University of Nottingham
UK | CHINA | MALAYSIA

Investigating the effect of N-terminal methionine addition, hydrophobic interaction enhancement and loop modification in modifying immunomodulatory and cancer-inhibitory activities of FIP-fve mutants

Chan Won Ting

Thesis submitted to the University of Nottingham for the degree of

Doctor of Philosophy

July 2019

Abstract

FIP-fve is an immunomodulatory protein isolated from edible enokitake mushroom *Flammulina velutipes* and grouped under fungal immunomodulatory proteins (FIPs) family. FIPs are well documented for their immunomodulation, anti-allergy and anti-tumour activities. Herein, this study is motivated by a lack of understanding in regard to structural and functional relationship of FIP-fve as well as other FIPs in the FIP family in association to immunomodulatory and cancer-inhibitory activities. The knowledge in structure-function paradigm may reveal fundational characteristics of FIP-fve in delivering its associated functions. The three-dimensional (3D) structure of FIP-fve is the first protein structure that is determined in FIPs family, by which it is also one of the most well delineated FIP structure. Examination to the structural data of FIP-fve revealed three important aspects that may be crucial in determining and/or enhancing its bioactivities. Firstly, it is hypothesized that reinforcing of hydrophobic interaction in N-terminal inter-helices via hydrophobic amino acid substitution would further improve its functional activities. Secondly, possible mutational benefits with addition of highly conserved N-terminal methionine in FIPs family to beginning of N-terminal of FIP-fve were investigated. Thirdly, it is believed that loops that connect beta-strands in FIP-fve are responsible in determining its bioactivities, and adoption of loops from Ling Zhi-8 (LZ-8), FIP from *Ganoderma lucidum* might strengthen bioactivities of FIP-fve. It is expected that LZ-8 that is isolated from medicinal mushroom *Ganoderma lucidum* possesses higher curative status in comparison to FIP-fve that is extracted from cuisine mushroom *Flammulina velutipes*. Following *in vitro* evaluation of functional activities, a few important findings were demonstrated. Mutants with reinforcing of N-terminal dimerization showed enhancement in its immunostimulatory and lung cancer A549 cell-inhibitory activities, presumably via increasing protein stability that led to prolong protein half-life. Mutations of loop DE and hinge residue E61K were crucial in directing immune

response towards T helper 1 (T_H1) and displayed significant inhibition towards breast cancer MDA-MB-231 cell viability, while mutations of loop FG and hinge residue I97D were important for inhibiting cell viability of A549 lung cancer cell and MCF-7 breast cancer cell. Loop DE adoption (LZ-8) also abolished haemagglutination ability of FIP-fve mutant, making it suitable for therapeutic use. The residues that are important in determining bioactivities of FIP-fve are tabled out. This study demonstrated for the first time that immunomodulatory and anti-cancer activities of FIP-fve can be enhanced via strengthened dimerization and loop modification. The research lays a foundation for other FIPs as immuno-therapeutic candidate in future.

List of conference abstracts

- Chan, W.T., Then S.M., and Kan M.S. 2016. Molecular cloning and expression of recombinant fungal immunomodulatory protein from *Flammulina velutipes* (FIP-fve) and mutants proteins. Monash Science Symposium 2016, 21-23 November 2016, Subang Jaya, Selangor.

- Chan, W.T., Then S.M., and Kan M.S. 2017. Unravelling the structural-functional relationship of an immunomodulatory protein from enokitake mushroom (FIP-fve). International Conference on Molecular Biology and Biotechnology, 1 – 2 November 2017, Kuala Lumpur, Malaysia.

- Chan, W.T., Tan, C.Y., Lai, K.M., Jonet, M.A., Then S.M., and Kan M.S. 2018. Identifying the potent amino acid residues in fungal immunomodulatory protein from *Flammulina velutipes* (FIP-fve) that attributes to its immunomodulatory and cancer-inhibitory activities. 47th Annual Scientific Meeting of the Australasian Society for Immunology, 2 – 6 December 2018, Perth, Australia.

Acknowledgements

The work presented in this thesis would not have been possible without the support of several people. I take this opportunity to extend my gratitude and appreciation to all those who made completion of this doctoral thesis possible.

First and foremost, I would like to express my sincere gratitude to my principal supervisor, Dr Kan Mun Seng for introducing me to this exciting field of science, for his valuable guidance, scholarly inputs, patience, continuous motivation and support throughout my PhD study. His integral view on research and his mission on coaching a doctoral student has allowed me to grow as a research scientist. For all that, I am thankful for his mentorship during the course of study.

My special words of thanks also go to my co-supervisor, Dr Then Sue-Mian for her guidance, insightful comments, and support especially during writing of this thesis.

I express my heart-felt gratitude to Dr Fang Chee Mun for his immense knowledge and guidance on immunology study.

I am grateful to Dr Mohd Jonet Anuar from Malaysian Genomics Institute who guided and gave me permission to use facility in his laboratory for X-ray crystallography study.

A special mention of thanks to my friends in University of Nottingham Malaysia Campus, especially Ms Tham Shiau Ying and Ms Loh Fei Kean for their companionship and constant support throughout the study.

Last but not least, my deepest gratitude go to my family and Mr Chu Ket Lee for the unconditional love, support and encouragement throughout these years.

Table of contents

Abstract i

List of conference abstracts iii

Acknowledgement iv

Table of contents v

Abbreviations viii

List of Figures xvii

List of Tables xxv

Chapter 1 General Introduction **1**

Chapter 2 Literature Review **10**

2.1 Biological characteristics of fungal immunomodulatory proteins from *Flammuline velutipes* (FIP-fve) 10

2.1.1 FIPs family 10

2.1.2 Structural characteristics 13

2.1.3 Processing resistance properties 24

2.2 Bioactivities and medicinal activities of FIP-fve 25

2.2.1 Haemagglutination activity 25

2.2.2 Anti-inflammatory 30

2.2.3 Anti-cancer 33

2.3 Mechanism of action of FIP-fve 38

2.4 Molecular biology research of recombinant FIP-fve protein 44

2.4.1 Bacterial production system 44

2.4.2 Baculovirus/insect cell expression system 45

2.4.3 Yeast cell expression system 46

2.5 Overview of human immune system 48

2.5.1 Innate (non-specific) immunity 48

2.5.2 Adaptive immunity 49

2.5.3 $CD4^+$ effector T cells 54

2.5.4 $CD8^+$ effector T cells 58

Chapter 3 Construction of FIP-fve and Mutant Gene Cassettes and Corresponding Recombinant Expression Vectors 60

3.1 Introduction 60

3.2 Materials and methods 67

3.2.1 General materials and equipment 69

3.2.2 cDNA encoding FIP-fve 71

3.2.3 Design and construction of recombinant *FIP-fve* and its variants 78

3.3 Results 93

3.3.1 Generation of FIP-fve cDNA 93

3.3.2 Cloning vector construction 94

3.3.3 Generation gene cassettes 96

3.3.4 Colony PCR 103

3.3.5 Verification of positive recombinant vectors 105

3.4 Discussion 107

3.5 Conclusion 112

Chapter 4 Protein Expression and Purification of Recombinant FIP-fve and Mutants from *Escherichia coli*..... 113

4.1 Introduction 113

4.2 Materials and methods 118

4.2.1 General materials and specialised equipment 118

4.2.2 Expression of recombinant FIP-fve and mutants proteins from Escherichia coli system 118

4.3 Results 125

4.3.1 Protein expression at different temperatures 125

4.3.2 Protein purification 126

4.4 Discussion 130

4.5 Conclusion 136

Chapter 5 Evaluation on Immunomodulatory Activities of FIP-fve mutants 137

5.1 Introduction 137

5.2 Methods and materials 142

5.2.1 General materials and equipment 142

5.2.2 Immunomodulation activity assay 143

5.2.3 Haemagglutination assay 147

5.2.4 Statistical analyses 148

5.3 Result 149

5.3.1 Microscopic visualization of splenocytes interactions 149

5.3.2 Proliferative responses of stimulated mice splenocytes 151

5.3.3 Cytokine profiling of stimulated splenocytes culture 155

5.3.4 *In vitro* immunological characterization of stimulated splenocytes 159

5.3.5 Haemagglutination activity 175

5.4 Discussion 177

5.5 Conclusion 188

Chapter 6 Evaluation on Anti-Cancer Activities of FIP-fve Mutants 190

6.1 Introduction 190

6.2 Materials and methods 194

6.2.1 General materials and specialised equipment 194

6.2.2 Cell viability inhibition assay 195

6.2.3 Cell migration assay 197

6.2.4 Statistical analyses 197

6.3 Results 198

6.3.1 Determination of optimal concentration in cancer cell inhibition 198

6.3.2 Determination of optimal treatment time in cancer cell inhibition 204

6.3.3 Cell inhibition assessment 210

6.3.4 Anti-migration assessment 220

6.4 Discussion 232

6.5 Conclusion 243

Chapter 7 X-ray Crystallography 245

7.1 Introduction 245

7.2 Methods and material 250

7.2.1 General materials and equipments 252

7.2.2 Further purification of fusion protein H-CWT6-Ek-GFP 252

7.2.3 Further purification of H-CWT6 253

7.2.4 Crystallization 254

7.2.5 X-ray analysis 255

7.3 Results 256

7.3.1 Enterokinase-digestion reaction 256

7.3.2 Purification of H-CWT6 257

7.3.3 Crystallization 261

7.3.4 X-ray analysis 266

7.4 Discussion 269

7.5 Conclusion 273

Chapter 8 General Discussion 274

References xxvii

Appendices xlviii

Abbreviations

MPD	2,4-methyl pentanediol
Brdu	5-bromo-2'-deoxyuridine
X-gal	5-bromo-4-chloro-3-indolyl-β-d-galactoside
A_{260}	absorbance at 260 nm wavelength
A_{280}	absorbance at 280 nm wavelength
A_{370}	absorbance at 370 nm wavelength
A_{570}	absorbance at 570 nm wavelength
A_{600}	absorbance at 600 nm wavelength
ATP	adenosine triphosphate
α	alpha
ATCC	American Type Cell Collection
ANOVA	analysis of variance
Ta	annealing temperature
APCs	antigen-presenting cells
H_A or H_B	N-terminal alpha-helices
Bp	base pair
S_A or S_B	beta-strands
β	beta
BLAST	Basic Local Alignment Search Tool

BM-DCs	bone-marrow dendritic cells
BSA	bovine serum albumin
Ca^{2+}	calcium ion
CBP	calmodulin binding peptide
CBM	carbohydrate-binding module
CO_2	carbon dioxide
CD40L	CD40 ligand
CTLs	$CD8^+$ cytotoxic T lymphocytes
Co^{2+}	cobalt ion
Co-CMA	cobalt(II)-carboxylmethylaspartate
Con A	concanavalin A
C_H	constant-light
Cu^{2+}	copper ion
CTLA	cytotoxic T-lymphocyte-associated antigen
˚C	degree celcius
DCs	dendritic cells
dNTP	Deoxynucleotides
Der m	*Dermatophagoides microceras*
Der p	*Dermatophagoides pteronyssinus*
DMSO	dimethyl sulfoxide

Na_2HPO_4	disodium phosphate
DTT	dithiothreitol
EMSA	electrophoretic mobility shift assay
Ek	enterokinase cleavage site
ELISA	enzyme-linked immunosorbent assay
EGFR	epidermal growth factor receptor
ER	estrogen receptor
EDTA	ethylenediaminetetraacetic acid
EMEA	European Medicines Agency
FACS	fluorescence-activated cell sorting
FBS	fetal bovine serum
FDA	Food and Drug Administration
FIP	fungal immunomodulatory protein
FIP-gap	fungal immunomodulatory protein from *Ganoderma applanatum*
FIP-app	fungal immunomodulatory proteins from *Auricularia polytricha*
FIP-cru	fungal immunomodulatory proteins from *Chroogomphis rutilus*
FIP-dsq2	fungal immunomodulatory proteins from *Dichomitus squalene*

FIP-fve	fungal immunomodulatory proteins from *Flammuline velutipes*
FIP-gja	fungal immunomodulatory proteins from *Ganoderma japoncium*
LZ-9	fungal immunomodulatory proteins from *Ganoderma lucidum*
FIP-gmi	fungal immunomodulatory protein from *Ganoderma microsporum*
FIP-gsi	fungal immunomodulatory protein from *Ganoderma sinense*
FIP-gts	fungal immunomodulatory protein from *Ganoderma tsugae*
FIP-lrh	fungal immunomodulatory proteins from *Lignosus rhinocerotis*
FIP-ppl	fungal immunomodulatory proteins from *Postia placenta* Mad-698-R
FIP-sch3	fungal immunomodulatory proteins from *Stachybotrys chartarum*
FIP-tvc	fungal immunomodulatory proteins from *Trametes versicolor*
FIP-vvo	fungal immunomodulatory proteins from *Volvariella volvacea*
FNIII	fibronectin III
GST	glutathione S-transferase
G	gram
GFP	green fluorescent protein

C_H	heavy chain
6xHis	hexahistidine
HF	High Fidelity
HER-2	human epidermal growth factor receptor 2
hPMBCs	human peripheral blood mononuclear cells
NMC23	human nonmetastatic clone 23
HPV	human papillomavirus
HCl	hydrochloric acid
HIC	hydrophobic interaction
AHR	airway hyperresponsiveness
V_H	hypervariable region from heavy chain
V_L	hypervariable region from light chain
IDA	iminodiacetic acid
IMAC	immobilised metal affinity chromatography
IgG	immunoglobulin G
IFN-γ	interferon-gamma
IDT®	Integrated DNA Technologies
IL	interleukin
IEX	ion exchange chromatography
IPTG	isopropyl β-D-1-thiogalactopyranoside

Kbp	kilo-base pair
kDa	kilo-Dalton
LZ-8	Ling Zhi-8
LCN2	lipocalin 2
L	litre
LB	Luria Bertani
$MgCl_2$	magnesium chloride
MHC	major histocompatibility complex
MBP	maltose binding protein
MMP2	matrix metalloproteinase
µl	microliter
mL	milliliter
mM	millimolar
Min	minute
M	molar
KH_2PO_4	monopotassium phosphate
NK	natural killer
NEB®	New England biolabs
NMR	Nuclear Magnetic Resonance
Ni^{2+}	nickel ion

Ni-NTA	nickel(II)-nitrilotriacetic acid
NSCLC	non-small-cell lung carcinoma
POD	peroxidase
PBS	phosphate-buffered saline
PAI-1	plasminogen activator inhibitor type-1
PES	polyethersulfone
PEG	polyethylene glycol
PCR	polymerase chain reaction
KCl	potassium chloride
PR	progesterone receptor
PD	programmed death
PDB	Protein Data Bank
ANOVA	one-way analysis of variance
OD	optical density
OVA	ovalbumin
RacGAP1	Rac GTPase-activating protein 1
rFIP-fve	recombinant FIP-fve gene
RBCs	red blood cells
x g	relative centrifugal force expressed in units of gravity
RSV	respiratory syncytial virus

RE	restriction enzyme
RPM	revolutions per minute
RT-PCR	reverse transcriptase-polymerase chain reaction
RT	room temperature
s	second
SDM	site-directed mutagenesis
SEC	size exclusion chromatography
SC	small-cell lung carcinoma
NaCl	sodium chloride
SDS-PAGE	sodium dodecyl sulfate polyacrylamide gel electrophoresis
SD	standard deviation
SI	stimulation index
TcR	T cell receptor
TMB	tetramethylbenzidine
T_H1	T helper 1
T_H2	T helper 2
T_H17	T helper 17
3D	three-dimensional
TVAI	*Thermoactinomyces vulgaris* R-47 α-amylase I
UK	United Kingdom

USA	United States of America
UV	ultraviolet
VEGF	vascular endothelial growth factor
v	voltage
v	volume
w	weight
x	times

List of Figures

		Page
Figure 1.1:	Three-dimensional structure of FIP-fve that is deposited in Protein Data Bank as 1OSY.	3
Figure 1.2:	Comparative structural analysis of protein structure of monomers of FIP-fve (cyan) and LZ-8 (yellow).	7
Figure 2.1:	Overall crystal structure of FIP-fve that is deposited in Protein Data Bank as 1OSY.	14
Figure 2.2:	Schematic diagram illustrating 3D domain swapping in FIP-fve	16
Figure 2.3:	Three dimensional structure of immunoglobulin G is adopted from PDB ID: 1igt.	19
Figure 2.4:	Superposition of 3D protein structure of the monomers of FIP-fve, LZ-8, FIP-gmi and FIP-ppl.	21
Figure 2.5:	Importance of proline.	23
Figure 2.6:	Haemagglutination assay.	26
Figure 2.7:	Histological staining on lung tissue sections of OVA-sensitized mice that showed effects of FVE treatment on lung inflammation and remodelling.	32
Figure 2.8:	Schematic diagram of structural comparison on Ig-like structure between FIP-fve and domain N of *T. vulgaris* R-47 α-amylase I.	39

Figure 2.9:	Multiple sequence alignment of FIP-fve, LZ-8, FIP-gts, FIP-gja, FIP-gsi, LZ-9, FIP-gmi, FIP-cru, FIP-gap, FIP-nha, FIP-dsq2, FIP-vvo, FIP-lrh, FIP-sch3, FIP-tvc and FIP-ppl	40
Figure 2.10:	Proposed site of mechanism of FIP-fve-modulated IFN-γ secretion.	43
Figure 2.11:	T lymphocyte activation.	51
Figure 2.12:	The biological action of IL-2	53
Figure 2.13:	Characteristics of T_H1, T_H2 and T_H17 subsets of $CD4^+$ T cells	55
Figure 2.14:	Cross-presentation pathway of antigens to $CD8^+$ T cells.	59
Figure 3.1:	Demonstration of the major regions of FIP-fve involved in mutagenesis.	63
Figure 3.2:	Multiple sequence alignment of amino acid sequences of FIP-fve (WT), CWT-1, CWT-2, CWT-3, CWT-4, CWT-5, CWT-6, CWT-7, and CWT-8	64
Figure 3.3:	A methodology workflow describing the process involved in the construction of recombinant vectors for *FIP-fve* and variants	68
Figure 3.4:	Fruiting body of *Flammulina velutipes* that was used as starting material.	72
Figure 3.5:	Vector map of linearized pGEM®-T easy with single 3'-terminal thymidine at both ends	75
Figure 3.6:	Vector map of pGLO	82

Figure 3.7:	Schematic diagram of the internal mutagenic primer design for overlap PCR extension approach	83
Figure 3.8:	Overlap PCR extension for site-directed mutagenesis involved several steps.	87
Figure 3.9:	PCR amplification profiles of FIP-fve cDNA	93
Figure 3.10:	Bacterial transformants resulted from transformation of TOP10 cells with ligation products	94
Figure 3.11:	Schematic diagram of the generated cloning vector, pGEM-FIPfve with *FIP-fve* cDNA as insert	95
Figure 3.12:	PCR amplification profile of gene cassette for *H_6-rFIPFVE-Ek*.	96
Figure 3.13:	PCR amplification profile of gene cassette for *H_6-CWT1-Ek*.	97
Figure 3.14:	PCR amplification profile of gene cassette for *H_6-CWT2-Ek*.	98
Figure 3.15:	PCR amplification profiles of fragment AB, fragment CD and gene cassette *H_6-CWT3-Ek* (fragment AD)	99
Figure 3.16:	PCR amplification profiles of *CWT-4*, *CWT-5*, gene cassette *H_6-CWT4-Ek* and gene cassette *H_6-CWT5-Ek*.	100
Figure 3.17:	PCR amplification profiles of fragment AB, fragment CD and gene cassette *H_6-CWT6-Ek* (fragment AD).	101
Figure 3.18:	PCR amplification profiles of *CWT-7*, *CWT-8*, gene cassette *H_6-CWT7-Ek*, and gene cassette *H_6-CWT8-Ek*.	102

Figure 3.19:	PCR amplification profiles of colony PCR screening	104
Figure 3.20:	Schematic diagram of the generated pGLO:: insert-GFP expression vector.	105
Figure 4.1:	Model of interaction between (a) histidine residues in affinity tag and Ni(II)-nitrilotriacetic acid matrix and (b) histidine residues in affinity tag and Co(II)-carboxylmethylaspartate.	115
Figure 4.2:	Diagram illustrating theory of size exclusion chromatography (SEC).	117
Figure 4.3:	Setup of size exclusion chromatography.	123
Figure 4.4:	Comparison of protein expression level based on fluorescence intensity of GFP containing tag in fusion proteins.	125
Figure 4.5:	SDS-PAGE profile of coomassie blue-stained 1 µg of recombinant proteins.	127
Figure 4.6:	Native-PAGE profile of (a) unstained and (b) coomassie-blue stained of 1 µg of recombinant proteins.	128
Figure 5.1:	Microscopic visualization of splenocytes agglutination at 100x magnification.	150
Figure 5.2:	Proliferative responses of balb/c mice splenocytes.	152
Figure 5.3:	Proliferative responses of balb/c mice splenocytes.	154
Figure 5.4:	Secretion profile of cytokines (a) IFN-γ and (b) IL-2 from mice splenocytes after 48 hr of stimulation.	156

Figure 5.5:	Secretion profile of cytokines (a) IFN-γ and (b) IL-2 from mice splenocytes after 48 hr of stimulation.	158
Figure 5.6:	FACS analysis of stimulated mice splenocytes.	160
Figure 5.7:	Immunophenotyping of lymphocyte population in mice splenocytes.	163
Figure 5.8:	Immunophenotyping of lymphocyte population in mice splenocytes.	166
Figure 5.9:	Immunophenotyping of lymphocyte population in mice splenocytes.	170
Figure 5.10:	Immunophenotyping of lymphocyte population in mice splenocytes.	174
Figure 5.11:	Haemagglutination activities of rFIP-fve and mutants towards mice and human red blood cells.	176
Figure 6.1:	Effect of different concentrations of rFIP-fve and mutants in inhibiting lung cancer A549 cell lines.	199
Figure 6.2:	Effect of different concentrations of rFIP-fve and mutants in inhibiting breast cancer MDA-MB-231 cell lines.	201
Figure 6.3:	Effect of different concentrations of rFIP-fve and mutants in inhibiting breast cancer MCF-7 cell lines.	203
Figure 6.4:	Effect of different time treatment of rFIP-fve and mutants in inhibiting lung cancer A549 cell lines.	205

Figure 6.5:	Effect of different time treatment of rFIP-fve and mutants in inhibiting breast cancer MDA-MB-231 cell lines.	207
Figure 6.6:	Effect of different time treatment of rFIP-fve and mutants in inhibiting breast cancer MCF-7 cell lines.	209
Figure 6.7:	Effect of rFIP-fve and mutant group with putative enhanced dimerization on A549 cell viability.	211
Figure 6.8:	Effect of rFIP-fve and mutant group with putative enhanced dimerization on MDA-MB-231 cell viability.	212
Figure 6.9:	Effect of rFIP-fve and mutant group with putative enhanced dimerization on MCF-7 cell viability.	213
Figure 6.10:	Effect of rFIP-fve and mutant group with loop modification on A549 cell viability.	215
Figure 6.11:	Effect of rFIP-fve and mutant group with loop modification on MDA-MB-231 cell viability.	217
Figure 6.12:	Effect of rFIP-fve and mutant group with loop modifications on MCF-7 cell viability.	219
Figure 6.13:	Effect of rFIP-fve and mutant group of putative enhanced dimerization on A549 cell migration.	222
Figure 6.14:	Effect of rFIP-fve and mutant group of putative enhanced dimerization on MDA-MB-231 cell migration.	225
Figure 6.15:	Effect of rFIP-fve and mutant group of loops modification on A549 cells migration.	228

Figure 6.16:	Effect of rFIP-fve and mutant group of loops modification on MDA-MB-231 cell migration.	231
Figure 7.1:	Vapour diffusion methods.	247
Figure 7.2:	Schematic representation of workflow conducted for X-ray crystallography study	251
Figure 7.3:	Rigaku Micromax-007 rotating-anode X-ray generator	255
Figure 7.4:	SDS-PAGE profile of coomassie blue-stained protein samples from enterokinase-digested reaction of fusion protein.	256
Figure 7.5:	Further purification of digested fusion protein H-CWT6-EK-GFP using ion exchange chromatography.	258
Figure 7.6:	Further purification of digested fusion protein H-CWT6-EK-GFP using IMAC and followed by IEX.	260
Figure 7.7:	Crystals grown from initial screening condition of D10 Index HT	261
Figure 7.8:	Crystals grown from the initial crystallization screening	263
Figure 7.9:	Crystals formed from the optimization by varying PEG concentration, pH value and additive addition.	265
Figure 7.10:	X-ray diffraction pattern of orthorhombic-like crystal.	267
Figure 7.11:	X-ray diffraction pattern of the tetragonal-like crystals.	268

Figure 8.1:	Tabulation of importance of the amino acids sites in determining the immunoregulatory and cancer-inhibitory activities of FIP-fve.	283
Figure A3.1:	Alignment of sequencing results for FIP-fve cDNA	lxvi
Figure A3.2:	Alignment between FIP-fve cDNA and FIP-fve mRNA (GU388420.1)	lxvi
Figure A4.1:	Fluorescence visualization of collected protein fractions containing GFP tag in tubes from protein purification using IMAC.	lxxvii
Figure A4.2:	Fluorescence visualization of collected protein fractions containing GFP tag in tubes from protein purification using SEC.	lxxvii
Figure A5.3	FACS analysis of ConA-stimulated mice splenocytes.	lxxxvii

List of Tables

		Page
Table 2.1:	List of FIPs that have been discovered from 1989 to 2017.	12
Table 2.2:	Specificities of FIPs on agglutination of different types of red blood cells	29
Table 3.1:	Programmed Thermal Cycler Conditions	73
Table 3.2:	Reaction components for ligation reaction	75
Table 3.3	List of gene cassettes with description of desired mutation generated for *rFIP-fve* and its eight derivatives.	79
Table 3.4:	List of primers designed for site-directed mutagenesis and gene cassettes construction	84
Table 3.5:	Naming of recombinant expression vectors generated for genes *rFIP-fve*, *CWT-1*, *CWT-2*, *CWT-3*, *CWT-4*, *CWT-5*, *CWT-6*, *CWT-7* and *CWT-8*.	106
Table 4.1:	Protein yields of synthesized recombinant H-rFIPFVE-Ek-GFP and derivatives proteins in 1 L of bacterial culture.	129
Table 5.1:	List of generated recombinant rFIP-fve and mutants proteins.	139
Table 5.2:	Combination of marker antibodies used in FACS analysis	147
Table 5.3:	Comparison of immunomodulatory and haemagglutination activities of recombinant FIP-fve and derivatives proteins.	189

Table 6.1:	Comparison of cell viability inhibition and anti-migration activities of rFIP-fve and mutants	244
Table A3.1:	Hydrophobicity index for common amino acids.	xlviii
Table A4.4a:	Composition of resolving gel for SDS-PAGE	lxxix
Table A4.4b:	Composition of stacking gel for SDS-PAGE	lxxix
Table A4.4c:	Composition of resolving gel for Native-PAGE	lxxix
Table A4.4d:	Composition of stacking gel for Native-PAGE	lxxix

Chapter 1 General Introduction

The discovery of a few small fungal proteins with similar structural and functional characteristics has led to the creation of a protein family known as fungal immunomodulatory protein (FIP) family (Ko *et al.*, 1995). The FIPs members share sequence homologies of 60-70% among the family members. FIPs are small proteins with estimated molecular mass of approximately 12 to 13 kDa (Li, Wang and Zhou, 2011). The immunomodulatory and cancer-inhibitory properties of FIPs have been reported over the years; for instance, the FIPs are capable of stimulating mitogenesis of human peripheral blood lymphocytes cells by inducing generation of various cytokines (Kino *et al*., 1989; Haak-Frendscho *et al.*, 1993; Ko *et al.*, 1995; and Hsu *et al.*, 1997) that are effective in alleviating allergy reaction (Hsieh *et al.*, 2003; Lee *et al*., 2013; Chang *et al*., 2015; and Chu *et al*., 2017) and in inhibiting tumor growth through immune-regulating pathway (Chang *et al.*, 2010). In addition to their immunoregulatory abilities, FIPs are also capable of initiating inhibition in cancer cell growth and inducing cytotoxicity against cancer cells (Wu *et al*., 2011; Chang *et al*., 2013; Li *et al.*, 2016 ; Li *et al.*, 2017; and Lin *et al.*, 2017). With regard to the reports that have been documented thus far, FIPs appear to possess both direct and indirect anti-cancer capabilities. One of the earliest FIPs – Ling Zhi-8 (LZ-8) was identified in medicinal mushroom *Ganoderma lucidum*, as known as Ling Zhi or Reishi in China (Kino *et al.*, 1989). Thereafter, another FIP was isolated from edible mushroom *Flammulina velutipes* as known as enokitake or golden needle mushroom, and named as FIP-fve (Ko *et al.*, 1995). This was followed by further characterization of FIPs in 14 other mushroom species.

Presently, three-dimensional protein structures of the three FIPs, **FIP-fve** (Protein Data Bank (PDB) ID: 1OSY) (Paaventhan *et al.*, 2003), **LZ-8** (PDB ID: 3F3H) (Huang *et al.*, 2009) and **FIP-gmi** (*Ganoderma microsporum*) (PDB ID: 3KCW) (Wu *et al.*, 2007) were resolved and deposited in Protein Data Bank. Both FIP-fve and LZ-8 exist as a homodimer in their native state, while FIP-gmi stays as tetramer in its native state. The structural data of FIP-fve was the first protein structure that was presented in FIPs family. It is also regarded as the most well defined FIP structure with the most available structural data. Although the protein structures of LZ-8 and FIP-gmi were resolved, the structural data was not as considerably delineated as compared to FIP-fve. Additionally, FIP-fve appears as one of the potential candidates in immunotherapy as it has been reported repeatedly for its immunomodulatory ability. FIP-fve is one of the most well documented FIPs for its abilities in mitigating allergy reaction (Hsieh *et al.*, 2003; Lee *et al*., 2013; Chang *et al*., 2015; and Chu *et al*., 2017) and inhibiting cancer cell growth (Ding *et al.*, 2009; Chang *et al.*, 2010) via regulation of host immune response. Essentially, FIP-fve demonstrated stable activity when it was administered orally (Hsieh *et al.*, 2003; Chang *et al.*, 2010, 2015; Lee *et al.*, 2013; Chu *et al.*, 2017), which makes it a suitable candidate to be developed for pharmaceutical use. Therefore, FIP-fve is chosen as the protein of interest in this research. The research question of this study arises from a lack of understanding in regard to relationship between structure and functions of FIP-fve as well as other FIPs in the FIP family as research area has been mainly focused on evaluating the bioactivities of FIPs. Hence, it drives the current research to investigate on the structural and functional association of FIP-fve in relation to its immunomodulatory and cancer-inhibitory activities. Further understanding on the structural and functional relationship of FIP-fve is considered as one of the prerequisites in developing and applying FIP-fve for future therapeutic use. Given high structural similarities among FIPs, the knowledge and understanding of which could contribute to potential enhancement of bioactivities of FIP-fve as well as other FIPs members via genetic engineering approach.

The three-dimensional structure of FIP-fve was taken as an essential and integral reference for the present research. As shown in **Figure 1.1**, FIP-fve exists as a homodimer with dumbbell shape. Each subunit of FIP-fve comprised of an N-terminal alpha (α)-helix (H_A or H_B) and beta (β)-strand (S_A or S_B) that is connected to a fibronectin III (FNIII)-type fold domain. The N-terminal α-helices of the two subunits interact through hydrophobic interaction whereas β-strands form an antiparallel β-sheet; this region represents the N-terminal dimerization site. The FNIII fold is made up of seven β-strands that are organized into a two β-sheets sandwich. These strands are linked by loops (Ko *et al.*, 1995). Topology of FNIII-type fold is highly similar to that of immunoglobulin (Ig)-like domains; one apparent difference between these two folds is the presence of disulfide bond in Ig-like domains, while FNIII-type fold lacks of the disulfide bonds (Kessel and Ben-Tal, 2018). In specific, an examination to the structural data of FIP-fve revealed three important aspects that are worth inspecting, which are described below.

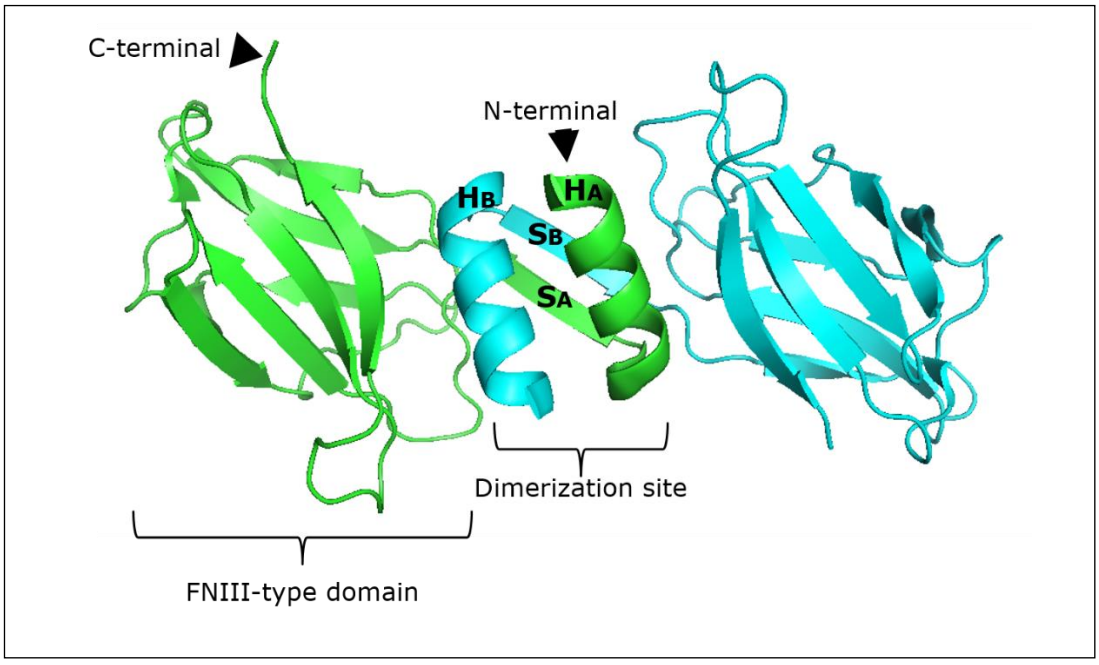


Figure 1.1. Three-dimensional structure of FIP-fve that is deposited in Protein Data Bank as 1OSY. Each subunit of FIP-fve comprises of an N-terminal α-helix and β-strand that is connected to a FNIII-type fold domain. The two monomers in the homodimer of FIP-fve are called molecule A and molecule B. The N-terminal α-helices are labelled as H_A and H_B; β-strands are labelled as S_A and S_B. (Paaventhan *et al.*, 2003).

Firstly, it has been proposed that the dimerization states of the FIPs are necessary for their immunomodulatory function. The speculation was deduced from the study of research groups of Lin (1997) and Paaventhan (2003). In FIP-gts, the α-helices (residues 1-13) are found to play a crucial role in dimerization of FIP-gts. It was demonstrated that recombinant deletion mutant FIP-gtsΔ1-13 and FIP-gtsΔLeu5/Phe7/Leu9 failed to dimerize, leading to loss of immunomodulatory function (Lin *et al*., 1997). Hence, the N-terminal α-helices that are responsible for FIPs dimeric structure are deemed crucial and needed for the functional role of FIPs in immune regulating activity (Lin *et al*., 1997). In fact, the subsequent structural determination of FIP-fve has substantiated their finding and revealed an important hydrophobic interaction between the alpha-helices. The two alpha-helices in FIP-fve are amphipathic. Each of the helix comprised of hydrophobic residues (Ala2, Leu5, Leu9, Leu12 and Val13) that are situated on the hydrophobic face. The side chains of these residues pack well against the hydrophobic residues of other helix, allowing the helices to bind to each other through hydrophobic interaction. The hydrophobic interaction between the two alpha-helices serves as one of the most important subunit-subunit interaction between the FIP-fve dimer where it functions to bind and stabilize the two monomers of FIP-fve (Paaventhan *et al.*, 2003). In view of this notion, it is hypothesized that the immunomodulatory ability of FIP-fve could be further enhanced by strengthening the hydrophobic interaction between the α-helices via hydrophobic amino acid substitution, which could potentially result in improvement of protein stability in homodimer form.

Secondly, one peculiar characteristic FIP-fve possesses is that it does not carry methionine residues while most of the FIPs harboured N-terminal methionine including LZ-8. In fact, all 16 discovered FIPs consist of N-terminal methionine residue except three FIPs, which are FIP-fve, FIP-vvo and FIP-ppl. The reason of initiator methionine conservation in most of the native FIPs except FIP-fve is unknown. Hence, the possible

mutational benefits as a result of addition of the highly conserved N-terminal Met to the beginning of N-terminal of FIP-fve are of interest to be investigated as well. Since N-terminal α-helices of FIP-fve are responsible in establishing dimerization between the two FIP-fve monomers (Paaventhan *et al.*, 2003), the added N-terminal methionine might influence dimerization of FIP-fve.

Thirdly, the potentiality of loops in FNIII-type fold that might act as functional domains in FIP-fve was explored as well. Considering that FNIII-type fold in FIP-fve is highly similar to that of Ig-like domains, IgG is viewed as an important reference in the exploration of functional sites that may be important in determining the immune-regulating function of FIP-fve as structural biology of IgG has been studied extensively. The stacking of β-sheets in Ig-type folding allows: (1) hydrophobic residues to be packed in protein core and (2) side chains of stacking sheets to be able to interact with each other. This arrangement leads to stabilization of the protein core. The stable protein core serves as a solid and reliable scaffold for functional sites, whereas the six loops in arm of the antibodies (three loops from each chain) are responsible in determining the antigen binding specificity. (Kessel and Ben-Tal, 2018). Likewise, comparative protein structural analysis between FIP-fve and LZ-8 also revealed significant conformational differences in loop DE and loop FG regions, while the rest of the structures aligned almost perfectly to each other as shown in **Figure 1.2**. In comparison to LZ-8, the α-carbons of loop DE in FIP-fve are positioned differently, leading to different orientation of the side chains in this segment; whereas, the loop FG in FIP-fve is longer and extended to a different angle (Huang *et al.*, 2009). Despite conservation of high sequence similarities among FIPs, the FIPs members have been shown to display distinctive bioactivities (Huang *et al*., 2009 and Bastiaan-Net *et al*., 2013). For instance, LZ-8 showed stronger direct cancer-inhibiting activity, whereas FIP-fve demonstrated a less effective direct cancer-inhibiting activity (Huang *et al.*, 2009). Rather, FIP-fve has been shown to display strong anti-

inflammation activity in allergic-induced mice (Hsieh *et al*., 2003; Lee *et al*., 2013; Chang *et al*., 2015 and Chu *et al*., 2017). It could be the reason why majority of studies have been focused on examining of its anti-allergic activities, and there were fewer studies carried out on investigating its anti-cancer activities. Although no previous studies have been performed to compare the immunomodulatory activities between FIP-fve and LZ-8, it is believed that adoption of loops region from LZ-8 could enhance the immune-regulating activity (besides anti-tumour activity) of FIP-fve. This is because medicinal mushroom *Ganoderma lucidum* has long been used in traditional Chinese medicine to promote physical wellness and long life. On the other hand, edible mushroom *Flammuline velutipes* has been used in East Asian cuisine. In light of these facts, LZ-8 that is isolated from *Ganoderma lucidum* is expected to possess higher curative status in comparison to FIP-fve that is extracted from *Flammulina velutipes*. Hence, it is hypothesized that the mutation involving the possibly potent loop regions from LZ-8 might enhance the functional activities of FIP-fve. Taking these into account, it is believed that the loops that connect the β-strands in FIP-fve are responsible for its bioactivities, and adoption of loops from LZ-8 might strengthen immunomodulatory properties as well as its anti-cancer activities of FIP-fve. Additionally, putative hinge residues right before the start of loop DE and FG regions are also found to differ in FIP-fve and LZ-8. It is postulated that the putative hinge residues are crucial in positioning the loops. Therefore, the putative hinge residues were also included as complements to the mutation of loop regions to determine its effect in protein bioactivities.

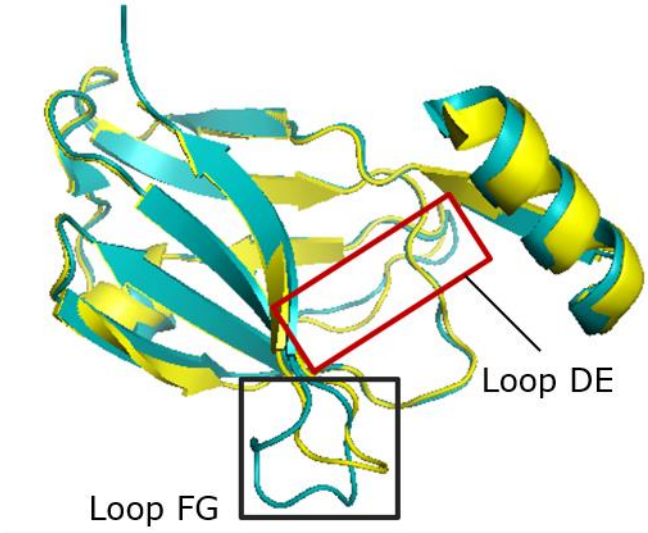


Figure 1.2. Comparative structural analysis of protein structure of monomers of FIP-fve (cyan) and LZ-8 (yellow). The differences in loop DE and FG regions are indicated in the red and black boxes respectively (Huang *et al*., 2009).

The core of this study is to determine the structural and functional relationship of FIP-fve with regard to its immunomodulation and cancer-inhibition abilities. Genetic modification was utilised to design and create FIP-fve mutants that harboured the intended mutations in **Chapter 3**. The gene encoding FIP-fve was extracted from the fruiting of *Flammulina velutipes* and served as the starting template. A total of eight FIP-fve gene derivatives were synthesized, which specifically targeted on N-terminal alpha-helices and loops regions. Expression cassettes were designed to include fusion of hexahistidine and green fluorescent protein (GFP) tags at the respective N- and C-terminal of the genes of interest. Bacterial pGLO plasmid vector was used as the expression vector in this study.

Chapter 4 describes the expression and purification of recombinant FIP-fve and derivatives proteins. The recombinant proteins were produced using bacterial expression system. Immobilised metal affinity chromatography (IMAC) was used as the primary purification method for the recombinant proteins, and followed by further purification using size exclusion chromatography (SEC).

Chapter 5 presents the immunomodulatory studies of purified recombinant FIP-fve and derivatives proteins. Balb/c mice splenocytes was used as the host cells in examining the *in vitro* immune-regulating activities of the recombinant proteins. Following stimulation of mice splenocytes with the respective proteins, the immune responses were evaluated based on proliferation of splenocytes, secretion profiles of T helper (T_H) 1 cytokines and characterization of immune cells. In addition, haemagglutination abilities of recombinant FIP-fve and mutants proteins were assessed using human and mice red blood cells.

Chapter 6 demonstrates the anti-cancer studies of purified recombinant FIP-fve and mutants proteins. Human lung and breast cancer cells were adopted as the cell lines in assessing the cancer-inhibiting abilities of the recombinant proteins. The anti-cancer activities were evaluated after cancer cells treatment with recombinant FIP-fve and derivatives proteins in term of their abilities in inhibition of cell viability and suppression of cell migration.

Chapter 7 describes the elucidation of the crystal structure of FIP-fve mutant that showed promising results in immunomodulation and anti-cancer studies. The derivative protein was subjected to further purification and followed by crystallization screening and optimization. The obtained crystals were subjected to X-ray analysis.

Overall, the ultimate goal of this study was to identify the potent amino acid residues that contribute to the immunomodulatory and anti-cancer activities of FIP-fve, which is a potential candidate for immunotherapy. To accomplish this, the study proposed the following specific objectives:

(i) To design and generate genes encoding FIP-fve and FIP-fve mutants;

(ii) To construct bacterial expression cassettes containing FIP-fve and FIP-fve mutants;

(iii) To purify the bacterial-expressed recombinant proteins FIP-fve and FIP-fve mutants;

(iv) To evaluate the immune-regulating and cancer-inhibiting activities of FIP-fve and FIP-fve mutants; and

(v) To determine the three-dimensional protein structure of FIP-fve mutant that showed promising results for the development as immunotherapy candidate via X-ray crystallography

Chapter 2 Literature Review

2.1 Biological characteristics of fungal immunomodulatory proteins from *Flammuline velutipes* (FIP-fve)

Study of protein structure and function allows insight into understanding on role as well as mechanism of action of a certain protein drug in biological system. With improved structural knowledge, positive impact can be attained via potential manipulation of particular protein using genetic modification techniques, and the resultant enhanced protein drug is introduced with higher specificity in treating disease (Whitford, 2005). In view of this, structural information of a protein is highly appreciated. Herein, the biological characteristics of FIP-fve that encompass its structural information from basic composition to overall protein structure are presented.

2.1.1 FIPs family

FIP-fve belongs to a protein family known as fungal immunomodulatory proteins (FIPs). FIP is a protein family that was proposed and created in 1995 since the discovery of a few small fungal proteins, which possess similar functional and structural characteristics (Ko *et al*. 1995). FIPs share sequence homologies of 40-70% among the family members. They consist of 110 to 125 amino acids residues, with estimated molecular masses of approximately 12 to 14 kDa (Li *et al*., 2011). All 16 discovered FIPs are listed in **Table 2.1**. Ling Zhi-8 (**LZ-8**) is the first FIP that was isolated from *Ganoderma lucidum*, a higher basidiomycetes (Kino *et al.*, 1989). Since then, several other FIPs have been extracted and characterized from other mushroom species such as *Flammulina velutipes* (**FIP-fve**) (Ko *et al.*, 1995), *Volvariella volvacea* (**FIP-vvo**) (Lin and Chou, 1984), *Ganoderma tsugae* (**FIP-gts**) (Lin *et al*., 1997), *Auricularia polytricha* (**FIP-app**) (Sheu *et al.*, 2004), *Ganoderma japoncium* (**FIP-gja**) (Bai *et al*., 2005), *Ganoderma microsporum* (**FIP-gmi**) (Wu *et al.*, 2007), *Ganoderma sinense* (**FIP-gsi**)

(Zhou *et al.*, 2009), *Ganoderma applanatum* (**FIP-gap**) (Lin *et al.*, 2011), *Trametes versicolor* (**FIP-tvc**) (Li *et al.*, 2012), *Ganoderma lucidum* (**LZ-9)** (Bastiaan-Net *et al.*, 2013), *Postia placenta* Mad-698-R (**FIP-ppl**) (Li *et al.*, 2015), *Chroogomphis rutilus* (**FIP-cru**) (Lin *et al.*, 2016), *Lignosus rhinocerotis* (**FIP-lrh**) (Pushparajah *et al.*, 2016), *Stachybotrys chartarum* (**FIP-sch3**) (Li *et al.*, 2016) and *Dichomitus squalens* (**FIP-dsq2**) (Li *et al.*, 2017).

Several research groups have reported on the medicinal properties of FIPs where FIPs are shown capable of inducing host immune system to generate a variety of cytokines that are effective in relieving allergy reaction and inhibiting tumour development (Li, Wang and Zhou, 2011). Other than LZ-8 that has been widely studied on both of its immunomodulatory and anti-cancer properties, research have been targeting on examination of the immunomodulatory activities of FIPs when they were first discovered. In recent years, the cancer-inhibiting capability of the newly discovered FIPs have been explored. Despite the fact that FIPs member share high similarity in their primary sequence, they are quite different in biological activities. For examples, FIP-fve is shown to display great anti-anaphylaxis effect in mice model (Hsieh *et al.*, 2003; Lee *et al.*, 2013; Chang *et al.*, 2015; Chu *et al.*, 2017). On the other hand, LZ-8 is reported to possess strong anti-tumour activity (Huang *et al.*, 2009). While both FIP-fve and LZ-8 showed capabilities of directing immune responses towards T helper (T_H) 1 by inducing T_H1-specific cytokine (Kino *et al.*, 1989; Ko *et al.*, 1995), FIP-vvo was shown to stimulate not only T_H1-specific cytokine, but also interleukin-4 (T_H2-specific cytokine) (Lin and Chou, 1984). The induction of interleukin-4 directs immune system towards T helper 2-specific response, leading to generation of IgE that promotes inflammation (Abbas, Lichtman and Pillai, 2015). In view of this, FIP-fve and LZ-8 are deemed to be suitable to be developed as therapeutic proteins as they are able to stimulate T_H1-specific response selectively. The bioactivities of FIP-fve are discussed further in the **Section 2.2**.

Table 2.1. List of FIPs that have been discovered from 1989 to 2017.

FIPs	Genbank	PDB ID	Species	Division	Identity of residues to FIP-fve (%)
LZ-8	EU680479.1	3F3H	*Ganoderma lucidum*	Basidiomycota	63.1
FIP-fve	ADB24832.1	1OSY	*Flammulina velutipes*	Basidiomycota	-
FIP-vvo	-	-	*Volvariella volvacea*	Basidiomycota	53
FIP-gts	-	-	*Ganoderma tsugae*	Basidiomycota	61
FIP-gja	AY987805.1	-	*Ganoderma japonicum*	Basidiomycota	60
FIP-gmi	-	3KCW	*Ganoderma microsporum*	Basidiomycota	61
FIP-gsi	-	-	*Ganoderma sinense*	Basidiomycota	61
FIP-gap	AEP68179	-	*Ganoderma applanatum*	Basidiomycota	65
FIP-tvc	XM_008039818.1	-	*Trametes Versicolor*	Basidiomycota	43
FIP-nha	XM_003043608.1	-	*Nectria haematococca*	Ascomycota	56
LZ-9	-	-	*Ganoderma lucidum*	Basidiomycota	63.1
FIP-ppl	KJ818121.1	-	*Postia placenta*	Basidiomycota	42
FIP-cru	KT210088	-	*Chroogomphis rutilus*	Basidiomycota	63
FIP-lrh	-	-	*Lignosus rhinocerotis*	Basidiomycota	51
FIP-sch3	KEY70185	-	*Stachybotrys chartarum* IBT 7711	Ascomycete	56
FIP-dsq2	XP 007363541.1	-	*Dichomitus squalens*	Basidiomycota	50

2.1.2 Structural characteristics

FIP-fve exists as a small homodimer protein with a molecular weight of 25500 Da in its native state. Each monomer of FIP-fve consists of 114 amino acid residues with molecular mass of 12746.3 Da (Seow *et al.*, 2003). It has an acetylated serine residue at N-terminal end and lacking of methionine, cysteine and histidine residues (Ko *et al.*, 1995). Crystal structure of FIP-fve was determined using single anomalous diffraction based on bromide ions signal in the crystal for structure delineation, revealing that FIP-fve exists as a homodimer with dumbbell shape (Paaventhan *et al.*, 2003). The 3D structural database of FIP-fve was deposited in Protein Data Bank (PDB) with PDB ID as 1OSY. FIP-fve serves as a representative protein structure for other members in FIPs family as its protein structure was first reported in FIPs family. Subsequently, crystal structure of LZ-8 was later reported, revealing that it bears close resemblance to FIP-fve. Similar to FIP-fve, the native state of LZ-8 is homodimer with dumbbell shape as well (Huang *et al.*, 2009).

Each subunit of FIP-fve comprised of an N-terminal α-helix (H_A or H_B) and β-strand (S_A or S_B) that is connected to a fibronectin III (FNIII)-type fold domain as shown in **Figure 2.1**. The N-terminal α-helices of the two subunits interact through hydrophobic interaction whereas β-strands form an antiparallel β-sheet. Both α-helices and β-strands are crucial in dimerizing FIP-fve. The FNIII fold is made up of seven β-strands that are organized into a two β-sheets sandwich, sheet I (strands A, B and E) and sheet II (strands C, C', F and G) that run antiparallel to each other. These strands are linked by loops. The dimerization of the two monomers is stabilized through three different interactions within the homodimer: (i) hydrophobic interaction between two α-helices (H_A and H_B, residues 2 to 14) in N-terminal (ii) hydrogen bonding interaction between two β-sheets (S_A and S_B, residues 14 to 19) and (iii) hydrogen bonding and ordered water molecule interactions between N-terminal α-helices and FNIII domain of the opposite monomers. All of these

three interactions are responsible in strengthening the dimeric interaction state between the two subunits (Paaventhan *et al.*, 2003). Hereby, a more holistic assessment on the structural elements of FIP-fve are described in the following **Sections (2.1.2.1 - 2.1.2.5)**. The secondary structures in each subunit of FIP-fve are arranged and organized to support each other while having its own role.

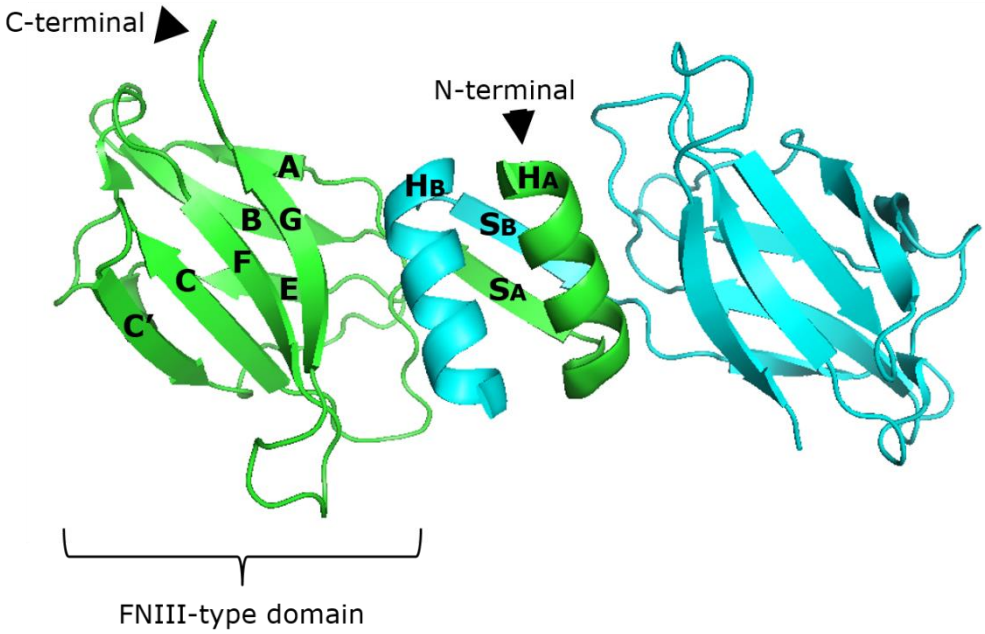


Figure 2.1. Overall crystal structure of FIP-fve that is deposited in Protein Data Bank as 1OSY. Each subunit of FIP-fve comprises of an N-terminal α-helix and β-strand that is connected to a FNIII-type fold domain. FNIII-type domain comprised of a sandwich of two sheets, I and II, which is formed by β-strands E-B-A and G-F-C-C' respectively. The two monomers in the homodimer of FIP-fve are called molecule A and molecule B. The N-terminal α-helices are labelled as H_A and H_B; β-strands are labelled as S_A and S_B; and FNIII-type domain β-sheets are labelled as A, B, C, C', E, F and G according to the chronological sequence of β-strands that are linked from N-terminal β-strand (S_A) (Paaventhan *et al.*, 2003).

2.1.2.1 Importance of N-terminal dimerization

The two α-helices of FIP-fve are suggested to dimerize via three-dimensional (3D) domain swapping mechanism as shown in **Figure 2.2** (Bennett, Schlunegger and Eisenberg, 1995; Liu and Eisenberg, 2002; Paaventhan *et al.*, 2003). The segments of N-terminal α-helices (H_A and H_B) in FIP-fve homodimer appear to swap, which allow them to interact with their complementary regions in another subunits (Paaventhan *et al*., 2003). This swapping mechanism is common in proteins that are identical in forming oligomeric proteins from monomers (Bennett, Schlunegger and Eisenberg, 1995). Beside FIP-fve and LZ-8, FIP-gts was also predicted to exist as homodimer in nature where α-helix is formed from residues 1-13 (Lin *et al*., 1997). It was discovered that recombinant mutant with deletion, FIP-gtsΔ1-13 and FIP-gtsΔLeu5/Phe7/Leu9 failed to dimerize, leading to loss of immunomodulatory function (Lin *et al*., 1997). Therefore, it is proposed that the N-terminal α-helices are responsible for FIPs dimeric structure, which are crucial and necessary for the functional role of FIPs in immune regulating activities (Lin *et al*., 1997; Paaventhan *et al*., 2003).

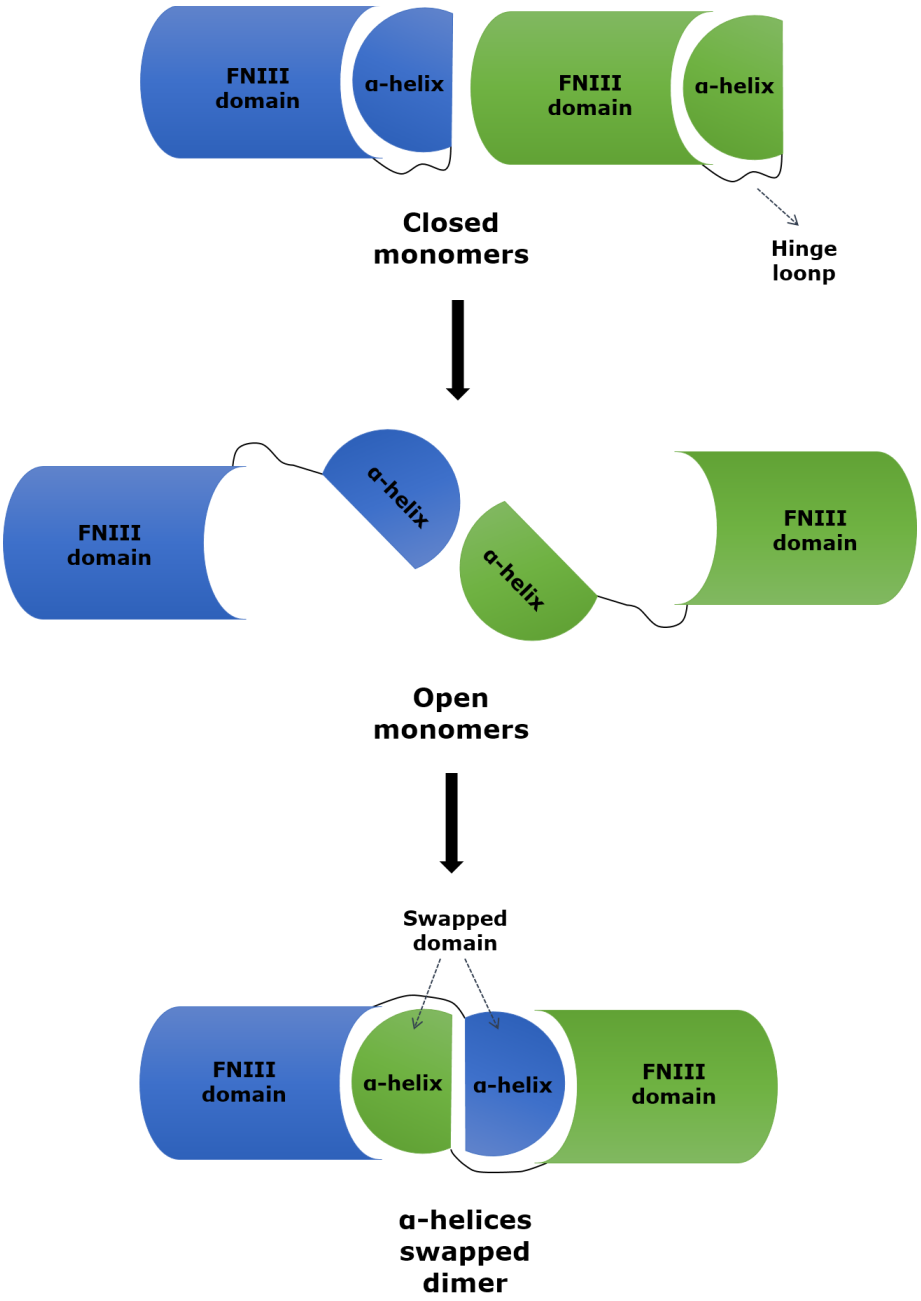


Figure 2.2. Schematic diagram illustrating 3D domain swapping in FIP-fve as modified according to research groups of Bennett (1995) and Liu and Eisenberg (2002).

2.1.2.2 Importance of FNIII fold

The β-sandwich arrangement in FIP-fve was found to be most alike to domains with FNIII-type fold (Paaventhan *et al.*, 2003), which is found commonly in proteins related to binding and signaling functions in cell (Cota and Clarke, 2000). In fact, the FNIII-type fold is topologically highly similar to one of the most generally known complex folds in proteins called immunoglobulin (Ig) fold. One apparent difference between these two folds is the presence of conserved disulfide bond in Ig fold, whereas FNIII-type fold lacks of the disulfide bond (Kessel and Ben-Tal, 2018). It is however important to note that although FIP-fve has FNIII-type fold, it does not bear significant sequence homology to other Ig-like fold proteins. For this reason, it is assumed that these domains are not evolutionarily related. It is suggested that amino acid chemistry in FNIII-type fold FIP-fve and Ig-like fold proteins might favor particular structural packing and arrangement that give rise to their structural resemblance. Nonetheless, FIP-fve does share one important feature with other Ig-like domains whereby both of them similarly possess hydrophobic cores. In the hydrophobic core of FIP-fve, hydrophobic residues that are situated in the central strands (B, C, E and F) of β-sandwich exhibit less than 10% relative surface exposure. The hydrophobic residues in the central strands are listed as followed: Ile33, Leu36, Phe38 and Val51 in B strand; Tyr47, Tyr49 and Val52 in C strand; Gly71, Gly72 and Ile74 in E strand; and Ile91, Val93 and Val95 in F strand (Paaventhan *et al.*, 2003). The stacking of β-sheets in β-sandwich arrangement leads to packing of hydrophobic residues in the protein core. This allows the side chains of stacking sheets to interact with each other, leading to stabilization of the protein core. Essentially, the stable protein core serves as a solid and reliable scaffold for functional sites (Kessel and Ben-Tal, 2018).

2.1.2.3 Importance of loop

IgG is viewed as an important reference in the aspect of discovery of immune-regulating function of FIP-fve as the structural biology of IgG has been studied extensively. The three dimensional structure of IgG was deposited in PDB at PDB ID: 1igt. IgG is composed of four polypeptide chains, two short chains and two large chains, which are referred as light and heavy chains respectively as shown in **Figure 2.3**. All the polypeptide chains are arranged into β-sandwich form and connected sequentially by linkers, which are assembled into a shape of letter Y structure. The "stem" of the Y-shaped IgG is made up of constant region from heavy chain (C_H), which is almost indistinguishable in all antibodies, whereas the "arm" consisting of hypervariable regions from light chain (V_L) and heavy chain (V_H), which are distinct among the antibodies. Hypervariable region indicates variation of amino acid in a certain region. Hence, the hypervariable region in the "arm" of the antibody is the one that contributes and determines the unique antigen-binding sites. Specifically, the binding site is built from two Ig folds, one contributed by hypervariable region of heavy chain, and the other provided by the hypervariable region of light chain. Each Ig fold is built from nine β-strands and three loops. The six loops in the arm of the antibodies (three loops from each chain) are responsible in determining the antigen binding specificity instead of the β-strands. This phenomenon could be explained by the nature of the loops as they are highly flexible and lack an ordered structure, which could therefore tolerate high degree of sequence variability in the antigen binding site and adapt the resulting structural changes (Kessel and Ben-Tal, 2018). The capability of loops in undergoing conformational changes spontaneously allows the antibody to bind to different antigens (James and Tawfik, 2003).

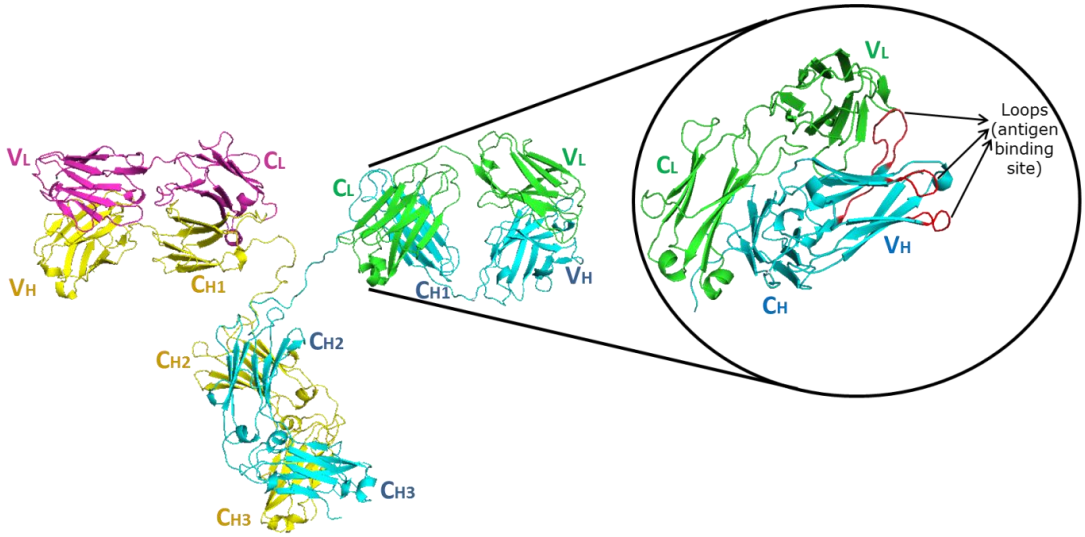


Figure 2.3. Three dimensional structure of immunoglobulin G is adopted from PDB ID: 1igt. The constant-light (C_L), constant-heavy (C_H), variable-light (V_L) and variable-heavy (V_H) domains are denoted in the diagram. Loops for antigen-binding site are highlighted in red colour.

Given the same underlying logic, the importance of loops in FIPs was first suggested by Huang and collegues (2009). Based on the comparative structural analysis, it was initially revealed that large conformational changes occurred at two loops regions (loop DE and FG) in FIP-fve and LZ-8, while the rest of the regions aligned well to each other as shown in **Figure 2.4a.** Both of the loops are exposed at the surface like IgG. In comparison to LZ-8, the α-carbons of loop DE in FIP-fve are positioned differently, leading to changed orientation of side chains in this segment; whereas, the loop FG in FIP-fve is longer and extended to another direction. As shown in **Figure 2.4b**, loop DE region consists of five different residues, whereas loop FG region contains difference of two gaps and one residue (Huang *et al.*, 2009). Subsequently, the 3D protein structure of FIP-ppl was built using homology modelling based on published crystal structures of FIP-fve (PDB ID: 1OSY), LZ-8 (PDB ID: 3F3H) and FIP-gmi (PDB ID: 3KCW), and thereafter used to compare to all these three crystal structures. The predicted structure of FIP-ppl superimposed well on the FIP-fve except four regions which are N-terminal alpha-helix,

loop AB, loop DE and loop FG as shown in **Figure 2.4a**. The difference in N-terminal α-helix and loop AB regions of FIP-ppl as compared to known FIPs structure was first reported in FIP-ppl. In comparison, FIP-fve is the only one that confers large difference in loop DE and FG regions to LZ-8, FIP-gmi, and FIP-ppl (Li *et al.*, 2015). In addition to this, it was subsequently shown that the 3D modelled protein structure of FIP-dsq2 also possesses similar loop DE and FG regions to LZ-8, but different to FIP-fve (Li *et al*., 2017). This could possibly serve as the reason of why FIP-fve demonstrated great activity in anti-anaphylaxis, while LZ-8, FIP-gmi, FIP-ppl, and FIP-dsq2 showed strong anti-tumour activities (Li *et al*, 2015;2017). In fact, it has been reported that loops in FNIII-type domain containing protein such as carbohydrate binding domains, cytokine receptors, cell adhesion molecules and cell hormones are frequently involved in specific recognition activity. Furthermore, it was shown that improved binding activity in antibody can be achieved by engineering loops in the hypervariable regions (Koide *et al*., 2002). Besides that, novel binding sites such as Src SH3 domain, tumour necrosis factor-α and estrogen receptor α were successfully generated in human fibronectin 10^{th} type III domain by altering length of loops DE and FG randomly (Koide *et al*., 1998; Karatan *et al*., 2004). Overall, the role of residues in loop regions in FIPs are worth to be investigated to explore the potential in further improvement of bioactivities or introduction of novel medicinal activities.

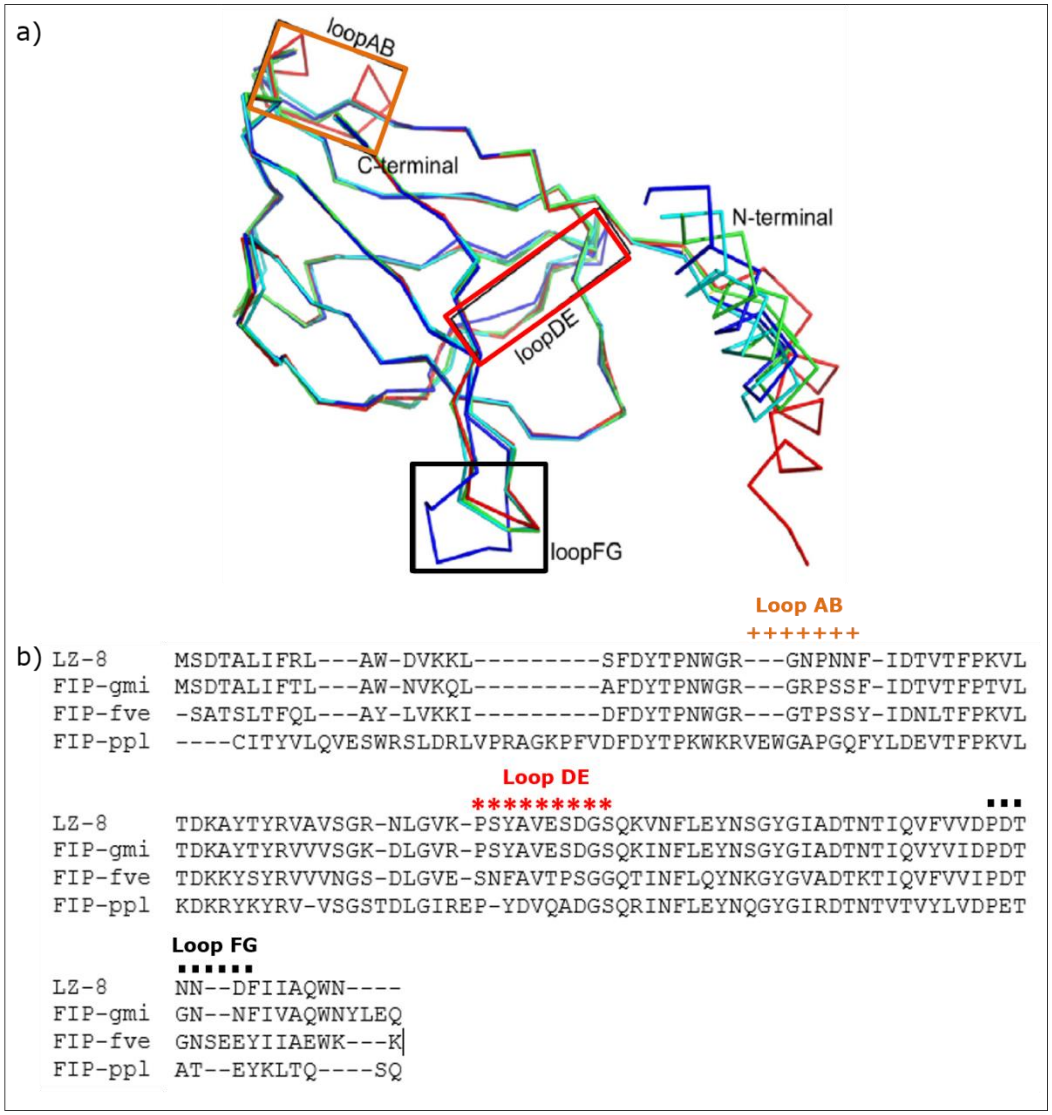


Figure 2.4. (a) Superposition of 3D protein structure of the monomers of FIP-fve (blue), LZ-8 (cyan), FIP-gmi (green) and FIP-ppl (red). The differences in loop AB, DE and FG regions are indicated in orange, red and black boxes respectively. (b) Multiple sequence alignment of FIP-fve, LZ-8, FIP-gmi and FIP-ppl generated using MAFFT multiple sequence alignment software. The amino acid residues involved in loop AB, DE and FG are indicated by symbol plus, asterisks and dots correspondingly at the top of the sequence alignment. Image adopted from Huang *et al.* (2009) and Li *et al.* (2015).

2.1.2.4 Importance of proline

Other than hydrophobic nucleus, four proline residues are found situated in the beginning or end of the β-strands and loops, which are proline 22, 29, 39, 68 and 98. These proline residues are vital to maintain the stability of FNIII-type fold. Particularly, Pro22 seems to convene a vital role in the 3D domain swapping mechanism as it is situated at the end of hinge part, which is simultaneously the start of strand A (**Figure 2.5a**) (Paaventhan *et al*., 2003). Unlike other amino acids, proline is unique as its side chain bends back from alpha carbon to bond to backbone nitrogen covalently, which leads to formation of a static conformation of cyclic pyrolidine ring as shown in **Figure 2.5b**. The presence of cyclic ring secures the phi backbone angle (N-C_α bond) and causes the backbone region to be rigid and inflexible. Therefore, Pro22 may function to consolidate polypeptide main chain and maintain its dynamics, and at the same time allowing arm to elongate while preventing the arm to interact with the core (Bergdoll *et al.*, 1997; Paaventhan *et al.*, 2003).

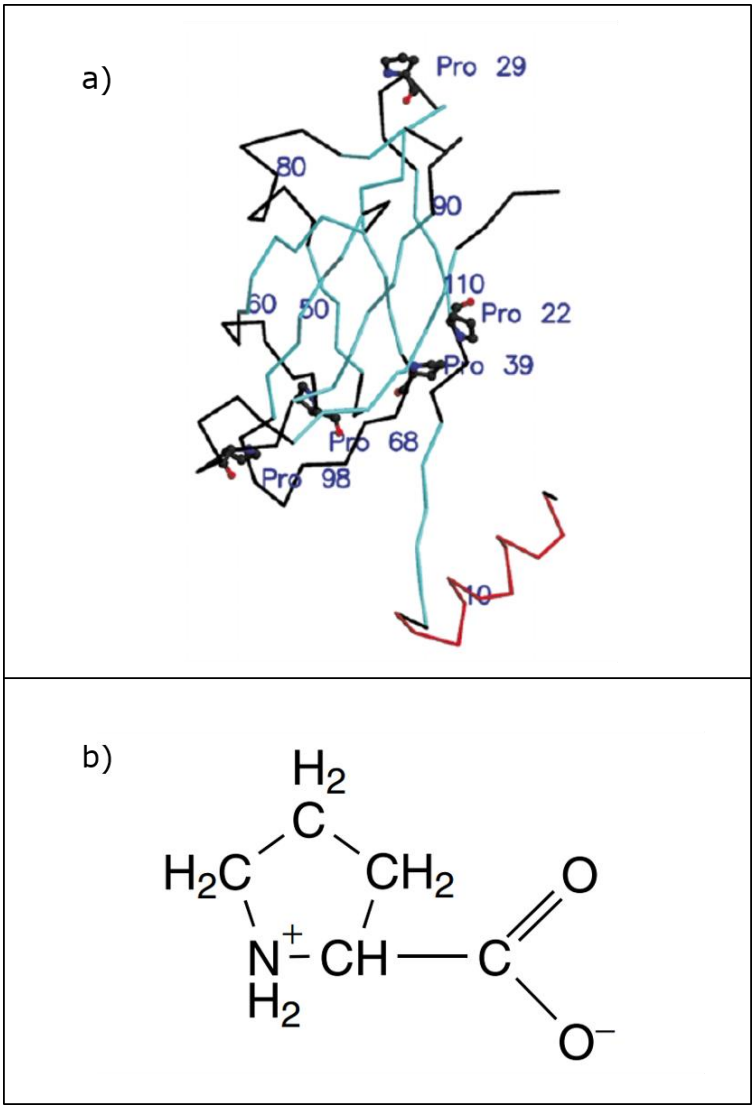


Figure 2.5. (a) The positions of proline residues 22, 29, 39, 68 and 98 are illustrated herein. In particular, Pro 22 that is situated at the initial of strand A appeared to play a critical role in domain swapping mechanism in FIP-fve. Image adopted from Paaventhan *et al.* (2003). (b) The structure of proline consisting of a five-membered pyrrolidine ring that is unique as compared to other 19 amino acids found in protein (Whitford, 2005).

2.1.3 Processing resistance properties

The properties of FIP-fve and LZ-8 in association to their processing resistance to sterilization, heating, freezing and exposure to acid/alkali conditions were reported (Tong *et al.*, 2008). It was found that both of the FIPs were able to retain more than 82% of induced mice splenocytes cell proliferation and interferon-gamma (IFN-γ) secretion abilities as compared to the control when they were treated with freezing (-80˚C, 24 h), boiling (100˚C, 30 min) and autoclaving (121˚C, 15 min). Nonetheless, most of the immune-regulating activities were destroyed when FIP-fve and LZ-8 were exposed to 100˚C treatment for more than 90 min. In addition, FIP-fve and LZ-8 were discovered to be able to sustain more than 98% of their immuno-properties after undergoing acidification of 0.6 M hydrochloric acid (pH 2, 2 hr). On the other hand, FIP-fve and LZ-8 were observed to be more sensitive towards alkali treatment with 5 M sodium hydrate (pH 13, 2 h) as they were only able to maintain about 50 to 70% of its immuno-properties. Besides that, the subjected dehydration treatment has reduced splenocytes cell proliferation abilities of FIP-fve and LZ-8 to 86% and 74% respectively. The treatment has also rendered a great reduction in IFN-γ-induction abilities in both FIP-fve and LZ-8, where they maintained only 54% and 40% of IFN-γ stimulatory activities respectively. Altogether, the study suggested that FIP-fve and LZ-8 have a remarkable tolerance towards freezing, thermal and acidification treatments and an intermediate tolerance to dehydration and alkali treatments (Tong *et al.*, 2008).

2.2 Bioactivities and medicinal activities of FIP-fve

FIP-fve has been demonstrated to exert its anti-inflammatory (Hsieh *et al.*, 2003; Lee *et al*., 2013; Chang *et al*., 2015; and Chu *et al*., 2017) and anti-cancer properties (Ding *et al.*, 2009; Chang *et al.*, 2010) via modulation of host immune system. In fact, FIP-fve is one of the most studied FIPs on its capability in alleviation of allergic reaction. Complementary to its immunoregulatory ability, FIP-fve is also capable of initiating direct inhibition against lung cancer cell growth (Chang *et al.*, 2013). Collectively, FIP-fve is proposed to possess both direct and indirect anti-tumour capabilities. Besides that, FIP-fve also shown haemagglutination activity towards red blood cells, which is one of the signature bioactivities observed in FIPs. With this background, the bioactivities of FIP-fve are presented in this context, specifically focused on its functional activities in haemagglutination, anti-inflammatory and anti-cancer.

2.2.1 Haemagglutination activity

Haemagglutination is a process where an agglutinin is capable of interacting with specific oligosaccharides epitopes on red blood cells (RBCs) and interlinks them, forming a mass of multicellular aggregates (Sharon and Lis, 1989). Different blood group systems express different components of terminal oligosaccharides epitope on cell surface. Owing to unique surface epitope, saccharides-binding compounds can identify and bind to individual blood groups (Adamová, Malinovská and Wimmerová, 2014). Haemagglutination assay is a simple and convenient method that is employed to detect agglutination of RBCs in presence of virus, antigen, antibody or lectin (Li, Wang and Zhou, 2011; Sajid *et al.*, 2012). To perform this method, a suspension of RBC is mixed with a sample and observed with naked eyes or microscope afterward. Whereas positive agglutination results in an interwoven mat of agglutinated RBC, negative agglutination

gives a distinct precipitate of non-agglutinated RBC at bottom of well (Adamová, Malinovská and Wimmerová, 2014) as shown in **Figure 2.6.**

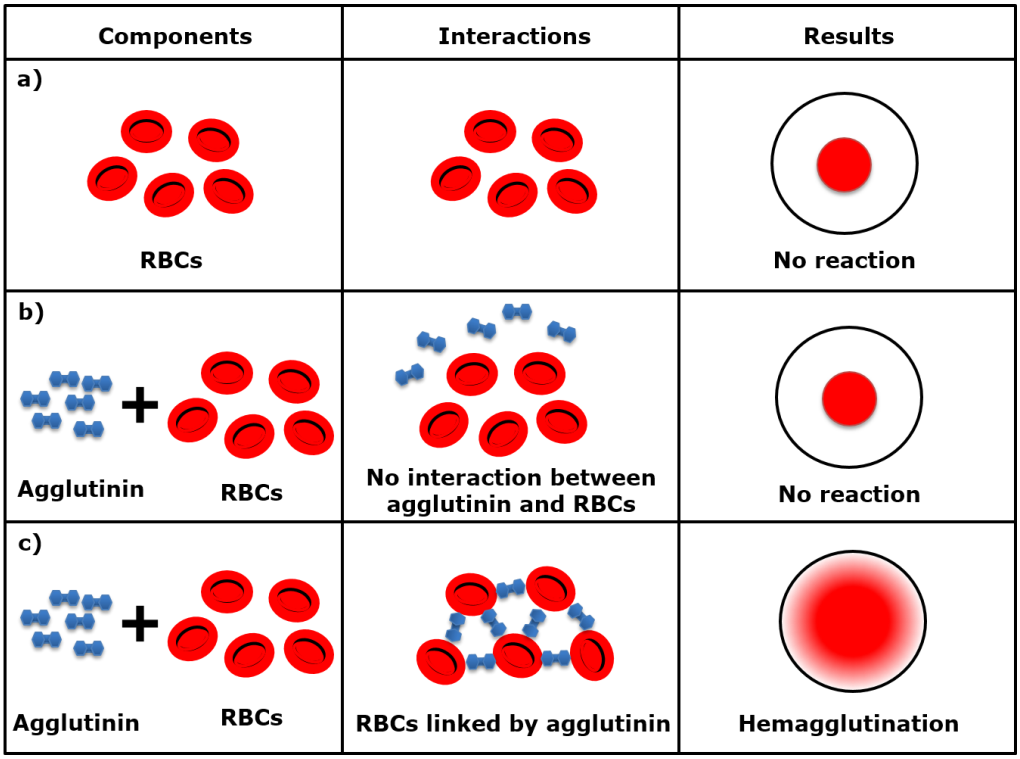


Figure 2.6. Haemagglutination assay. (a) Negative agglutination reaction in absence of agglutinin, and results in RBCs settle in bottom of well. (b) Negative agglutination reaction when agglutinin is unable to bind to epitope on RBCs, and results in RBCs settle in bottom of well. (c) Positive agglutination reaction in presence of interaction between agglutinin and RBCs, and results in RBCs forming a mat in well.

Rather than using the haemagglutination assay for detection of virus or antigen, the assay is used to assess abilities of FIPs in recognizing sugar moieties on RBC surface. As shown in **Table 2.2**, FIPs displayed different specificities toward different types of RBCs. The capability of FIPs in haemagglutination was first observed in LZ-8. LZ-8 successfully induced haemagglutination in sheep RBCs at concentrations larger than 6.25 µg/ml (Kino *et al.*, 1989). However, it failed to agglutinate all four types of human RBCs (A, B, AB and O) when tested with a range of concentrations from 0.03 to 50 µg/ml (Kino *et al.*, 1989). On the other hand, FIP-fve was able to haemagglutinate all four types of

human RBCs (A, B, AB and O) at 2 µg/ml (Ko *et al*., 1995). FIP-vvo showed haemagglutination activities toward RBCs of rats, rabbit and mice at concentrations of 0.52 µg/ml, 0.13 µg/ml and 1.11 µg/ml respectively; yet, haemagglutination activities were not seen when as high as 175 µg/ml of FIP-vvo was applied on all four types of human RBCs (Lin and Chou, 1984). Recombinant FIP-tvc exhibited haemagglutination activities in mouse and rat RBCs at concentrations of more than 4 µg/ml (Li *et al*., 2012). For the newly discovered FIPs, recombinant FIP-ppl showed agglutination activity towards rabbit RBCs at 64 µg/ml, while no agglutination activities were shown toward human RBCs type A, B, AB and O (Li *et al.*, 2015). Recombinant FIP-lrh was demonstrated to agglutinate both human and mice RBCs at 5 µg/ml, with stronger hemagglutination ability shown towards human RBCs (Pushparajah *et al.*, 2016). Recombinant FIP-cru showed hemagglutination activities towards mouse and sheep RBCs at 2 µg/ml, but it was unable to agglutinate human RBCs when the concentration was increased to 16 µg/ml (Lin *et al.*, 2016). The FIPs members possess different haemagglutination activities toward different types of RBC, of which the reason that caused the diversity of sugar moieties binding preferences in FIPs is not clear.

Asides from that, contradictory results were observed in native FIPs and recombinant FIPs that were expressed using different expression systems. Both native FIP-fve and recombinant FIP-fve (produced using *Pichia pastoris* GS115 system) were able to haemagglutinate all four types of human RBCs (A, B, AB and O) at 2 µg/ml (Ko *et al*., 1995; Lin *et al*., 2013). A contradicting result is noted in recombinant FIP-fve that was expressed using *P. pastoris* X-33 system where no agglutination activities were observed towards human, mouse and sheep RBCs; it only agglutinated rabbit RBCs at 5 µg/ml (Bastiaan-Net *et al.*, 2013). Additionally, the conflicting agglutination result was also shown in recombinant LZ-8 that was expressed in *P. pastoris* X-33 as it was able to agglutinate human RBCs (Bastiaan-Net *et al.*, 2013), unlike native LZ-8 that showed no

agglutination activity towards human RBCs (Kino *et al.*, 1989). Similarly, recombinant FIP-nha synthesized respectively using *P. pastoris* X-33 and *E. coli* expression systems displayed variation in the haemagglutination activities as well. For instance, a strong haemagglutination effect was shown towards rabbit RBCs at concentration of 1.275 µg/ml recombinant FIP-nha (expressed in *E. coli*), but it only weakly agglutinated human RBCs even at concentration of more than 100 µg/ml (Li *et al.*, 2014). For recombinant FIP-nha that was expressed in *P. pastoris* X-33, haemagglutination activities was shown toward human, mouse, rabbit and sheep RBCs at minimal concentrations of recombinant FIP-nha at 0.156, 1.25, 2.5 and 5 µg/ml respectively (Bastiaan-Net *et al.*, 2013). These results indicated that the expression systems used to generate recombinant FIPs appeared to affect the RBCs epitope specificities of recombinant FIPs, and therefore the choice of expression system should be taken into consideration in designing protein drugs that is suitable for pharmaceutical use in future.

Table 2.2. Specificities of FIPs on agglutination of different types of red blood cells

FIPs	Protein preparation methods	Red blood cells type				
		Human	**Mice**	**Rat**	**Rabbit**	**Sheep**
LZ-8	Native	No	-	No	No	Yes
	Generated using *P. pastoris* X-33	Yes	-	-	-	-
FIP-fve	Native	Yes	-	-	-	-
	Produced using *P. pastoris* GS115	Yes	-	-	-	-
	Generated using *P. pastoris* X-33	-	-	-	Yes	-
FIP-vvo	Native	Yes	Yes	Yes	Yes	-
FIP-tvc	Synthesized using *E. coli* BL21	No	Yes	Yes	-	-
FIP-cru	Produced using *P. pastoris* GS115	-	Yes	Yes	-	-
FIP-ppl	Generated using *E. coli* Rosetta	No	-	-	Yes	-
FIP-lrh	Produced using *E. coli* BL21	Yes	Yes	-	-	-
FIP-nha	Synthesized using *P. pastoris* X-33	Yes	-	-	Yes	-
	Produced using *E. coli* BL21	Yes	Yes	-	Yes	Yes

(No) indicates no agglutination activity on RBCs
(Yes) indicates agglutination activity is observed on RBCs
(-) indicates no experiments were performed on RBCs type

2.2.2 Anti-inflammatory

In some circumstances, particular kind of innocuous molecule can stimulate a primary adaptive immune response that generates immunological memory. Subsequently, secondary immune response is stimulated when the antigen is re-exposed to the immune system, causing inflammation and tissue damage. These redundant overreactions of immune responses due to harmless environmental antigens are known as allergic reactions or hypersensitivity reactions (Parham, 2015). One of the most prevailing inflammatory chronic diseases is asthma (Type I hypersensitivity reaction) that affects more than 300 million people around the world, especially in developed countries (Pal, Dahal and Pal, 2009; Bosnjak *et al.*, 2011). Some hallmark features of asthma include airway hyperresponsiveness, remodeling of airway, infiltrating cells of lung, enhancement of IgE, metaplasia of goblet cell and increased of cytokines IL-4 and IL-6 (Barrett and Austen, 2009). The current treatments are prescribing patients with drugs including corticosteroids, antihistamines and β-adrenergic bronchodilators that help to ease allergic symptoms; however effectiveness of these drugs vary depending on conditions of allergic patients (Chung *et al.*, 2014).

Several studies were conducted to study the effect of FIP-fve on allergic inflammation in mice. Abilities of FIP-fve in suppressing systemic anaphylaxis and local swelling in footpads of mice were first demonstrated by the research group of Ko (1995). Subsequently, Hsieh and colleagues (2003) demonstrated the potential use of oral administration of FIP-fve in mediating food allergy in mice model that were sensitized using ovalbumin (OVA), a derivative from chicken egg plus Alum to induce an artificial food allergy in mouse model. It was shown that FIP-fve-treated mice were protected from systemic anaphylaxis-like symptoms (Hsieh *et al.*, 2003). The outcome of this study has encouraged and directed more research toward exploring the use of oral-delivered FIP-fve on resolving allergic airway diseases.

Following the initial success, another five studies were conducted to examine effect of oral-administered FIP-fve on mice with induced airway inflammation using allergens such as **OVA** (Lee *et al.*, 2013, 2017), **respiratory syncytial virus (RSV)**, house dust mite (HDM) ***Dermatophagoides microceras*** **(Der m)** (Chang *et al.*, 2015) and HDM ***Dermatophagoides pteronyssinus*** **(Der p)** (Chu *et al.*, 2017). These findings consistently showed that oral-administered FIP-fve was capable of reversing the triggered-inflammation reactions in mice. Indeed, a recent research also showed that oral-adminstered FIP-fve was capable of alleviating chronic allergic airway inflammation in mice model. Moreover, the anti-inflammatory activity of FIP-fve in suppressing chronic asthma in mice appeared to have higher effectivity as compared to corticosteroid, an immunosuppressant drug (Lee *et al.*, 2017). Notably, one of the exceptional features of FIP-fve revealed from these studies was that FIP-fve was capable of skewing and directing immune response towards T helper 1 (T_H1) response, which in turn suppresses allergic airway inflammations that were triggered by T helper 2 (T_H2) cytokines, T helper 17 (T_H17) cytokines or IgE (Lee *et al*., 2013; Chang *et al*., 2014; Chang *et al*., 2015; Chu *et al*., 2017 and Lee *et al*., 2017). Furthermore, FIP-fve was capable of inhibiting RSV infection and the following RSV-stimulated inflammation by reducing RSV replication and interleukin (IL)-6 expression (Chang *et al.*, 2014). RSV is the most prevailing cause of severe acute lower respiratory disease in children, which is normally accompanied with long term complications such as asthma and recurrent wheezing (Swanson *et al.*, 2011).

Specifically, FIP-fve counteracted cardinal features of asthma in allergen-challenged mice in those studies as mentioned above by: (i) reducing airway hyperresponsiveness (AHR) in FVE-treated mice group; (ii) diminishing infiltration of inflammation cells such as eosinophils and neutrophils (iii) enhancing expression of T_H1 and Treg cytokines, including interferon (IFN)-γ, IL-12, transforming growth factor (TGF)-β and IL-10; (iv) decreasing expression of T_H2 cytokines such as IL-4, IL-5 and

IL-13 as well as expression of T_H17 cytokine, IL-17; (v) diminishing expression of IgE; and (vi) reducing inflammation, goblet cell metaplasia and epithelial cell thickness in lung tissue (**Figure 2.7**). Taken together, FIP-fve was shown to possess anti-inflammatory effects on OVA/Der m/Der p-induced airway inflammations in murine models, and the findings have been consistent thus far. Most importantly, it is noteworthy to mention that FIP-fve shown stable activity when it was delivered orally (Lee *et al*., 2013; Chang *et al*., 2014; Chang *et al*., 2015; Chu *et al*., 2017 and Lee *et al*., 2017). This excellent feature of FIP-fve allows convenience in protein drug administration that could helps to increase patient compliance, which makes it a great candidate to be developed for pharmaceutical use.

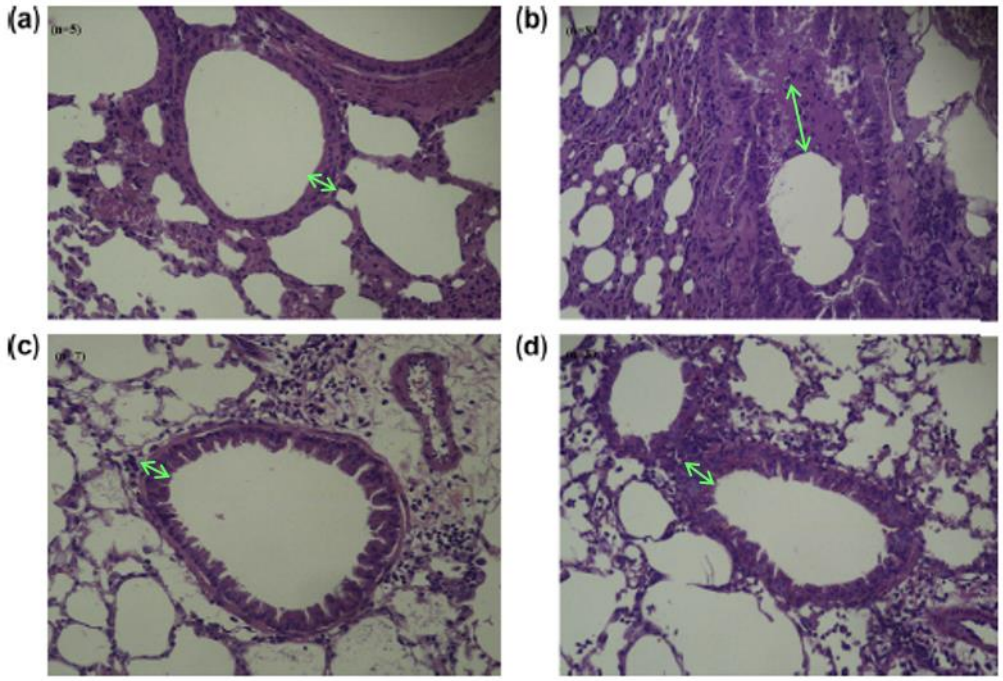


Figure 2.7. Histological staining on lung tissue sections of OVA-sensitized mice that showed effects of FVE treatment on lung inflammation and remodelling. Thickness in smooth muscles of lung were indicated with green arrows. (a) Negative control mice group that was fed with phosphate-buffered saline only. (b) Positive control mice group that was sensitized with OVA. Thickened smooth muscles were observed in lung tissue in this mice group. (c) OVA-sensitized mice group that received pre-treatment of FIP-fve. (d) OVA-sensitized mice group that received post-treatment of FIP-fve. Thickness in smooth muscles of lung were diminished in both pre and post FVE-treated mice. Image adopted from Lee *et al.* (2013).

2.2.3 Anti-cancer

Majority of the studies have been focused on the ability of FIP-fve in alleviating inflammatory responses. There were only three studies that were conducted to investigate on the cancer-inhibitory abilities of FIP-fve based on its direct and indirect inhibition (via immunomodulatory) mechanisms, which are described further in the following sections.

2.2.3.1 Direct inhibition mechanism

The direct anti-cancer effects of FIP-fve were examined *in vitro* on three lung cancer cell lines, A549, CaLu-1 and MRC-5 (Chang *et al.*, 2013). FIP-fve was demonstrated to be more effective in inhibiting proliferation of A549 cells in comparison to CaLu-1 and MRC-5 cells. Out of the three lung cancer cell lines, FIP-fve showed highest reduction of cell viability on A549 cells where it decreased cell viability in a concentration dependent manner from 92.5 to 375 µg/ml. At 375 µg/ml of FIP-fve treatment, cell viability A549 was diminished to 60%. Rather than inducing apoptosis, FIP-fve was demonstrated to reduce cell viability of A549 cells by inducing cell cycle G1 arrest. It was shown that there was an increase of G1 population, but less than 7% apoptotic cells were observed after 48 hr of FIP-fve treatment. The induction of G1 arrest may be a consequence of an increase of expression of main cell cycle arrest signals p21, p27 and p53. Apart from that, FIP-fve was found to be able to suppress migration of A549 cells by disrupting filopodia formation and actin assembly. Several genes that are related to lung cancer such as Rac GTPase-activating protein 1 (RacGAP1), lipocalin 2 (LCN2), matrix metalloproteinase (MMP2), plasminogen activator inhibitor type-1 (PAI-1) and human nonmetastatic clone 23 (NMC23) were also investigated for their mRNA expression after FIP-fve treatment. It was reported that mRNA expression of RacGAP1 was greatly reduced while expression of the other genes maintained after the treatment. In short, FIP-fve was shown to inhibit A549 cell proliferation via p53 activation pathway and to repress the cell migration through reduction of RacGAP expression (Chang *et al.*, 2013).

2.2.3.2 Indirect inhibition mechanism

Case study: Application of FIP-fve as an adjuvant against human papillomavirus cancer in mice

The feasibility of FIP-fve to be utilized as an adjuvant was investigated *in vivo* when it was immunized together with a model antigen, human papillomavirus (HPV)-16 E7 oncoprotein against HPV TC-1 cell lines induced tumour in mice (Ding *et al.*, 2009). HPV type 16 is one of the most prevalent existing genotypes, which caused at least 50% of all cervical cancers (Munoz *et al.*, 2003). Hence, many researches have been targeting HPV-16 E7 for development of vaccines for both prevention and control of HPV infections. Since the use of HPV-16 E7 alone has been shown insufficient to achieve efficient protection against tumour growth, the possibility of FIP-fve to be developed as alternative adjuvant molecule was explored (Ding *et al.*, 2009).

Co-administrations of FIP-fve together with HPV-16 E7 were shown effective in prolonging protection of mice against tumour challenge as well as enhancing survival of mice harbouring tumour (Ding *et al.*, 2009). In immunization test, 60% of mice that were immunized with both HPV-16 E7 and FIP-fve proteins were protected from tumour growth for 167 days after tumour challenge, while only 20% of mice that were immunized with HPV-16 E7 stayed tumour-free at that period. An interesting observation reported was that FIP-fve immunization alone conferred some inhibition effects on tumour growth where tumour size was shown smaller in FIP-fve-immunized mice as compared to control mice. Whereas in mice survival experiment, tumour-bearing mice that received the co-treatment demonstrated prolonged survival up to 120 days, while tumour-harbouring mice groups that were treated with HPV-16 E7, FIP-fve and phosphate-buffered saline (PBS) alone were unable to survive beyond 55 days. Altogether, FIP-fve was shown capable of: (i) enhancing immunization efficiency of an antigen-specific immune response and (ii) prolonging survival of immunized tumour-bearing mice (Ding *et al.*, 2009).

Further examination into mechanisms that underlied the tumour-protective enhancement by co-immunization of HPV-16 E7 and FIP-fve explained that the co-treatment led to boosting of both T_H1-directed humoral and cell-mediated specific immune responses as well as enhancement on phenotypic maturation of dendritic cells (DCs). It was demonstrated that production of HPV-16 E7-specific IgG1, IgG2c and IFN-γ were enhanced significantly in HPV-16 E7 and FIP-fve co-treated mice group. Additionally, the importance of T cells in anti-tumour mechanism induced by HPV-16 E7 and FIP-fve was highlighted in the research as well, which was illustrated using T cells adoptive experiment. In comparison to HPV-16 E7 treatment alone, tumour size was effectively suppressed when T cells from the co-treated mice was adoptively transferred into recipient mice that harboured tumour. It was suggested that the enhanced tumour inhibition efficacy might be due to either increased avidity of HPV-16 E7-specific T-cell or increased number of HPV-16 E7-specific effector T cells that were initiated by the co-administration. While both $CD4^+$ and $CD8^+$ subsets were crucial for antitumour immunity generated by the co-treatment of HPV-16 E7 and FIP-fve, it was demonstrated that $CD8^+$ subset played a principal role in tumour inhibition effect. Apart from that, FIP-fve was shown to be capable of modifying DCs ability by selectively induce phenotypic maturation of certain DCs, leading to preferential enhancement of OVA-specific $CD8^+$ T-cell immune response. It was shown that the co-culture of OVA/FVE-induced DCs greatly enhanced the generation of IFN-γ and IL-2 in $CD8^+$ T cells as compared to control mice group. Interestingly, this enhancement extent of cytokine production was not seen in co-culture of OVA/FVE-induced DCs and $CD4^+$ T cells, implying that the effect was specific to $CD8^+$ T cells. Hence, the results suggested that FIP-fve was capable of modifying capability of DCs by directing stimulation of specific DCs phenotypic maturation and preferentially enhance OVA-specific $CD8^+$ T-cell immune responses (Ding *et al.*, 2009).

On the whole, FIP-fve was demonstrated to possess great potential to be developed as an effective adjuvant for not only on HPV chimeric vaccines, but more of its capabilities could be explored on other anticancer vaccines as well. This is the first *in vivo* study that showed the possible mechanism of how FVE regulated and strengthen tumour-specific immune responses.

Case study: Oral-administered FIP-fve against hepatic cancer in mice

Another *in vivo* study on anti-tumour effect of FIP-fve was conducted by oral-delivered FIP-fve against hepatic cancer in mice (Chang *et al*. 2010). Oral treatment of FIP-fve has shown reduction in tumour development of hepatoma-bearing mice in relation to control mice group as well as prolonging survival duration of hepatoma-habouring mice via modulation of host immune response.

Several mechanisms were shown to be involved in anti-tumour activity of FIP-fve against hepatoma-bearing mice. Firstly, FIP-fve treatment was shown to enhance tumoricidal ability of peritoneal macrophages and splenocytes. The harvested peritoneal macrophages (belong to innate immunity) and splenocytes (belong to adaptive immunity) from hepatoma-bearing mice (FVE-administered) were used as effector cells against murine BNL 1MEA.7R.1 hepatoma cell line. As expected, the tumoricidal activities of both of the effector cells were markedly stronger in FIP-fve-administered mice group as compared to control group. In this regard, FIP-fve was suggested to be capable of strengthening both innate and adaptive immunity of the host (Chang *et al*. 2010). Secondly, FIP-fve also contributed to anti-tumour immunity by enhancing antigen-presenting ability of antigen-presenting cells (APCs) via upregulation of expression of major histocompatibility complex (MHC) class I, MHC class II and CD80 costimulatory molecules on APCs (Chang *et al*. 2010). Activation of T cell relies on recognition of antigenic peptides that is linked to MHC molecules expressed on APCs surface. Therefore, the enhancement in the expression of these molecules are critical to ensure priming of a

strong tumour-inhibiting effect in the host. Efficient antigen presentation and T-cells activation have been known to be responsible in dictating success of cancer immunotherapy (Abbas, Lichtman and Pillai, 2015). Thirdly, oral treatment of FIP-fve was shown to be able to inhibit pre-existing hepatic cancer cell proliferation and angiogenesis in mice. In comparison to control mice group, FIP-fve-treated hepatoma-bearing mice have demonstrated a great reduction in number of hepatic cancer cell as well as a remarkable reduction in amount of tumour blood vessel (Chang *et al*. 2010). Similarly, the abilities of FIP-fve in reducing cell viability and interrupting cell migration in A549 cells have been previously reported by Chang *et al*. (2013), indicating that the *in vitro* result was consistent with the *in vivo* findings.

It is also important to highlight that cytokine IFN-γ was found to contribute mainly to the efficient tumour-inhibiting mechanism of FIP-fve in hepatoma-harbouring mice. One of the examples was that neutralization of IFN-γ in FVE oral administered-hepatoma bearing mice has significantly reduced the cytotoxic activities of peritoneal macrophages and splenocytes. Hence, it is suggested that IFN-γ plays a crucial part in FIP-fve-mediated anti-tumour mechanism (Chang *et al*. 2010). In brief, oral administered-FVE showed enhanced anti-tumour immunity in hepatic-bearing mice by activating both innate and adaptive immunity of the hosts via enhancement in tumoricidal abilities of peritoneal macrophages and splenocytes as well as reinforcement in antigen-presenting ability of DCs, and all of which led to priming of an efficient immune response against hepatic cancer cells. FIP-fve was also capable of inhibiting cancer cell proliferation and angiogenesis in mice (Chang *et al*. 2010).

2.3 Mechanism of action of FIP-fve

Although it is known that FIP-fve exercises its immunostimulatory function through stimulation of IFN-γ production and secretion in human peripheral blood mononuclear cells (hPMBCs), the knowledge on site of interaction as well as mechanism of action of FIP-fve is limited. Likewise, understanding on mechanism of action of FIP-fve in exerting its anti-cancer activities is poor as well. Till date, only one study has examined the structural and functional relationship of FIP-fve in relation to its immunomodulation function. It was discovered that a carbohydrate-binding module (CBM)-34 in C-terminal region of FIP-fve is critical for establishing an interaction between FIP-fve and receptor-like glycoprotein on hPBMCs surface, and the contact of which is necessary for immunomodulatory functions of FIP-fve (Liu *et al.*, 2012). CBM is generally small and separated from catalytic domains of hydrolytic enzyme. The main function of CBMs is to act as a supporting role for its relative catalytic modules by (i) maintaining a proximity distance between enzyme and substrate, (ii) targeting distinct region in polysaccharides and subsequently influence ability of catalytic enzymes and (iii) disrupting polysaccharides structure (Boraston *et al.*, 2004).

Bioinformatics tool revealed that FNIII-type domain in FIP-fve protein is topologically similar to domain N in *Thermoactinomyces vulgaris* R-47 α-amylase I (TVAI) gene (PDB ID: 1UH4) as shown in **Figure 2.8a** (Liu *et al.*, 2012). Interaction between CBM-34 residues of both N domain of TVA I α-amylase and FNIII-type domain of FIP-fve and granule form starch molecule is shown in **Figure 2.8b**. Based on the analysis, it was revealed that FNIII-type domain of FIP-fve exhibits high similarity to N domain of TVA I α-amylase in term of number of key residues and architecture that are involved in the interaction. Indeed, several key residues (Ile43, Thr44, Trp65, Trp77, Asp75 and Asn 65) in surface cleft of CBM-34 of TVA1 are found conserved in FIP-fve (Ile91, Thr90, Trp111, Trp24, Asp34, and Thr28) (Liu *et al.*, 2012). The proposed key

residues of FIPs that are involved in CBM-34 are indicated with asterisk (*) as shown in **Figure 2.9**. Other than Thr28 in FIP-fve, multiple sequence alignment of the FIPs member showed that these key residues are also highly conserved among all discovered FIPs. To be specific, Trp24 and Asp34 are identical and conserved in all FIPs; Ile91 and Trp111 are conserved in all FIPs except FIP-ppl and; Thr90 is conserved in all FIPs except FIP-dsq2, FIP-lrh and FIP-tvc.

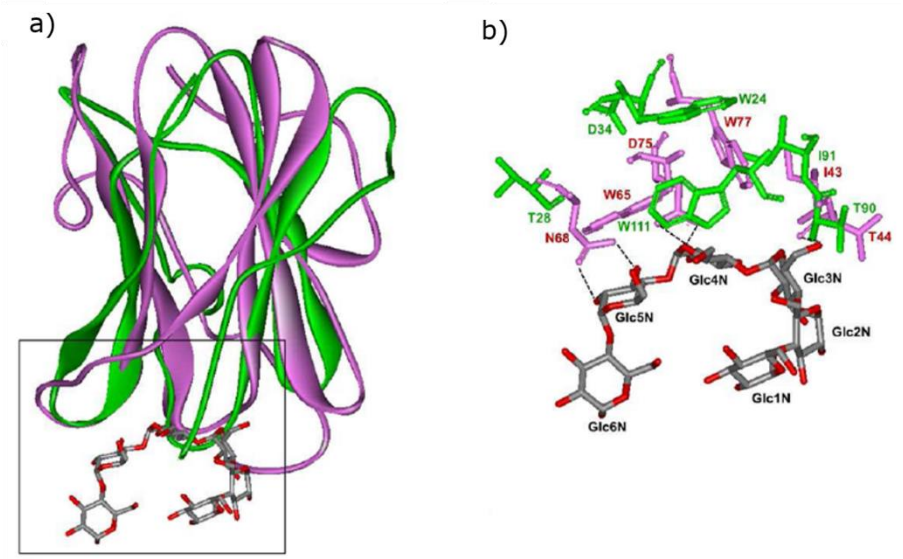


Figure 2.8. (a) Schematic diagram of structural comparison on Ig-like structure between FIP-fve and domain N of *T. vulgaris* R-47 α-amylase I. FIP-fve and domain N of *T. vulgaris* R-47 α-amylase I are represent in respective green and purple molecules. (b) The box illustrated interaction between CBM-34 of both α-amylase I and FIP-fve and granule starch. Hydrogen bonds involved in the interaction are indicated with dotted lines. Image adopted from Liu *et al*. (2012).

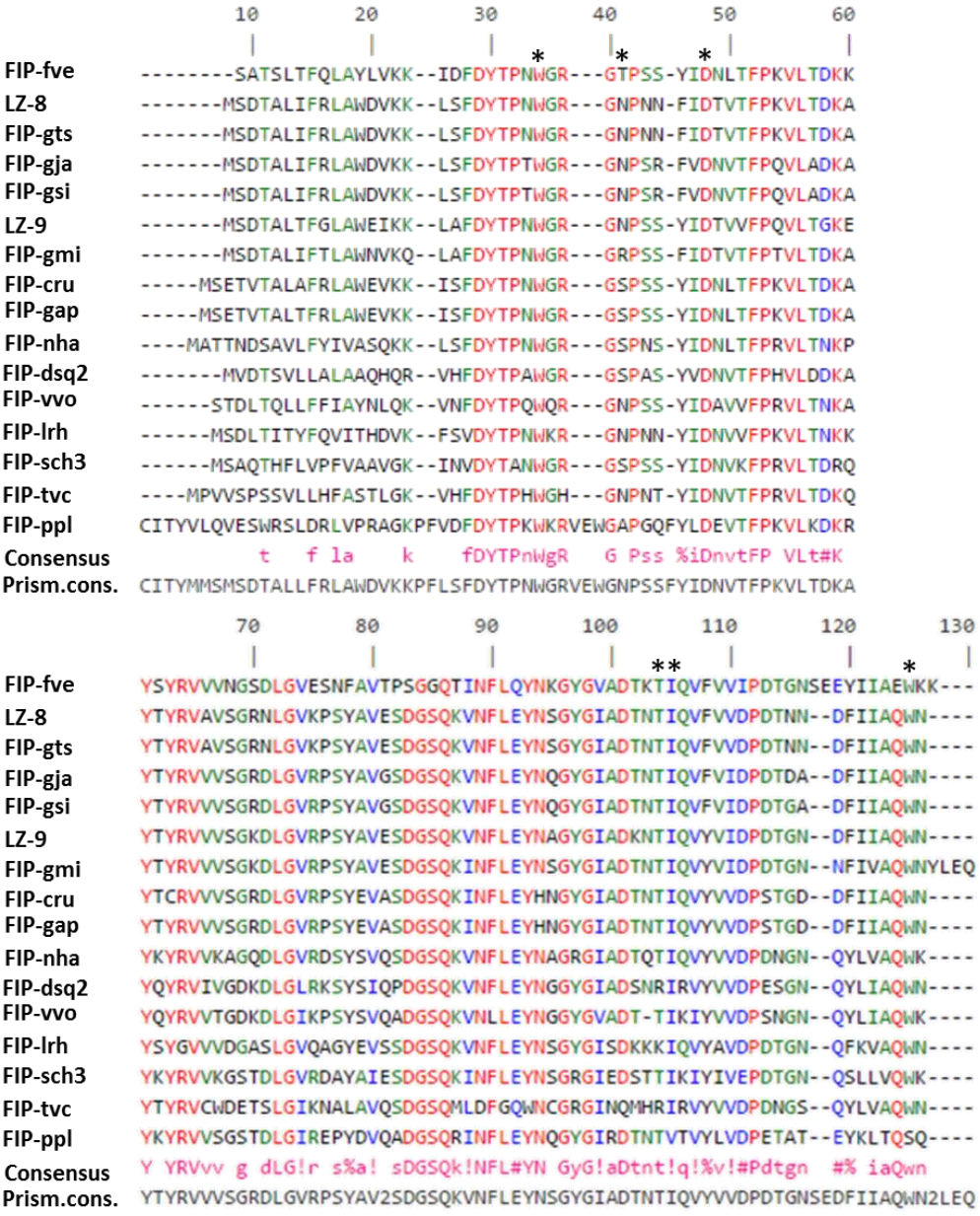


Figure 2.9. Multiple sequence alignment of FIP-fve, LZ-8, FIP-gts, FIP-gja, FIP-gsi, LZ-9, FIP-gmi, FIP-cru, FIP-gap, FIP-nha, FIP-dsq2, FIP-vvo, FIP-lrh, FIP-sch3, FIP-tvc and FIP-ppl were calculated using program MULTALIN. The key residues that are involved in CBM-34 are indicated by asterisks.

.

To verify if putative CBM-34 is responsible in glycoproteins binding on hPBMCs, α-amylase and β-amylase were used in ligand competitive assay. α-amylase and β-amylase represent non-catalytic and enzymatic activity domains respectively. It was shown that the non-catalytic domain on α-amylase instead of enzymatic activity domain on β-amylase was responsible in competing with FIP-fve, resulting in the reduced immunomodulatory ability. In other words, a similar CBM structure such as TVAI α-amylase can compete with FIP-fve that possesses CBM-34, with substrate binding ability relative to its immunomodulatory activity (Liu *et al.*, 2012).

The importance of these six putative key residues in CBM of FIP-fve were examined using site-directed mutagenesis. Results demonstrated that the key residues Trp24, Asp34, Ile91, and Trp111 in CBM-34 domain are critical for immunomodulatory activity of FIP-fve as substitution of these residues has caused little or no production of IFN-γ in hPMBCs (Liu *et al*., 2012). Substitution of Thr90 resulted in approximately 64% reduction of IFN-γ expression in hPBMCs, indicating that even though Thr90 is less crucial as compared to Trp24, Asp34, Ile91 and Trp111 in generation of IFN-γ, it is undeniably that Thr90 was also an important residue for carbohydrate-binding capability in FIP-fve. In contrast, there was no apparent effect in IFN-γ production when Thr28 was substituted with Asn that is conserved in FIPs such as LZ-8, FIP-gts, FIP-gja, FIP-gsi, LZ-9, FIP-vvo, FIP-lrh and FIP-tvc; therefore it appeared that Thr28 is not responsible for carbohydrate-binding ability in FIP-fve.

CBM-34 domain in C-terminal region of FIP-fve was identified as a type B CBM based on substrate specificity test. In substrate specificity test, a range of substrate-binding competitor was supplemented with FIP-fve to induce IFN-γ production in hPBMCs, and the amount of generated IFN-γ was measured. It is suggested that FIP-fve belongs to "glycan-chain binding" CBM, an extended ligand-binding site groove, which is able to accommodate distinctive sugar units of a stretch of glucose residues. FIP-fve has shown

strong binding to a wide range of substrate from monosaccharide N-acetylneuraminic acid (sialic acid) to oligosaccharides dextrin, maltotriose and cyclodextrin, and a moderate binding to water-soluble polysaccharides starch and disaccharide maltose. The result of substrate binding competition therefore concluded that FIP-fve favors complex polysaccharides to mono or divalent ligands, which is one of the features of avidity effect (Liu *et al*., 2012).

Apart from that, the immunomodulatory ability of FIP-fve was shown to be dependent on interaction between FIP-fve and membrane receptors on hPBMCs. It was found that cell surface glycans that are N- and/or O-linked to membrane receptors were crucial for FIP-fve binding in which the binding was necessary for IFN-γ induction in hPBMCs. **Figure 2.10** illustrated a summary of the proposed mechanism of FIP-fve on IFN-γ regulation in hPBMCs (Liu *et al*., 2012). In spite of the fact that CBM is necessary for immunomodulatory activity of FIP-fve, it is believed that the distinctive activities of FIP members are determined by other regions within the proteins as most of the FIPs member have conserved the same key residues in CBM. In short, CBM-34 in C-terminal region of FIP-fve is critical for establishment of an interaction between FIP-fve and receptor-like glycoprotein on hPBMCs surface, and the contact of which is necessary for immunomodulatory functions of FIP-fve (Liu *et al*., 2012).

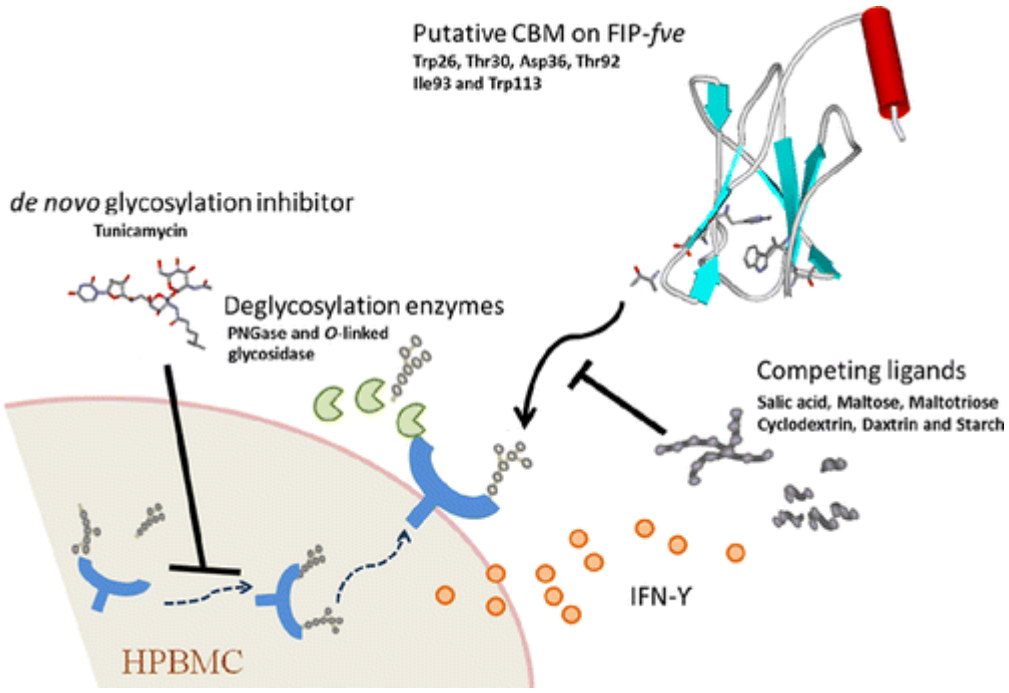


Figure 2.10. Proposed site of mechanism of FIP-fve-modulated IFN-γ secretion. The immunomodulatory activities were abolished when key residues Trp26, Thr30, Asp36, Thr92, Ile93 and Trp113 were substituted. FIP-fve has been shown to favor complex polysaccharides to mono or divalent ligands. The generation of IFN-γ was also inhibited when glycosylation mechanism was disrupted using de novo glycosylation inhibitor and deglycosylation enzymes. Image adopted from Liu *et al*. (2012).

2.4 Molecular biology research of recombinant FIP-fve protein

Since limited yield of FIP-fve protein was obtained when it was harvested directly from *Flammulina velutipes*, several research groups have worked on improving yield of FIP-fve using genetic engineering technique in order to obtain sufficient FIP-fve protein for research use. It was reported that 400 g of fruiting bodies yielded only about 35 mg of purified FIP-fve (Ko *et al*., 1995). Recombinant FIP-fve proteins have been successfully synthesized using prokaryotic and eukaryotic systems (Ko *et al.*, 1997; Wu *et al.*, 2008, 2013; Lin *et al.*, 2013), the methodology and findings of which are described further in **Sections 2.4.1 – 2.4.3**.

2.4.1 Bacterial production system

The first recombinant FIP-fve protein was expressed by Ko and colleagues (1997) using *Escherichia coli* strain TG1 with expression vector pGEX-2T harbouring FIP-fve and glutathione S-transferase (GST). The yield of purified recombinant fusion protein was 5 mg/L (Ko *et al.*, 1997). GST was fused at N-terminal of FIP-fve, and it was abbreviated as GST:FIP-fve. It was reported that the generated recombinant proteins was bioactive but it retained only 50% of lymphocyte stimulatory activity as compared to native FIP-fve (Ko *et al.*, 1997). Apart from that, another group of researcher also synthesized recombinant FIP-fve protein in *E. coli* strain BL21 (DE3) using expression vector pET30a-FIP-fve. The FIP-fve was produced in fusion protein with N-terminal hexahistidine (6xHis) tag, and was abbreviated as 6xHis:FIP-fve. The yield of purified recombinant fusion protein 6xHis:FIP-fve was approximately 29.1 mg/L. Immunomodulatory activity of generated 6xhis-FIP-fve was examined *in vivo* where it was shown that serum level of IL-2 and IFN-γ was significantly higher in FVE-treated mice group in comparison to control mice group, indicating that the generated 6xhis-FIP-fve was bioactive (Kong *et al.*, 2013).

2.4.2 Baculovirus/insect cell expression system

Other than bacterial system, FIP-fve was also produced using baculovirus/insect Sf21 cell expression system. A recombinant plasmid pAc$P_{10}SP_{bbx}$FVE was generated using vector pAcUW21 with bombyxin signal peptide and 6x-his tag fused at N and C-terminal of FIP-fve respectively, which was later utilised for generation of recombinant baculovirus vAc$P_{10}SP_{bbx}$FVE. The recombinant FIP-fve was expressed as a glycosylated protein and secreted into culture medium of vAc$P_{10}SP_{bbx}$FVE-infected cells (Wu *et al.*, 2008). In fact, it was subsequently reported that there are two N-glycosylation sites in FIP-fve, which are "Asn-Leu-Thr" and "Asn-Gly-Ser" (Bastiaan-Net *et al.*, 2013). The yield of purified recombinant FIP-fve was 6.25 mg/L.

In order to compare immune-regulating activities of recombinant FIP-fve proteins that were synthesized using different systems, recombinant GST:FIP-fve protein was produced in *E. coli* BL21 (DE3) cells as well to be used as a comparison to recombinant FIP-fve protein expressed by insect cell system. It is important to note that the GST:FIP-fve protein was first subjected to thrombin protease cleavage to release FIP-fve from GST prior to immunomodulatory activity test. It was demonstrated that 10 ug/ml of purified recombinant FIP-fve from insect and bacterial cells stimulated 503 and 165 pg/ml of IL-2 respectively. This indicates that recombinant FIP-fve expressed using insect cells exhibited stronger immunomodulatory activity as compared to recombinant FIP-fve produced using bacterial cells (Wu *et al.*, 2008). Nonetheless, it is thought that the difference in their immunomodulatory activities should not be attributed fully to the different expression systems as the difference in activities could be due to several factors as followed: (i) glycosylation site of recombinant FIP-fve may be crucial in improving its immune-regulating activity; (ii) proteins synthesized using insect cells are processed, folded and modified in a similar manner to native FIP-fve; or (iii) steric hindrance of protein structure due to inserted affinity tag. It is also noteworthy to mention that although

GST was removed from recombinant FIP-fve, there was possibility that the protein structure of FIP-fve had already perturbed. According to prior literature, N-terminal α-helices in FIP-fve homodimer are important for dimerization whereby the two α-helices are stabilized through hydrophobic interaction. The two α-helices are embedded inwards as the core centre of the two monomers (Paaventhan *et al.*, 2003). Therefore, it is postulated fusion of large fusion tag at N-terminal of FIP-fve might introduce steric hindrance to the protein structure, leading to reduced immunomodulatory activity in recombinant FIP-fve. Taking this into account, it is worthwhile to consider choice of fusion tag site in future study as little attention has been devoted to the impact of N- or C-terminal site choice for fusion tag in the generation of recombinant FIP-fve protein.

2.4.3 Yeast cell expression system

Apart from the two expression systems, recombinant FIP-fve was also expressed using yeast strain *P. pastoris* (GS115) using expression vector pPIC9-FIPfve. Similar to baculovirus/insect cell expression system, extraction process of recombinant FIP-fve protein expressed in *P. pastoris* is simpler as the protein is secreted extracellularly. The yield of purified recombinant FIP-fve protein from *P. pastoris* was 258.2 mg/L, which was much higher as compared to recombinant FIP-fve protein expression level produced in bacteria and insect cells. Interestingly, recombinant FIP-fve protein was expressed in three different molecular masses at approximately 14, 17 and 20 kDa, indicating that the proteins may be modified in different levels by *P. pastoris* (Lin *et al*., 2013). In fact, another study by Bastiaan-Net and colleagues (2013) also generated recombinant FIP-fve protein using *P. Pastoris* system; similarly, recombinant FIP-fve protein was also synthesized in three different molecular masses. Glycosylation staining revealed that the two out of the three determined molecular mass proteins were glycosylated recombinant FIP-fve protein (Lin *et al*., 2013). It is not known if glycosylation modification of recombinant FIP-fve would affect its bioactivities, and therefore it warrants further study

to investigate on the effect of such modifications. The immunomodulatory activity of recombinant FIP-fve protein (generated using *P. pastoris* system) was similar to native FIP-fve when they were compared based on the expression level of induced-IL-2 and -IFN-γ. For example, 10 μg/mL of both recombinant and native FIP-fve enhanced expression level of IL-2 in mice splenocytes to 503 and 509 pg/ml respectively, whereas 5 μg/mL of recombinant and native FIP-fve enhanced expression level of IFN-γ in splenocytes to 509 and 522 pg/ml respectively (Lin *et al*., 2013). Future study on synthesis of recombinant FIP-fve should take into consideration of some of the important aspects discussed above, which are effects of glycosylation and site of affinity tag.

2.5 Overview of human immune system

A general overview of the immune system is included herein so that the ability of FIP-fve protein in modulating the immune response and tackling cancer cells can be related. Immunological research demonstrated that immune responses can be induced against tumours that normally do not provoke an immune response (Parham, 2009). Human immunity system is made up of both innate immune response (non-specific) and adaptive immune response (specific). There are many connections between innate and adaptive immune systems. The response of innate immunity towards microbes initiates adaptive immunity and directs the nature of adaptive immune response. In turn, adaptive immunity enhances the combating mechanisms of innate immunity, enabling them to be more capable of eliminating pathogenic microbes (Abbas, Lichtman and Pillai, 2015). Most infections are stopped by innate immunity; when they fail, the innate immune response works to slow the spread of infection while adaptive immune response takes place to increase the focus of immune response. When successful, it clears the infection and provides long-lasting immunity that prevents its recurrence (Parham, 2009).

2.5.1 Innate (non-specific) immunity

Innate immunity is pre-existing defence mechanism that is designed to mount an immediate defence against the infectious agent (Wood, 2006). There are three major components in innate immunity that includes (i) physical and chemical barriers such as epithelia and antimicrobial chemicals produced at epithelia surface; (ii) dendritic cells, natural killer (NK) cells and phagocytic cells (macrophages, neutrophils); (iii) blood proteins such as mediators of inflammation and complement system. The physical and chemical barriers such as skin and mucosa exclude more than 99.9% of infectious organisms human are exposed to. However, when physical and chemical barriers fail, the physiologic barriers take place by elevating temperature, increasing pH acidity in stomach

and producing various soluble factors (Kindt *et al*., 2007). Hence, inflammatory response is executed to recruit macrophages, neutrophils and other factors from the bloodstream into tissues to aid the removal of pathogens and death cells via phagocytosis. Phagocytosis is the ingestion and destruction of microbes by macrophages and neutrophils (Abbas, Lichtman and Pillai, 2015).

2.5.2 Adaptive immunity

The adaptive immunity is brought into play only after the innate immune response has failed to eradicate the invading pathogen (Abbas, Lichtman and Pillai, 2015). There are two types of adaptive immune responses, which are humoral immunity and cell-mediated immunity. Humoral immunity is the main defense mechanism against extracellular microbes and their toxins. B lymphocytes (also known as B cells) are the principal cells that mediate humoral immunity, secreting antibodies to eliminate microbes by recognizing antigens and neutralizing microbe infectivity. On the other hand, cell-mediated immunity is mediated by T lymphocytes (also known as T cells). Intracellular microbes such as virus and bacteria may infect and proliferate inside phagocytes and other host cells, where they are inaccessible to circulating antibodies. Therefore, cell-mediated immunity is responsible in defending such intracellular infections by killing the infected cells. B and T lymphocytes use entirely different strategies of pathogen recognition where they recognize pathogen by using cell-surface receptors namely B-cell and T-cell receptors respectively. The adaptive immune system executes several benefits to immunological defences. One of the advantages is that a strong immune response can be precisely targeted against a particular pathogen by recognizing the specific pathogen from another. Additionally, some of the pathogen-specific B and T lymphocytes that proliferate during a first infection are retained long as memory cells after the infection has been terminated, which enables subsequent infections by the same pathogen to be terminated promptly (Parham, 2009). In this context, T lymphocytes will be focused particularly.

2.5.2.1 T lymphocytes

T lymphocyte originates in the bone marrow and reaches its maturity only when it migrates to thymus. The mature T lymphocytes then leave the thymus and circulate through the bloodstream and lymphoid tissue (Wood, 2006). The initial activation of naive T lymphocytes occurs mainly in secondary lymphoid organs, through which these cells normally circulate and where they may encounter antigens presented by mature dendritic cells. There are two major types of T lymphocytes, helper cells and cytotoxic cells, which are distinguished phenotypically by the expression of membrane glycoproteins $CD4^+$ and $CD8^+$ respectively. Both $CD4^+$ and $CD8^+$ T cells use T cell receptor (TcR) with different variable regions for recognising antigen. $CD4^+$ T cell recognizes antigen that is associated with major histocompatibility complex (MHC) class II molecules on the surface of dendritic cells (Wood, 2006). The activated $CD4^+$ T cell then play an important role in activating B cells, cytotoxic T cells, macrophages via production of various cytokines. $CD8^+$ T cell is cytotoxic in which its main function is to kill cells that have become infected with virus or some other intracellular pathogens (Parham, 2009).

2.5.2.2 Activation of T lymphocytes

The proliferation of T lymphocytes and their differentiation into effector and memory cells require antigen recognition, costimulation and cytokines (Abbas, Lichtman and Pillai, 2015). The first signal that is required for T cell activation is antigen recognition, which ensures that the antigen-specificity of the subsequent immune response. Dendritic cells play a critical role in initiating naive T cell via presentation of antigenic peptide as dendritic cells are strategically situated at the common sites of foreign antigens and in tissues that may be colonized by microbes. Additionally, molecules such as MHC-peptide complex and costimulatory molecules are highly expressed by mature dendritic cells, which are crucial for naive T lymphocytes induction (Abbas, Lichtman and Pillai, 2015).

As shown in **Figure 2.11**, activated APCs express costimulatory molecules B7-1 (CD80) and B7-2 (CD86) on its surface, which bind to T cell surface receptor CD28. The costimulators are expressed only on APCs when necessary (Abbas, Lichtman and Pillai, 2015). The resting APCs have a very low expression of costimulators. In fact, numerous stimuli such as microbial products that engage TLR and cytokine such as IFN-γ generated in innate immunity enhance the expression of costimulators. Besides that, costimulator CD40 ligand (CD40L) is induced on the activated T lymphocyte, which interacts with CD40 on APCs; the engagement leads to a further enhancement of B7 molecules expression, resulting in an increase antigen-presenting ability of APCs (Abbas, Lichtman and Pillai, 2015).

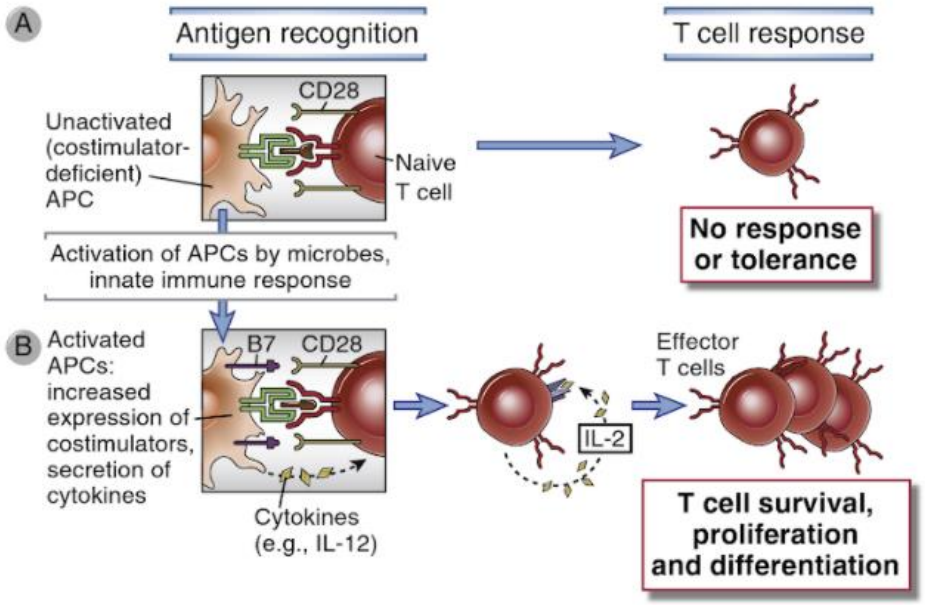


Figure 2.11. T lymphocyte activation. (A) The resting APC without costimulators is unable to activate naive T lymphocytes, leading to tolerance response from T lymphocyte. (B) B7 molecule is expressed by activated APC, increasing its antigen-presenting capability. APCs can be activated by microbes encountered or cytokines generated during innate immune response. Cytokine IL-12 that is produced by activated APC induces differentiation of naive T cell into effector T cell. Image adopted from Abbas, Lichtman and Pillai (2015).

A combination of antigen recognition together with costimulatory molecules initiates several responses in T lymphocyte such as (i) cytokine secretion, mainly interleukin-2; (ii) proliferation that results in clonal expansion, an increase of numbers of cells in the antigen-specific clones; and (iii) naive cells differentiation into effector and memory lymphocytes. Hereby, T cell-derived cytokine, interleukin-2 is presented as it is greatly involved in T lymphocyte activation (Abbas, Lichtman and Pillai, 2015).

Interleukin-2

Interleukin-2 (IL-2) is a growth, survival, and differentiation factor for T lymphocytes (Abbas, Lichtman and Pillai, 2015). IL-2 is secreted by $CD4^+$ T cell early once it is activated by antigen and costimulator molecule. Besides its biologic action in regulating survival, proliferation and differentiation of T lymphocytes, IL-2 also involves in the control of immune response. The biological action of IL-2 is summarized in **Figure 2.12**. IL-2 promotes survival of cells by inducing anti-apoptotic protein Bcl-2. It stimulates cell cycle progression through synthesis of cyclins and by relieving a block in cell cycle progression through degradation of cell inhibitor p27. In addition, IL-2 increases production of effector cytokines such as IFN-γ and IL-2. IL-2 serves as an autocrine growth factor in T cell proliferation whereby the antigen-induced cells that synthesize IL-2 also preferentially respond to it, assuring that the antigen-specific T lymphocytes are the one that proliferate the most. The consequence of T cell proliferation is a clonal expansion of cells from a small pool of antigen-specific T cells, which produces an immense amount of cells necessary to eradicate foreign antigen or microbes. Other than that, IL-2 is also necessary in controlling immune response by modulating the survival and function of regulatory T cells, which is important to suppress immune responses against self and other foreign antigens. IL-2 is the sole cytokine that is responsible in maintaining functional regulatory T cells (Abbas, Lichtman and Pillai, 2015).

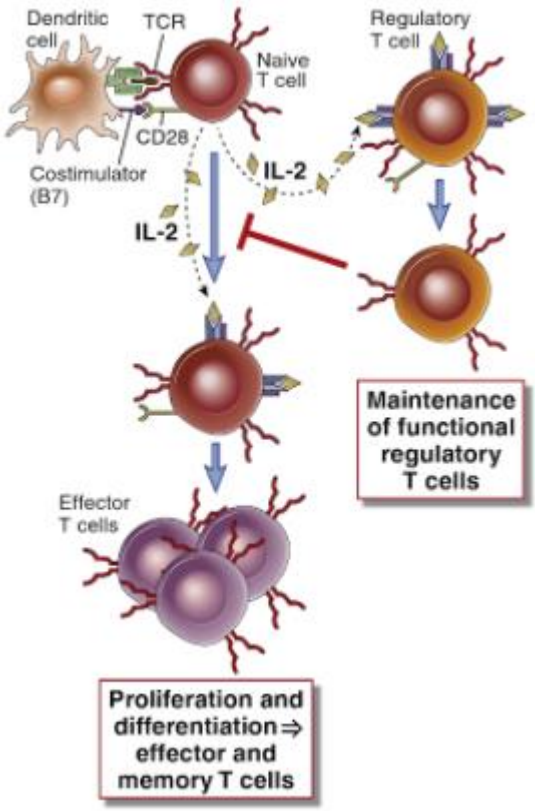


Figure 2.12. The biological action of IL-2 is summarized in the diagram. Two major roles of IL-2 include (i) stimulation of survival, proliferation and differentiation of T cells; and (ii) controlling immune response by maintaining functional regulatory T cells. Image adopted from Abbas, Lichtman and Pillai (2015).

2.5.2.3 Major histocompatibility complex molecules and antigen presentation to T lymphocytes

MHC molecules are expressed on host cell surface (Abbas, Lichtman and Pillai, 2015). They are responsible for presenting antigen that is derived from host cell during antigen recognition by T cell receptor on $CD4^+$ and $CD8^+$ T cells. MHC class I molecules are expressed in all nucleated cells, while MHC class II molecules are presented only in dendritic cells, phagocytes, B lymphocytes, and endothelial cells. In fact, the pattern of MHC molecule expressions are associated to the roles of MHC class I-restricted and class II-restricted T cells. $CD4^+$ helper T cells are restricted to bind class II MHC-associated peptides, whereas $CD8^+$ T cells are restricted to recognize class I MHC-bound peptides (Abbas, Lichtman and Pillai, 2015).

In MHC class I antigen presentation, the internal cytosolic protein antigens are processed via class I MHC pathway for generation of class I-linked peptides and subsequently recognized by $CD8^+$ T cells. Majority of the cytosolic foreign proteins are synthesized by viruses, bacteria or other intracellular microbes that infect the host cells. Protein antigens may also be generated by the mutated or overexpressed genes in tumour cells. Besides that, microbes and other particulate antigens may be phagocytosed and transported from vesicle to cytosol, which are later subjected to MHC class I pathway via cross presentation mechanism. In MHC Class II pathway, specialized APCs capture protein antigens from extracellular environment, internalized into endosome, and process via class II pathway to be presented to $CD4^+$ T cells. The nature of T cell responses based on the presentation of class I or class II MHC pathways allow the immune response to effectively guide $CD4^+$ and $CD8^+$ T cell subsets in respond to infection. Class I MHC-restricted $CD8^+$ T cells come into play to eradicate the cells that endogenously synthesized antigens; in contrary, class II MHC-restricted $CD4^+$ T cells act on eliminating extracellular microbes by recognizing the internalized antigens that are processed into class II-binding antigens by APCs (Abbas, Lichtman and Pillai, 2015).

2.5.3 $CD4^+$ effector T cells

There are three major subsets of $CD4^+$ effector T cells, which are T_H1, T_H2 and T_H17 cells (Abbas, Lichtman and Pillai, 2015). Each of the $CD4^+$ effector T cells has a distinct role in host defence against various types of infectious pathogens, which are described further in **Sections 2.5.3.1 and 2.5.3.2**. $CD4^+$ effector T cells are differentiated from naive $CD4^+$ T cells in response to cytokines that are produced by APCs such as DCs, macrophages, NK cells, mast cells or basophils that are present in lymphoid organs where the immune response is initiated. The characterization of the $CD4^+$ effector cells is based on the signature cytokines they generate as shown in **Figure 2.13** (Abbas, Lichtman and Pillai, 2015).

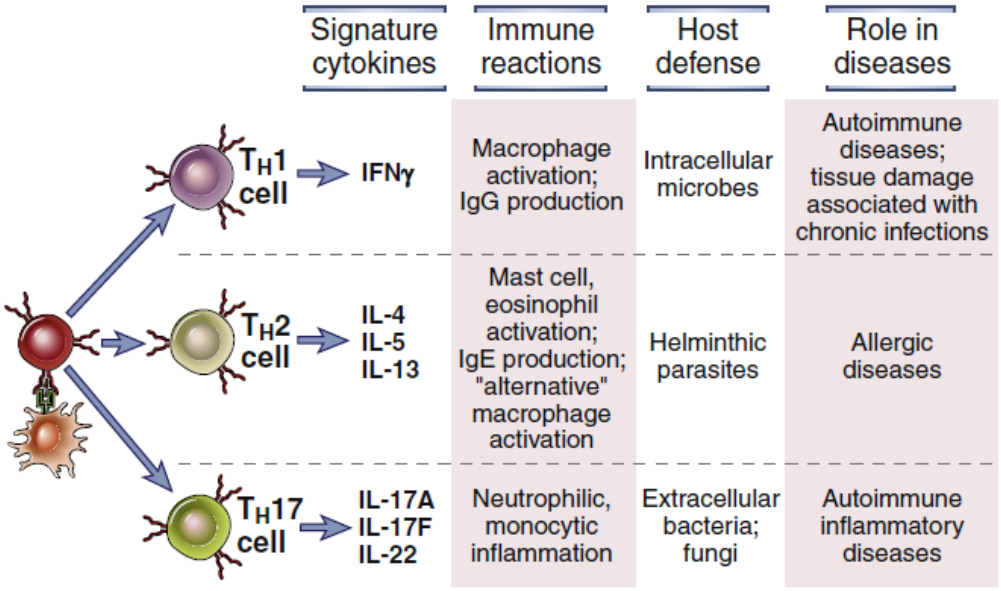


Figure 2.13. Characteristics of T_H1, T_H2 and T_H17 subsets of $CD4^+$ T cells. The signature cytokines, immune reactions, host defence and role in diseases of each of these subsets are listed correspondingly. Image adopted from Abbas, Lichtman and Pillai (2015).

2.5.3.1 T_H1 subsets

T_H1 subset is the principal mediator of cell-mediated immunity as well as phagocyte-mediated host defence (Abbas, Lichtman and Pillai, 2015). T_H1 subset differentiation is induced in response to intracellular microbes that activate dendritic cells, macrophages and NK cells, leading to differentiation of antigen-induced $CD4^+$ T cells to T_H1 effectors cells. The generation of cytokines IL-12 and IFN-γ are mainly responsible in directing and promoting the T_H1 cells development of antigen-activated $CD4^+$ T cells (Abbas, Lichtman and Pillai, 2015).

Interferon-γ

IFN-γ is the major macrophage-activating cytokine and plays critical functions in immunity against intracellular microbes (Abbas, Lichtman and Pillai, 2015). IFN-γ is also called immune or type II interferon. IFN-γ is produced by $CD4^+$ T cells, $CD8^+$ T cells and NK cells. There are four main functions of IFN-γ. Firstly, IFN-γ induces classical macrophage activation that leads to enhanced phagocytosis and microbial killing activity

in macrophages. The macrophage activation relies on two signals, which are expression of CD40L on T_H1 cell surface and secretion of IFN-γ by T_H1 cells. The CD40L and IFN-γ are induced when T_H1 cells are stimulated by antigens. Both of the signals synergize and work together for macrophage activation. The activated macrophage responds to the stimuli, leading to enhanced immune response both directly and indirectly. Its direct mechanism includes killing of phagocytosed microbes via production of reactive oxygen species, nitric oxides and lysosomal enzymes. Its indirect mechanism includes secretion of IL-12 cytokines that stimulate T_H1 cells differentiation into effector cells; and inflammatory cytokines such as TNF, IL-1, and chemokines that recruit more leukocytes to enhance immune response of host. Additionally, initiated macrophages also increased its surface expression of class II MHC molecules and B7 costimulators, enhancing its ability as antigen-presenting cells and resulting in intensification of cell-mediated immunity (Abbas, Lichtman and Pillai, 2015).

Secondly, IFN-γ is involved in stimulation of IgG subclasses switching in B lymphocytes as well as inhibiting of switching to IL-4-dependent isotypes such as IgE. It was found that IFN-γ especially promotes subclasses switching to IgG2a or IgG2c in the study of mice. Moreover, the produced IgG antibodies as a result of IFN-γ induction enhance phagocyte-mediated elimination of microbes through (i) binding to Fc receptors on phagocytes and initiating complement and (ii) opsonizing microbes for phagocytosis (Abbas, Lichtman and Pillai, 2015).

Thirdly, IFN-γ plays a crucial role in the differentiation of $CD4^+$ T cells to the T_H1 subset and inhibits the development of T_H2 and T_H17 cells, promoting the polarization of the immune response in one direction. The developed T_H1 cells secrete IFN-γ that promotes more T_H1 differentiation, which amplifies the cell-mediated immune reaction (Abbas, Lichtman and Pillai, 2015).

Fourthly, IFN-γ enhances MHC-related antigen presentation and intensification of T cell-dependent immune reactions by inducing expression of various proteins that contribute to the beneficial effect. For example, the expression of MHC molecules, B7 costimulators on APC and HLA-DM are elevated, contributing to enhanced T-cell dependent immunity (Abbas, Lichtman and Pillai, 2015).

2.5.3.2 T_H2 subset

T_H2 subset is the regulator of phagocyte-independent defence whereby eosinophils and mast cells are largely involved in the immunity reaction, which functions to eradicate helminthic infections and to eliminate microbes in mucosal tissues (Abbas, Lichtman and Pillai, 2015). Other than that, T_H2 subset also contributes to the development of allergic diseases. The fact that common human parasites have been eradicated from the developed countries has indirectly turned the effector mechanism of IgE to harmless protein antigens that are derived from common animals or plants as IgE has lost its natural substrate (Parham, 2015). Out of the three signature cytokines in T_H2 subset (IL-4, IL-5 and IL-13), cytokine IL-4 plays a major role in T_H2-mediated immunity. IL-4 induces antibody IgE-, mast cell- and eosinophil-mediated reactions to eradicate helminthic infection or to induce allergic reaction (Abbas, Lichtman and Pillai, 2015).

IL-4

IL-4 functions as both inducer and effector cytokine in T_H2 subset. The stimulation of T_H2 differentiation relies on cytokine IL-4 that occurs when the $CD4^+$ naive T cell encounters helminths or allergens (Abbas, Lichtman and Pillai, 2015). Nonetheless, it is unknown the origin of IL-4 that first leads to the T_H2 differentiation. It is suggested that small amount of IL-4 is secreted from antigen-stimulated $CD4^+$ T cells; and when the trigger reaction is persistent, a high concentration of IL-4 is gradually accumulated that resulted in increasing differentiation of naive T cells to T_H2 subset. The developed T_H2

generates more IL-4, which serves to amplify the reaction and inhibit the development of T_H1 and T_H17 cells (Abbas, Lichtman and Pillai, 2015).

IL-4 also induces B cell Ig heavy chain switching to IgE isotype. IgE is pivotal to the T_H2 arm of adaptive immunity that is committed to defend the human body against helminth worms and other parasitic multicellular animals (Abbas, Lichtman and Pillai, 2015). These parasites pose two challenges to the human body as they are naturally less antigenic and bigger size as compared to other pathogens; therefore they are not readily phagocytosed by neutrophils or macrophages. To eliminate these parasites from human body, CD4 T_H2 cell induces the production of IgE, leading to coordinated mast cell degranulation that results in massive inflammatory responses such as increased mucus secretion, sneezing, coughing, vomiting and diarrhea. These violence mechanisms dislodge embedded parasites from tissues and eject them from human body (Parham, 2015).

Furthermore, IL-4 also contributes to elimination of surface microbes by working together with IL-13 to initiate peristalsis in gastrointestinal. IL-13 also enhances secretion of mucus from airway and gut epithelial cells. IL-4 and IL-13 also stimulate the recruitment of leukocytes, especially eosinophils. (Abbas, Lichtman and Pillai, 2015).

2.5.4 $CD8^+$ effector T cells

The viruses are unable to be destroyed when they invade cytosol as they are inaccessible to extracellular killing mechanisms (Abbas, Lichtman and Pillai, 2015). Therefore, the immunity system has evolved to eliminate the viruses in the cells by killing the infected cells, restricting ability of virus to survive and replicate in the cells. In adaptive immunity, $CD8^+$ cytotoxic T lymphocytes (CTLs) orchestrate in the killing of virus-infected cells and eradication of tumour. CTLs also produce IFN-γ, the signature cytokine of T_H1 subsets (Abbas, Lichtman and Pillai, 2015).

The activation of naive $CD8^+$ T cells is dependent on a specific pathway of antigen presentation in a specialized subset of dendritic cells and may also require the help from $CD4^+$ T cell (Abbas, Lichtman and Pillai, 2015). Similar to other naive T cells, dendritic cells are the best APCs to initiate the activation of naive $CD8^+$ T cells. Nonetheless, the viruses are not consolidated to infect only the DCs as they might infect many other cell types. Additionally, antigens of tumours that are derived from cells other than DCs may occur as well. The mechanism nature of class I MHC antigen presentation pathway requires antigen to be present in cytosol of infected cells so that the antigen can be processed and presented via MHC class I pathway. Therefore, cross-presentation pathway is utilised under this circumstances where specialized dendritic cells are involved in the process by ingesting infected cells, tumor cells or protein expressed by these cells, transferring the protein antigens into the cytosol, and processing the antigens to enter the class I MHC antigen presentation pathway for recognition by $CD8^+$ T cells (Abbas, Lichtman and Pillai, 2015). The cross-presentation pathway is shown in **Figure 2.14**.

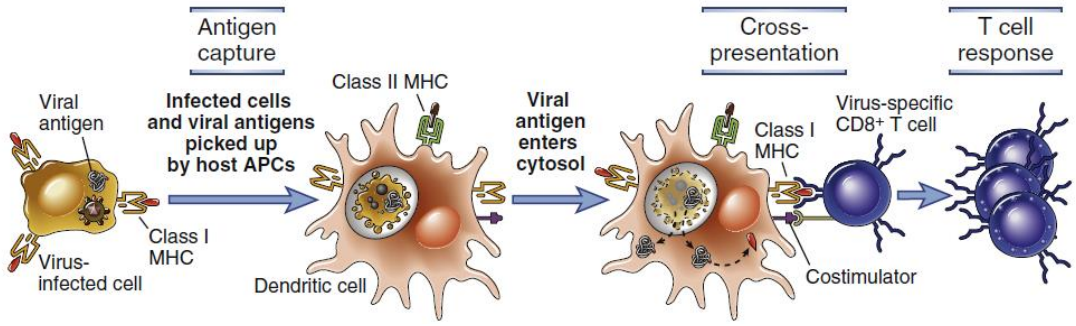


Figure 2.14. Cross-presentation pathway of antigens to $CD8^+$ T cells. Dendritic cell ingests infected microbes and processed via MHC class I pathway, generating class I MHC-antigen complex that is able to activate $CD8^+$ T cells. Image adopted from Abbas, Lichtman and Pillai (2015).

Chapter 3 Construction of FIP-fve and Mutant Gene Cassettes and Corresponding Recombinant Expression Vectors

3.1 Introduction

Mutagenesis of protein is crucial for understanding of the structural-functional relationship of a protein (Ling and Robinson, 1997). The structural and functional roles of amino acid residues in a protein of interest can be examined by comparing the mutant proteins harbouring alteration in amino acid residues to wild type protein. Before the advancing in mutagenesis technology, the means of obtaining a mutant were either selecting a naturally occurring mutant or inducing mutations using mutagenic agents; generally, both of which methods are unable to create a specific mutation that is desired and generate a randomly distribution of mutations, therefore the selection process of desired mutants is tedious and time-consuming. Site-directed mutagenesis (SDM) has revolutionized the methods of obtaining the desired mutants. Specific residues can be substituted, removed, or added precisely by using SDM approach. The technique has been applied in protein functional study and protein engineering, which includes creation of a protein with improved stabilization, introduction of novel catalytic activities and humanization of antibodies (Ling and Robinson, 1997).

Chapter 3 describes the upstream gene construction approaches utilised to generate recombinant FIP-fve and mutants proteins using SDM in conjunction with *Escherichia coli* recombinant protein production system. Construction of recombinant vectors harbouring gene of FIP-fve (*FIP-fve*) and genes of its derivatives that lead to subsequent production of functional recombinant proteins was the ultimate aim in **Chapter 3**. Strategies used in obtaining *FIP-fve* cDNA template; designing SDM of *FIP-fve* derivatives; designing and generating gene cassettes; and construction of recombinant vector are presented herein.

In efforts to produce recombinant FIP-fve and derivatives proteins, this study was initiated by obtaining *FIP-fve* cDNA template. Since enokitake mushroom is readily available in supermarket, the method of direct total RNA isolation from *Flammulina velutipes* and subsequent generation of *FIP-fve* cDNA was utilized. Therefore, this technique is considered simple given that the source of cDNA template is conveniently accessible.

Based on the hypotheses as discussed in **Chapter 1**, mutagenesis was conducted by targeting on the three main aspects. Firstly, N-terminal methionine residue that was highly conserved in FIPs family was inserted at the N-terminal of FIP-fve. Secondly, Ala2 (hydrophobicity index: 41) was substituted with Leu (hydrophobicity index: 97) that has a higher hydrophobicity index based on the amino acid hydrophobicity index (**Appendix A3.1**) to enhance N-terminal dimerization of FIP-fve. Ala2 is the amino acid residue with the least hydrophobicity among the residues that are situated on the hydrophobic face of the helix in FIP-fve. There are another two residues that have higher hydrophobicity index than Leu, which are Phe and Ile. However, Leu was chosen as the residue for Ala2 replacement because Phe is the hydrophobic residue with aromatic side chain, while Ile is the hydrophobic residue with larger side chain than Leu whereby the side chains of these two residues may interfere the binding interaction between the two helices. Thirdly, loop DE and FG regions of FIP-fve were substituted with the loop DE and FG regions of LZ-8. The functional effects of single adoption of each of the loops as well as both of the loops were explored. Additionally, it is postulated that the distinctive putative hinge residues (for loop DE and FG) in FIP-fve and LZ-8 might be crucial in positioning the loops. Thus, the putative hinge residues were also included as complements to the mutation of loop regions to determine the effect of adoption of both loop and putative hinge residues in protein functional activities.

In connection therewith, eight derivatives of *FIP-fve* were synthesized using SDM in which the modifications were performed on several regions of FIP-fve as shown in **Figure 3.1** by: (a) adopting methionine residue [*CWT-1*]; (b) enhancing N-terminal dimerization [*CWT-2*]; (c) adopting loop DE region from LZ-8 [*CWT-3*]; (d) adopting loop FG region from LZ-8 [*CWT-4*]; (e) adopting both loop DE and FG regions from LZ-8 [*CWT-5*]; (f) adopting loop DE region and putative hinge residue (for loop DE) from LZ-8 [*CWT-6*]; (g) adopting loop FG region and putative hinge residue (for loop FG) from LZ-8 [*CWT-7*]; and (h) adopting loop DE and FG regions and putative hinge residues for both loop DE and FG from LZ-8 [*CWT-8*]. The bioactivities of synthesized FIP-fve wild type and derivatives proteins were examined and compared in **Chapter 5 and 6** for their respective immunomodulation and anti-cancer activities. To demonstrate a better representation of mutations imposed on the FIP-fve derivatives, an alignment of amino acid sequences of the FIP-fve and mutants are shown in **Figure 3.2**.

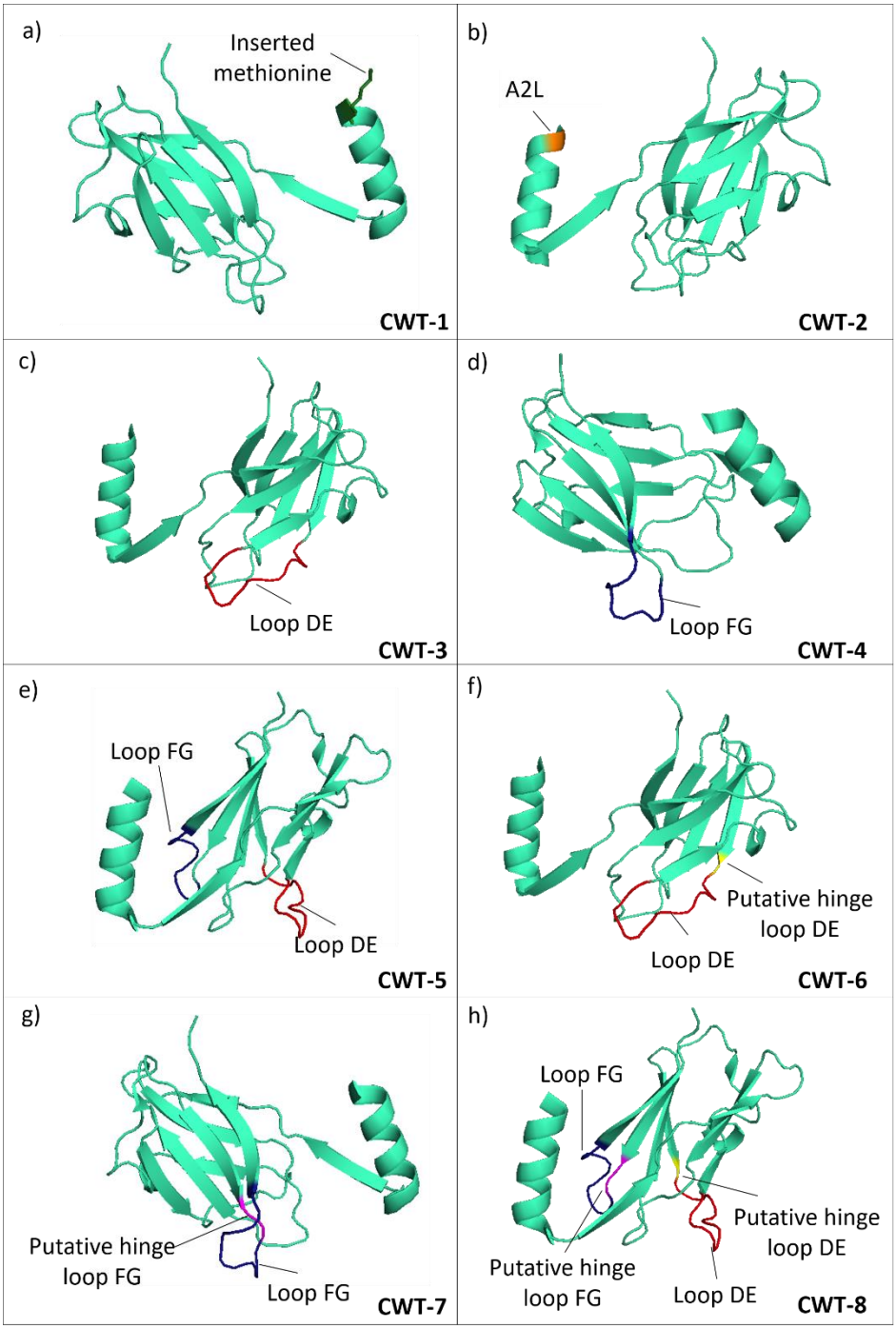


Figure 3.1. Demonstration of the major regions of FIP-fve involved in mutagenesis. FIP-fve monomer is used as a representative structure for illustration purpose. The FIP-fve monomers were adjusted to demonstrate the best view of the regions indicated. The major regions of FIP-fve that are targeted for mutagenesis are highlighted in colour. *CWT-1* consists of inserted methionine (S1InsM) (dark green); *CWT-2* comprises of substituted residue for enhanced hydrophobicity (A2L) (orange); *CWT-3* consists of loop DE region (S62P, N63S, F64Y, T67E, P68S, S69D, G71S) (red); *CWT-4* consists of loop FG region (G101N, S103Del, E104Del, E105D, Y106F) (dark blue); *CWT-5* consists of both loop DE and FG region; *CWT-6* comprised of loop DE region and putative hinge residue for loop DE (E61K) (yellow colour); *CWT-7* consists of loop FG region and putative hinge residue for loop FG (I97D) (purple colour); and *CWT-8* comprises of loop DE, FG and putative hinge residues for loop FG and DE.

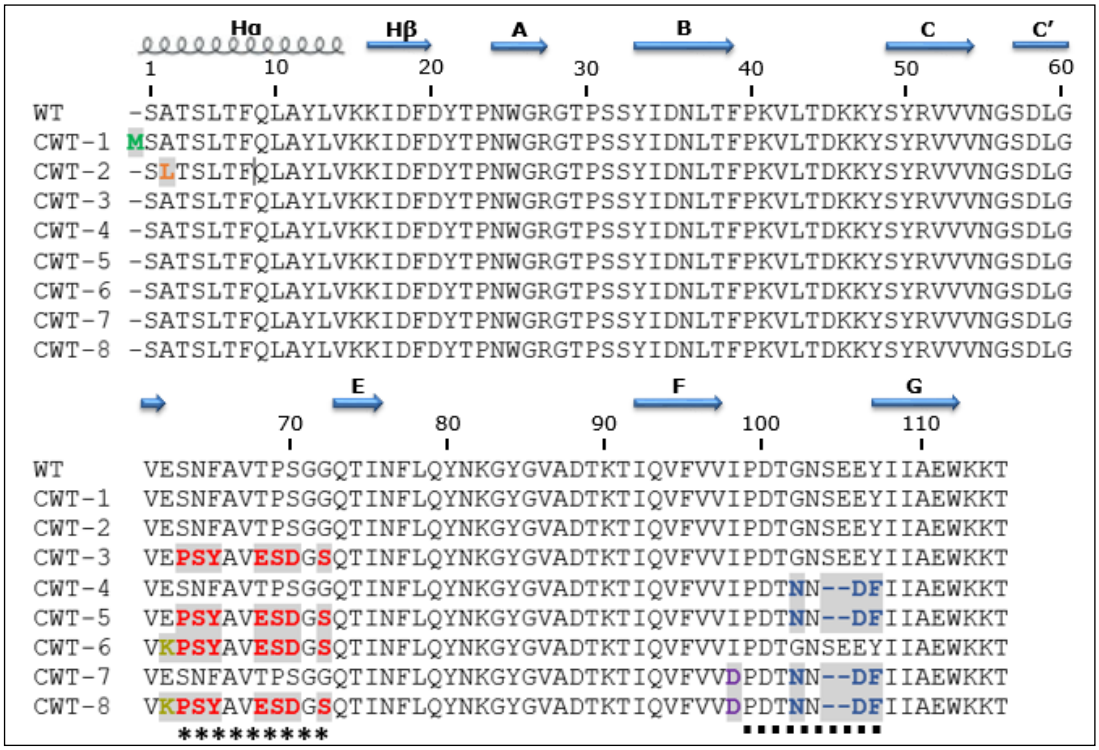


Figure 3.2. Multiple sequence alignment of amino acid sequences of FIP-fve (WT), CWT-1, CWT-2, CWT-3, CWT-4, CWT-5, CWT-6, CWT-7, and CWT-8 generated using MAFFT multiple sequence alignment software. The N-terminal alpha helix and beta-strand are denoted as Hα and Hβ respectively. The beta-strands in FNIII domain (strands A, B, C, C', E, F and G) are indicated as respective A, B, C, C', E, F and G. The main regions of FIP-fve that are targeted for mutagenesis are highlighted as followed: dark green colour indicated inserted methionine (S1InsM); orange colour indicated residue for enhanced hydrophobicity (A2L); red colour indicated loop DE region (S62P, N63S, F64Y, T67E, P68S, S69D, G71S); blue colour indicated loop FG region (G101N, S103Del, E104Del, E105D, Y106F); yellow colour indicated putative hinge residue for loop DE (E61K); purple colour indicated putative hinge residue for loop FG (I97D). The amino acid residues in loop DE and FG regions are indicated as asterisk and dots respectively.

As discussed in **Chapter 2 Section 2.4**, functional FIP-fve has been successfully generated in both prokaryotic and eukaryotic system (Ko *et al.*, 1997; Wu *et al.*, 2008; Lin *et al.*, 2013). In this study, *Escherichia coli* expression system was employed as it offered advantages such as simple media requirement, high growth rate, and cost-effective (Baeshen *et al.*, 2014) for production of recombinant FIP-fve and eight variants proteins, allowing a fairly comprehensive analysis to be completed within planned time frame. In addition, FIP-fve is a small protein with a size of 12.7 kDa in monomer form (Seow *et al.*, 2003), therefore it is suitable to be expressed using *E. coli* system. *Escherichia coli* has

been widely used to produce recombinant proteins that largely contributed to healthcare industrial applications as well as protein structural studies (Rosano and Ceccarelli, 2014). For instance, about 30% of the recombinant biopharmaceuticals that are licensed up to 2016 by United State Food and Drug Administration (FDA) and European Medicines Agency (EMEA) were obtained using *E.coli*, including growth factors, interferons, antibody fragments, and hormones (Berlec and Štrukelj, 2013; Baeshen *et al.*, 2014; Sanchez-Garcia *et al.*, 2016). Besides that, approximately 90% of the protein structures that are deposited in Protein Data Bank was also generated in *E.coli* (Nettleship *et al.*, 2010).

Although *E. coli* recombinant protein expression system can be applied to generate and accumulate a high amount of soluble proteins in the host cells, the excessive production may result in detrimental effects on protein folding (formation of inclusion bodies) as well as on host itself (Costa *et al.*, 2014). The synthesizing of recombinant protein requires a successful interconnection between expression of gene, solubility of protein, and purification of protein. In this respect, one of the most important aspects to consider in this chapter is to construct an expression vector that is capable of producing functional recombinant proteins. The pGLO expression vector was employed in this study. pGLO vector comprised of the easily modulated pBAD promoter that is a moderately strong promoter associated with tight regulation, allowing achievement of a moderately high protein expression that is sufficient for recombinant protein production for subsequent analysis assay (Guzman *et al.*, 1995).

For the ease of protein purification, affinity tag was included in the design and construction of recombinant proteins in this study. Hexahistidine (6xHis) tag was introduced to allow subsequent protein purification via immobilized metal affinity chromatography (IMAC). Besides that, green fluorescent protein gene (*gfp*) was also incorporated during the construction. The unique fluorescent feature of GFP makes it a

great fusion partner as it allows visibility of the protein presence through fluorescent visualization along expression and purification procedure, permiting continuation to the subsequent steps with confidence (Chalfie *et al.*, 1994). The 6xHis tag was introduced at the N-terminal of the recombinant proteins, whereas GFP tag was fused at the C-terminal of the recombinant proteins. Hexahistidine encoding sequence was added to the genes of interest via polymerase chain reaction (PCR), whereas GFP encoding gene was harboured by pGLO vector, which was fused to the C-terminal of the target gene when the gene cassette was cloned into the vector. Additionally, encoding sequence of enterokinase cleavage site was incorporated at the C-terminal of recombinant genes (in between of the coding sequences of target proteins and GFP). The GFP can be cleaved off using enterokinase in case if GFP influences the protein characteristics.

Hence, the specific objectives of this chapter are: (i) to generate *FIP-fve* cDNA template; (ii) to design and synthesize *FIP-fve* derivatives using the cDNA template; (iii) to design and construct gene cassettes harbouring individual genes of *FIP-fve* and its variants in fusion with coding sequences of hexahistidine tag and enterokinase cleavage site; (iv) to integrate the generated gene cassettes into pGLO expression vector that harboured *gfp*.

3.2 Materials and methods

The research was initiated with isolation of total mRNA from golden needle mushroom, *Flammulina velutipes* in order to obtain *FIP-fve* cDNA as a template for subsequent DNA mutagenesis. The acquired *FIP-fve* cDNA was cloned into a cloning vector. A total of eight *FIP-fve* variants were synthesized using site-directed mutagenesis. To construct expression vectors, gene cassettes for *FIP-fve* and mutants were first generated. Subsequently, the gene cassettes were subjected to (i) restriction enzyme digestion, (ii) ligation with expression vector, and (iii) transformation into bacterial cells. The successfully transformed bacterial colonies harbouring the recombinant vectors were identified using colony PCR screening and verified using DNA sequencing. A schematic workflow involved in the generation of cDNA encoding FIP-fve and design and construction of recombinant *FIP-fve* and mutants is presented in **Figure 3.3**.

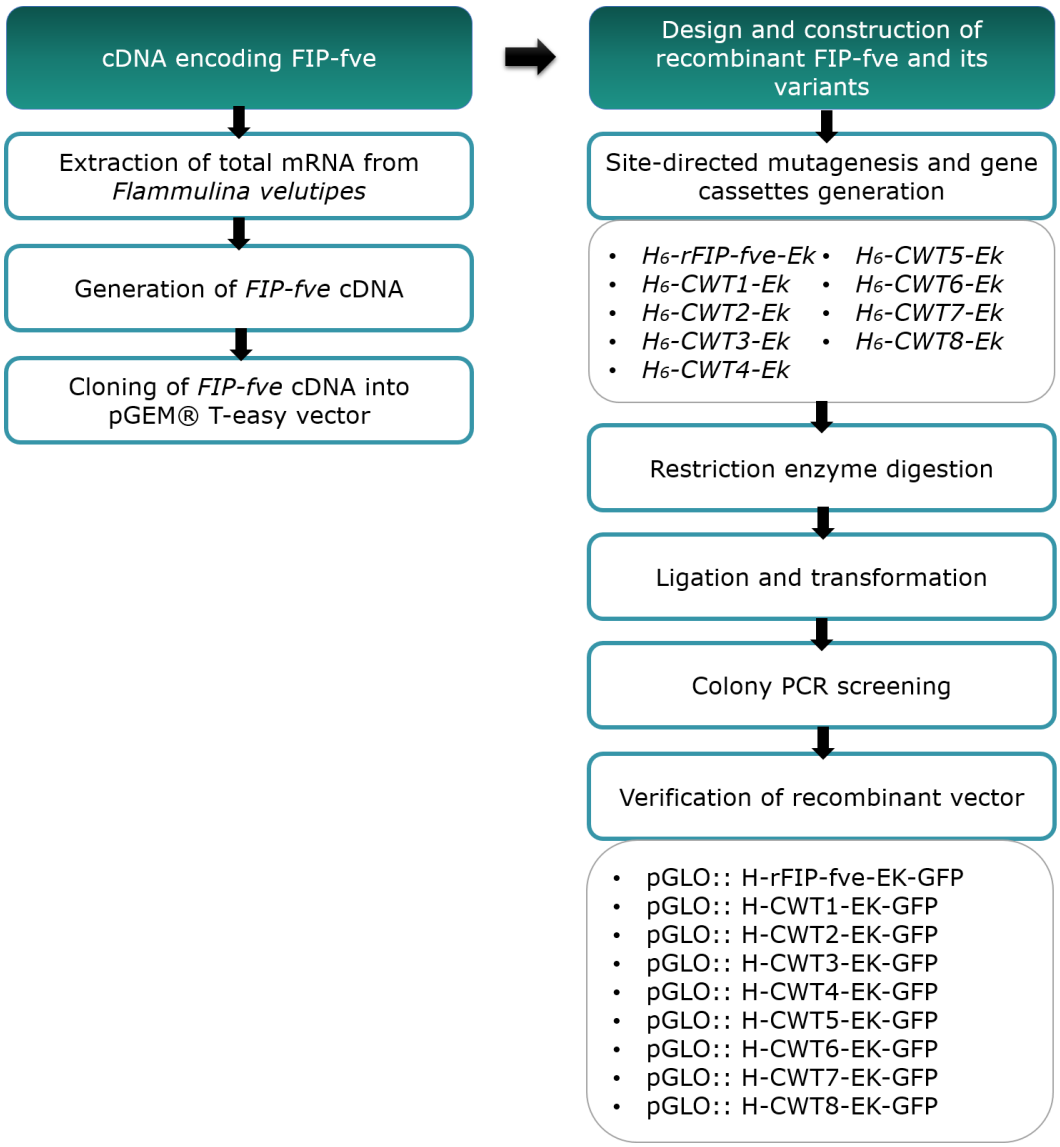


Figure 3.3. A methodology workflow describing the process involved in the construction of recombinant vectors for *FIP-fve* and variants in this research.

3.2.1 General materials and equipment

The general materials (including bacterial culture agar and broth and DNA agarose gel), specialized equipment, and primer and DNA sequencing services used in this study are described as below.

3.2.1.1 Agar and broth culture preparation

Luria Bertani (LB) Lennox was used as the growth medium for *Escherichia coli*. The components in LB Lennox medium include 10 g/L tryptone, 5 g/L yeast extract and 5 g/L sodium chloride. LB Lennox broth medium was prepared by suspending 20 g of LB Lennox powder (Novagen®, United States of America (USA)) in 1 L distilled water, and distributed into culture erlemenyer flasks before subjected to autoclave at 15 min for 121˚C. The volume of LB culture medium prepared was 10% of the flask volume. LB Lennox agar medium was prepared by suspending 20 g of LB Lennox powder (CONDA pronadisa, Spain) and 15 g of agar powder in 1 L distilled water, and autoclaved at 15 min for 121˚C. For LB medium agar plate, the agar medium was poured directly into sterile agar plate dishes. When antibiotic supplement was necessary, the agar medium was allowed to cool to 55˚C and supplemented with a final concentration of 100 µg/ml of filter-sterilized antibiotic ampicillin (Nacalai Tesque, Japan), and poured into sterile agar plate dishes. The plate-pouring procedure was carried out in laminar air flow (ESCO Airstream®). The agar plates were stored at 4˚C for up to 1 month.

3.2.1.2 Specialised equipment

PCR was carried out using Mastercycler® nexus (Eppendorf, Germany). DNA gel electrophoresis was performed using Sub-Cell® GT Cell DNA gel electrophoresis system (Bio-Rad Laboratories, USA). Image of electrophoresed gel was captured using Gel Doc™ XR system (Bio-Rad Laboratories, USA), and analyzed using Quantity One 1-D analysis software (Bio-Rad Laboratories, USA). DNA concentration was measured using

Epoch microplate spectrophotometer with Take3 micro-volume plate (BioTek®, USA) and analysed using Gen5 Data Analysis Software (BioTek®, USA). Centrifugation was performed using centrifuge 5810 R (Eppendorf™, USA). Sample incubation at controlled temperature was carried out using water bath (Memmert, Germany) or Thermomixer® (Eppendorf®, Germany). Bacterial culture plate was incubated in BINDER Microbiological Incubator (Binder, Germany), while bacterial culture flask was incubated in SI-600 incubator shaker (Lab Companion, USA). Optical density of bacterial culture was measured using BioPhotometer Plus (Eppendorf®, Germany).

3.2.1.3 Agarose gel DNA electrophoresis

DNA fragment of PCR amplicon and digestion-product of restriction enzyme were analysed using agarose gel electrophoresis. Agarose gel was made with TBE buffer (89 mM Tris, 89 mM boric acid, 2 mM ethylenediaminetetraacetic acid, pH 8.3) containing 1% (w/v) agarose, and pre-stained with 1:10000 dilution of SYBR™ Safe DNA gel stain (Invitrogen, USA). With the prepared agarose gel soak in TBE running buffer, DNA electrophoresis was performed at 100 V for 60 min. The size of DNA fragments was determined using 1 kb DNA ladder (ThermoFisher Scientific, USA) as reference DNA ladder.

3.2.1.4 Primer synthesis and DNA sequencing

Primers were synthesized by Integrated DNA Technologies (Integrated DNA Technologies (IDT®), USA). DNA sequencing service was performed by 1st Base laboratory (1st Base, Malaysia). Sequencing data were analysed using BioEdit and Nucleotide Blast®.

3.2.2 cDNA encoding FIP-fve

This section presents on generation of *FIP-fve* cDNA (**Appendix A3.2**), which served as a template for subsequent synthesis of *FIP-fve* derivatives and their gene cassettes. Total RNA was first isolated from enokitake mushroom *Flammulina velutipes*, and converted into cDNA. The *FIP-fve* cDNA was amplified with *FIP-fve* gene-specific primers. The DNA sequences of the amplified products were confirmed using DNA sequencing. *FIP-fve* DNA fragment was then cloned into a cloning vector.

3.2.2.1 Isolation of total RNA from *Flammulina velutipes*

A packet of fresh golden needle mushroom, *Flammulina velutipes* was purchased from local Tesco supermarket and used as starting material for this project (**Figure 3.4a and b**). The upper one quarter of the fruiting bodies were excised with a scalpel and placed in liquid nitrogen. The excised tissues were then ground thoroughly by using autoclaved pestle and mortar. An amount of 100 mg ground tissue powder were weighed and decanted into a liquid-nitrogen-cooled 1.5 ml microcentrifuge tube, which were processed immediately by using RNeasy Plant Mini Kit (QIAGEN®, Germany) to purify total RNA from the fruiting bodies. The protocol of RNA isolation was perfomed according to manufacturer's instruction as shown in **Appendix A3.3**.

a)



b)



Figure 3.4. a) Fruiting body of *Flammulina velutipes* that was used as starting material. b) Packaging of the golden needle mushroom that was produced in China.

3.2.2.2 Generation of FIP-fve cDNA

QIAGEN One Step RT-PCR kit® was used to amplify and clone FIP-fve coding region from extracted total RNA. The QIAGEN enzyme mix contains Omniscript and Sensiscript Reverse Transcriptases and HotStarTaq DNA polymerase, which are blend specifically for the use of both reverse transcription and PCR amplification.

The reaction mixture containing QIAGEN OneStep RT-PCR Buffer (1X), QIAGEN OneStep RT-PCR Enzyme Mix, deoxynucleotides (dNTPs) mix (10 mM of each dNTPs), forward primer (0.6 µM), reverse primer (0.6 µM,) template DNA (1.5 µg) and top up with RNase-free distilled water to 50 µl were prepared. A negative control (consisting all components without template RNA) was prepared as well. The forward and reverse primers used are FIPfve-FP (5'-ATGTCCGCCACGTCGCTCACCTT-3') and FIP-fve-RP (5'-CTTCTTCCACTCAGCGATGATGTACTCCTCCGAGT-3') respectively, which are designed according to FIP-fve gene (GU388420.1) from GenBank database. The thermal cycler was programmed according to the program outlined in **Table 3.1**, which included steps for both reverse transcription and PCR. Different activation temperature requirements of reverse transcriptase and DNA polymerase allowed both reactions to take place in a single tube. The thermal cycler was pre-heated to 50˚C before loading the sample tubes. The first step of 50˚C allowed reverse transcription to take place efficiently. Subsequently, HotStarTaq® DNA polymerase required initial activation by incubation at 95˚C for 15 min before amplification of target gene take place. Meanwhile, the reverse transcriptase was inactivated at this incubation step.

Table 3.1. Programmed Thermal Cycler Conditions

Programmed steps	Time	Temperature
Reverse transcription	30 min	50˚C
Initial PCR activation step	15 min	95˚C
3-step cycling: 30 cycles		
Denaturation	1 min	94˚C
Annealing	1 min	59˚C
Extension	1 min	72˚C
Final extension		
Final extension	10 min	72˚C
Infinite hold	-	10˚C

3.2.2.3 Verification of *FIP-fve* cDNA

OneStep RT-PCR amplified *FIP-fve* cDNA (10 µl) were analyzed using gel electrophoresis and visualized using gel imaging system. A 100 bp ladder (GeneRuler™ 100bp DNA Ladder, Thermo Scientific™) was used to determine the size of amplified *FIP-fve* cDNA. Gel/PCR DNA Fragments Extraction Kit (Geneaid, Taiwan) was used to purify *FIP-fve* cDNA from the remaining 40 µl of OneStep RT-PCR product according to the PCR clean-up protocol as shown in **Appendix A3.4.**

3.2.2.4 Ligation

pGEM-T® easy vector (Promega, USA) was used to clone *FIP-fve*. The vector map is shown in **Figure 3.5**. pGEM-T® easy is a linearized vector with a size of 3015 bp and possesses single 3'-terminal thymidine at both ends. It is a high-copy-number vector that encodes an alpha-peptide coding region of enzyme β-galactosidase with an internal multiple cloning site. Ligation reactions were set up as according to **Table 3.2**, where positive and background controls were included as well. The reactions were mixed by pipetting and incubated overnight at 4˚C to get maximum number of transformants. Ratio 3:1 of the *FIP-fve* cDNA to pGEM-T® easy vector was used in this ligation reaction. The transformant of pGEM-T® easy vector and *FIP-fve* cDNA is designated as pGEM-FIPfve.

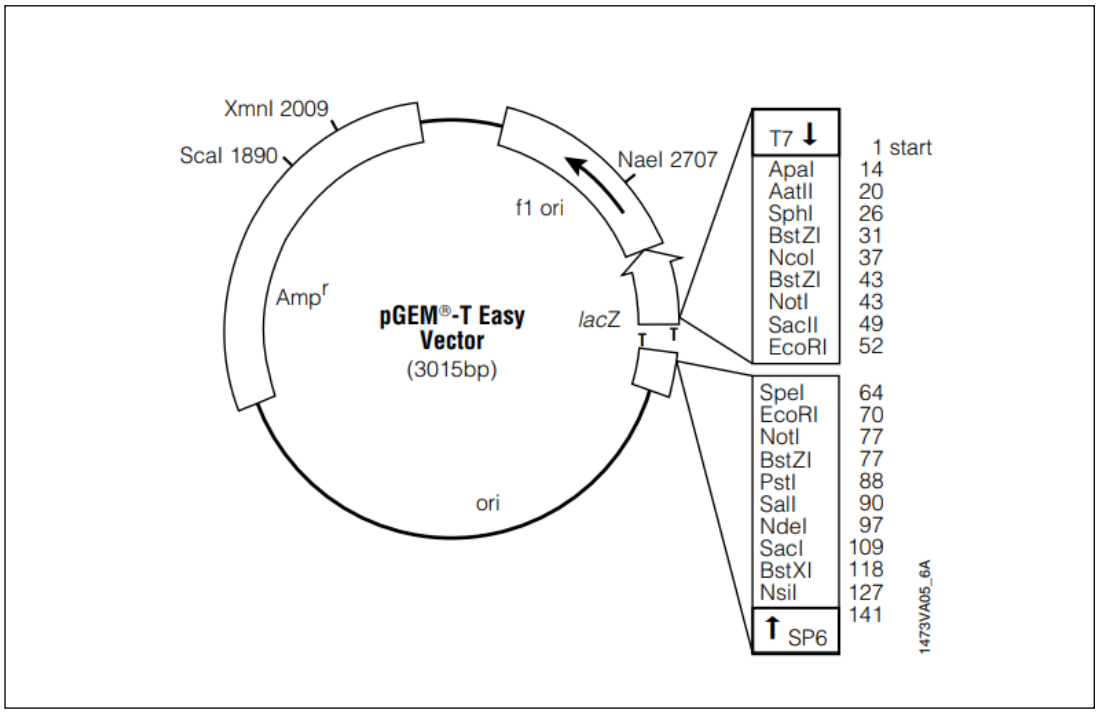


Figure 3.5. Vector map of linearized pGEM®-T easy with single 3'-terminal thymidine at both ends. Image adopted from Promega Corporation (2015).

Table 3.2. Reaction components for ligation reaction

Reaction component	Standard Reaction	Positive Control	Background control
2X Rapid Ligation Buffer, T4 DNA Ligase	5µl	5µl	5µl
pGEM-T® easy vector (50ng)	1µl	1µl	1µl
FIP-fve cDNA	1µl	-	-
Control Insert DNA	-	2µl	-
T4 DNA Ligase (3 Weiss units/µl)	1µl	1µl	1µl
Nuclease-free water to a final volume of	2µl	1µl	3µl

3.2.2.5 Calcium chloride competent cells preparation

TOP10 *Escherichia coli* cells (Invitrogen™, USA) was used as the host cell. The genotype of the TOP10 *E. coli* cell is F- *mcrA*, Δ(*mrr-hsd*RMS-*mcr*BC), Φ80*lac*ZΔM15, Δ *lac*X74 *rec*A1 *ara*D139, Δ(*araleu*)7697, *gal*U, *gal*K, *rps*L, (StrR), *end*A1, and *nup*G. TOP10 competent cell was prepared using calcium chloride method according to the protocol described by Tu and colleagues (2005) with some modifications to the method used for starter culture preparation. While the glycerol stock of *E. coli* was used by Tu *et al*. (2005) directly for competent cells preparation, starter culture was first prepared using bacteria colony that was streaked on LB agar plate. The starter culture was incubated at 37˚C for 16 hr with a speed of 180 rpm. After 16 hr of incubation, 200 µl of the bacterial culture was transferred into a new conical flask containing 20 ml of LB broth and incubated at 37˚C until OD_{600} of the culture reached 0.4-0.5. The bacterial culture was then used for competent cells preparation according to the protocol that was described in **Appendix A3.5**. The prepared competent cells were distributed into single-aliquot tubes and kept at -80˚C.

3.2.2.6 Bacterial cell transformation

Prior to cell transformation procedure, the competent cells were removed from -80˚C and thawed on ice. Once the cells were thawed, 2 µl of each ligation reaction was added to 50 µl of competent cells. The cells with the ligation reaction were mixed gently by flicking the tube and incubated on ice for 30 min. The cells were then heat-shock precisely at 42˚C in a water bath for 45 s. The tubes were returned immediately to ice for 2 min. An amount of 950 µl of LB medium (room temperature) was added to the tubes containing the transformants and incubated at 37˚C and 300 rpm for 1.5 hours. Each of the 200µl transformants were plated onto duplicate LB agar plates containing 100 µg/ml ampicillin, 0.5 mM isopropyl β-D-1-thiogalactopyranoside (IPTG) and 80 µg/ml 5-bromo-4-chloro-3-indolyl-β-d-galactoside (X-Gal) and incubated at 37˚C for 16 hours. The LB agar

medium with supplements was prepared as followed: LB agar medium was first autoclaved at 121˚C for 15 min, and once the temperature was cooled to 55˚C, it was supplemented with filter-sterilized ampicillin, IPTG and X-gal before plates pouring. Subsequently, recombinant clones were identified by blue-white screening on the LB/ampicillin/IPTG/X-Gal agar plates.

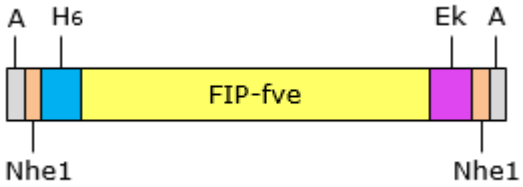
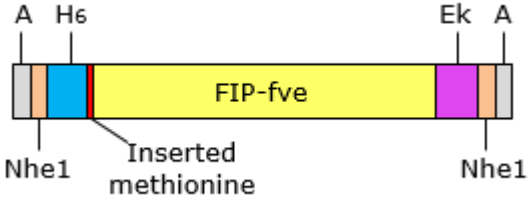
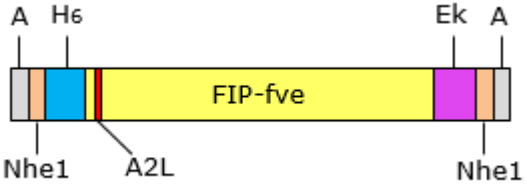
3.2.2.7 Isolation of recombinant vector clones

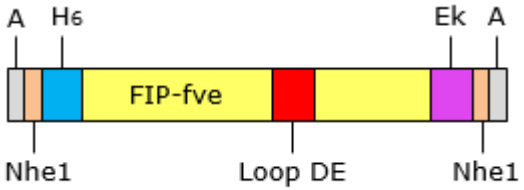
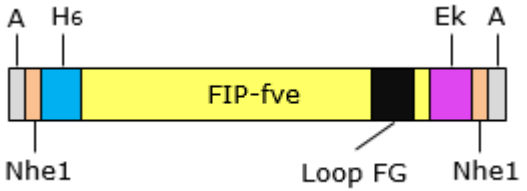
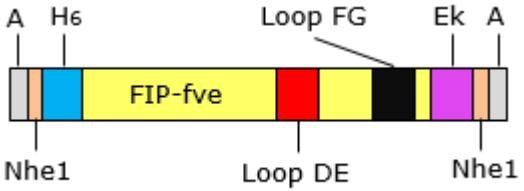
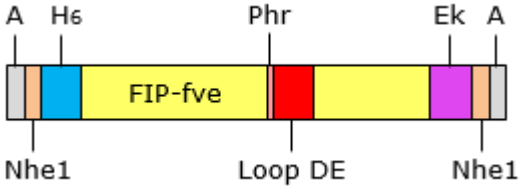
A white colony was randomly selected from plate with transformants and inoculated individually in 250 ml erlemenyer flask containing 20 ml LB broth with 100 µg/ml ampicillin, and incubated on incubator shaker for 16 hr at 37˚C with speed of 180 rpm. The procedure was conducted within sterile field created by Bunsen burner flame. High-speed Plasmid Mini Kit (Geneaid, New Taipei City, Taiwan) was used for plasmid extraction as per manufacturer's instruction (**Appendix A3.6**).

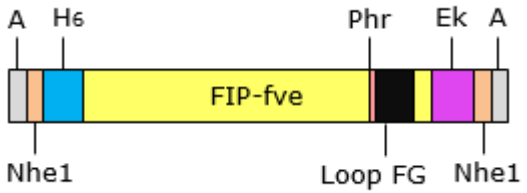
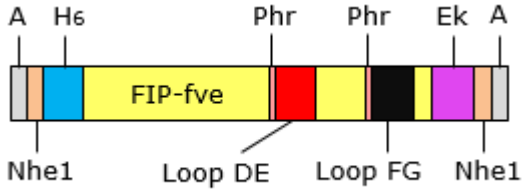
3.2.3 Design and construction of recombinant *FIP-fve* and its variants

Design and construction of genes of recombinant FIP-fve (*rFIP-fve*) and derivatives are presented herein. Eight variants of *rFIP-fve* were constructed using SDM and prepared as individual gene cassettes to be inserted into expression vector. The encoding sequences of 6xHis tag and enterokinase cleavage site were incorporated at the N-terminal and C-terminal of the genes respectively. NheI restriction sites were added at both flanks of the sequence for subsequent digestion and ligation into the expression vector. The insertion of gene cassettes into the expression vector introduced *gfp* at the C-terminal of the gene cassettes. The list of gene cassettes for *rFIP-fve* and mutants is shown in **Table 3.3**.

Table 3.3. List of gene cassettes for *rFIP-fve* and its eight derivatives. The nucleotide and amino acid sequences of each of the gene cassettes were included in the appendices.

No.	Name of gene cassettes	Description of mutation imposed	Schematic diagram of gene cassettes of FIP-fve and its derivatives for recombinant vectors construction	Appendix
1	*H_6-rFIPFVE-EK*	-		**A3.3**
2	*H_6-CWT1-Ek*	S1insM		**A3.4**
3	*H_6-CWT2-Ek*	A2L		**A3.5**

4	*H_6-CWT3-Ek*	**Loop DE:** S62P, N63S, F64Y, T67E, P68S, S69D, G71S		**A3.6**
5	*H_6-CWT4-Ek*	**Loop FG:** G101N, S103Del, E104Del, E105D, Y106F		**A3.7**
6	*H_6-CWT5-Ek*	**Loop DE:** S62P, N63S, F64Y, T67E, P68S, S69D, G71S **Loop FG:** G101N, S103Del, E104Del, E105D, Y106F		**A3.8**
7	*H_6-CWT6-Ek*	**Putative hinge residue:** E61K **Loop DE:** S62P, N63S, F64Y, T67E, P68S, S69D, G71S		**A3.9**

8	*H_6-CWT7-Ek*	**Putative hinge residue:** I97D **Loop FG:** G101N, S103Del, E104Del, E105D, Y106F		**A3.10**
9	*H_6-CWT8-Ek*	**Putative hinge residue (loop DE):** E61K **Loop DE:** S62P, N63S, F64Y, T67E, P68S, S69D, G71S **Putative hinge residue (loop FG):** I97D **Loop FG:** G101N, S103Del, E104Del, E105D, Y106F		**A3.11**

Denotation:

A – Additional nucleotides
H_6 – 6xhis tag
Ek – Enterokinase cleavage site
NheI – NheI restriction site
Phr – Putative hinge residue
Loop DE – Loop DE mutation region
Loop FG – Loop FG mutation region

3.2.3.1 Vector

pGLO vector (Bio-Rad Laboratories, USA) was used in this study to harbor and express genes of wild type and mutated *FIP-fve* in TOP10 *E. coli*. As shown in **Figure 3.6**, pGLO vector comprised of numerous DNA sequences that includes pBAD promoter; *gfp* encoding 'cycle 3' mutant GFP; *araC* encoding regulatory protein for pBAD promoter; and *bla* encoding enzyme beta lactamase, which degrades antibiotic ampicillin. pBAD is an inducible promoter that is regulated by AraC protein, which acts as both positive and negative regulators (Guzman *et al.*, 1995). pBAD transcription is activated only in the presence of an inducer agent, L-arabinose (Rosano and Ceccarelli, 2014).

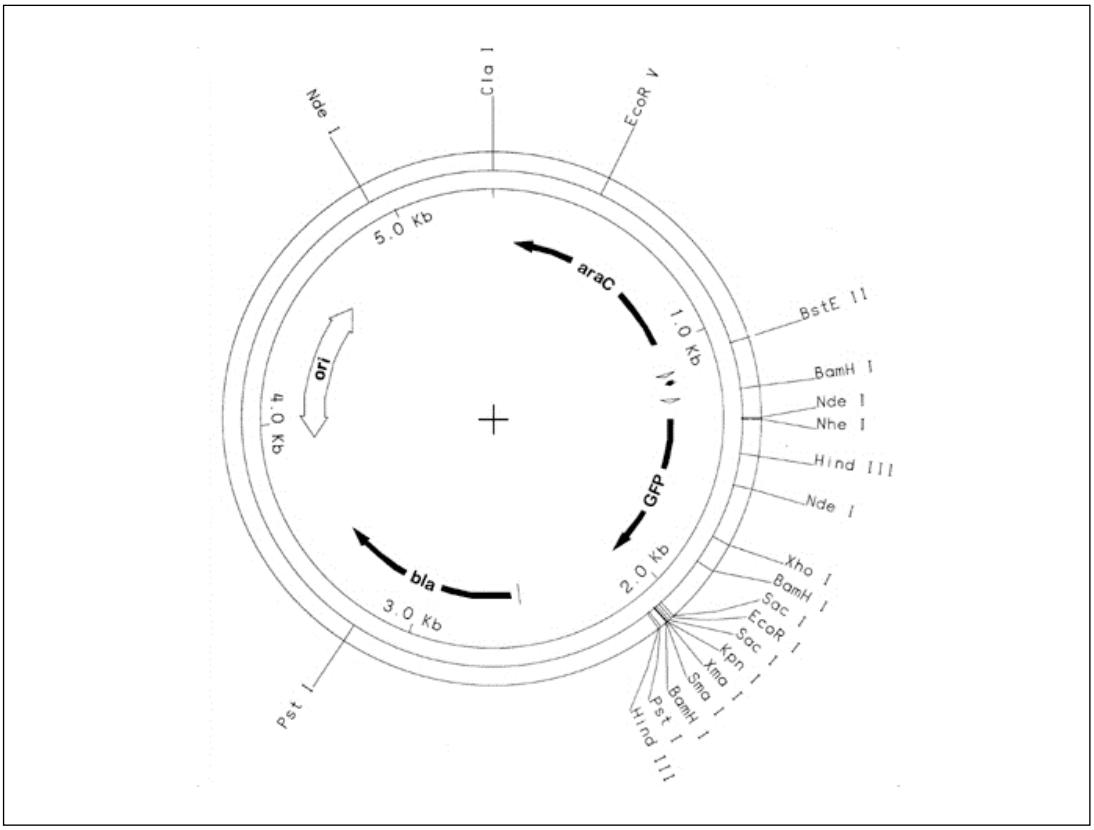


Figure 3.6. Vector map of pGLO consisting of DNA sequences of pBAD promoter, *bla*, *gfp* 'cycle 3' mutant, *araC* and multiple cloning site. Image adopted from Bio-Rad (2014).

3.2.3.2 Primer design

All primer pairs were designed manually and analyzed for primer melting temperature, GC content and secondary structures possibilities using OligoAnalyzer 3.1 (IDT®, USA). It is important to note that the internal mutagenic primer pairs for one of the SDM methods, overlap extension PCR was designed according to primer design scheme demonstrated in the study of Liu and Naismith (2008). As shown in **Figure 3.7**, overlapping sequences (complementary sequences) was included at 5' end of the primer pair, while non-overlapping sequences was included at the 3' end of the primer pair; this design helps to minimize dimerization of primer-primer. Mutation sites were incorporated at both overlapping and non-overlapping regions.

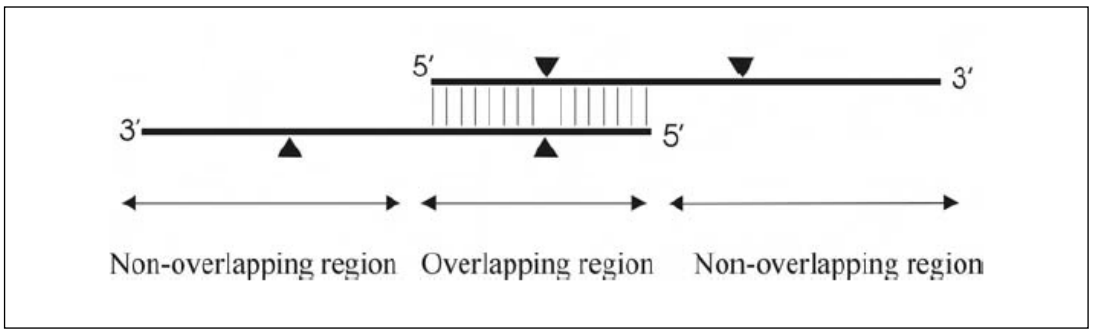


Figure 3.7. Schematic diagram of the internal mutagenic primer design for overlap PCR extension approach. Image adopted from Liu and Naismith (2008).

In addition to SDM, the fragments of *rFIP-fve* and mutants were also prepared in the form of gene cassettes for subsequent cloning into pGLO vector. Primers for gene cassettes were designed to include hybridization sequence, mutation (only for terminal changes and internal mutagenic primers), NheI restriction site (5'-GCTAGC-3'), additional nucleotides (5'-GCATAA-3'), 6xHis tag sequence (5'-CACCATCACCATCACCAT-3') and enterokinase cleavage site (5'-GACGACGACGACAAGATC-3'). Hybridization sequence is the region that allows primer to bind to the gene specific sequence; NheI restriction site is the DNA sequence that is recognized and cut by NheI restriction enzyme; additional nucleotides are the extra

base pairs added at the 5' end of restriction enzyme recognition site that assist restriction enzyme cutting. A list of the primers that are designed for SDM and gene cassettes construction was shown in **Table 3.4**.

Table 3.4. List of primers designed for site-directed mutagenesis and gene cassettes construction

Genes	**Primer pairs**	**Sequences (5'-3')**	**Annealing temperature (˚C)**
rFIP-fve	H_6-Fve-FP	GCATAAGCTAGCCACCATCACCATC ACCATTCCGCCACGTCGCTCAC	66
	Ek-Fve-RP	CGTGCTGCTAGCGATCTTGTCGTCGT CGTCAGTCTTCTTCCACTCAGCGAT	
CWT-1	H_6-MFve-FP	GCATAAGCTAGCCACCATCACCATC ACCATATGTCCGCCACGTCGCTC	66
	Ek-Fve-RP	CGTGCTGCTAGCGATCTTGTCGTCGT CGTCAGTCTTCTTCCACTCAGCGAT	
CWT-2	Dimer-FP	GCATAAGCTAGCCACCATCACCATC ACCATTCCCTCACGTCGCTCACC	66
	Ek-Fve-RP	CGTGCTGCTAGCGATCTTGTCGTCGT CGTCAGTCTTCTTCCACTCAGCGAT	
CWT-3	H_6-Fve-FP	GCATAAGCTAGCCACCATCACCATC ACCATTCCGCCACGTCGCTCAC	66
	LoopDE_RP	ACCGTCCGATTCCACTGCGTAGCTG GGCTCGAC	
	LoopDE_FP	CAGTGGAATCGGACGGTTCGCAGAC CATCAACTTCCTCCAG	66
	Ek-Fve-RP	CGTGCTGCTAGCGATCTTGTCGTCGT CGTCAGTCTTCTTCCACTCAGCGAT	
CWT-4	FIPFve-FP	ATGTCCGCCACGTCGCTCACCTT	61.3
	LoopFG-RP	AGTCTTCTTCCACTCAGCGATGATGA AGTCGTTGTTGGTATCTGGAATGAC	
	H_6-Fve-FP	GCATAAGCTAGCCACCATCACCATC ACCATTCCGCCACGTCGCTCAC	66
	Ek-Fve-RP	CGTGCTGCTAGCGATCTTGTCGTCGT CGTCAGTCTTCTTCCACTCAGCGAT	
CWT-5	FIPFve-FP	ATGTCCGCCACGTCGCTCACCTT	61.3
	LoopFG-RP	AGTCTTCTTCCACTCAGCGATGATGA AGTCGTTGTTGGTATCTGGAATGAC	
	H_6-Fve-FP	GCATAAGCTAGCCACCATCACCATC ACCATTCCGCCACGTCGCTCAC	66
	Ek-Fve-RP	CGTGCTGCTAGCGATCTTGTCGTCGT CGTCAGTCTTCTTCCACTCAGCGAT	

CWT-6	H_6-Fve-FP	GCATAAGCTAGCCACCATCACCATC ACCATTCCGCCACGTCGCTCAC	66
	LoopDE-Phr-RP	CCGTCCGATTCCACTGCGTAGCTGG GCTTGACGC	
	LoopDE-FP	CAGTGGAATCGGACGGTTCGCAGAC CATCAACTTCCTCCAG	66
	Ek-Fve-RP	CGTGCTGCTAGCGATCTTGTCGTCGT CGTCAGTCTTCTTCCACTCAGCGAT	
CWT-7	FIPFve-FP	ATGTCCGCCACGTCGCTCACCTT	61.3
	LoopFG-Phr-RP	CTTCTTCCACTCAGCGATGATGAAGT CGTTGTTGGTATCTGGATCGACAAC	
	H_6-Fve-FP	GCATAAGCTAGCCACCATCACCATC ACCATTCCGCCACGTCGCTCAC	66
	Ek-Fve-RP	CGTGCTGCTAGCGATCTTGTCGTCGT CGTCAGTCTTCTTCCACTCAGCGAT	
CWT-8	FIPFve-FP	ATGTCCGCCACGTCGCTCACCTT	61.3
	LoopFG-Phr-RP	CTTCTTCCACTCAGCGATGATGAAGT CGTTGTTGGTATCTGGATCGACAAC	
	H_6-Fve-FP	GCATAAGCTAGCCACCATCACCATC ACCATTCCGCCACGTCGCTCAC	66
	Ek-Fve-RP	CGTGCTGCTAGCGATCTTGTCGTCGT CGTCAGTCTTCTTCCACTCAGCGAT	

Denotation:
Grey highlight – Additional nucleotides
Green highlight – NheI restriction enzyme recognition sequence
Blue highlight – Hexahistidine sequence
Purple highlight – Enterokinase cleavage site sequence
Yellow highlight – Hybridization sequence
Red bold wording – Mutations imposed
Underline wording – Overlapping sequences

3.2.3.3 Site-directed mutagenesis and gene cassettes generation

Two methods of SDM namely overlap PCR extension and/or terminal PCR changes approaches were employed to generate the *FIP-fve* variants depending on the positions of desired SDM as shown in **Table 3.3**. Terminal changes PCR technique was applied when the intended mutation is situated within approximately 30 bp of either end of the target PCR fragment (Ling and Robinson, 1997). Overlap extension PCR approach was practiced when the desired mutation is located in the center of the target PCR fragment (Ling and Robinson, 1997).

All PCR reactions for the SDM of *FIP-fve* gene and generation of gene cassettes were carried out by using MyTaq™ Mix (Bioline, London). PCR mixtures were prepared as described: MyTaq Mix (1x), forward primer (0.4 µM), reverse primer (0.4 µM), DNA template and topped up with distilled water to 50 µl. PCR programme was initiated at 95˚C for 1 min, and followed by 30 cycles of denaturation at 95˚C for 15 s, annealing at 61.3-66˚C for 15 s and extension at 72˚C for 10 s. The respective annealing temperature and primer pairs used for different gene cassettes are presented in **Table 3.4**. The generation of mutant gene with terminal changes was rather straightforward where terminal changes PCR approach can be achieved in one single round of PCR using flanking primers that contain intentional mutations, resulting in the generation of amplified PCR product with sequence modification.

On the other hand, several steps were involved in overlap extension PCR technique (Pogulis, Vallejo and Pease, 1996) as shown in **Figure 3.8**. Two pairs of primers were utilized in this approach, which were the flanking primer pair (A & D) and internal mutagenic primer pair (B & C). Mutations were illustrated as round black dots. Firstly, fragments AB and CD were generated in the first PCR cycle (a). The fragments were then gel purified using Gel/PCR DNA fragments kit (Geneaid, Taiwan); the protocol is described in **Appendix A3.16**. An equimolar of the two fragments was used as template

for second PCR cycle. Internal mutagenic primers were designed to carry mutations and share overlap DNA sequences, allowing fragments that were generated in first PCRs to merge in second round of PCR. Second PCR cycle was started for 3 cycles without the addition of primers A and D to allow the extension of annealed overlap AB and CD fragment (b). During PCR cycle, the 5' end of fragment CD hybridized with the 3' end of fragment AB; the overlapping strands acted as a 'megaprimer' for each other. DNA polymerase then worked on extending the overlapping strands, resulting in full-length mutated fusion PCR product (AD). After the 3 cycles of extension, the flanking primers A and D was added to the PCR reaction to amplify the full-length template AD (c).

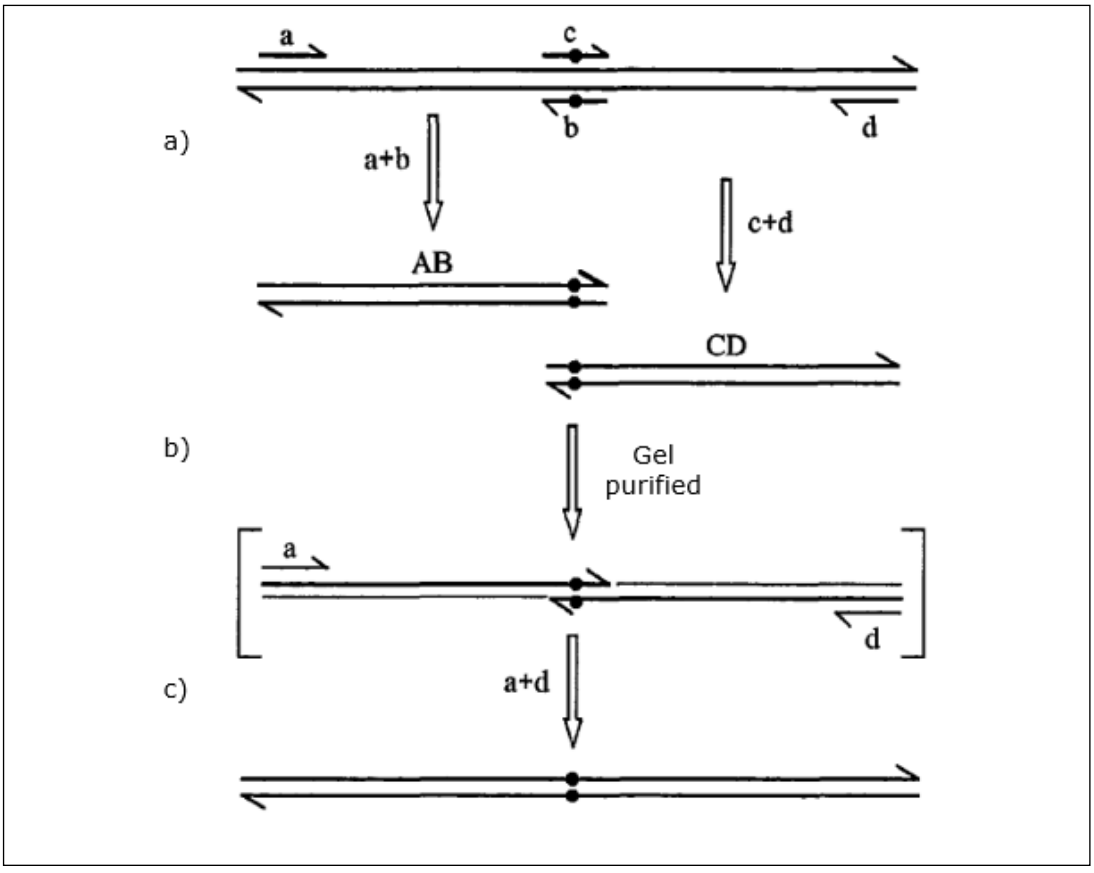


Figure 3.8. Overlap PCR extension for site-directed mutagenesis involves several steps. Two pairs of primers were utilized in this approach, which were flanking primer pair (A & D) and internal mutagenic primer pair (B & C). (a) Mutations were illustrated as round black dots. Firstly, fragments AB and CD were generated in the first PCR cycle. (b) The fragments were then gel purified and used as template for second PCR cycle. Second PCR cycle was started for 3 cycles without the addition of primers A and D to allow the extension of annealed overlap AB and CD fragment, generating the intermediate product as indicated in bracket. (c) After the 3 cycles of extension, primers A and D was added to the PCR reaction to amplify the extended templates (Pogulis, Vallejo and Pease, 1996).

The details including DNA templates and primers involved in the mutagenesis and generation of each gene cassettes were described as below:

rFIP-fve

Gene cassette of *rFIP-fve* was generated by using pGEM-FIPfve vector as template. Forward (H_6-Fve-FP) and reverse primers (Ek-Fve-RP) was used to add in the flanking regions (containing encoding sequences of 6xhis tag, enterokinase cleavage site, NheI restriction sites and additional nucleotides via PCR reaction).

CWT-1

Derivative of *rFIP-fve*, *CWT-1* was designed to be mutated by inserting an additional amino acid, methionine at the N-terminal of *rFIP-fve*. Terminal changes PCR technique was performed for mutation as well as addition of flanking regions using pGEM-FIPfve vector as DNA template and forward (H_6-MFve-FP) and reverse primer (Ek-Fve-RP).

CWT-2

Derivative of *rFIP-fve*, *CWT-2* was designed to be mutated at A2L. Terminal changes PCR technique was conducted for mutation as well as addition of flanking regions using pGEM-FIPfve vector as DNA template and forward (Dimer-FP) and reverse primer (Ek-Fve-RP).

CWT-3

Derivative of *rFIP-fve*, *CWT-3* was designed to be mutated at loop DE region by adopting amino acid residues of loop DE in LZ-8. Overlap extension PCR approach was carried out by using both flanking and internal primer pairs. The flanking forward and reverse primers were H_6-Fve-FP (A) and Ek-Fve-RP (D), respectively; while the internal forward and reverse primers were LoopDE-FP (C) and LoopDE-RP (B), respectively. pGEM-

FIPfve vector was used as DNA template in the first round of PCR; while fragments AB and CD were utilized as DNA templates in the second round of PCR.

CWT-4

Derivative of *rFIP-fve*, *CWT-4* was designed to be mutated at loop FG region by adopting amino acid residues of loop FG in LZ-8. Terminal changes PCR technique was carried out using pGEM-FIPfve vector as DNA template. The forward and reverse primers used were FIPfve-FP and LoopFG-RP respectively. The resulting PCR products were subjected to PCR clean-up and used as template for another round of PCR using forward (H_6-Fve-FP) and reverse primers (Ek-Fve-RP) to add in flanking regions.

CWT-5

Derivatives of *rFIP-fve*, *CWT-5* was designed to be mutated at both loop DE and FG regions by adopting amino acid residues of loop DE and FG in LZ-8. Terminal changes PCR approach was conducted by using *CWT-3* as DNA template. The forward and reverse primers used were FIPfve-FP and LoopFG-RP respectively. The resulting PCR products were subjected to PCR clean-up and used as template for another round of PCR using forward (H_6-Fve-FP) and reverse primers (Ek-Fve-RP) to add in flanking regions.

CWT-6

Derivative of *rFIP-fve*, *CWT-6* was designed to be mutated at (i) loop DE region and (ii) putative hinge-residue for loop DE by adopting the amino acid residues of loop DE and putative hinge residue in LZ-8. Overlap extension PCR approach was carried out by using flanking and internal primer pairs. The flanking forward and reverse primers were H_6-Fve-FP (A) and Ek-Fve-RP (D), respectively; while the internal forward and reverse primers were LoopDE-FP (C) and LoopDE-Phr-RP (B), respectively. pGEM-FIPfve vector was used as DNA template in the first round of PCR; while fragments AB and CD were utilized as DNA templates in the second round of PCR.

CWT-7

Derivative of *rFIP-fve*, *CWT-7* was designed to be mutated at (i) loop FG region and (ii) putative hinge-residue for loop FG by adopting the amino acid residues of loop FG and putative hinge residue in LZ-8. Terminal changes PCR technique was carried out using pGEM-FIPfve vector as DNA template. The forward and reverse primers used were FIPfve-FP and LoopFG-Phr-RP respectively. The resulting PCR products were subjected to PCR clean-up and used as template for another round of PCR using forward (H_6-Fve-FP) and reverse primers (Ek-Fve-RP) to add in flanking regions.

CWT-8

Derivatives of *rFIP-fve*, *CWT-8* was designed to be mutated at (i) loop DE, (ii) loop FG regions, (iii) putative hinge-residue for loop DE, and (iv) putative hinge-residue for loop FG, by adopting the amino acid residues of loop DE, loop FG, putative hinge residue of loop DE and FG in LZ-8. Terminal changes PCR approach was conducted by using *CWT-6* as DNA template. The forward and reverse primers used were FIPfve-FP and LoopFG-Phr-RP respectively. The resulting PCR products were subjected to PCR clean-up and used as template for another round of PCR using forward (H_6-Fve-FP) and reverse primers (Ek-Fve-RP) to add in flanking regions.

3.2.3.4 Restriction enzyme digestion

Restriction digestion reaction for pGLO vector and gene cassettes were prepared in individual reaction tubes as followed: 1 µg of DNA, 1X NEBuffer™ 1.1 (10 mM Bis-Tris-propane-hydrochloride acid (HCl), 10 mM magnesium chloride ($MgCl_2$), 100 µg/ml bovine serum albumin (BSA), pH 7) (New England biolabs (NEB®), USA), 10 units of NheI-High Fidelity (HF®) restriction enzyme (NEB®, USA), and topped up to 50 µl with distilled water. The reaction tubes were incubated at 37˚C for 3 hours. For pGLO vector reaction tube, 1 unit of TSAP Thermosensitive Alkaline Phosphatase (Promega, USA) was added into the reaction mixture after first hour of incubation, and the incubation was continued at 37˚C for 2 hr. The alkaline phosphatase was utilized to prevent recircularization and religation of linearized pGLO vector DNA during ligation by catalyzing the removal of 5' phosphate group from the vector DNA. After 3 hours of incubation, the pGLO vector and gene cassettes reaction tubes were incubated at 80˚C for 20 min to heat inactivate the enzymes.

3.2.3.5 Ligation and transformation

NheI-digested inserts were ligated individually to dephosphorylate NheI-digested pGLO vector at 1:7 molar ratio. Ligation reactions were prepared as followed: 50 ng of vector DNA, 25.2 ng of insert DNA, 1X T4 DNA ligase buffer (50 mM Tris-HCl, 10 mM $MgCl_2$, 1 mM adenosine triphosphate (ATP), 10 mM dithiothreitol (DTT), pH 7.5) (NEB®, USA), 1 µl of T4 DNA ligase (NEB®, USA), and topped up with distilled water to 20 µl. A background control was set up as well by including the dephosphorylated NheI-digested pGLO vector DNA without insert in the ligation mixture. The ligation mixtures were incubated at 16˚C for 16 hr. After 16 hr, the reaction mixtures were incubated at 65˚C for 10 min to heat-inactivate the T4 DNA ligase. The prepared TOP10 competent cells were

transformed with the ligation mixture according to the protocol described in **Section 3.2.2.6**. The transformants were plated on LB agar containing of 100 µgml^{-1} ampicillin and incubated at 37˚C for 16 hr.

3.2.3.6 Colony PCR screening

Recombinant clones were identified by using colony PCR screening. Seven single colonies were individually picked using sterile pipette tips and swirled in 20 µl of sterile distilled water to ensure sufficient mixing. The bacteria-water mixtures were then subjected to incubation at 95˚C for 15 min to lyse the bacterial cell and release plasmid DNA. The mixtures were centrifuged at 15000 x g for 1 min to remove the cell debris. Subsequently, PCR mixtures were prepared as described: MyTaq Mix (1x), forward primer pBAD-FP (0.4 µM), reverse primer FIPfve-RP (0.4 µM), 1 µl of bacteria-water suspension and topped up with distilled water to 25 µl. Backbone-specific forward primer pBAD-FP (5'-ATGCCATAGCATTTTTATCCATAAGATTAGCGGATCC-3') and insert-specific reverse primer FIPfve-RP (5'-CTTCTTCCACTCAGCGATGATGTACTCCTCCGAGT-3') were used to determine the presence and orientation of the insert. PCR programme was initiated at 95˚C for 1 min, and followed by 30 cycles of denaturation at 95˚C for 15 s, annealing at 58˚C for 15 s and extension at 72˚C for 10 s. The PCR products were gel-electrophoresed to identify the positive clones with correct orientation.

3.2.3.7 Verification of recombinant vectors

The identified positive recombinant clones were cultured in individual 250 ml erlemenyer flask containing 20 ml of LB broth with 100 µg/ml ampicillin, and incubated on incubator shaker for 16 hr at 37˚C with speed of 180 rpm. The procedure was conducted within sterile field created by Bunsen burner flame. The recombinant vectors were extracted with High-Speed Plasmid Mini Kit using protocol according to **Appendix A3.6**. The extracted recombinant vectors were sent for DNA sequencing service.

3.3 Results

3.3.1 Generation of FIP-fve cDNA

The RNA concentration of isolated *F. velutipes* total RNA was 1155.7 ng/µl with A_{260}/A_{280} ratio of 2.2. Total RNA was converted into cDNA and the amplified PCR products of approximately 342 bp were displayed in **Figure 3.9**. The amplified PCR product was verified to carry the coding sequence of FIP-fve based on the analyzed sequencing result as shown in **Appendix A3.17**.

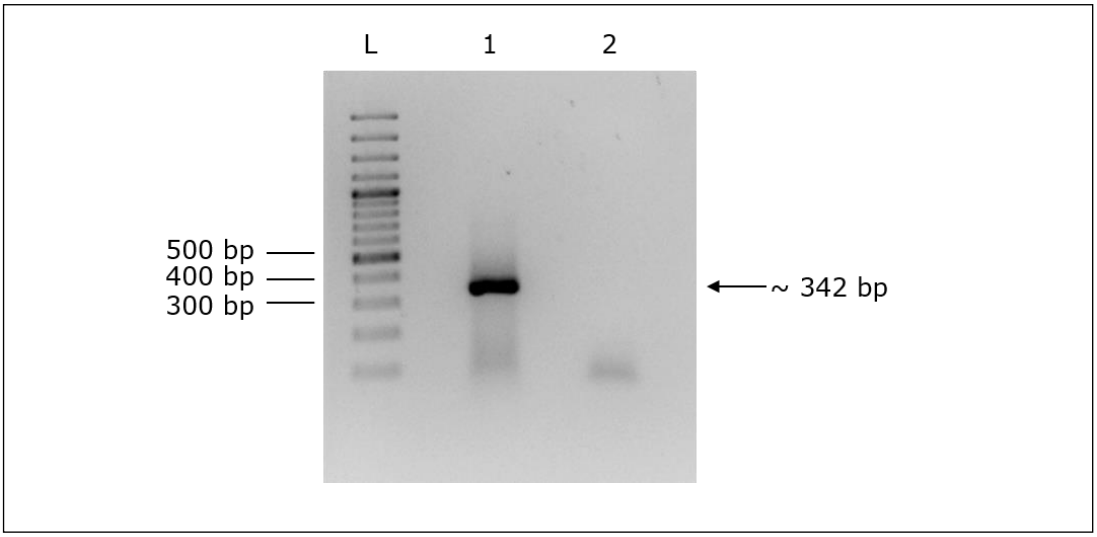


Figure 3.9. PCR amplification profiles of FIP-fve cDNA with estimated size of 342 bp. Lane Lane L: GeneRuler™ 100bp DNA Ladder; Lane 1: FIP-fve cDNA; Lane 2: Negative control.

3.3.2 Cloning vector construction

Bacterial plates with transformants were observed as shown in **Figure 3.10**. A number of white and blue colonies formed on plate with ligation product of FIP-fve cDNA and pGEM® T-easy vector. Some white and blue colonies were observed on plate with ligation product of control insert DNA and pGEM® T-easy vector, indicating that the ligation process was efficient. No colony was seen on plate with ligation product of only pGEM® T-easy vector; indicating that the pGEM® T-easy vector was well-linearized with tailed overhang thymidine. Based on these observations, the white colonies that were formed on plate with ligation product of FIP-fve cDNA and pGEM® T-easy vector were considered as a result of successful ligation and transformation. The presence of FIP-fve coding sequence was verified in the isolated plasmids from white colony based on the analyzed sequencing result as shown **Appendix A3.18**. Schematic diagram of the generated cloning vector, pGEM-FIPfve with FIP-fve cDNA as insert was shown in **Figure 3.11**.

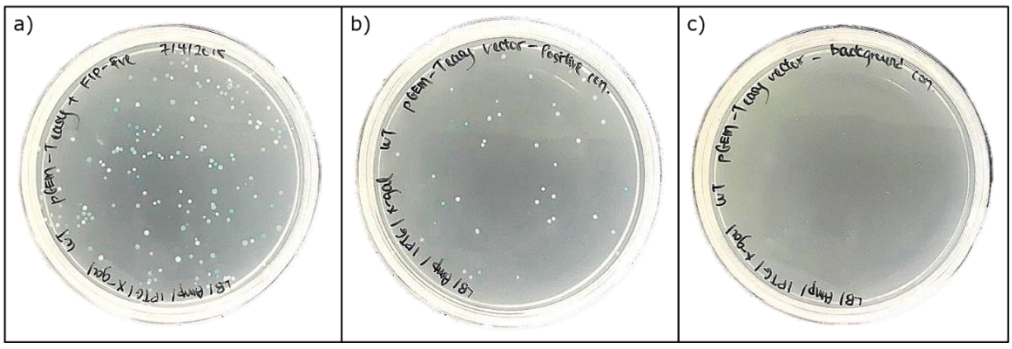


Figure 3.10. Bacterial transformants resulted from transformation of TOP10 cells with ligation products of (a) *FIP-fve* cDNA and pGEM® T-easy vector; (b) control insert DNA and pGEM® T-easy vector and (c) pGEM® T-easy vector only.

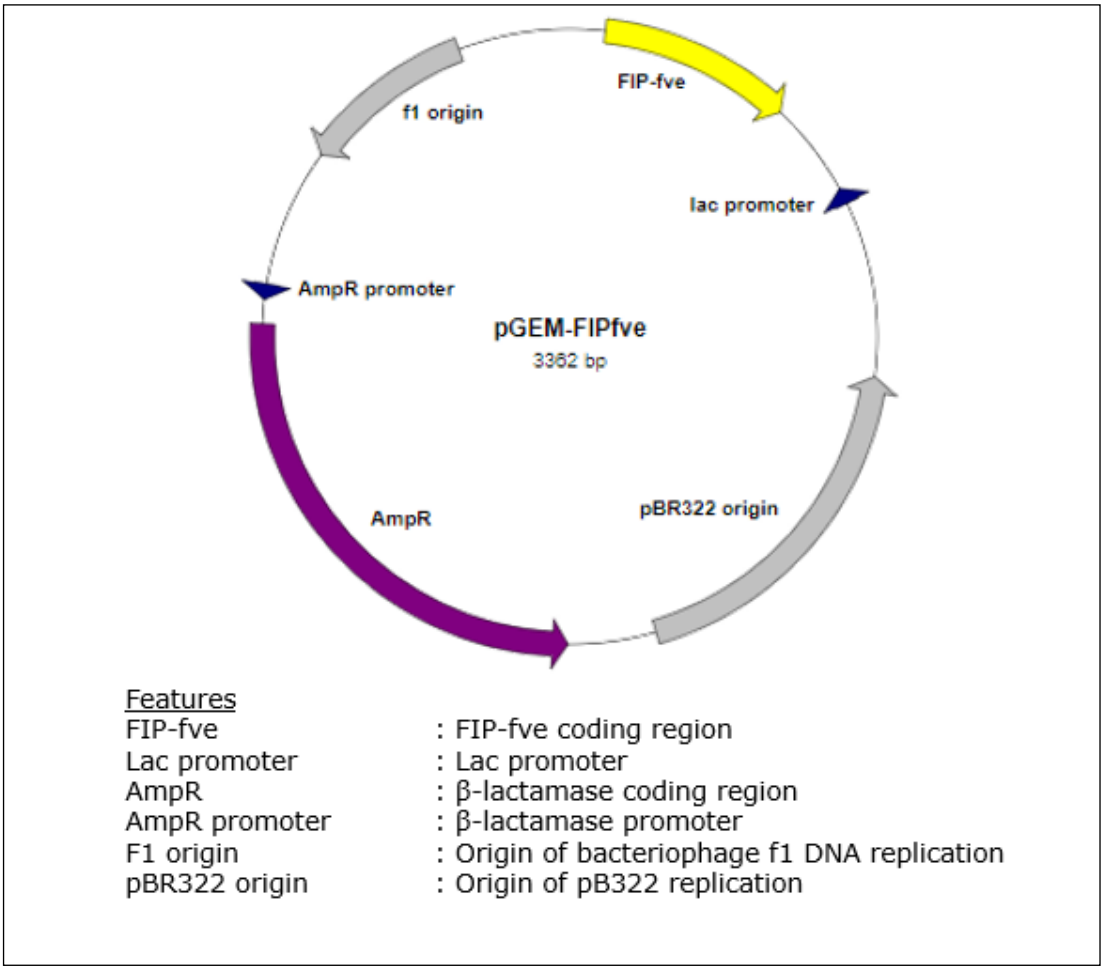


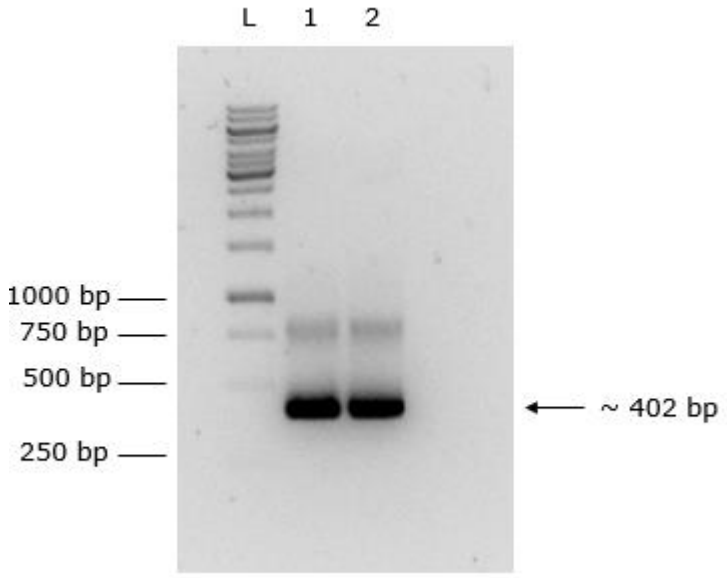
Figure 3.11. Schematic diagram of the generated cloning vector, pGEM-FIPfve with *FIP-fve* cDNA as insert

3.3.3 Generation gene cassettes

All the synthesized gene cassettes were incorporated with DNA sequences of N-terminal 6xhis tag, C-terminal enterokinase, NheI restriction site and additional sequence.

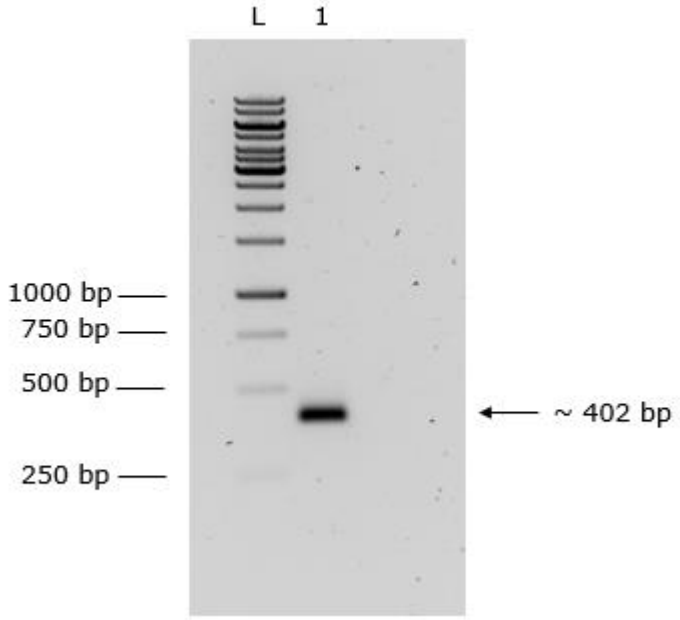
3.3.3.1 rFIP-fve, CWT-1 and CWT-2

PCR amplification profiles of gene cassettes for *rFIP-fve*, *CWT-1* and *CWT-2* were demonstrated in **Figure 3.12**, **Figure 3.13** and **Figure 3.14** respectively. The estimated sizes of generated gene cassettes were 402 bp.



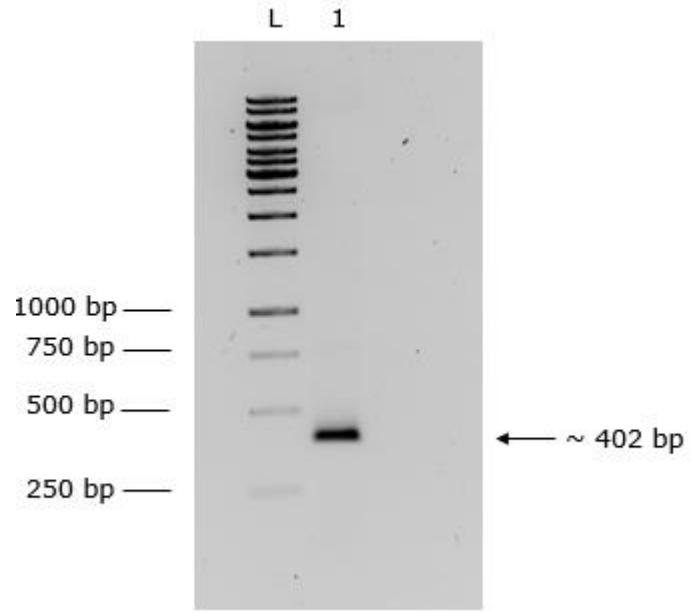
Lane	Gene cassettes	Estimated size
L	GeneRuler 1kb DNA ladder	-
1	*H_6-rFIPFVE-Ek*	402 bp
2	*H_6-rFIPFVE-Ek*	402 bp

Figure 3.12. PCR amplification profile of gene cassette for *H_6-rFIPFVE-Ek*.



Lane	Gene cassettes	Estimated size
L	GeneRuler 1kb DNA ladder	-
1	*H_6-CWT1-Ek*	402 bp

Figure 3.13. PCR amplification profile of gene cassette for *H_6-CWT1-Ek*.

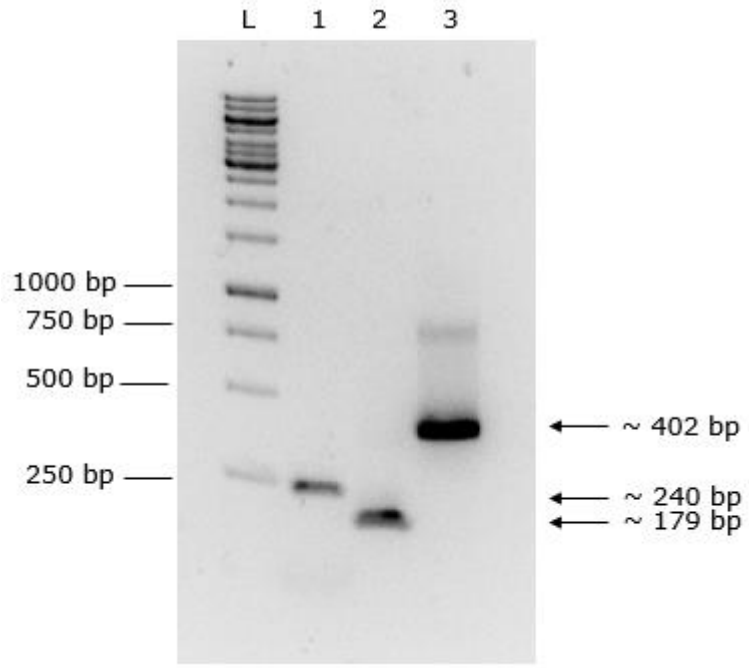


Lane	Gene cassettes	Estimated size
L	GeneRuler 1kb DNA ladder	-
1	*H_6-CWT2-Ek*	402 bp

Figure 3.14. PCR amplification profile of gene cassette for *H_6-CWT2-Ek*.

3.3.3.2 CWT-3

For *CWT-3*, PCR amplification profiles of fragments AB, CD, and full-length *H_6-CWT3-Ek* (fragment AD) with estimated sizes of 240, 179 and 402 bp respectively were displayed in **Figure 3.15**.

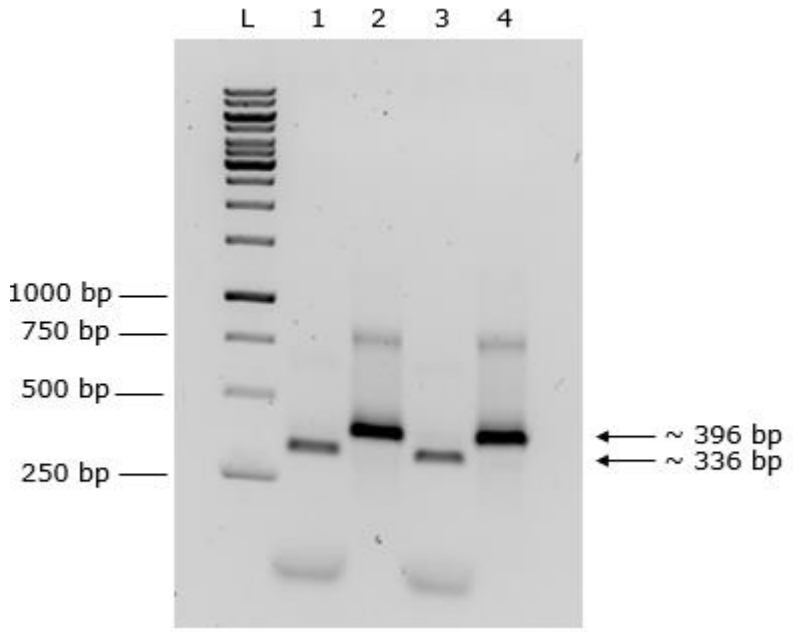


Lane	Gene cassettes	Estimated size
L	GeneRuler 1kb DNA ladder	-
1	Fragment AB (*CWT-3*)	240 bp
2	Fragment CD (*CWT-3*)	179 bp
3	*H_6-CWT3-Ek*	402 bp

Figure 3.15. PCR amplification profiles of fragment AB, fragment CD and gene cassette *H_6-CWT3-Ek* (fragment AD).

3.3.3.3 CWT-4 and CWT-5

PCR amplification profiles of *CWT-4*, *CWT-5*, *H_6-CWT4-Ek* and *H_6-CWT5-Ek* with estimated sizes of 336, 336, 396 and 396 bp respectively were shown in **Figure 3.16**.

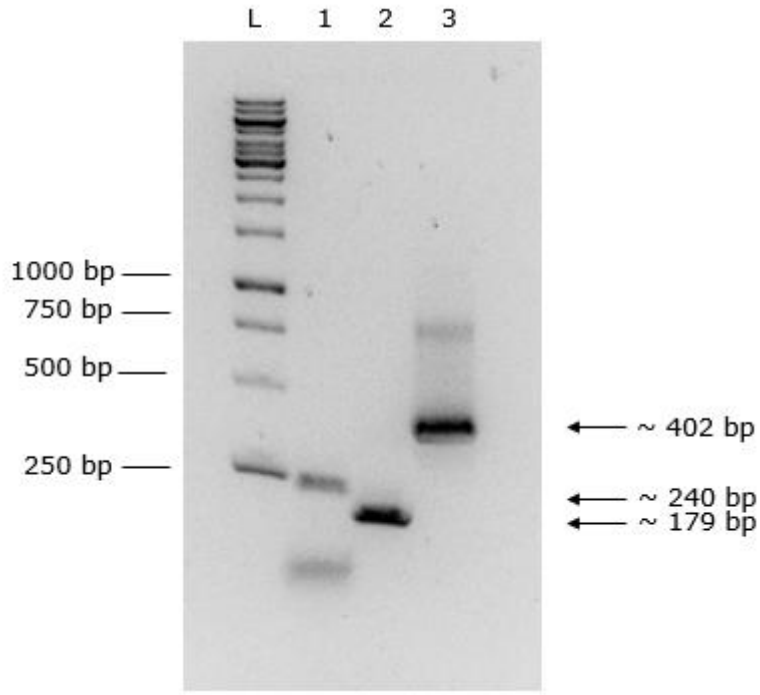


Lane	Gene cassettes	Estimated size
L	GeneRuler 1kb DNA ladder	-
1	*CWT-4*	336 bp
2	*H_6-CWT4-Ek*	396 bp
3	*CWT-5*	336 bp
4	*H_6-CWT5-Ek*	396 bp

Figure 3.16. PCR amplification profiles of *CWT-4*, *CWT-5*, gene cassette *H_6-CWT4-Ek* and gene cassette *H_6-CWT5-Ek*.

3.3.3.4 CWT-6

For *CWT-6*, PCR amplification profiles of fragments AB, CD, and full-length *H_6-CWT6-Ek* (fragment AD) with estimated sizes of 240, 179 and 402 bp respectively were presented in **Figure 3.17**.

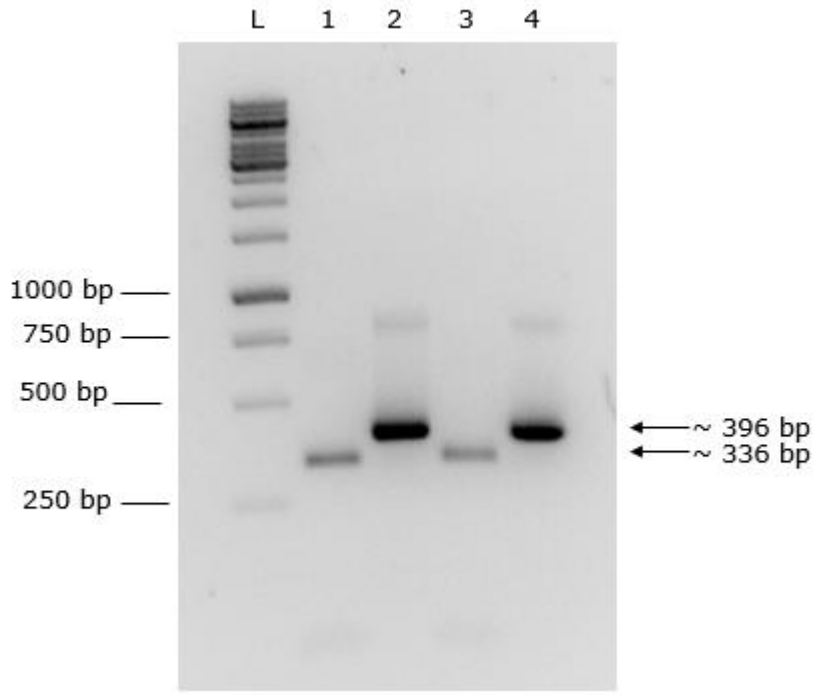


Lane	Gene cassettes	Estimated size
L	GeneRuler 1kb DNA ladder	-
1	Fragment AB (*CWT-6*)	240 bp
2	Fragment CD (*CWT-6*)	179 bp
3	*H_6-CWT6-Ek*	402 bp

Figure 3.17. PCR amplification profiles of fragment AB, fragment CD and gene cassette *H_6-CWT6-Ek* (fragment AD).

3.3.3.5 CWT-7 and CWT-8

PCR amplification profiles of *CWT-7*, *CWT-8*, *H_6-CWT7-Ek* and *H_6-CWT8-Ek* with estimated sizes of 336, 336, 396 and 396 bp respectively were shown in **Figure 3.18**.

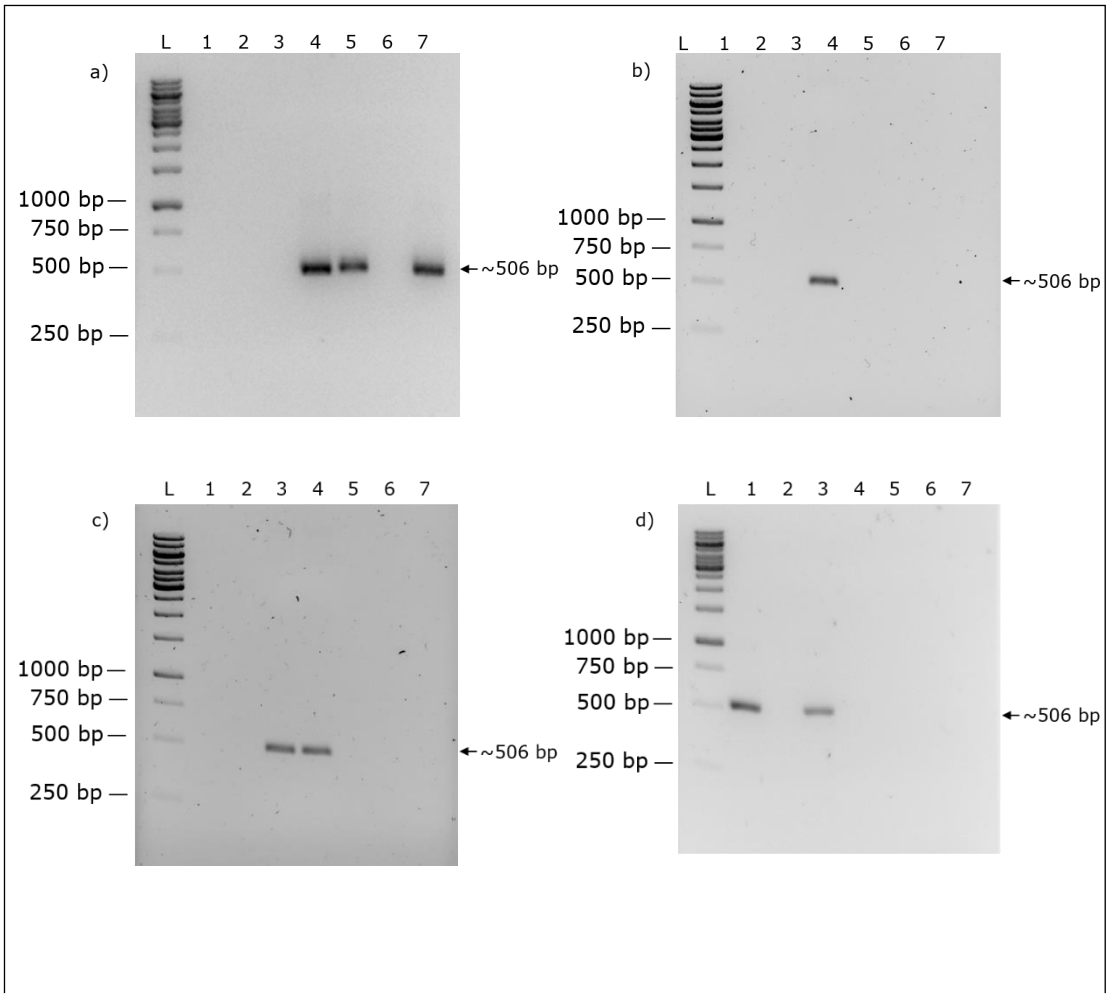


Lane	Gene cassettes	Estimated size
L	GeneRuler 1kb DNA ladder	-
1	*CWT-7*	336 bp
2	*H_6-CWT7-Ek*	396 bp
3	*CWT-8*	336 bp
4	*H_6-CWT8-Ek*	396 bp

Figure 3.18. PCR amplification profiles of *CWT-7*, *CWT-8*, gene cassette *H_6-CWT7-Ek*, and gene cassette *H_6-CWT8-Ek*.

3.3.4 Colony PCR

In colony PCR, positive clones with presence of insert as well as correct orientation of insert resulted in generation of PCR products at estimated size of 506 bp. As shown in **Figure 3.19**, three positive clones were resulted from transformants with *H_6-rFIPFVE-Ek* insert (a); one positive clone was resulted from transformant with *H_6-CWT1-Ek* insert (b); two positive clones were resulted from transformants with *H_6-CWT2-Ek* insert (c); two positive clones were resulted from transformants with *H_6-CWT3-Ek* insert (d); one positive clone was resulted from transformant with *H_6-CWT4-Ek* insert (e); one positive clone was resulted from transformant with *H_6-CWT5-Ek* insert (f); three positive clones were resulted from transformants with *H_6-CWT6-Ek* insert (g); two positive clones were resulted from transformants with *H_6-CWT7-Ek* insert (h); and four positive clones were resulted from transformants with *H_6-CWT8-Ek* insert (i).



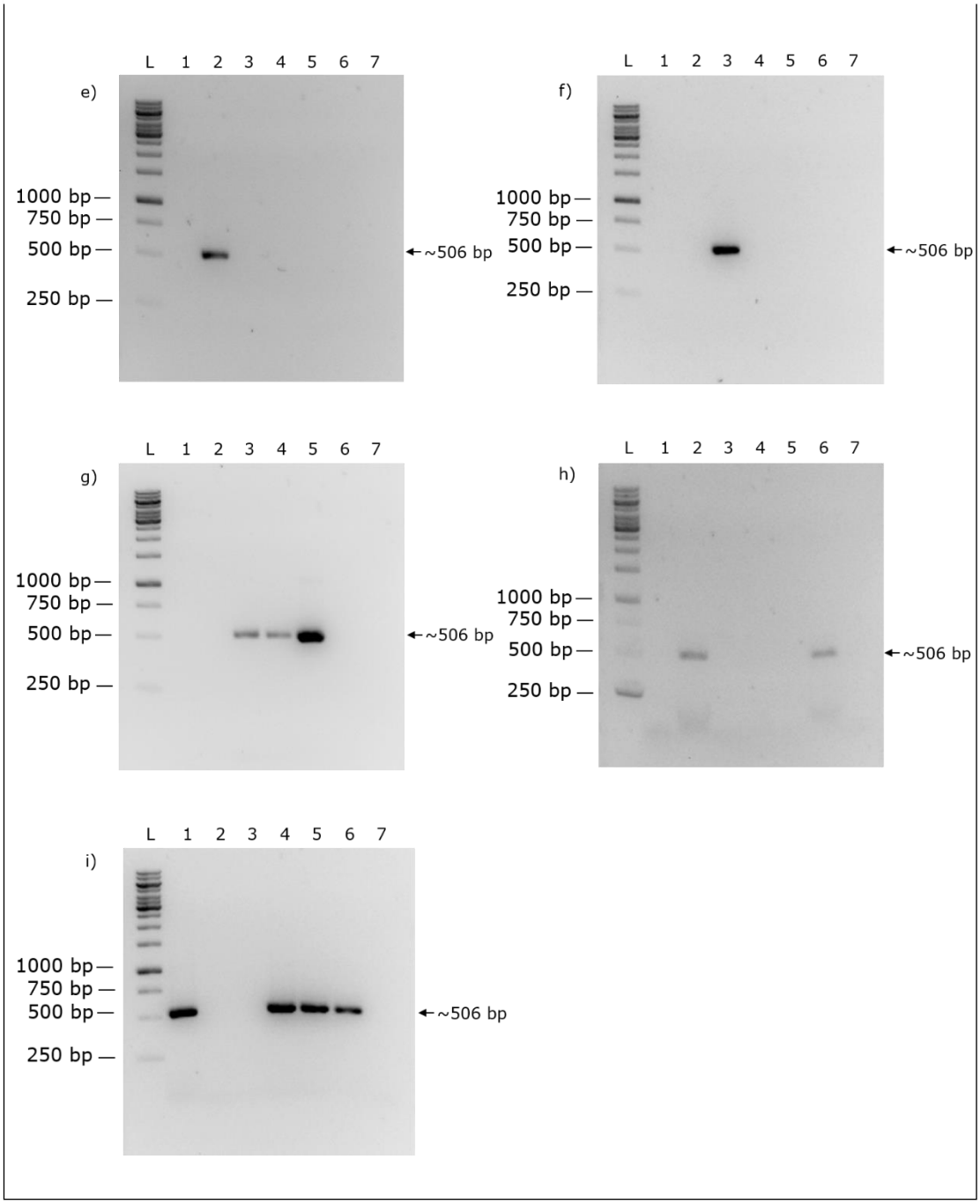


Figure 3.19. PCR amplification profiles of colony PCR screening on transformants with insert of (a) *H_6-rFIPfve-Ek*, (b) *H_6-CWT1-Ek*, (c) *H_6-CWT2-Ek*, (d) *H_6-CWT3-Ek*, (e) *H_6-CWT4-Ek*, (f) *H_6-CWT5-Ek*, (g) *H_6-CWT6-Ek*, (h) *H_6-CWT7-Ek* and (i) *H_6-CWT8-Ek*. Amplification of PCR products at estimated size of 506 indicates positive clones with presence of insert as well as correct orientation of insert.

3.3.5 Verification of positive recombinant vectors

Analysis of sequencing result confirmed that all generated recombinant expression vectors harbored the correct nucleotide sequences with no occurrence of unintended mutation or frameshift. The sequencing results are shown in **Appendix A3.19 – A3.27**. Schematic vector map of a general representation of the generated pGLO:: insert-GFP expression vector with gene cassettes of rFIP-fve and eight mutants as inserts is shown in **Figure 3.20**. The recombinant vectors are named accordingly as listed in **Table 3.5**.

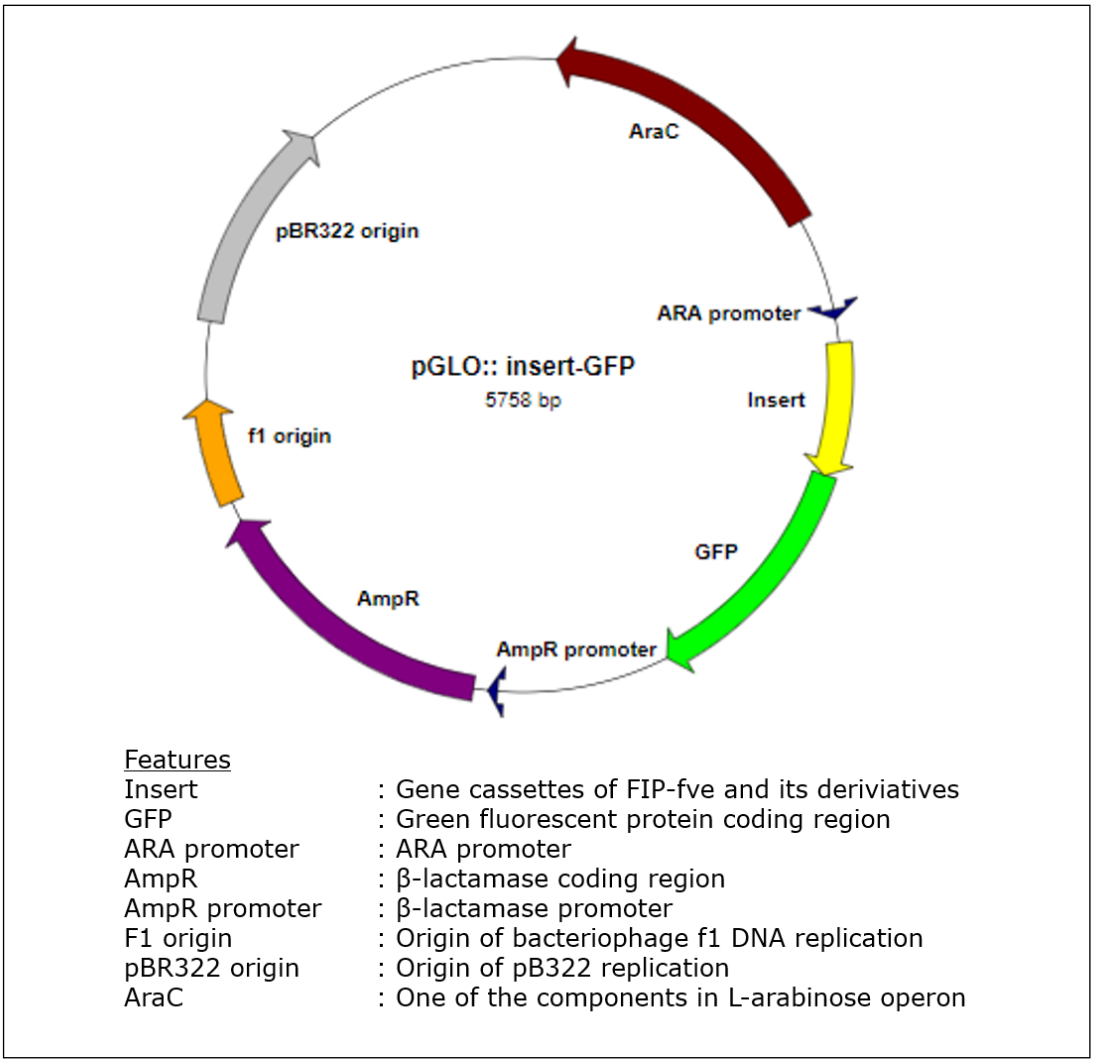


Figure 3.20. Schematic diagram of the generated pGLO:: insert-GFP expression vector as a general representation of the recombinant vector with gene cassettes of rFIP-fve and eight variants genes as inserts.

Table 3.5. Naming of recombinant expression vectors generated for genes *rFIP-fve*, *CWT-1*, *CWT-2*, *CWT-3*, *CWT-4*, *CWT-5*, *CWT-6*, *CWT-7* and *CWT-8*. pGLO indicated plasmid backbone; H indicated hexahistidine fusion tag; Ek indicated enterokinase cleavage site; GFP indicated green fluorescent protein fusion tag. Sequencing results of each of the recombinant clones are shown respectively in **Appendix A3.19** to **A3.27**.

Genes	**Recombinant vectors**	**Appendix**
rFIPFVE	pGLO:: H-rFIPFVE-Ek-GFP	**A3.19**
CWT-1	pGLO:: H-CWT1-Ek-GFP	**A3.20**
CWT-2	pGLO:: H-CWT2-Ek-GFP	**A3.21**
CWT-3	pGLO:: H-CWT3-Ek-GFP	**A3.22**
CWT-4	pGLO:: H-CWT4-Ek-GFP	**A3.23**
CWT-5	pGLO:: H-CWT5-Ek-GFP	**A3.24**
CWT-6	pGLO:: H-CWT6-Ek-GFP	**A3.25**
CWT-7	pGLO:: H-CWT7-Ek-GFP	**A3.26**
CWT-8	pGLO:: H-CWT8-Ek-GFP	**A3.27**

3.4 Discussion

This chapter describes the upstream procedures for the production of recombinant FIP-fve and eight variants in *E.coli* cells, which focused on the (i) isolation of *FIP-fve* cDNA template; (ii) design and SDM of *FIP-fve* variants; (iii) design and generation of *FIP-fve* and mutants gene cassettes; and (iv) construction of recombinant vector.

Herein, SDM was used to introduce desired mutations into the target DNA sequences. There are various methods of SDM. One of the most commonly known techniques was developed by Strategene called QuikChange™ Site-Directed Mutagenesis System, which is also known as inverse PCR method (Zheng, Baumann and Reymond, 2004). In this system, a complementary mutagenic primer pair anneals to plasmid DNA template during PCR, and extends a new strand of plasmid DNA that is incorporated with the mutation, producing a plasmid pool consisting of parental and mutant DNA. DpnI restriction enzyme is used to treat the DNA pool, digesting and eradicating the parental methylated DNA while retaining the newly generated unmethylated mutant plasmid DNA that is resistant to DpnI digestion. The remaining plasmid DNA was then transformed into *E. coli* where the host repair enzymes ligate the nick in the plasmid (Zheng, Baumann and Reymond, 2004). Nonetheless, the QuikChange™ SDM System poses several challenges. As the length of plasmid DNA is usually more than 3 kb, *Pfu* or *Vent* polymerases are preferentially used in SDM as they possess 3'-5' exonuclease activity that "proofread" any nucleotide-misincorporation errors resulted from 5'-3' DNA polymerase reaction in order to increase the sequence fidelity of the PCR products (Cline, 1996; Ling and Robinson, 1997). *Pfu* or *Vent* polymerases possess 6 to 15 times the sequence fidelity of *Taq* polymerase, which lacks the "proofread" ability (Cline, 1996). Nonetheless, the preferred *Pfu* is more expensive than *Taq* polymerase and therefore it increases the experimental cost. Furthermore, incomplete digestion of DpnI could cause the recovery of parental plasmid DNA besides mutated plasmid DNA, which reduces the success rate

of mutagenesis. Moreover, DNA sequencing is necessary to check and verify the selection of successfully developed mutants as verification via PCR amplification using specific primer or restriction enzyme digestion is not appropriate in which the PCR reaction is unable to differentiate a few nucleotides change in mutant DNA from parental DNA.

Instead of using inverse PCR technique, the SDM methods that were employed in this study was terminal changes PCR and/or overlap extension PCR techniques based on the positions of desired mutations. Terminal changes PCR technique provides a means of incorporating mutation in the beginning or end of a PCR fragment; whereas, the overlap extension PCR approach serves as a method of introducing mutations in the center of a PCR fragment (Pogulis, Vallejo and Pease, 1996). The resulting fragments of FIP-fve and variants were subsequently cloned into pGLO vector. This method separated the generation of PCR mutagenic fragments and construction of recombinant vectors into two steps, yet it offered almost 100% mutagenesis efficiency as mutations are certainly present in PCR products prior to cloning. DpnI digestion was not required to eliminate the parental strand like QuikChange™ system as the confirmed mutagenic fragments were used as the inserts for the subsequent cloning into vector. Therefore, the resulted transformants should harbor the mutagenic fragments. Notably, the overall mutagenesis process is simple and commercial kit is not needed, thus reducing the experimental cost.

As shown in **Figure 3.12**, **3.15-3.18**, there were faint bands that appeared on top of the DNA bands with the estimated sizes of PCR products. Generally, protein-nucleic acid complex has a slower migration rate as compared to the nucleic acid alone (Hellman and Fried, 2007), hence the faint band that moved slower may represents the DNA polymerase-nucleic acid complexes rather than a result of unspecific DNA amplification. Analysis of sequencing result has further validated the successful generation of a single species of the individual rFIP-fve and variants genes.

pGLO vector comprised of the easily modulated pBAD promoter that is a moderately strong promoter associated with tight regulation. This is one of the advantages of pBAD promoter possesses over other strong promoter as problem that may arise from excessive production of protein can be avoided when protein is moderately expressed (Guzman *et al.*, 1995). The strong promoter expression systems may generate an overproduction of protein yield exceeding 50% of total cellular proteins, which results in adverse effect on the folding of newly synthesized protein such as formation of inclusion bodies (Baneyx and Mujacic, 2004). In high level protein expression, there is a high chance of interaction between the hydrophobic stretches of polypeptide that are present at crowded concentration, leading to protein instability and aggregation that is known as inclusion bodies (Rosano and Ceccarelli, 2014). In addition, the over-saturated of recombinant proteins also burden protein quality control mechanism of molecular chaperones, which act to ensure the correct folding of newly synthesized polypeptide. Under oversaturation condition, some newly synthesized polypeptides may "escape" from the quality control mechanism and fold incorrectly, resulting in formation of inclusion bodies. In some cases, hyper-production of protein may also cause destruction of rRNA and ribosome, accumulation of heat shock proteins, and lethality of the host cells (Dong, Nilsson and Kurland, 1995). On the other hand, pBAD vectors have been shown to be able to achieve a moderately high expression that is sufficient for recombinant protein production, yet the production level is modulated within the boundary that may otherwise cause detrimental effect on host cells like the strong promoter. In fact, the substitution of strong vector in use with pBAD vector was shown to alleviate the protein overproduction complication such as formation of inclusion bodies and lethality (Guzman *et al.*, 1995). In this regard, the moderate pBAD promoter was used in this study to reduce the protein production rate as well as the cellular protein concentration, ensuring sufficient time for the newly synthesized recombinant proteins to fold correctly.

In recombinant production strategy, one of the most important aspects to consider during gene cassettes design was to purify the target proteins efficiently and inexpensively (Costa *et al.*, 2014). For this reason, the recombinant proteins were designed to be affinity tagged using hexahistidine tag for IMAC purification. In addition to affinity tag, a GFP reporter tag was also included where its fluorescent properties allow an additional round of purification to complement the affinity tagging via manual size-exclusion chromatography (SEC). In this research, the SEC was conducted manually without the use of automated chromatography system, in such manner information such as chromatogram was not available for protein peak detection. Therefore, the fluorescent from GFP serves as an indicator of the recombinant proteins, allowing collection of the GFP-tagged recombinant proteins via fluorescent visualization. The protocol of protein purification is discussed further in **Chapter 4**.

In selecting N or C termini for the fusion tag, the nature of FIP-fve structure based on PDB ID: 1OSY together with the rationale discussed in **Chapter 2 Section 2.4.2** were taken into consideration. According to FIP-fve structure that is deposited in PDB, the two N-terminal α-helices of FIP-fve that are crucial for dimerization are embedded inwards and serve as the core centre of the two monomers, whereas C-terminal of FIP-fve protrude outwards from the main domain of FIP-fve. Hence, it is hypothesized large size fusion tags such as GST or GFP that are introduced at the N-terminal of FIP-fve could possibly cause steric hindrance to the structure, while C-terminal serve as a better choice for tagging large size fusion tag. In fact, the previous finding by Kong and colleagues (2013) also substantiated this hypothesis where it was shown that the expression level of 6xhis:rFIP-fve was six times higher than GST:rFIP-fve that was produced by Ko and research group (1997); the recombinant proteins in these two studies were synthesized using *E.coli*. The introduced GST at the N-terminal of FIP-fve is much larger as compared to 6xhis tag, which could affect the folding of rFIP-fve and explain the difference of

expression level in the two studies. On the other hand, the small histidine tag would not affect the N-terminal structure of the protein of interest, maintaining its structural characteristics (Gräslund *et al.*, 2008). Taking into account above discussion, the site of fusion tags in this study were designed as followed: the smaller size of hexahistidine fusion tag was inserted at the N-terminal of recombinant proteins, while the larger size of GFP fusion tag was incorporated at the C-terminal of the recombinant proteins. Apart from that, an enterokinase cleavage site was introduced at the C-terminal of recombinant proteins (in between of the target protein and GFP coding sequence). The enterokinase cleavage site was added so that GFP can be cleaved off in case if GFP interferes the protein characteristics. Enterokinase cleavage site allows recognition by a specific protease called enterokinase at cleavage site of Asp-Asp-Asp-Asp-Lys (Hosfield and Lu, 1999).

3.5 Conclusion

In conclusion, the expression cassettes for FIP-fve and eight mutant genes were constructed and cloned into pGLO vectors successfully. A total of nine recombinant clones were generated, namely pGLO:: H-rFIPFVE-Ek-GFP, pGLO:: H-CWT1-Ek-GFP, pGLO:: H-CWT2-Ek-GFP, pGLO:: H-CWT3-Ek-GFP, pGLO:: H-CWT4-Ek-GFP, pGLO:: H-CWT5-Ek-GFP, pGLO:: H-CWT6-Ek-GFP, pGLO:: H-CWT7-Ek-GFP and pGLO:: H-CWT8-Ek-GFP. TOP10 *Escherichia coli* host cells were transformed with these recombinant vectors, and were ready to be used for protein expression, by which details are presented in **Chapter 4**.

Chapter 4 Protein Expression and Purification of Recombinant FIP-fve and Mutants from *Escherichia coli*

4.1 Introduction

The successful production of recombinant protein is dependent on correlation between expression of gene, solubility of protein and purification of protein (Costa *et al.*, 2014). The rationale underlying choice of expression vector used to express recombinant proteins as well as the selection of fusion tags incorporated to facilitate protein purification have been discussed in Chapter 3. This chapter focuses on strategy taken in expression and purification of recombinant FIP-fve and mutant proteins in *Escherichia coli*. In recombinant protein production, it is known that protein purification generally accounts for the highest expenses. Thus, protein purification strategy is one of the most important aspects to be considered to ensure that the protein production method is simple, direct and cost-effective. Affinity tag is usually designed to be attached to target protein using recombinant DNA technology, benefiting the subsequent purification strategy by simplifying the purification process. Affinity chromatography also permits the proteins to maintain its properties without direct interaction with matrix (Costa *et al.*, 2014).

In affinity chromatography, proteins are separated via a reversible interaction between the protein of interest and a specific ligand linked to a matrix. In this purification pipeline, the target protein is first captured by the ligand under favourable conditions for that interaction. The weakly bound-proteins and impurities are washed out of the column in washing step. Subsequently, the bound target proteins are eluted using a competitive ligand or changing polarity, ionic strength or pH (GE healthcare, 2010). Some of the commonly used affinity tags include histidine, glutathione S-transferase (GST), maltose binding protein (MBP), and calmodulin binding peptide (CBP) (Kimple, Brill and Pasker, 2013).

Herein, immobilized metal-affinity chromatography (IMAC) was used to purify recombinant proteins carrying hexahistidine residues. IMAC is a commonly employed technique to purify recombinant proteins harbouring a peptide affinity tag of polyhistidine residues (Bornhorst and Falke, 2000). It offers high selectivity with strong and specific binding coupled with mild elution condition, therefore most of the commercial expression vectors and purification reagents provided are related to the polyhistidine tag. Histidine tag normally comprised of six consecutive histidine residues but the number of residues can vary from two to ten residues (Kimple, Brill and Pasker, 2013). Immobilized metal ions such as Ni^{2+}, Cu^{2+}, Co^{2+}, Fe^{3+}, Ca^{2+} and Zn^{2+} have been used to purify polyhistidine fused-proteins as the histidine quickly establishes coordination bonds with these metal ions (Kimple, Brill and Pasker, 2013). There are various immobilized metal matrices that are commercially available for IMAC. Iminodiacetic acid (IDA) was utilized initially as IMAC matrix to chelate immobilized metals via three coordination sites (Bornhorst and Falke, 2000). Nonetheless, the weak interaction (three coordination sites) formed between IDA matrix and metal ion causes metal leaching from matrix, resulting in loss of protein yield (Crowe *et al.*, 1994). Therefore, nickel(II)-nitrilotriacetic acid (Ni-NTA) matrix and cobalt(II)-carboxylmethylaspartate (Co-CMA) are developed subsequently to improve the feasibility of IMAC system. Ni-NTA and Co-CMA secure the linked metal ions via four coordination sites. The two of the immobilized metal coordination sites are exposed to interact with polyhistidine residues that are carried by recombinant proteins. Molecular models of these interactions are demonstrated in **Figure 4.1**. One additional benefit of IMAC is that it recognizes histidine residues without relying on the conformation of the peptide tag, making the purification condition amendable if denaturing condition is required for purification of insoluble proteins (Bornhorst and Falke, 2000).

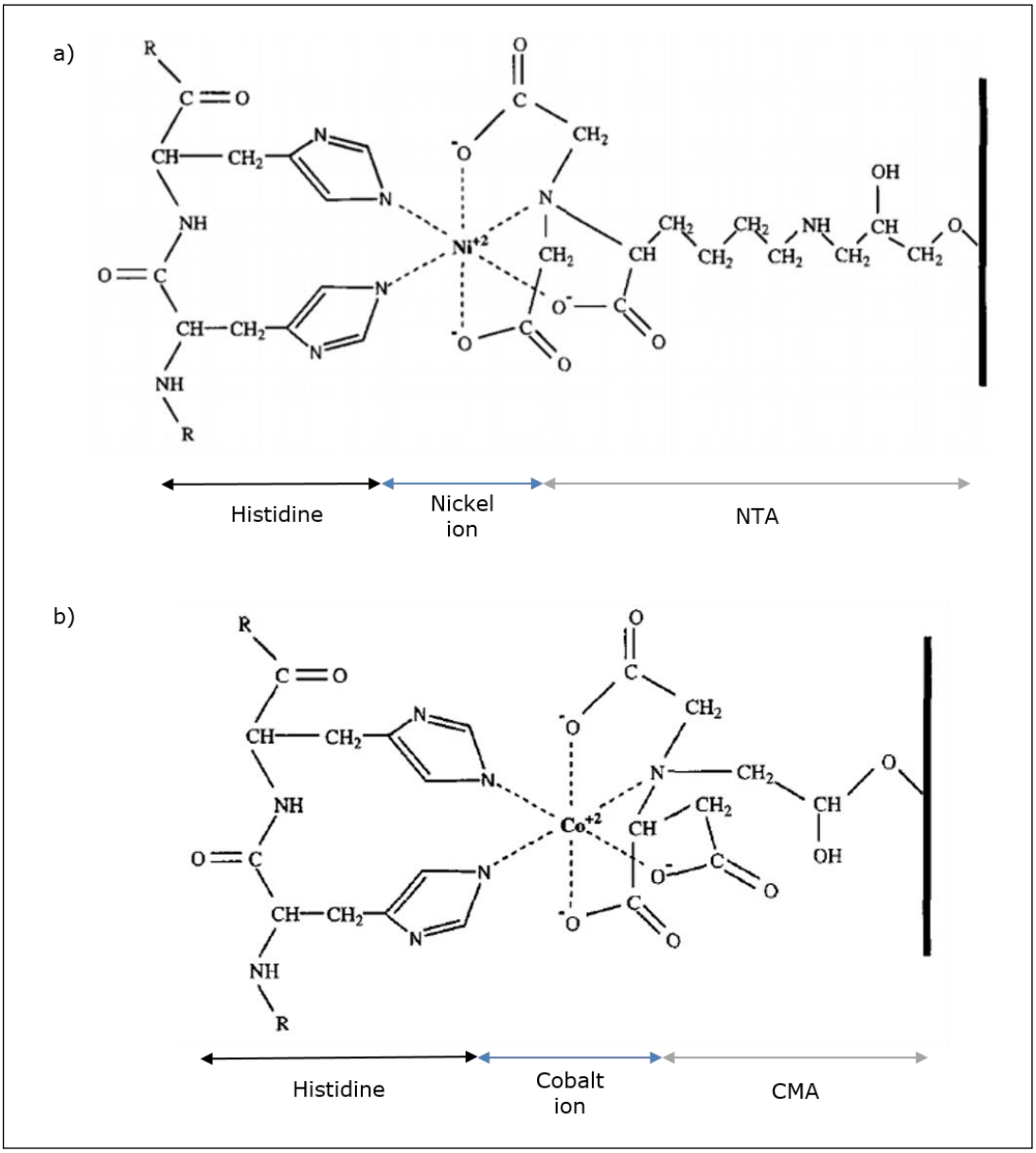


Figure 4.1. Model of interaction between (a) histidine residues in affinity tag and nickel-nitrilotriacetic acid (Ni-NTA) matrix. Image adopted from Crowe *et al.* (1994) and (b) histidine residues in affinity tag and cobalt-carboxylmethylaspartate (Co-CMA). Image adopted from Bornhorst and Falke (2000).

Additional physiochemical-based chromatography methods are usually added to the purification process to complement the affinity purification. For example, the approaches include size exclusion chromatography (SEC), hydrophobic interaction chromatography (HIC) and ion exchange chromatography (IEX) that separate and purify the proteins based on size, hydrophobicity and charge respectively (GE healthcare, 2010). SEC was employed in this study as a polishing step for buffer exchange of the recombinant proteins that was first purified using IMAC. As mentioned in Chapter 3, a GFP fluorescent reporter tag was also incorporated to the recombinant proteins in addition to affinity tag for the purpose of polishing step via SEC, which was conducted manually without the use of automated chromatography system in this study. In such manner, automatic protein peak detection in the form of chromatogram was not available. For this reason, the fluorescent from GFP fusion partner serves as an indicator for the recombinant proteins, allowing collection of GFP-tagged recombinant proteins via fluorescent visualization. SEC is a simple and efficient method that is able to get rid of low molecular weight and transfer the protein sample into desired buffer (GE healthcare, 2010). SEC resins comprised of porous matrix of spherical particles that are lack of adsorptive and reactivity properties. The flow rate of the molecules varies based on the molecule size as molecules with different sizes have varying degree of penetration into the pore. As shown in **Figure 4.2**, large molecules are eluted first as they are larger than the pores, therefore unable to diffuse into the beads. Smaller molecules such as proteins enter the pores in the resin at different extent and elute later than the large molecules. Other low molecular weight substances or salt enter the total pore volume of the resin, and elute last (GE healthcare, 2010). Therefore, SEC served as a technique that was used to exchange the buffer that contained high concentration of imidazole that was introduced during the elution step of IMAC, removing the small molecule imidazole.

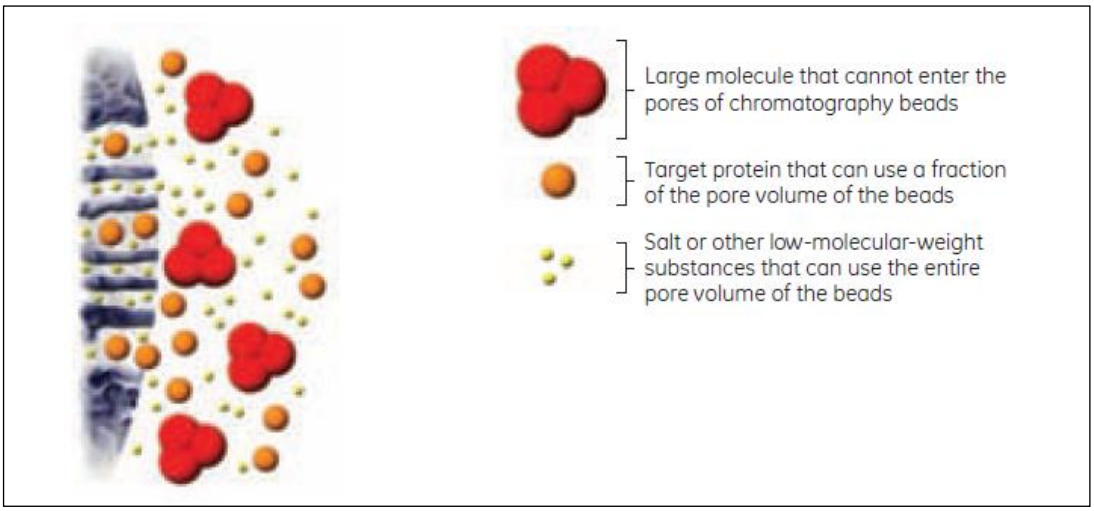


Figure 4.2. Diagram illustrating theory of size exclusion chromatography (SEC). Image adopted from GE healthcare (2010).

Chapter 4 describes and discusses on the generation and construction of recombinant expression vectors for *rFIP-fve* and mutants. In this chapter, protein expression and purification of the recombinant FIP-fve and deriviative proteins that were synthesized in TOP10 *Escherichia coli* cells harbouring pGLO:: H-rFIPFVE-Ek-GFP, pGLO:: H-CWT1-Ek-GFP, pGLO:: H-CWT2-Ek-GFP, pGLO:: H-CWT3-Ek-GFP, pGLO:: H-CWT4-Ek-GFP, pGLO:: H-CWT5-Ek-GFP, pGLO:: H-CWT6-Ek-GFP, pGLO:: H-CWT7-Ek-GFP and pGLO:: H-CWT8-Ek-GFP are presented and discussed. The nine recombinant proteins were produced in TOP10 *E. coli* cells by using L(+)-arabinose as protein expression inducer agent. The bacterial cells were subsequently ruptured using sonication to release crude lysates. IMAC was used to purify the target recombinant proteins containing hexahistidine tag under native condition. Subsequently, IMAC-purified proteins were subjected to SEC as a mean of buffer exchange to substitute the buffer that contained a high concentration of imidazole into buffer that is suitable for subsequent functional assay study. Hence, the specific objectives for this chapter are: (i) to produce recombinant proteins in *E.coli* cells; (ii) to release the synthesized recombinant proteins from *E.coli* cells; (iii) to purify target recombinant proteins using IMAC; (iv) to change the buffer composition of IMAC-purified recombinant proteins using SEC.

4.2 Materials and methods

4.2.1 General materials and specialised equipment

The general materials such as bacterial culture agar and broth as well as specialized equipment used in this study are described in this section.

4.2.1.1 Agar and broth culture preparation

LB Lennox agar and broth medium were prepared according to the protocols as described in **Chapter 3 Section 3.2.1.1**.

4.2.1.2 Specialised equipment

For the incubation temperature of 20˚C and 25˚C, bacterial culture plate was incubated in FOC 120i cooled incubator (VELP® Scientifica, USA) (Binder, Germany). For the incubation temperature at 37˚C, bacterial culture plate was incubated in BINDER Microbiological Incubator (Binder, Germany). Bacterial cultivation in flask was carried out using FOC 120i cooled incubator and TS-520 orbital shaker (YIH DER, China); the shaker was placed into the cooled incubator. The cooled incubator allows adjustable temperature from 3 to 50˚C. Optical density of bacterial culture was measured using BioPhotometer Plus (Eppendorf®, Germany). Centrifugation was performed using centrifuge 5810 R (Eppendorf™, USA).

4.2.2 Expression of recombinant FIP-fve and mutants proteins from Escherichia coli system

Recombinant FIP-fve and mutants proteins were expressed in TOP10 cells carrying recombinant vectors pGLO:: H-rFIPFVE-Ek-GFP, pGLO:: H-CWT1-Ek-GFP, pGLO:: H-CWT2-Ek-GFP, pGLO:: H-CWT3-Ek-GFP, pGLO:: H-CWT4-Ek-GFP, pGLO:: H-CWT5-Ek-GFP, pGLO:: H-CWT6-Ek-GFP, pGLO:: H-CWT7-Ek-GFP and pGLO:: H-CWT8-Ek-GFP.

4.2.2.1 Bacterial agar plates

As the transformants cells were stored in frozen glycerol stocks for long term storage of recombinant plasmids, bacterial cell recovery was conducted prior to protein expression induction. Sterile loops were used individually to scrape some of the frozen TOP10 cells harbouring recombinant vectors and streaked over LB agar surface using 4-ways streaking technique, and incubated at 37˚C for 16 hr to isolate individual clonal population. The procedure was conducted within sterile field created by Bunsen burner flame.

4.2.2.2 Optimization of protein expression

The temperature that was suitable for the protein expression was determined by incubating the bacterial culture at different temperatures. Each of the transformants was streaked on two LB agar plate supplemented with filter-sterilized 0.2% (w/v) L-(+)-arabinose (Sigma-aldrich®, Germany), and the respective plates were incubated at 20˚C, 25˚C and 37 ˚C for 48, 48 and 16 hr respectively. The bacterial plates were visualized for the fluorescence intensity of GFP as a result of expression of fusion recombinant proteins carrying GFP tag using Gel Doc™ XR system (Bio-Rad Laboratories, USA) and analyzed using Image Lab™ Software (Bio-Rad Laboratories, USA).

4.2.2.3 Starter culture

Bacterial colonies carrying the recombinant vectors were picked individually from the agar plates and inoculated in 250 ml erlemenyer flasks containing 20 ml LB broth with 100 µg/ml ampicillin, and incubated in incubator shaker for 16 hr at 37˚C with speed of 180 rpm. The inoculation procedure was carried out within sterile field created by Bunsen burner flame.

4.2.2.4 Protein induction

After 16 hr of incubation, starter cultures were diluted individually in 1:100 into a fresh 1L erlemenyer flask containing 200 mL LB broth with 100 µg/ml ampicillin. The cells were allowed to grow until optical density $(OD)_{600}$ reached 0.6. Subsequently, filtered-sterilized inducing agent L-(+)-arabinose was added into the individual bacterial culture to a final concentration of 0.2% (w/v) L-(+)-arabinose, which is the recommended concentration according to manufacturer protocol for pGLO vector (Bio-Rad laboratories, USA). The procedure was carried out within sterile field created by Bunsen burner flame. Sterile cotton plug was used to cap the mouth of the flasks, which permitted free passage of air into the flask. Erlenmenyer flasks containing bacterial culture were incubated at 20˚C for 48 hr with a speed of 180 rpm.

4.2.2.5 Protein extraction

After 48 hr of incubation, bacterial cells were pelleted individually using centrifugation at 8,000 x g for 5 min. Cell pellets were stored in -20˚C until further use. The cell pellets were resuspended in 5 mL of chilled lysis buffer (50 mM Tris-HCl pH 7.5, 200 mM sodium chloride, 10% glycerol) and kept on ice. Sonicator probe microtip with diameter of 1/4" was immersed into cell suspension (in 50 mL falcon tube that was placed on ice), and sonicated at 35% amplitude with 5 short burst of 10 s followed by interval of 10 s cooling using Q500 sonicator (QSONICA, USA). The cell suspension was centrifuged at 8,000 x g for 15 min to pellet debris. The cell lysates were collected. The collected cell lysates were stored in -20˚C. As the pellet debris may contain unlysed cells, the extraction process was repeated for another round to ensure adequate lysis of cell.

4.2.2.6 Immobilized metal-ion affinity chromatography

IMAC was performed to capture and isolate the 6xhis-tag fused recombinant proteins using HIS-Select Nickel Affinity Gel (Sigma-aldrich®, USA). An amount of 10 mL of 50% suspension (in 30% ethanol) of HIS-Select Nickel Affinity Gel was transferred to a chromatography column. The affinity gel was washed with 2 volumes of deionized water and followed by 3 volumes of Equilibrium Buffer (50 mM sodium phosphate pH 8.0, 0.3 M sodium chloride, and 10 mM imidazole). The cell lysates were loaded onto the column. After loading of lysates, the column was washed with Wash Buffer (50 mM sodium phosphate pH 8.0, 0.3 M sodium chloride, and 10 mM imidazole). The recombinant proteins carrying histidine tag were eluted using Elution Buffer (50 mM sodium phosphate pH 8.0, 0.3 M sodium chloride and 250 mM imidazole), and the fractions were collected in 2 mL microcentrifuge tubes. Fluorescence of all tube fractions were visualized using Gel Doc™ XR system (Bio-Rad Laboratories, USA) and analyzed using Image Lab™ Software (Bio-Rad Laboratories, USA) to select fractions that fluoresced attributed to the GFP tag containing in fusion recombinant proteins. An example of which is shown in **Appendix A4.1**.

4.2.2.7 Size exclusion chromatography

SEC was used to further purify and exchange buffer of IMAC-purified recombinant proteins via separation of samples according to molecular weight using gel matrix Sephacryl® S200HR (Sigma-aldrich, USA) and Econo™ Gradient Pump (Bio-Rad Laboratories, USA). The gel matrix Sephacryl® S200HR was transferred into a chromatography column (1.5 x 50 cm). The Econo™ gradient pump is a peristaltic two-channel bidirectional pump. The setup of SEC is shown in **Figure 4.3**. Channel I of Econo™ Gradient Pump was linked to desired injection solution, whereas Channel II of Econo™ Gradient Pump was connected to chromatography column with gel matrix. The solution was drawn from the injection solution and directed into chromatography gel

matrix at a control designated flow rate. The column was first equilibrated with 2 column volumes of buffer (0.05 M sodium phosphate, 0.15 M sodium chloride, pH 7) at flow rate of 3 ml/min. The flow was paused when approximately 1 ml of buffer was left on top of the gel. The IMAC-purified recombinant protein was then loaded on top of the gel media and the flow was resumed at flow rate of 1 ml/min. The protein was eluted with 1 column of buffer at flow rate of 1 ml/min. The buffer of IMAC-purified recombinant proteins that contained high concentration of imidazole (250 mM) was removed during the process. The flow of recombinant proteins with fluorescent GFP tag were constantly checked with hand-held UV light (excitation wavelength: 395nm). The protein fractions were subsequently collected in 2 mL tubes. Fluorescence of all tube fractions were visualized to select fractions that fluoresced attributed to the GFP tag containing in fusion recombinant proteins. An example of which is shown in **Appendix A4.2**.

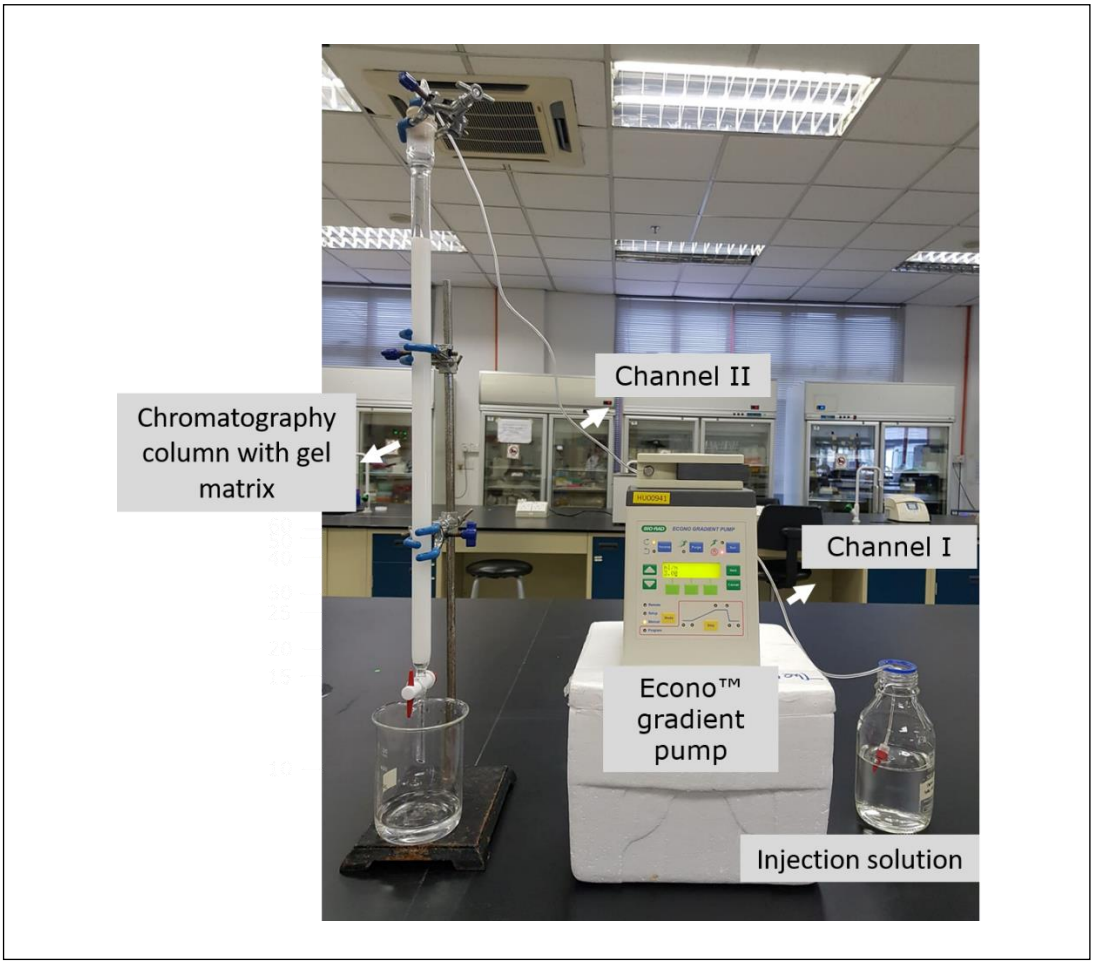


Figure 4.3. Setup of size exclusion chromatography. Channel I and II of Econo™ Gradient Pump was connected to injection solution and chromatography column with gel matrix Sephacryl® S200HR respectively. Econo™ Gradient Pump drawn and directed solution into the chromatography gel matrix at a control designated flow rate.

4.2.2.8 Protein concentration determination

Protein concentration was measured using Epoch microplate spectrophotometer with Take3 micro-volume plate (BioTek®, USA) and analysed using Gen5 Data Analysis Software (BioTek®, USA). The extinction coefficient and estimated protein molecular weight of the recombinant proteins were determined based on the amino acid sequences using EMBOSS Pepstats (**Appendix A4.3**).

4.2.2.9 SDS-PAGE

Sodium dodecyl sulfate polyacrylamide gel electrophoresis (SDS-PAGE) was performed using gel electrophoresis system (Amersham Biosciences, United Kingdom). A 12% resolving gel and a 4% stacking gel was used to determine the purity and molecular weight of the purified proteins. The formulations of resolving and stacking gel are shown in **Appendix 4.4**. About 1 µg of each of the recombinant proteins was mixed with SDS sample loading buffer and incubate at 95˚C for 10 min prior to electrophoresis. The SDS gel was soak in SDS running buffer (25 mM Tris, 192 mM glycine, 0.1% SDS, pH 8.3), and the electrophoresis was performed at 110 V for 90 min. The electrophoresed gel was stained with Coomassie brilliant blue R250 for 2 hr. After 2 hr, the gel was destained overnight using distilled water. The destained gel was captured using Gel Doc™ XR system. The protein bands of each lane in SDS-PAGE were analysed using Image Lab™ software in order to determine the protein purity.

4.2.2.10 Native PAGE

Native-PAGE gel electrophoresis was performed using gel electrophoresis system (Amersham Biosciences, UK). A 12% resolving gel and a 4% stacking gel was used to visualize the fluorescent intensity of the purified proteins. The formulations of resolving and stacking gel are shown in **Appendix 4.4**. About 1 µg of each of the recombinant proteins was mixed with native sample loading buffer and loaded into the gel for gel electrophoresis. The electrophoresed gel was visualized using UV transilluminator and gel image was captured using camera with filter kit (#58 green) (Peca® Products Inc., USA). The electrophoresed gel was subsequently stained with Coomassie brilliant blue R250 for 2 hr. After 2 hr, the gel was destained overnight using distilled water. The destained gel was captured using Gel Doc™ XR system and analyzed using Image Lab™ software.

4.3 Results

4.3.1 Protein expression at different temperatures

The expression of proteins at different temperatures was compared based on the fluorescence intensity of GFP tag containing in fusion proteins that were expressed by TOP10 *Escherichia coli* cells carrying pGLO, pGLO:: H-rFIPFVE-Ek-GFP, pGLO:: H-CWT1-Ek-GFP, pGLO:: H-CWT2-Ek-GFP, pGLO:: H-CWT3-Ek-GFP, pGLO:: H-CWT4-Ek-GFP, pGLO:: H-CWT5-Ek-GFP, pGLO:: H-CWT6-Ek-GFP, pGLO:: H-CWT7-Ek-GFP and pGLO:: H-CWT8-Ek-GFP. As shown in **Figure 4.4**, the fluorescence intensity of bacterial cell harbouring pGLO was the highest at 20˚C, but remained similar at 25˚C and 37˚C. Whereas, the fluorescence intensity of bacterial cell carrying recombinant vectors varied among the mutant strains as well as differed at different temperature. The optimum protein expression of the bacterial harboring recombinant vectors was determined at 20˚C as the fluorescence intensity of the bacterial was the highest at this temperature. Therefore, the recombinant proteins were expressed at 20˚C for the subsequent experiment.

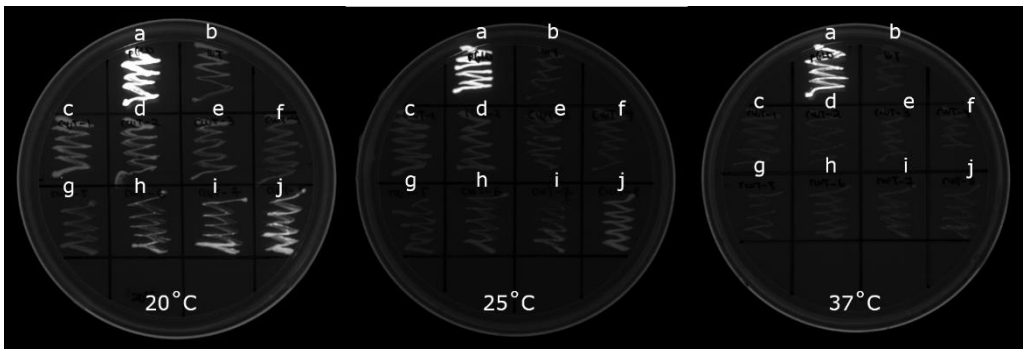
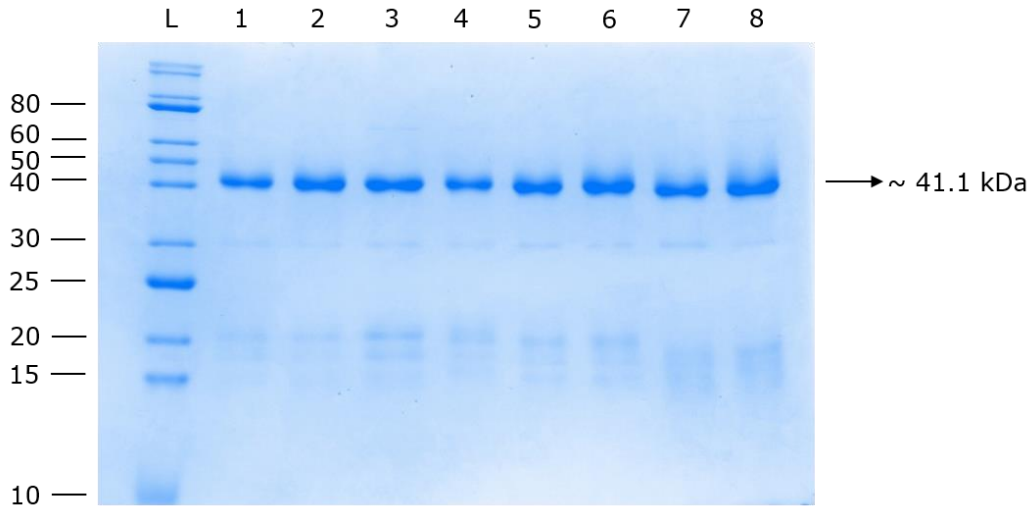


Figure 4.4. Comparison of protein expression level based on fluorescence intensity of GFP containing tag in fusion proteins that were synthesized by bacterial harbouring (a) positive control pGLO, (b) pGLO:: H-rFIPFVE-Ek-GFP, (c) pGLO:: H-CWT1-Ek-GFP, (d) pGLO:: H-CWT2-Ek-GFP, (e) pGLO:: H-CWT3-Ek-GFP, (f) pGLO:: H-CWT4-Ek-GFP, (g) pGLO:: H-CWT5-Ek-GFP, (h) pGLO:: H-CWT6-Ek-GFP, (i) pGLO:: H-CWT7-Ek-GFP and (j) pGLO:: H-CWT8-Ek-GFP at 20˚C, 25˚C and 37˚C.

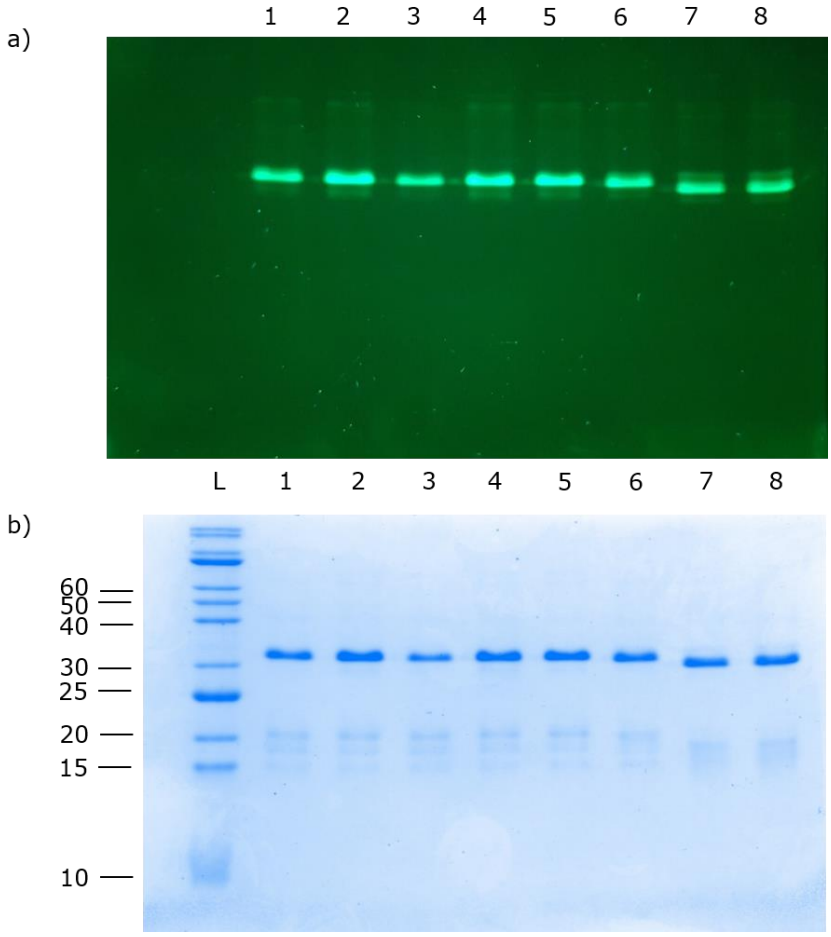
4.3.2 Protein purification

All of the recombinant proteins have been successfully expressed and purified from TOP10 *Escherichia coli* cells carrying pGLO:: H-rFIPFVE-Ek-GFP, pGLO:: H-CWT1-Ek-GFP, pGLO:: H-CWT2-Ek-GFP, pGLO:: H-CWT3-Ek-GFP, pGLO:: H-CWT4-Ek-GFP, pGLO:: H-CWT6-Ek-GFP, pGLO:: H-CWT7-Ek-GFP and pGLO:: H-CWT8-Ek-GFP at estimated size of 41.1 kDa except pGLO:: H-CWT5-Ek-GFP as demonstrated in **Figure 4.5**. H-CWT5-Ek-GFP was unable to be recovered from the crude lysates of TOP10 cells with pGLO:: H-CWT5-Ek-GFP as it was eluted in Washing Buffer during the washing step. The purity of all recombinant proteins following purification via two-steps purification were over 70% as determined by SDS-PAGE. The analysis report of protein purity is included in **Appendix A4.5**. As shown in native PAGE (**Figure 4.6**), all of the purified recombinant proteins containing GFP tags fluoresced when they were viewed under UV transilluminator, whereas no fluorescence was detected in other protein bands. This further confirmed the identity of the purified recombinant proteins.



Lane	Sample	Estimated size (kDa)	Purity (%)
L	Unstained Protein Standard, Broad Range (10-200 kDa)	-	-
1	H-rFIPFVE-EK-GFP	~41.1	83.6
2	H-CWT1-EK-GFP	~41.1	94.6
3	H-CWT2-EK-GFP	~41.1	73.0
4	H-CWT3-EK-GFP	~41.1	81.0
5	H-CWT4-EK-GFP	~41.1	81.2
6	H-CWT6-EK-GFP	~41.1	77.4
7	H-CWT7-EK-GFP	~41.1	78.3
8	H-CWT8-EK-GFP	~41.1	70.0

Figure 4.5. SDS-PAGE profile of coomassie blue-stained 1 µg of recombinant proteins H-rFIPFVE-EK-GFP, H-CWT1-EK-GFP, H-CWT2-EK-GFP, H-CWT3-EK-GFP, H-CWT4-EK-GFP, H-CWT6-EK-GFP, H-CWT7-EK-GFP, and H-CWT8-EK-GFP that were recovered from two-steps purification using IMAC and SEC. The purity of the purified recombinant proteins are presented herein.



Lane	Sample
L	Unstained Protein Standard, Broad Range (10-200 kDa)
1	H-rFIPFVE-Ek-GFP
2	H-CWT1-Ek-GFP
3	H-CWT2-Ek-GFP
4	H-CWT3-Ek-GFP
5	H-CWT4-Ek-GFP
6	H-CWT6-Ek-GFP
7	H-CWT7-Ek-GFP
8	H-CWT8-Ek-GFP

Figure 4.6. Native-PAGE profile of (a) unstained and (b) coomassie-blue stained of 1 µg of recombinant proteins H-rFIPFVE-Ek-GFP, H-CWT1-Ek-GFP, H-CWT2-Ek-GFP, H-CWT3-Ek-GFP, H-CWT4-Ek-GFP, H-CWT6-Ek-GFP, H-CWT7-Ek-GFP, and H-CWT8-Ek-GFP that were recovered from two-step purification using IMAC and SEC.

The yield of the rFIP-fve and mutants proteins generated and purified from 1 L bacterial culture was listed in **Table 4.1**. The amount of protein expression was in correlation to the fluorescent intensity of bacterial cells harboring the recombinant vectors as shown in **Figure 4.4**. In other words, the higher the fluorescent intensity, the higher the amount of recombinant protein expression. Among all of the synthesized and purified recombinant proteins, the protein yield of purified recombinant proteins H-CWT7-EK-GFP and H-CWT8-Ek-GFP were the highest; whereas the protein yield of purified recombinant protein H-CWT4-Ek-GFP was the lowest.

Table 4.1. Protein yield of synthesized recombinant H-rFIPFVE-Ek-GFP and derivatives protein in 1 L bacterial culture.

Recombinant proteins	**Protein yield (mg/L)**
H-rFIPFVE-Ek-GFP	6.00
H-CWT1-Ek-GFP	19.00
H-CWT2-Ek-GFP	5.75
H-CWT3-Ek-GFP	7.50
H-CWT4-Ek-GFP	1.07
H-CWT6-Ek-GFP	19.00
H-CWT7-Ek-GFP	34.00
H-CWT8-Ek-GFP	35.50

4.4 Discussion

TOP10 *Escherichia coli* was used in this study as the host cells for recombinant protein production. Wild type *E. coli* strain can use L-(+)-arabinose as a source of carbon and energy, whereas TOP10 strain is a modified strain with genotypes of araEFGH^{+} and araBADC^{-} that allow transportation of L-(+)-arabinose but lack of capability of metabolizing the L-(+)-arabinose (Invitrogen, 2010). It is important to mention that the pGLO vector employed in this study comprised of an araBAD promoter system that relies on the presence of an inducer, L-(+)-arabinose in initiating the target gene transcription and followed by protein expression. Hence, TOP10 strain is the suitable host for araBAD promoter system as the level of L-(+)-arabinose remains constant inside the cells, which permits the recombinant protein expression to take place steadily.

The araEFGH proteins are involved in the transportation of L-(+)-arabinose in *E.coli*. There are two transport systems in *ara* system, which are low and high affinity transport systems. In low affinity transport system, *araE* encoding for transporter attaches to inner membrane and employs electrochemical potential for arabinose transportation. In high affinity transport system, the araFGH genes encodes for proteins components of an ABC transporter in which: AraF is periplasmic arabinose-binding protein; AraG is ATP-binding component; and, AraH is membrane-bound component (Kolodrubetz and Schleif, 1981). With araEFGH^{+}, TOP10 strain is able to transport the L-(+)-arabinose into the cell (Bachmann, 1990).

While araEFGH proteins are engaged in the L-(+)-arabinose transportation, the four genes, *araB*, *araA*, *araD*, and *araC* encoding for enzymatic proteins that are responsible for conversion of L-arabinose to D-xylulose-5-phosphate (Gross and Englesberg, 1959). AraA is an L-arabinose isomerase that converts L-(+)-arabinose to L-ribulose; AraB is a kinase that phosphorylates L-ribulose; and AraD is an epimerase that

converts L-ribulose-phosphate to D-xylulose-phosphate (Englesberg, 1961). The conversion process of L-arabinose to D-xylulose-5-phosphate relies on AraC protein as it plays the main role in regulating the transcription in araBAD promoter. AraC protein possesses dual roles as activator or repressor (Wilcox *et al.*, 1974). Owing to the fact that these four genes are involved in the metabolism of L-arabinose in wild type *E.coli*, the four genes were removed in TOP10 strain, making it unable to metabolize arabinose.

The pGLO vector is designed to harbour the *araC* gene in which the gene products, AraC protein is responsible in modulating the transcription in araBAD promoter. In the absence of L(+)-arabinose inducer, AraC dimer represses transcription by contacting to O_2 and I_1 sites of the *araBAD* operon, forming a protein-DNA loop that prevents RNA polymerase from binding to pBAD promoter (Soisson *et al.*, 1997). In the presence of the inducer, L-arabinose interacts directly with AraC dimer, releasing binding from O_2 site and contact the I_2 site that is adjacent to I_1; this allows RNA polymerase to bind to the promoter, and subsequently gene expression takes place (Soisson *et al.*, 1997). Due to the reasons discussed above, pGLO vector must be complemented with TOP10 *E.coli* as it allows the level L-(+)-arabinose to remain stable in the cells, and the L-(+)-arabinose in turn serves to activate the transcription of gene of interest.

The optimized temperature for protein synthesis was determined using three different temperatures at 20˚C, 25˚C and 37˚C. The fluorescent intensity of the GFP tag containing generated recombinant protein was used as an indicator for the recombinant protein expression level. According to **Figure 4.4**, bacteria cultivation at 20˚C was optimum for recombinant proteins expression in this study, whereas higher cultivation temperature at 25˚C and 37 ˚C showed reduction of protein synthesis. Indeed, lower temperature is often used in bacteria cultivation for protein synthesis to decrease protein aggregation by slowing down the protein synthesis rate and folding kinetics, which allows the molecular chaperones to process formation of folding intermediates efficiently

(Schumann and Ferreira, 2004). A further reduction on bacterial expression temperature was not explored in this study as over-reduction of temperature may affect rate of replication, transcription and translation, leading to reduction of bacterial growth and protein synthesis yield (Costa *et al.*, 2014). Hence, the condition of bacterial cultivation was set at 20˚C and complemented with a longer period of incubation (48 hr) in this research.

As shown in **Table 4.1**, the generated recombinant protein yields varied among the bacterial strains of rFIP-fve and mutant. The reason of which might be that the recombinant proteins possess different protein folding efficiencies, which influence their protein solubility. Therefore, the generated soluble protein yields were different among the recombinant proteins. For instances, the synthesized polypeptides of H-CWT7-Ek-GFP and H-CWT8-Ek-GFP may be more readily to fold into soluble proteins, thus the recovered soluble protein yield was considerably high. On the contrary, the generated polypeptide H-CWT4-Ek-GFP may be less favorable to fold into soluble proteins, hence the recovered soluble protein yield was low. The speculation will need further experiment to be verified. For example, circular dichroism is one well-established technique that can be used to assay the secondary structure of protein *in vitro* as different secondary structure contents represent different stages in protein folding and aggregation. It is important to note that neither possible insoluble fraction of the protein was retrieved for protein refolding nor cultivation condition was optimized to achieve higher soluble protein yield of the recombinant proteins. Considering the fact that it is time-consuming to conduct optimization for each of the recombinant proteins, the synthesized soluble proteins were made use of without further optimization. More bacterial cultivations were prepared to obtain sufficient protein in case if higher amount of recombinant proteins were needed for the functional studies. Therefore, this cultivation condition was proceeded as the ultimate

aim of the research was to produce sufficient recombinant proteins for determination of the structural and functional relationship of FIP-fve.

In term of protein purity, the purity of all recombinant proteins ranged from 70 to 95% where some of the impurities appeared to remain after two-steps purification procedure. This is a common problem encountered in the histidine affinity tag application as there is possibility that the untagged proteins could bind non-specifically to the immobilized ions (Bornhorst and Falke, 2000). Some cellular proteins may contain two or more naturally occurred adjoining histidine residues, which have affinity towards IMAC matrix and therefore co-elute with target protein. In fact, the problem of impurities contaminant is usually more pronounced in systems other than *E. coli*; for example in mammalian system, proteins with consecutive histidine residues are present abundantly (Crowe *et al.*, 1994). Further purification can be conducted to increase the homogeneity of the protein samples. However, the purity of purified recombinant proteins synthesized herein was regarded as adequately high, thus the purified proteins were applied for subsequent functional studies.

All of the designed recombinant proteins were successfully synthesized and purified except H-CWT5-Ek-GFP. It was the only recombinant protein that was unable to be purified in this study. The fluorescence intensity of bacterial cell carrying pGLO:: H-CWT5-EK-GFP was the lowest among bacterial cells harboring other recombinant vectors as demonstrated in **Figure 4.4**, which might indicate that majority of this particular protein was incorrectly folded, leading to the formation of insoluble protein. As the amount of the soluble H-CWT5-Ek-GFP in the crude extract was low, a total of 2 L of bacterial culture was prepared for this particular strain to increase the final amount of retrieved H-CWT5-Ek-GFP. However, H-CWT5-Ek-GFP was unable to be recovered in IMAC purification as it was eluted during washing step. It is unlikely that the H-CWT5-Ek-GFP was washed out due to incorrect binding conditions or high washing stringency as the other

recombinant proteins were successfully purified using the same condition. Hence, the reason of H-CWT5-Ek-GFP being washed out could be due to buried hexahistidine tag within the protein structure (as a result of improper folding), making it unable to bind onto the immobilized ions. H-CWT5-Ek-GFP is the derivative with adoption of both loop DE (S62P, N63S, F64Y, T67E, P68S, S69D, G71S) and FG (G101N, S103Del, E104Del, E105D, Y106F) regions from LZ-8. These mutations appeared to affect the protein structure of the recombinant protein H-CWT5-Ek-GFP. Interestingly, H-CWT8-Ek-GFP with only two amino acid residues differences to H-CWT5-Ek-GFP demonstrated much higher protein expression level as compared to H-CWT5-Ek-GFP. H-CWT8-EK-GFP carries the same mutation regions as H-CWT5-Ek-GFP, but H-CWT8-Ek-GFP also harbours two additional modifications at hinge loop DE residue (E61K) and hinge loop FG residue (I97D). This indicates that the amino acid residues E61K and I97D are potentially crucial for proper protein folding in the mutant that adopts both of the loop DE and FG regions, which may be responsible in positioning the loop regions outward without interrupting the protein structure.

Generally, a final polishing step is included in purification procedure to substitute the buffer composition of the purified protein sample in order to prepare the purified protein before the end application. In this research, SEC was applied to exchange the buffer of IMAC-purified protein sample that contained a high concentration of imidazole, which may potentially interfere subsequent biological assay. Apart from SEC, another commonly used buffer exchange method includes dialysis (GE healthcare, 2010). Dialysis utilises a selectively permeable membrane that allows diffusion of small molecules through permeable membranes and retains only large molecules within the membrane. In protein dialysis, protein sample is contained in a sealed dialysis membrane and immersed in desired buffer, then equilibrium of small molecules takes place slowly between protein sample and dialysate. Normally, several rounds of dialysis are required to achieve

sufficient level of buffer exchange (Andrew, Titus and Zumstein, 2001). Therefore, dialysis requires a large volume of buffer during dialysis process and it is time-consuming, which could pose a risk in protein degradation when buffer exchange process is prolonged. On the other hand, gel filtration offers an efficient and rapid approach to process buffer exchange of a protein sample. Depending on the sample volume, there are different formats available for gel filtration such as: single use column (small sample volume), gravity-flow column (small sample volume) and chromatography system (large sample volume). The single use column is quick and convenient but it is limited to processing of small sample volume and it is expensive as the column cannot be reused (GE healthcare, 2010). Hence, SEC chromatography column was used in this study as it offers several advantages over the other methods: (i) SEC allows processing of larger sample volume; (ii) SEC column can be reused; (iii) duration required for SEC process is much shorter than dialysis; and (iv) SEC approach is cost-effective.

4.5 Conclusion

In summary, the recombinant H-rFIPFVE-Ek-GFP, H-CWT1-Ek-GFP, H-CWT2-Ek-GFP, H-CWT3-Ek-GFP, H-CWT4-Ek-GFP, H-CWT6-Ek-GFP, H-CWT7-Ek-GFP and H-CWT8-EK-GkP proteins were successfully synthesized in TOP10 *E.coli* cells and purified using two-step purification systems that comprised of IMAC and SEC. The fact that H-CWT5-Ek-GFP was found unable to be recovered using IMAC in additional to its low protein production yield implies that the hinge loop DE residue (E61K) and hinge loop FG residue (I97D) are potentially crucial for proper protein folding in recombinant protein that adopts both loop DE and FG regions. Hence, the remaining eight proteins that were successfully produced and purified were subjected to functional assay studies, which are presented in Chapter 5 and Chapter 6.

Chapter 5 Evaluation on Immunomodulatory Activities of FIP-fve mutants

5.1 Introduction

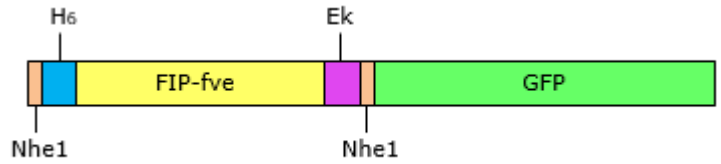
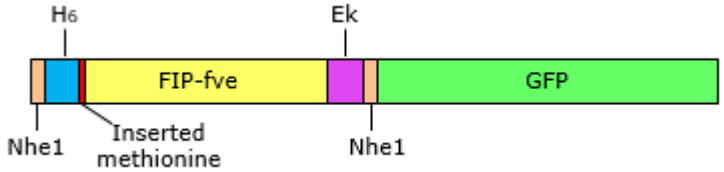
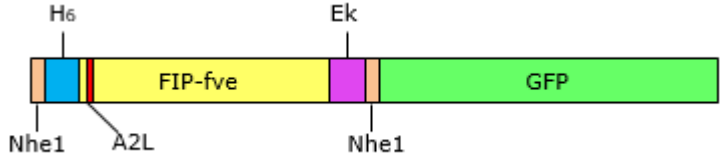
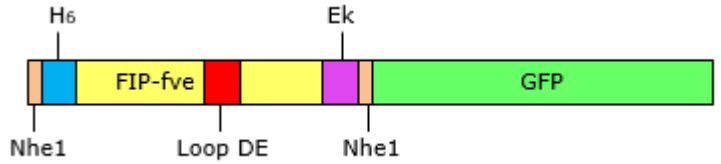
Protein engineering is a technique that is used to develop novel proteins with desired properties and functions. It has been used to create a large variety of proteins with applications that range from food and detergent industry to medical, research, environment and nanobiotechnology applications in the last 30 years. There are many protein engineering approaches available nowadays. When knowledge on the structure and mechanism of the target protein is poorly understood, random mutagenesis such as saturation mutagenesis, error prone PCR or chemical mutagenesis can be utilized. On the other hand, when structural and/or mechanism of the protein of interest is established, rational design via site-directed mutagenesis such as overlap PCR approach or whole plasmid single round PCR can be applied (Turanli-Yildiz, Alkim and Cakar, 2012).

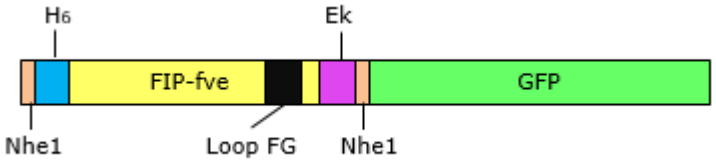
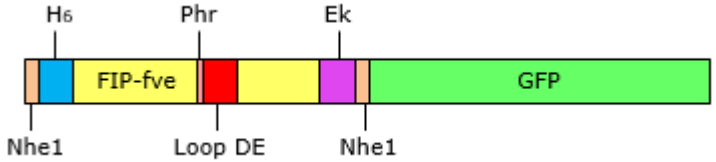
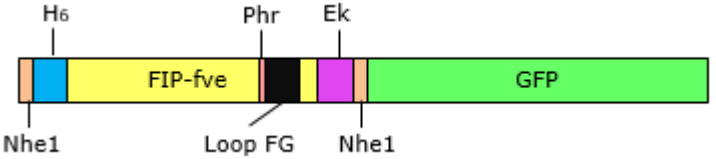
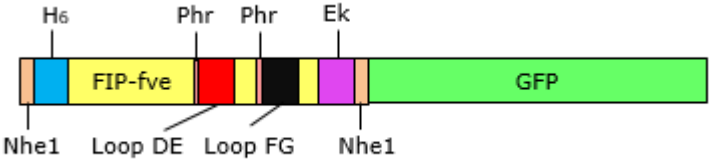
In biomedical application, one of the first protein-based therapeutic generated using recombinant DNA technology was human insulin, which was established by Genentech (Genentech, 1978). Numerous insulin analogs with rapid and prolonged reactions were engineered to improve the properties of native insulin; the rapid-acting insulin analogs include insulin lispro (Howey *et al.*, 1994), insulin aspart (Simpson and Spencer, 1999) and insulin gelusine (Becker, 2007), whereas the long-acting insulin analogs include insulin glargine (Owens *et al.*, 2000) and insulin detemir (Wada *et al.*, 2008). Subsequently, an enhanced version of insulin analog, "zinc" stapled insulin hexamer was developed using supramolecular protein engineering method based on the clinical results shown from the earlier utilized insulin analogs. The "zinc" stapled insulin hexamer possesses properties of both prolonged action and enhanced specificity; it was shown to be able to distinguish between mitogenic insulin-like growth factor receptor and insulin receptor at stringency of 30 times higher than insulin glargine that is marketed

under brand named Lantus® (Phillips *et al.*, 2010). Currently, the work of engineering of insulin analogs is still actively ongoing to further improve its pharmacokinetics (Poluri and Gulati, 2017). The mutagenesis of insulin derivatives represents a great success of structure-based design, which has since inspired the development of many other protein-therapeutic drugs such as recombinant PEGlylated L-asparaginase for leukaemia treatment (Pasut, Sergi and Veronese, 2008), recombinant PEGlylated PEG-interferon-α2a for chronic hepatitis B/C (Perry and Jarvis, 2001), and recombinant engineered interleukin-2 for metastatic melanoma (Vazquez-Lombardi, Roome and Christ, 2013; Poluri and Gulati, 2017).

In this research, site-directed mutagenesis was used to generate FIP-fve derivatives based on its protein structural information (PDB ID: 1OSY). The design and construction of recombinant vectors for *rFIP-fve* and mutants were described in **Chapter 3**, while the production of the recombinant proteins was discussed in **Chapter 4**. The list of recombinant rFIP-fve and mutants proteins generated is presented in **Table 5.1** for ease of reference; annotation (applicable in functional studies - **Chapter 5 and 6**) and schematic diagram of recombinant rFIP-fve and mutants as well as the description of mutations imposed were included.

Table 5.1. List of generated recombinant rFIP-fve and mutants proteins.

No.	Annotation of recombinant proteins	Description of mutation imposed	Schematic diagram of synthesized recombinant proteins
1	**rFIP-fve**: H-rFIPFVE-Ek-GFP	-	
2	**CWT-1**: H-CWT1-Ek-GFP	S1insM	
3	**CWT-2**: H-CWT2-Ek-GFP	A2L	
4	**CWT-3**: H-CWT3-Ek-GFP	**Loop DE:** S62P, N63S, F64Y, T67E, P68S, S69D, G71S	

5	**CWT-4**: H-CWT4-Ek-GFP	**Loop FG:** G101N, S103Del, E104Del, E105D, Y106F	
6	**CWT-6**: H-CWT6-Ek-GFP	**Putative hinge residue:** E61K **Loop DE:** S62P, N63S, F64Y, T67E, P68S, S69D, G71S	
7	**CWT-7**: H-CWT7-Ek-GFP	**Putative hinge residue:** I97D **Loop FG:** G101N, S103Del, E104Del, E105D, Y106F	
8	**CWT-8**: H-CWT8-Ek-GFP	**Putative hinge residue (loop DE):** E61K **Loop DE:** S62P, N63S, F64Y, T67E, P68S, S69D, G71S **Putative hinge residue (loop FG):** I97D **Loop FG:** G101N, S103Del, E104Del, E105D, Y106F	

Denotation:

H6 – 6xhis tag
Ek – Enterokinase cleavage site
NheI – NheI restriction site
Phr – Putative hinge residue
Loop DE – Loop DE mutation region
Loop FG – Loop FG mutation region

Herein, the immunomodulation effects of the synthesized mutants were investigated *in vitro* using mice splenocytes. The splenocytes were harvested from mice spleens and subsequently stimulated with the recombinant FIP-fve and derivatives proteins. After a period of stimulation, the immunomodulatory activities of the mutants were examined based on the previously employed methods in analysing immune-regulating activities of FIP-fve (Kino *et al.*, 1989; Ko *et al.*, 1995, 1997; Wu *et al.*, 2008; Lin *et al.*, 2013); the approaches utilised include splenocytes proliferation 5-bromo-2'-deoxyuridine (BrdU) enzyme-linked immunosorbent assay (ELISA), secretory cytokines release ELISA, immunophenotyping flow cytometry, and haemagglutination. The BrdU splenocytes proliferation assay was used to investigate the stimulatory capabilities of rFIP-fve and mutants on splenocytes proliferation; cytokines release ELISA was used to measure the release of cytokines that were induced by rFIP-fve and mutants in which interferon-γ (IFN-γ) and interleukin-2 (IL-2) were targeted; immunophenotyping flow cytometry was utilised to characterize the immune cell types that were activated by rFIP-fve and mutants; and haemagglutination assay was used to explore the differences of capabilities of rFIP-fve and mutants in agglutinating human and mice red blood cells.

Hence, the specific objectives for this chapter are: (i) to test a hypothesis that enhanced dimerization in FIP-fve would further improve its immune-regulating activities; (ii) to investigate the possible mutational benefit of adjoining highly conserved methionine to the N-terminal of FIP-fve; (iii) to examine the immunomodulation and haemagglutination effects of loops modification in FIP-fve, which were adoption of loop DE, adoption of loop FG, adoption of loop DE and E61K hinge residue, adoption of loop FG and I97D hinge residue, adoption of both loop DE and FG, and adoption of loop DE, loop FG, hinge residue E61K and hinge residue I97D.

5.2 Methods and materials

5.2.1 General materials and equipment

5.2.1.1 Cell culture reagents

RPMI 1640 (Nacalai Tesque, Japan) containing L-glutamine, D-(+)-glucose, and phenol red was supplemented with 10% fetal bovine serum (FBS) (Sigma-aldrich, USA) and 100 unit/mL penicillin and 100 µg/ml streptomycin antibiotic (Gibco™, USA). The supplemented RPMI 1640 was referred as complete RPMI in this context. Phosphate-buffered saline (PBS) (137 mM sodium chloride (NaCl), 2.7 mM potassium chloride (KCl), 10 mM disodium phosphate (Na_2HPO_4) and 1.8 mM monopotassium phosphate (KH_2PO_4), pH 7.2) was sterilized by autoclaving at 121˚C for 15 min.

5.2.1.2 Specialised equipment

Carbon dioxide (CO_2) incubator (Mermmert, Germany) was used for incubation of splenocytes cells. The absorbance reading was conducted using Epoch microplate spectrophotometer (BioTek®, USA) and analysed using Gen5 Data Analysis Software (BioTek®, USA). Centrifugation was performed using centrifuge 5810 R (Eppendorf™, USA).

5.2.1.3 Protein samples

Recombinant rFIP-fve and derivatives proteins were prepared as described in **Chapter 4**. All of the two-steps purified recombinant proteins were concentrated to 2 mg/ml using Macrosep® advance centrifugal device (PALL, USA) and filter-sterilized using sterile polyethersulfone (PES) 0.22 µM syringe filters (Membrane Solutions, China). Small aliquots of proteins were prepared and stored at -20˚C. Recombinant rFIP-fve and derivatives proteins were prepared freshly for three independent courses of splenocytes stimulation.

5.2.2 Immunomodulation activity assay

5.2.2.1 Spleen collection, splenocytes harvesting and blood collection

Five mice (Balb/c; 8-10 weeks) were obtained from Animal House in Monash University Malaysia per experiment. Mice blood collection and spleen extraction were performed with assistance and guidance from Mr Leong Kum Loong. Mice were exposed to carbon dioxide until consciousness were lost, followed by blood collection using cardiac puncture technique. The blood collected was used in haemagglutination assay that is described further in **Section 5.2.3**; approximately 3 mL of blood was collected per experiment. The mice death were assured by the use of secondary form euthanasia, cervical dislocation. Spleens were extracted from the mice aseptically in Class II Biological Safety Cabinet. The spleens were kept in complete RPMI media on ice, and transferred to lab in University of Nottingham Malaysia Campus. All animal procedures were performed according to approved protocols in accordance to Animal Welfare and Ethical Review Body Committee of University of Nottingham under approval reference number: UNMC 9.

The spleens were homogenized using frosted sides of two microscopic slides and suspended in RPMI. Spleen suspension was centrifuged at 350 x g for 5 min (4˚C). Supernatant was discarded. ACK lysis buffer (150 mM ammonium chloride, 10 mM potassium bicarbonate, 0.1 mM EDTA disodium salt, pH 7.2) was used to lyse red blood cells; 10 mL of sterile ACK lysis buffer (2 mL per spleen) was added to suspend the cells and incubated at room temperature for 3 min. After 3 min, 30 ml of sterile PBS was added into the suspension to remove activity of ACK lysis buffer, and the suspension was centrifuged at 350 x g for 5 min (4˚C). Supernatant was discarded and the cells were suspended with 15 ml complete RPMI. The suspension was filtered using BD Falcon™ 40 µM nylon cell strainer (BD Biosciences, USA). Cells were treated with Trypan Blue (Gibco™, USA) and counted using haemocytometer. Cells were resuspended to a

concentration of 5.333 x 10^6 cells/ml; 1.5 mL of the cell suspension (8 x 10^6 cells) was seeded in into each well of a 6-well plate.

5.2.2.2 Splenocytes culture and stimulation

Recombinant proteins were diluted to a final concentration of 10 µg/ml using complete RPMI; 1.5 mL of the diluted solutions were then added individually into each well of the 6-well plate. Positive and negative unstimulated controls were also included using 5 µg/ml Concanavalin A (Con A) (Sigma-aldrich, USA) and PBS respectively. Con A is lectin with sugar-binding capability, and it is isolated from *Canavalia ensiformis* (Jack bean). It is known to induce T cell activation and cytokine secretion (Wermerskirchen, LaTocha and Clarke, 2000). The treated cells were incubated at 37˚C in a 5% CO_2 humidified atmosphere for 48 hr.

5.2.2.3 Observation of splenocytes interaction

The interactions of splenocytes were observed at 24 hr using microscope. The images were captured using Nikon Eclipse TS 100 Inverted microscope (Nikon, Japan) and analysed using imaging software NIS-Elements D 3.0 (Nikon, Japan).

5.2.2.4 Splenocytes proliferation assay

Cell proliferation BrdU (colorimetric) ELISA (Roche, Switzerland) was employed to quantitate cell proliferation based on measurement of BrdU incorporation during DNA synthesis in proliferating cells. Splenocytes proliferation assay was performed according to manufacturer instructions as shown in **Appendix A5.1**. Each treatment sample has triplicate, including positive and unstimulated controls. The proliferative responses were expressed as stimulation index (SI), which was calculated using formula as below:

$$SI = \frac{A_{370}\ of\ stimulated\ splenocytes}{A_{370}\ of\ untreated\ splenocytes}$$

5.2.2.5 Secretory cytokines profiling

It was reported previously that FIP-fve stimulated splenocytes to enhance expression of cytokines such as IFN-y and IL-2 (Ko *et al.*, 1995; Wu *et al.*, 2008; Liu *et al.*, 2012; Lin *et al.*, 2013). Thus, the abilities of rFIP-fve and mutants in inducing generation of IFN-γ and IL-2 were also investigated in this study by measuring the amount of cytokines release from mice splenocytes using ELISA.

BD OptIEA™ mouse IFN-γ ELISA set (BD Biosciences, USA) and BD OptIEA™ mouse IL-2 ELISA set (BD Biosciences, USA) were employed to quantitate mouse IFN-γ and IL-2 in cell culture supernatants. Cell suspensions were transferred from each well in 6-well plate into 15 mL tubes. The tubes with cell suspension were centrifuged at 350 x g for 5 min. The supernatant was individually transferred from each tube to 2 mL microcentrifuge tubes, whereas pellet was used in flow cytometry for immune cell population determination (described in **Section 5.2.2.6**). The microcentrifuge tubes containing the supernatant were kept in -80˚C until further use. ELISA protocol for cytokine determination was performed according to instruction provided by BD OptIEA™ ELISA kits as shown in **Appendix A5.2**.

5.2.2.6 Fluorescence-activated cell sorting (FACs)

To explore the type of proliferated immune cells that rFIP-fve and mutants primed, phenotyping of T cells, B cells, $CD4^+$ T cells and $CD8^+$ T cells were performed using CD3-, CD19-, CD4- and CD8-antibodies respectively. The collected cell pellets from the same treatment in **Section 5.2.2.5** were resuspended using staining buffer (1X PBS with 0.5% bovine serum albumin (BSA) and 2 mM (ethylenediaminetetraacetic acid (EDTA)) and pooled in a single tube. Cells were mixed with trypan blue and counted using haemocytometer. An amount of 1 x 10^6 cells was aliquot from each treatment and

centrifuged at 450 x g for 5 min (4˚C). The cells were resuspended with 25 µl of staining buffer containing 10% normal rat serum (Sigma-aldrich, USA) and 1 µg Rat Anti-Mouse CD16/CD32 (Mouse Fc Block™ Clone: 2.4G2) (BD Pharmigen™, US). The CD16/CD32 antibody was employed to block non-specific antigen binding of immunoglobulins to receptors FcγII (CD32) and FcγIII (CD16) where the antibodies recognize a common non-polymorphic epitope on the extracellular domains of FcγII and FcγIII (Unkeless, 1979; Kulander, Ellison and Hall, 1984). The tubes were incubated on ice for 30 min in dark.

The staining antibodies were prepared in two marker combinations as shown in **Table 5.2**. Single stained controls were also prepared using $CD3^{APC}$ monoclonal antibody, $CD4^{PE}$ monoclonal antibody and $CD8a^{FITC}$ monoclonal antibody, and an unstained control was included as well. CD3 antibody is used to identify T cells; CD19 is utilized to differentiate B cells; CD4 is used to differentiate $CD4^+$ T cells; and, CD8 is used to distinguish $CD8^+$ T cells.

After 30 min, antibodies combination (**Table 5.2**) was added to fill each tube to 50 µl reaction. Each treatment group was stained with marker combinations A and B and incubated on ice for 30 min in dark; a single microcentrifuge tube was prepared for each antibodies combination. The stained cells were washed with 1 mL 1X PBS, and centrifuged at 450 x g for 5 min (4˚C). Supernatant was discarded. Cells were fixed with 100 µl of 2% paraformaldehyde and incubated at room temperature in dark for 10 min. The cells were centrifuged at 800 x g for 5 min (4˚C). Supernatant was discarded. The cells were resuspended in 500 µl 1X PBS and stored at 4˚C in dark. On the next day, cells were read using BD Accuri™ C6 Flow Cytometer (BD Biosciences, USA) where 50,000 events were acquired from each sample. Gating and fluorescence compensation were performed using the BD Accuri™ C6 software (BD Biosciences, USA).

Table 5.2. Combination of marker antibodies used in FACS analysis

No	Marker combination	Marker specificity
1	CD3 monoclonal antibody (Clone: 17A2) APC (eBioscience™, USA) at 1:200 dilution	T cells
	CD19 monoclonal antibody (Clone: eBio1D3(ID3) PE (eBioscience™, USA) at 1:400 dilution	B cells
2	CD3 monoclonal antibody (Clone: 17A2) APC (eBioscience™, USA) at 1:200 dilution	T cells
	CD4 monoclonal antibody (Clone: RM4-5) PE (eBioscience™, US) at 1:400 dilution	$CD4^+$ T cells
	CD8a monoclonal antibody (Clone: 53-6.7) FITC (eBioscience™, USA) at 1:400 dilution	$CD8^+$ T cells

5.2.3 Haemagglutination assay

Human O type blood was obtained from healthy volunteer who approved the use of their blood in this study. The human blood collection was performed by Heath centre Kumpulan Medic in University of Nottingham Malaysia Campus. The protocol of haemagglutination assay was adopted and modified from (Kino *et al.*, 1989). The collected human and mice blood in **section 5.2.2.1** were centrifuged at 500 x g for 5 min (4˚C). Plasma and white ghost layer at the top of the pellet were removed. The cells were washed five times with 10 mL of chilled 1X PBS and centrifuged at 500 x g for 5 min (4˚C). Supernatant was removed. After the last wash, the pelleted red blood cells were suspended to 1.5% (v/v) blood cells and kept at 4˚C until further use. Prior to agglutination assay, human red blood cells were mixed with 0.1% trypsin solution and incubated at 37˚C for 15 min, and followed by washing with 1X PBS and centrifugation at 500 x g for 5 min (4˚C). Trpsinisation of the cell renders the cell more sensitive to agglutination as it was found that human red blood cells without trypsinisation treatment were not responsive to agglutination activities (Sano and Ogawa, 2014).

To detect haemagglutination activity, suspension of 25 µl of 1.5% red blood cells, 75 µl of PBS with 0.2% gelatin and 25 µl of purified recombinant proteins (2, 5, 10, 20, 100 µg/ml) were placed in 96-well round bottom microplates. Two concentrations of concanavalin A at 5 µg/ml and 20 µg/ml were used as positive control in mice and human RBCs respectively. PBS was used as negative control. The plates were incubated at 37˚C for 2 hr, followed by examination for haemagglutination. The haemagglutination activity was captured using Gel Doc™ XR system (Bio-Rad Laboratories, USA) and analyzed using Image Lab™ Software (Bio-Rad Laboratories, USA). Result of haemagglutination activities were interpreted according to reasoning discussed in **Chapter 2 Section 2.2.1**.

5.2.4 Statistical analyses

All experiments were performed at least in triplicate in three independent experiments. All values are presented as mean ± SD of three independent experiments. Statistical analysis was performed using GraphPad Prism 7. One-way analysis of variance (ANOVA) was conducted followed by a Tukey multiple comparisons test to determine the significance degree of proliferative responses of mice splenocytes, secretory release of cytokines IFN-γ and IL-2 and changes of immune cell population in mice splenocytes stimulated by rFIP-fve and mutants. The significance levels were denoted at $P \leq 0.05$ with *, $P \leq 0.01$ with **, $P \leq 0.001$ with ***, and $P \leq 0.0001$ with ****.

5.3 Result

5.3.1 Microscopic visualization of splenocytes interactions

The interaction of splenocytes was observed at 24 hr after stimulation and the microscopic visualization images were captured using microscopes at 100x magnification. As shown in **Figure 5.1**, agglutinations of cells were observed in all of the stimulated splenocytes cell. The extent of cell agglutination varied among the mutants with higher amount of agglutinated cells observed in CWT-3, CWT-6 and CWT-8; moderate amount of agglutinated cells demonstrated in CWT-7; and lower amount of agglutinated cells shown in rFIP-fve, CWT-1, CWT-2, and CWT-4. Positive control Con A-induced splenocytes displayed agglutination, whereas no agglutination of cells were observed in negative control. The phenomenon of splenocytes agglutination was observed in Con A-stimulated cells, which was caused by binding of Con A to cells surface membrane, and bridging the surface binding sites of immune cells. This results in activation of lymphocytes or splenocytes blastogenesis (Wands, Podolsky and Isselbacher, 1976). Although it is not known which immune cell types that were bridged and caused cell agglutination, interaction between immune cells such as lymphocytes and macrophages is known to play a vital role in the development of immune response (Abbas, Lichtman and Pillai, 2015). On the basis of this assumption, it is suggested that the higher the extent of cell agglutination, the higher the degree of activation of splenocytes proliferation.

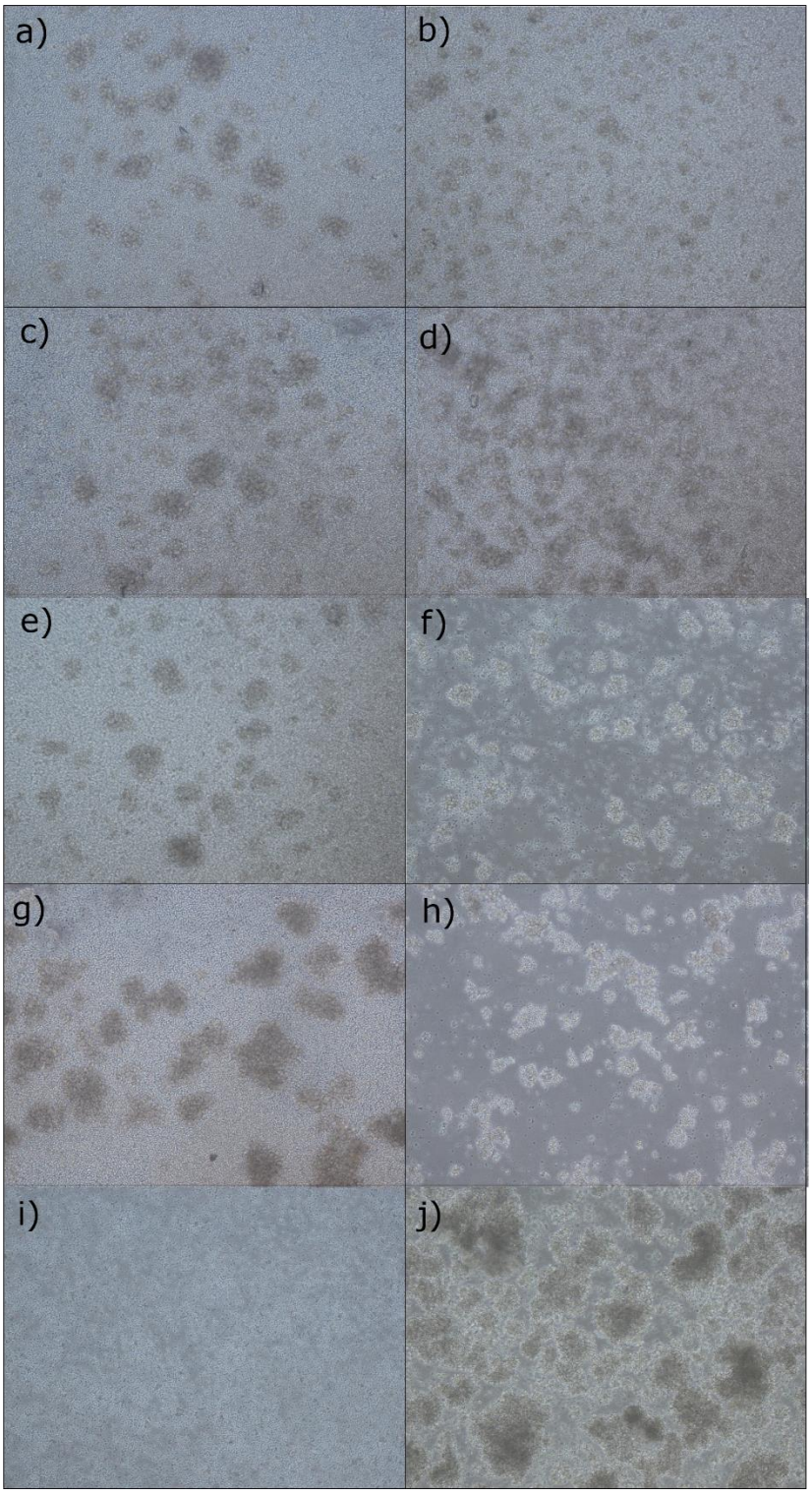


Figure 5.1. Microscopic visualization of splenocytes agglutination at 100x magnification. Interactions of mice splenocytes stimulated with the respective 10 µg/ml recombinant proteins are presented as: a) rFIP-fve; b) CWT-1; c) CWT-2; d) CWT-3; e) CWT-4; f) CWT-6; g) CWT-7 and h) CWT-8. Splenocytes interactions stimulated with PBS and Con A are displayed as (i) negative control and (j) positive control respectively. It is presumably that the higher the extent of cell agglutination, the higher the degree of activation of splenocytes proliferation.

5.3.2 Proliferative responses of stimulated mice splenocytes

The *in vitro* immunomodulatory activities of rFIP-fve and mutants were investigated by examining the splenocytes cell proliferation that were induced by the recombinant proteins. The comparison in terms of differences in proliferative responses among the mutants are classified into two groups: (i) mutant group with putative improved dimerization (**section 5.3.2.1**) and (ii) mutant group with loops modification (**section 5.3.2.2**).

5.3.2.1 Mutant group with putative improved dimerization

As shown in **Figure 5.2**, stimulation indexes of 10 µg/ml rFIP-fve, CWT-1 and CWT-2 toward mice splenocytes were 11.99 ± 1.76, 12.56 ± 2.93, and 22.16 ± 1.36 respectively. The stimulation index of 5 µg/ml ConA towards mice splenocytes was 18.22 ± 0.96. The splenocytes proliferative activity of CWT-2 was approximately one-fold higher as compared to rFIP-fve, whereas the splenocytes proliferative response of CWT-1 was not statistically different to rFIP-fve.

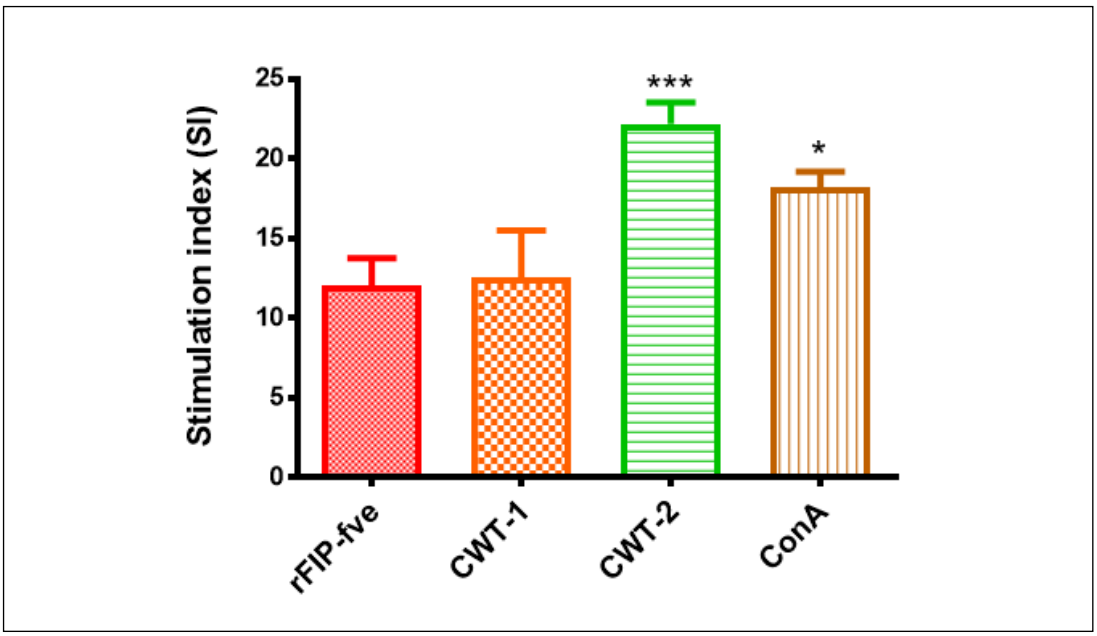


Figure 5.2. Proliferative responses of balb/c mice splenocytes were measured using BrdU cell proliferation ELISA. Mice splenocytes were treated with 10 µg/ml rFIP-fve, CWT-1, and CWT-2. Positive and negative controls were included using 5 µg/ml Con A-treated splenocytes and untreated splenocytes respectively. The proliferative responses were expressed as stimulation index (SI), which was calculated by dividing absorbance value of stimulated cells by absorbance value of untreated cells that was derived from wavelength of 370 nm with correction wavelength at 492 nm. Data represent mean ± SD of triplicates for three independent experiments. Tukey multiple comparisons test showed degree of significance between rFIP-fve-stimulated splenocytes in comparisons to mutants- and ConA- induced splenocytes; $P \leq 0.05$ with *, $P \leq 0.01$ with **, $P \leq 0.001$ with ***, and $P \leq 0.0001$ with ****. The splenocytes stimulatory activity of CWT-2 was apparently higher in comparison to rFIP-fve, whereas the splenocytes stimulatory activity of CWT-1 was not statistically different to rFIP-fve.

5.3.2.2 Mutant group with loops modification

Stimulation indexes of 10 µg/ml rFIP-fve, CWT-3, CWT-4, CWT-6, CWT-7 and CWT-8 toward mice splenocytes were 11.99 ± 1.78, 23.66 ± 0.51, 10.06 ± 0.91, 24.58 ± 1.74, 15.43 ± 1.58 and 17.30 ± 0.73 respectively as demonstrated in **Figure 5.3**. The stimulation index of 5 µg/ml ConA towards mice splenocytes was 18.22 ± 0.96. The splenocytes proliferative activities of CWT-3, CWT-6 and CWT-8 were significantly higher as compared to rFIP-fve, while CWT-4 and CWT-7 were not significantly different as compared to rFIP-fve. Both CWT-3 and CWT-6 displayed at least one-fold increase in the splenocytes proliferative activities in comparison to rFIP-fve. Additionally, both CWT-3 and CWT-6 also exhibited higher mice splenocytes stimulation indexes as compared to CWT-4, CWT-7 and CWT-8. The three mutants CWT-3, CWT-6 and CWT-8 comprised of mutations at loop DE region, which are adopted from loop DE in LZ-8; whereas CWT-4 and CWT-7 consist mutations at loop FG region that are adopted from loop FG from LZ-8.

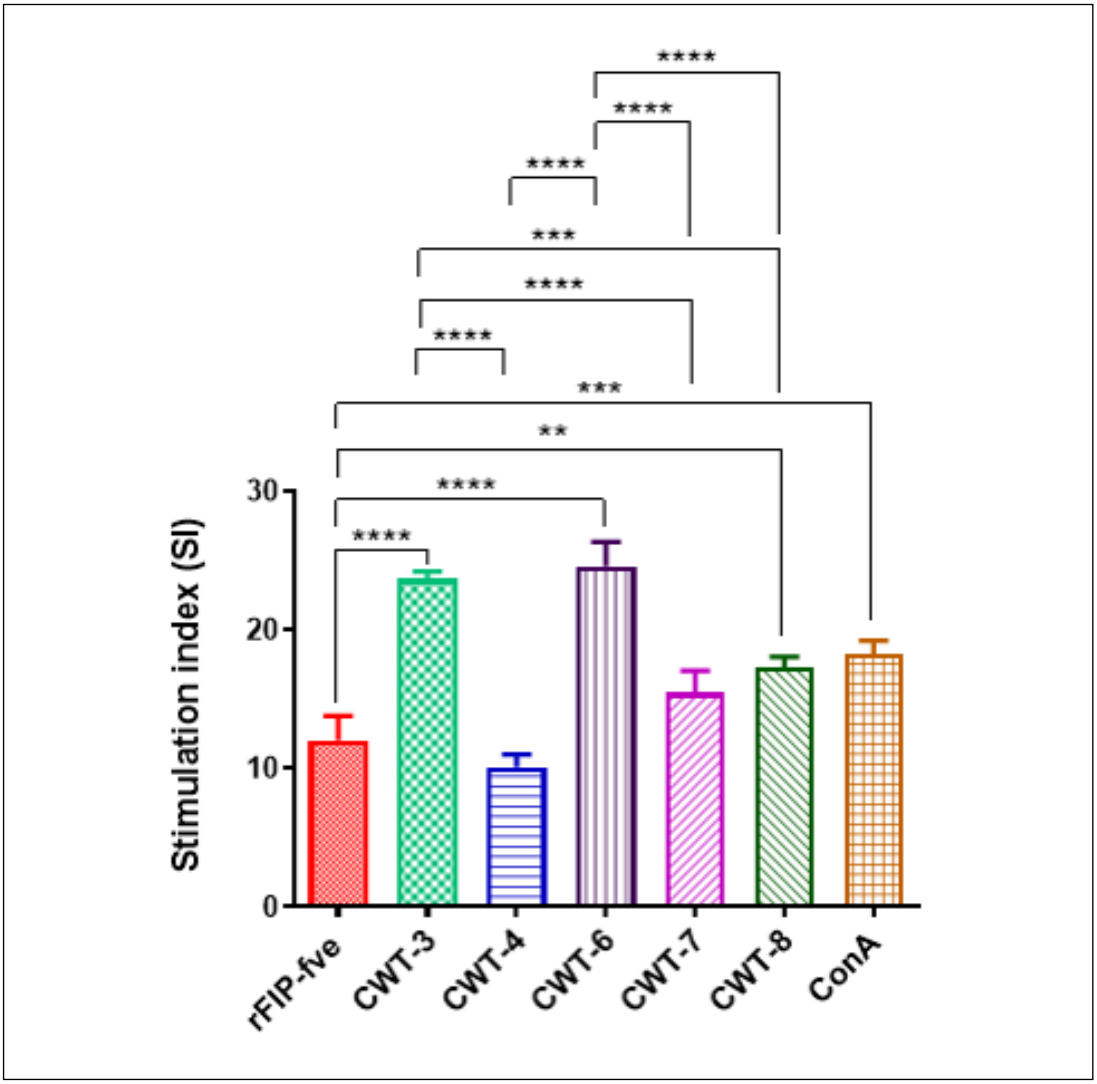


Figure 5.3. Proliferative responses of balb/c mice splenocytes were measured using BrdU cell proliferation ELISA. Mice splenocytes were treated with 10 µg/ml rFIP-fve, CWT-3, CWT-4, CWT-6, CWT-7 and CWT-8. Positive and negative controls were included using 5 µg/ml Con A-treated splenocytes and untreated splenocytes respectively. The proliferative responses were expressed as stimulation index (SI), which was calculated by dividing absorbance value of stimulated cells by absorbance value of untreated cells that was derived from wavelength of 370 nm with correction wavelength of 492 nm. Data represent mean ± SD of triplicates for three independent experiments. Tukey multiple comparisons test showed degree of significance between rFIP-fve-stimulated splenocytes in comparisons to mutants- and ConA- induced splenocytes as well as degree of significance among mutants-induced splencytes; $P \leq 0.05$ with *, $P \leq 0.01$ with **, $P \leq 0.001$ with ***, and $P \leq 0.0001$ with ****. All mutants with loop modifications displayed significantly higher proliferative activities as compared to rFIP-fve except CWT-4 and CWT-7. Both CWT-3 and CWT-6 displayed the best splenocytes proliferative responses in this group of recombinant derivative proteins.

5.3.3 Cytokine profiling of stimulated splenocytes culture

The cytokine profile of the cultured supernatant was investigated to further assess the polarisation effects of rFIP-fve and mutants on splenocytes. Results indicated that the recombinant proteins in this study were capable of stimulating splenocytes to enhance expression of cytokines IFN-y and IL-2, which were consistent with the previously reported finding (Ko *et al.*, 1995; Wu *et al.*, 2008; Liu *et al.*, 2012; Lin *et al.*, 2013). The comparison in terms of differences in induced-cytokines release among the mutants are classified into two groups: (i) mutant group with putative improved dimerization (**section 5.3.3.1**) and (ii) mutant group with loops modification (**section 5.3.3.2**).

5.3.3.1 Mutant group with putative improved dimerization

As shown in **Figure 5.4a**, result showed that 10 µg/ml rFIP-fve, CWT-1 and CWT-2 increased the level of IFN-γ cytokine secretions in murine splenocytes to 73.31 pg/ml ± 3.53, 113.38 pg/ml ± 3.53, and 397.15 pg/ml ± 62.86 respectively. The amount of CWT-2 induced-IFN-γ generation was at least five-fold higher as compared to rFIP-fve. Evidently, CWT-2 exhibited a stronger immunomodulatory activity than rFIP-fve. There was no significant difference between rFIP-fve and CWT-1 in IFN-γ expression level. Positive control 5 µg/ml Con A stimulated and enhanced IFN-γ to a level of 1695.02 pg/ml ± 53.62, while IFN-γ was not detected in negative control.

As demonstrated in **Figure 5.4b**, the amount of IL-2 secreted in mice splenocytes under treatments of 10 µg/ml rFIP-fve, CWT-1 and CWT-2 were 131.90 pg/ml ± 19.74, 97.17 pg/ml ± 2.89, and 167.25 pg/ml ± 6.10 respectively. Similar to the IFN-γ expression level, CWT-2 enhanced mice splenocytes to a higher level of IL-2 production as compared to rFIP-fve. There was no significant difference between rFIP-fve and CWT-1 in term of IL-2 expression level. Positive control 5 µg/ml concanavalin A stimulated and enhanced IL-2 to a level of 190.72 pg/ml ± 3.66, while IL-2 was not detected in negative control.

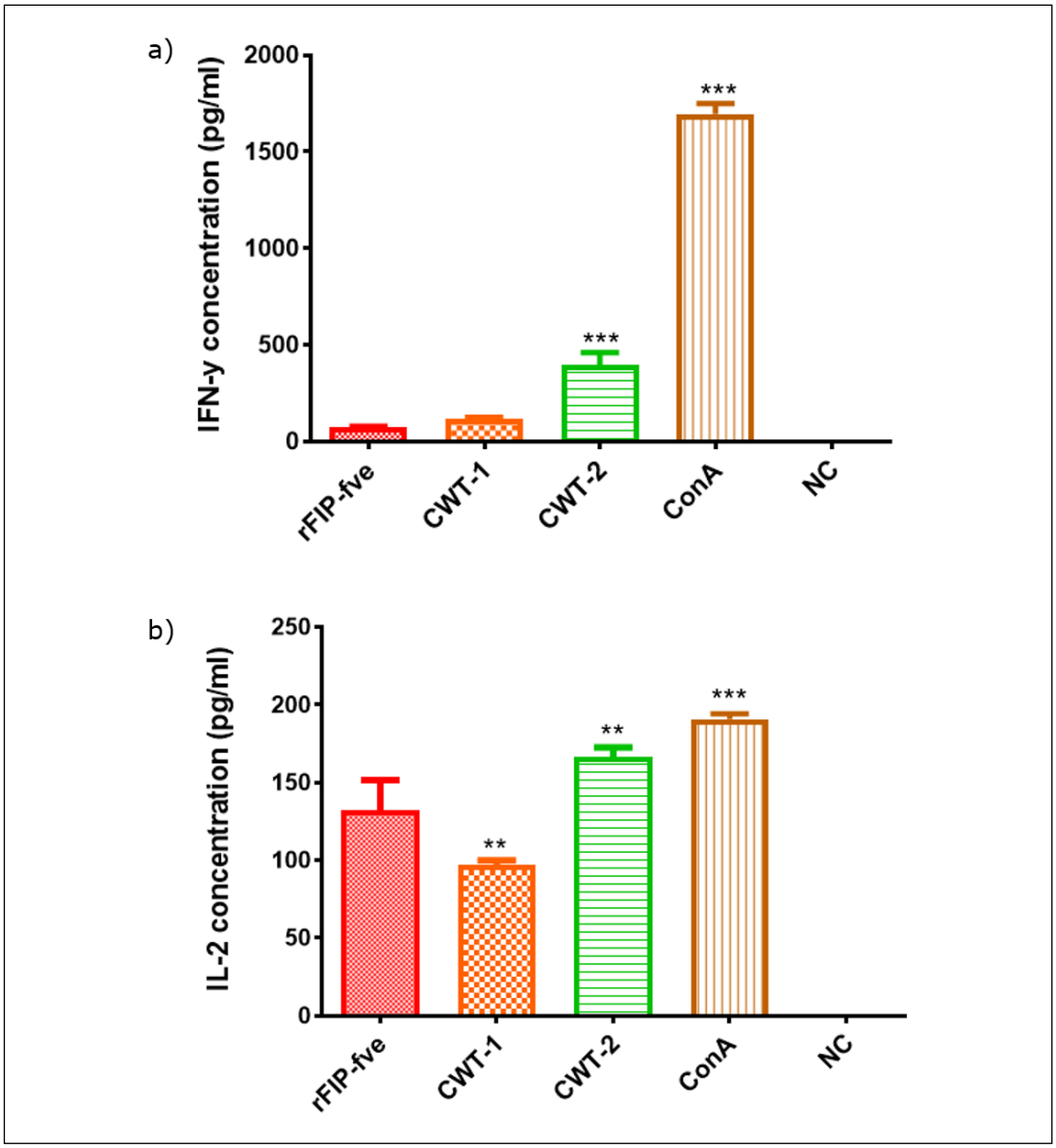


Figure 5.4. Secretion profile of cytokines (a) IFN-γ and (b) IL-2 from mice splenocytes after 48 hr of stimulation with rFIP-fve, CWT-1, CWT-2 and Con A. The recombinant proteins were tested at concentration of 10 µg/ml. The ConA-treated cells and untreated cells were used as positive and negative controls respectively. Data represent mean ± SD of triplicates for three independent experiments and were expressed as cytokine concentration (pg/ml) ± SD. Tukey multiple comparisons test showed degree of significance between rFIP-fve-stimulated splenocytes in comparisons to mutants- and ConA- induced splenocytes; $P \leq 0.05$ with *, $P \leq 0.01$ with **, $P \leq 0.001$ with ***, and $P \leq 0.0001$ with ****. CWT-2 with putative enhanced dimerization showed higher secretion of IFN-γ and IL-2 as compared to rFIP-fve, whereas CWT-1 displayed similar secretory IFN-γ level but lower IL-2 level in comparison to rFIP-fve.

5.3.3.2 Mutant group with loops modification

As shown in **Figure 5.5a**, result demonstrated that 10 µg/ml rFIP-fve, CWT-3, CWT-4, CWT-6, CWT-7 and CWT-8 increased the level of IFN-γ cytokine secretions in murine splenocytes to 73.31 pg/ml ± 11.48, 698.78 pg/ml ± 66.32, 57.78 pg/ml ± 11.75, 724.42 pg/ml ± 106.90, 413.22 pg/ml ± 31.18 and 476.04 pg/ml ± 25.91 respectively. The amount of IFN-γ released from mice splenocytes stimulated by CWT-3, CWT-6, CWT-7 and CWT-8 were significantly higher than rFIP-fve. The peak stimulatory effects were observed in mutants CWT-3 and CWT-6, which harbour mutations in loop DE that are adopted from loop DE in LZ-8. In fact, the enhancement of IFN-γ generation in both CWT-3 and CWT-6 were evidently higher than CWT-4, CWT-7 and CWT-8, which carry mutations in loop FG that are adopted from loop FG in LZ-8. CWT-4 had the lowest stimulated IFN-γ production level. This result was in correlation to the stimulation index of mice splenocytes as presented in **Section 5.3.2.2**.

As demonstrated in **Figure 5.5b**, result showed that rFIP-fve, CWT-3, CWT-4. CWT-6, CWT-7 and CWT-8 enhanced the IL-2 expression level to 131.9 pg/ml ± 13.65, 185.42 pg/ml ± 3.40, 114.47 pg/ml ± 7.99, 189.45 pg/ml ± 10.44, 176.73 pg/ml ± 4.67, 179.38 pg/ml ± 5.40 pg/ml respectively. The amount of IL-2 released from mice splenocytes stimulated by rFIP-fve were significantly lower than mutants CWT-3, CWT-6, CWT-7 and CWT-8, except CWT-4. In fact, the lowest induced IL-2 expression level was observed in CWT-4. There were no significant differences in IL-2 secretion among CWT-3, CWT-6, CWT-7 and CWT-8.

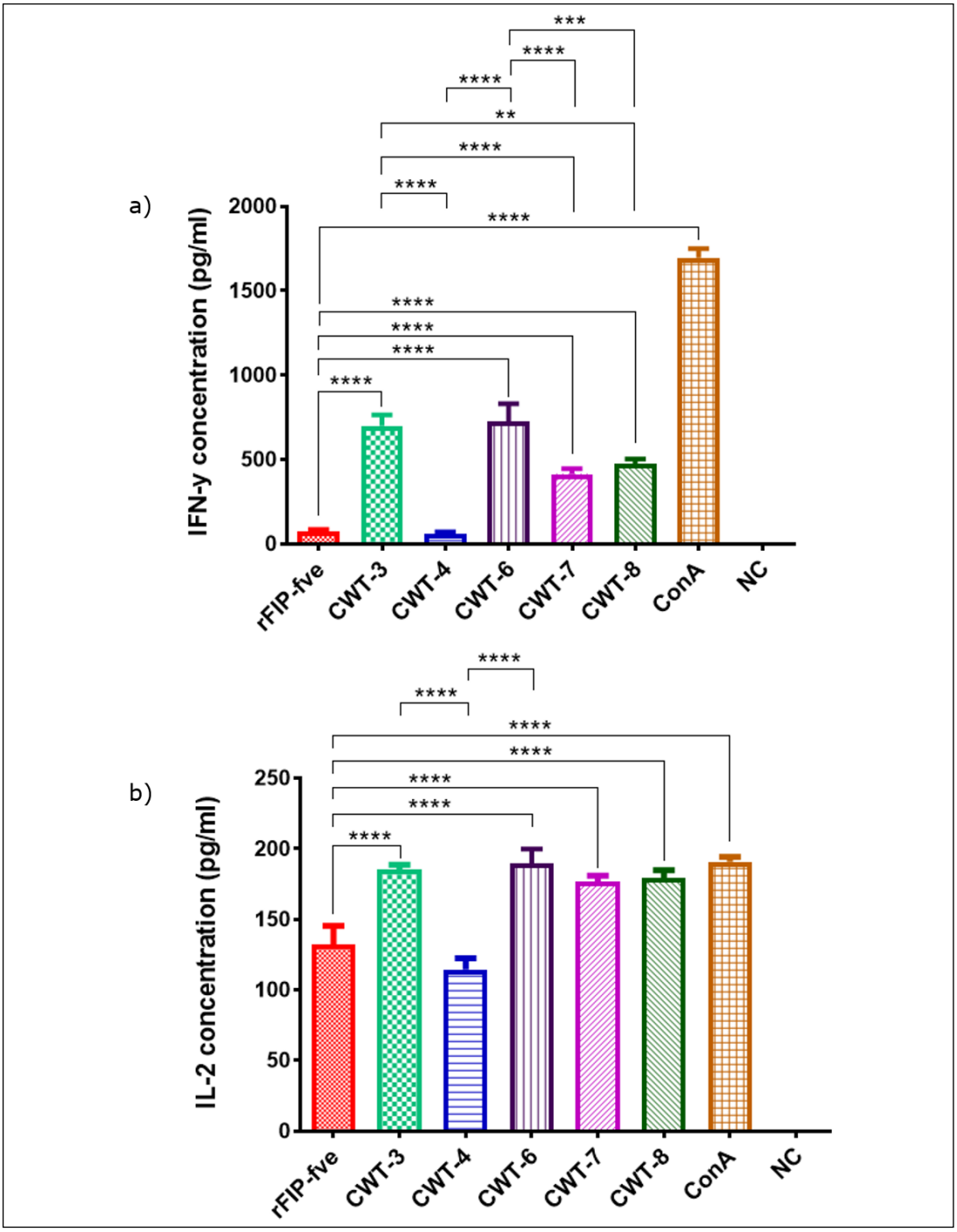


Figure 5.5. Secretion profile of cytokines (a) IFN-γ and (b) IL-2 from mice splenocytes after 48 hr of stimulation with rFIP-fve, CWT-3, CWT-4, CWT-6, CWT-7, CWT-8 and Con A. The recombinant proteins were tested at concentrations of 10 µg/ml. The ConA-treated cells and untreated cells were used as positive and negative controls respectively. Data represent mean ± SD of triplicates for three independent experiments and were expressed as cytokine concentration (pg/ml) ± SD. Tukey multiple comparisons test showed degree of significance between rFIP-fve-stimulated splenocytes in comparisons to mutants- and ConA- induced splenocytes as well as degree of significance among mutants-stimulated splenocytes; $P \leq 0.05$ with *, $P \leq 0.01$ with **, $P \leq 0.001$ with ***, and $P \leq 0.0001$ with ****. The amount of IFN-γ and IL-2 released from mice splenocytes stimulated by CWT-3, CWT-6, CWT-7 and CWT-8 were significantly higher than rFIP-fve. The peak stimulatory effects were observed in mutants CWT-3 and CWT-6.

5.3.4 *In vitro* immunological characterization of stimulated splenocytes

5.3.4.1 Gating of lymphocytes in total splenocytes population

The lymphocyte cells were gated based on cell properties that were determined from correlated measurement of forward-scattered light (FSC) and side-scattered light (SSC). A cell particle deflects incident laser light and results in light scattering, which is affected by factors such as cell size, shape, and internal complexity. FSC is proportional to cell surface area or size, whereas SSC is proportional to cell granularity including nucleus and any granular materials (BD Biosciences, 2002). Splenocytes consist of heterogeneous cell populations with various cell types. Therefore, FSC and SSC are used to distinguish the lymphocyte cells of interest. Debris and dead cells are normally found at the bottom left corner of the density plot as they have low level of FSC. Granulocytes are cells with bigger size and high granularity and thus, it has a higher FSC and SSC level. Monocytes has a higher FSC than lymphocytes as the size of monocytes size is bigger as compared to lymphocytes, so monocytes is generally found at the right side of lymphocytes in the density plot (Abbas, Lichtman and Pillai, 2015). Based on the light scatter pattern, the targeted lymphocyte region was gated and the monocytes, debris or dead cells were excluded as shown in **Figure 5.6.**

The use of single stained markers allows determination of the extent of fluorescence spillover from each fluorochrome. Based on the histogram of unstained control and histograms of single-stained marker $CD3^{APC}$, $CD4^{PE}$ and $CD8^{FITC}$, the fluorescence spillover were assessed. Results indicate that all three fluorochromes used in this experiment were correctly detected. Single stained APC control displayed only signal from cells stained with APC antibodies; single stained PE control shown only signal from cells stained with PE antibodies; and no signal was detected in single stained FITC control. CD8α-FITC antibody was used in the single stained FITC control, therefore the lack of signal indicated the cell with CD8α antigen that was specific for the antibody was absence

in the induced splenocytes. A minor colour compensation was conducted by correcting $CD4^{PE}$ via subtraction of a percentage of 5% $CD8^{FITC}$ and by correcting $CD3^{APC}$ through subtraction of a percentage of 5% $CD8^{FITC}$. The comparison in terms of differences in changes of primed immune cells among the mutants are classified into two groups: (i) mutant group with putative improved dimerization (**section 5.3.4.2**) and (ii) mutant group with loops modification (**section 5.3.4.3**).

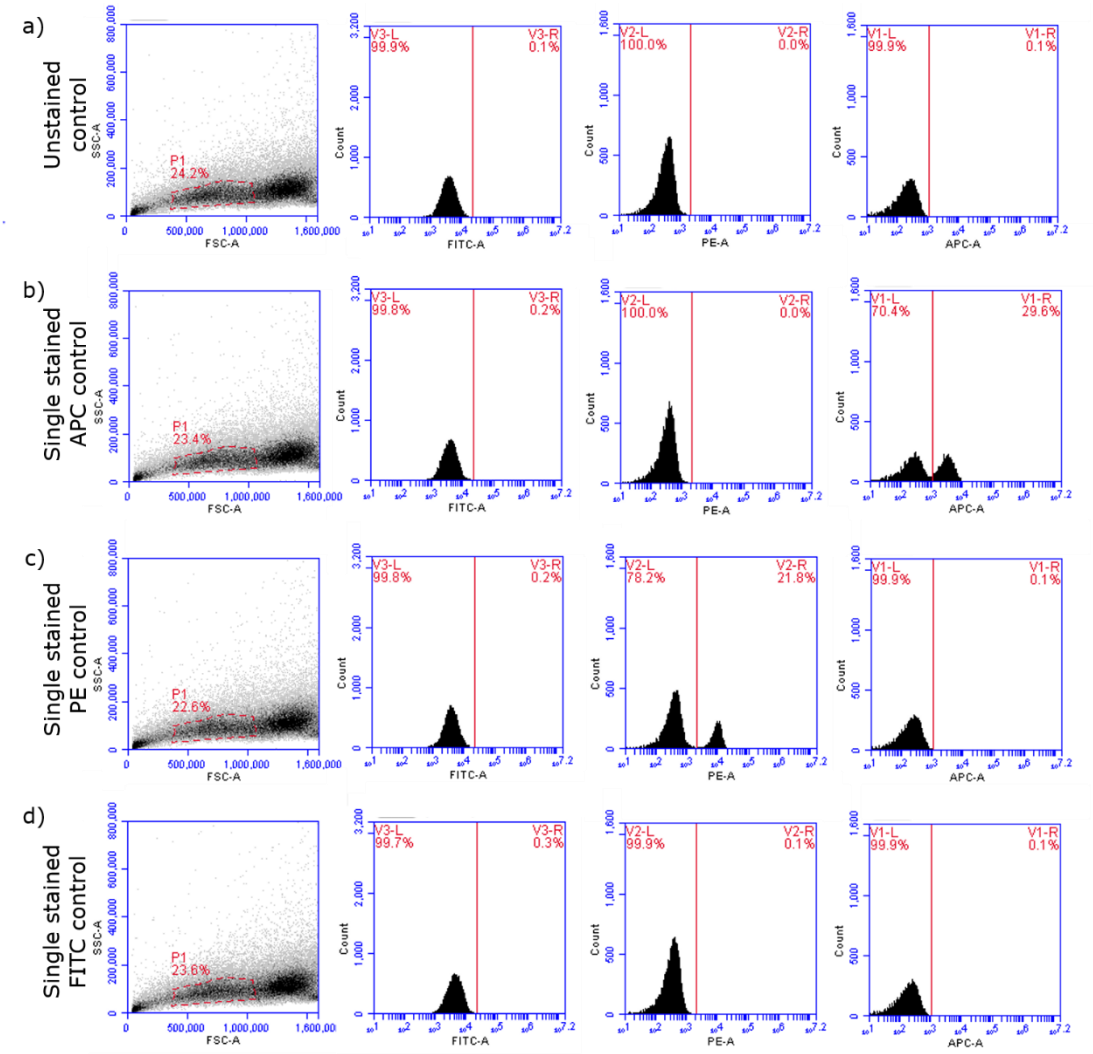


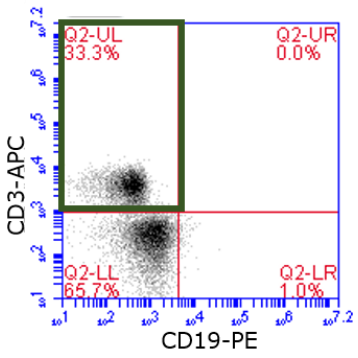
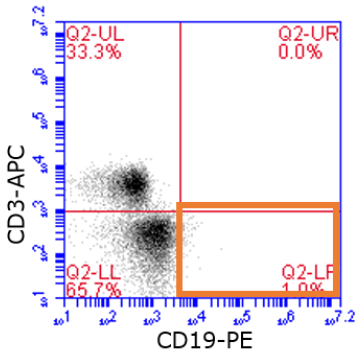
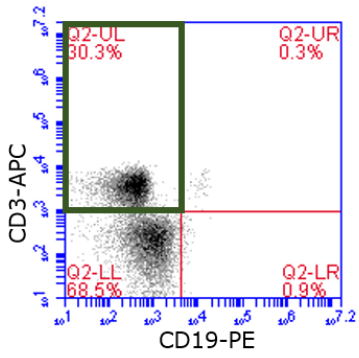
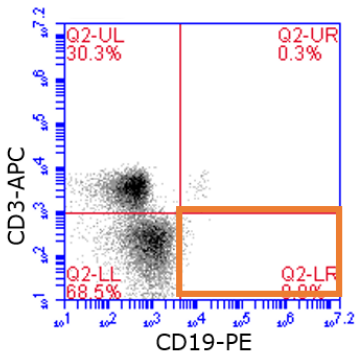
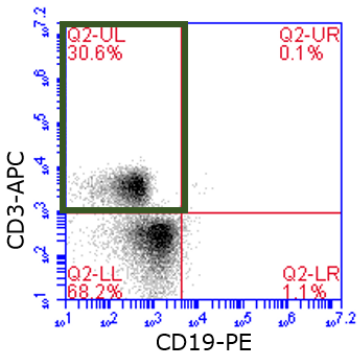
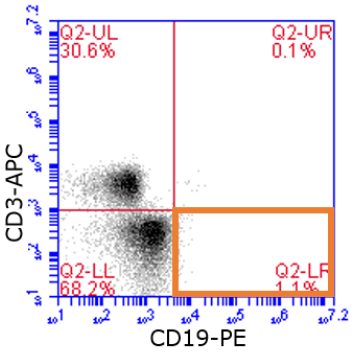
Figure 5.6. FACS analysis of stimulated mice splenocytes. The stimulated splenocytes from rFIP-fve and mutants were pooled and subjected single staining with antibodies $CD3^{APC}$, $CD4^{PE}$ and $CD8^{FITC}$. An unstained control was included as well. The lymphocytes population was first gated based on FSC and SSC. Based on the histogram of (a) unstained control and histograms of single-stained marker (b) $CD3^{APC}$, (c) $CD4^{PE}$ and (d) $CD8^{FITC}$, the fluorescence spillover were assessed. Results indicate that all three fluorochromes used in this experiment were correctly detected. A minor colour compensation was performed by correcting $CD4^{PE}$ via subtraction of a percentage of 5% $CD8^{FITC}$ and by correcting $CD3^{APC}$ through subtraction of a percentage of 5% $CD8^{FITC}$.

5.3.4.2 Mutant group with putative improved dimerization

(A) Immunophenotyping of T cells and B cells

T cells and B cells are characterized by cells that are stained with CD3- and CD19-antibodies respectively. As shown in **Figure 5.7**, the percentage of T cells (CD3-stained cells) in splenocytes with treatment of 10 µg/ml rFIP-fve, CWT-1 and CWT-2 were 33.67% ± 2.08, 30.37% ± 4.60 and 30.93% ± 2.08 respectively; whereas the percentage of B cells (CD19-stained cells) in splenocytes with treatment of 10 µg/ml rFIP-fve, CWT-1 and CWT-2 were 1.13% ± 0.23, 0.33% ± 0.06 and 0.87% ± 0.21 respectively. This indicates that rFIP-fve, CWT-1 and CWT-2 primarily induced T cells proliferation where only a minimal population of B cells was detected. There were no significant differences in percentage of T and B cells in splenocytes with treatment of 10 µg/ml rFIP-fve, CWT-1 and CWT-2. The immunophenotyping result of ConA-stimulated splenocyte culture is included in **Appendix A5.3**.

a)

Treatment	T cells (Dark green box)	B cells (Orange box)
rFIP-fve		
CWT-1		
CWT-2		

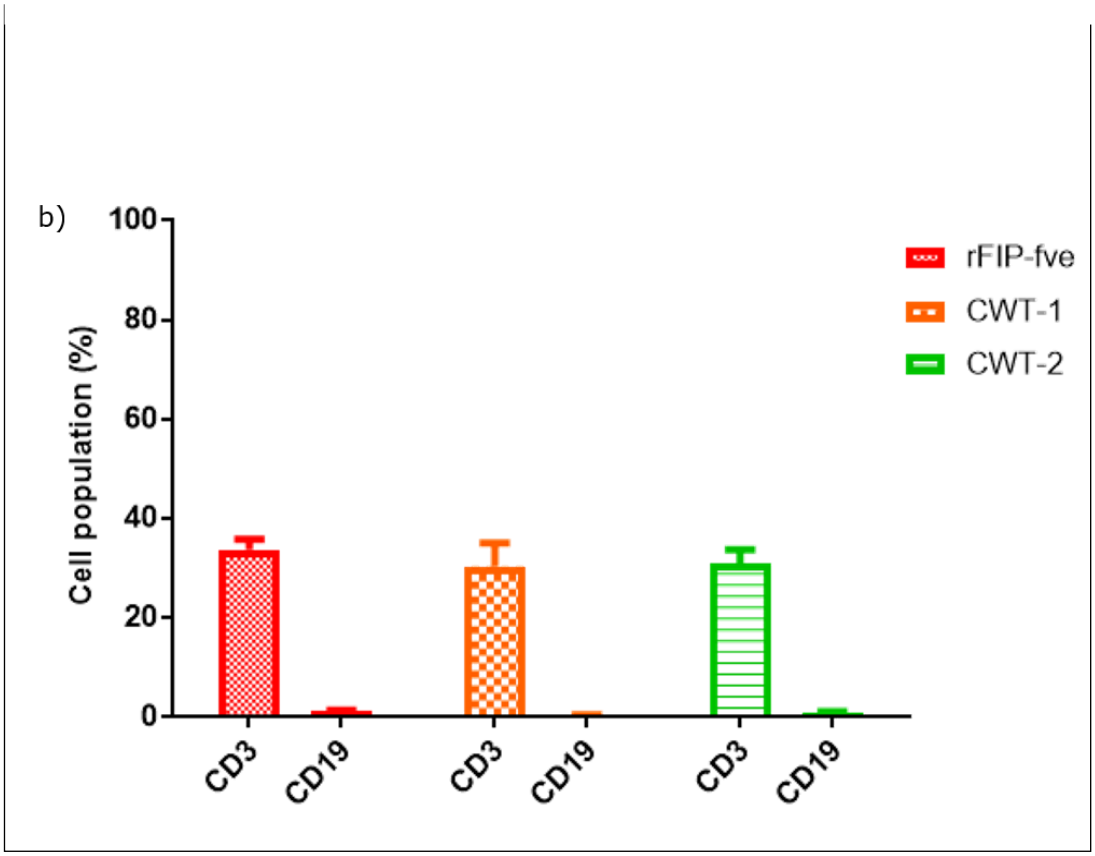
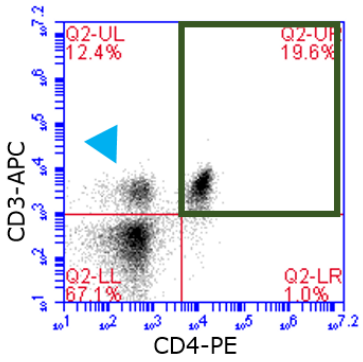
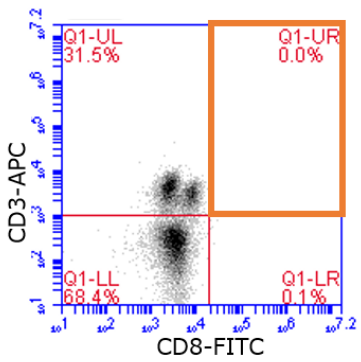
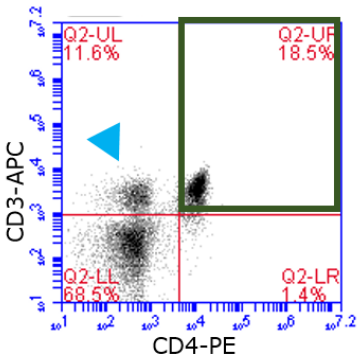
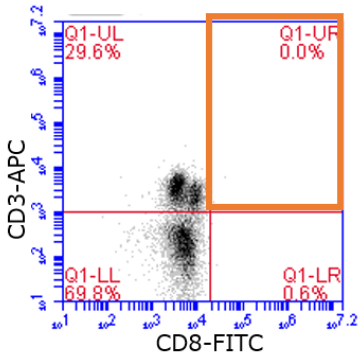
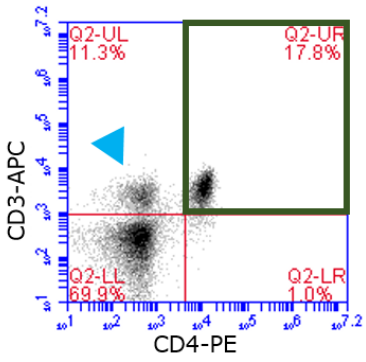
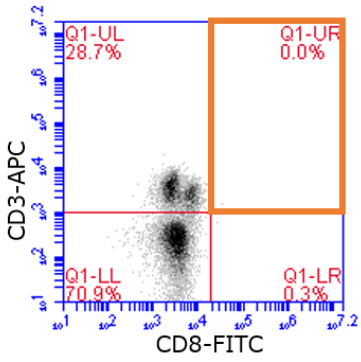


Figure 5.7. Immunophenotyping of lymphocyte population in mice splenocytes. Changes in cell populations of T cells (CD3) and B cells (CD19) were determined using FACS analysis following stimulation with rFIP-fve, CWT-1 and CWT-2 for 48 hr. (a) The plots are representatives of three independent experiments. CD3-stained cells represented T cells (indicated by dark green box), whereas CD19-stained cells represented B cells (indicated by orange box). (b) Data were expressed as mean of percentage of cell population (%) ± SD from three independent experiments. There were no significant differences in the cell population of T cells and B cells in rFIP-fve-, CWT-1- and CWT-2-stimulated splenocytes.

(B) Immunophenotyping of T cells, $CD4^+$ T cells, and $CD8^+$ T cells

T cells, $CD4^+$ T cells and $CD8^+$ T cells are characterized by cells that are stained with CD3-, CD4-, and CD8-antibodies respectively. As shown in **Figure 5.8**, the percentage of T cells (CD3-stained cells) in splenocytes with treatment of 10 µg/ml rFIP-fve, CWT-1 and CWT-2 were 32.2% ± 2.59, 30.07% ± 2.77 and 29.67% ± 4.16 respectively; while the percentage of $CD4^+$ T cells (CD4-stained cells) in splenocytes with treatment of 10 µg/ml rFIP-fve, CWT-1 and CWT-2 were 19.43% ± 3.71, 18% ± 3 and 18.13% ± 2.80 respectively. The $CD4^+$ T cells made up more than 50% of the T cells that were induced by the mutants and rFIP-fve, whereas the $CD8^+$ T cells were not detected in induced splenocytes. Interestingly, there was a population of cells that were stained positively with CD3-antibody yet stained negatively with CD4-antibody as well as CD8-antibody as indicated with blue arrows in **Figure 5.8a**; this indicates that the cell population was made up of uncharacterized T cells as they were neither $CD4^+$ T cells nor $CD8^+$ T cells. The percentage of the uncharacterized T cells in splenocytes with treatment of rFIP-fve, CWT-1 and CWT-2 were 12.77% ± 2.07, 11.13% ± 1.19, and 11.53% ± 0.97 % respectively. Taken together, there were no significant differences in the percentages of T cells, $CD4^+$ T cells, and uncharacterized T cells in splenocytes that were treated by rFIP-fve, CWT-1 and CWT-2.

a)

Treatment	CD4⁺ T cells (dark green box)	CD8⁺ T cells (orange box)
rFIP-fve		
CWT-1		
CWT-2		

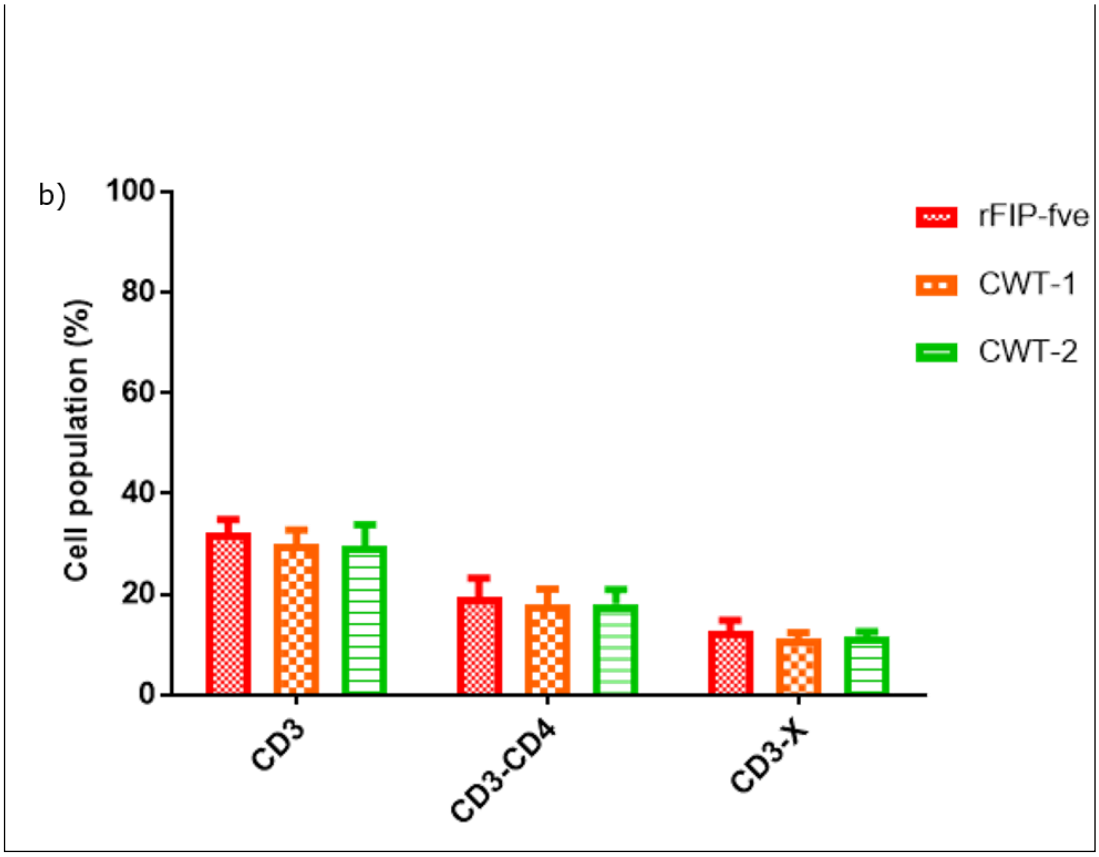


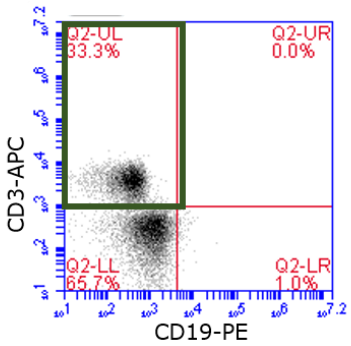
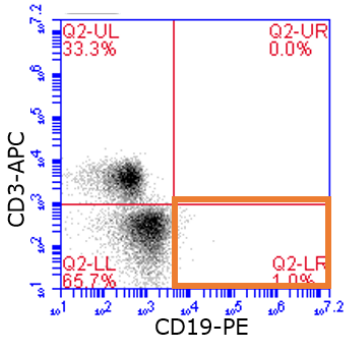
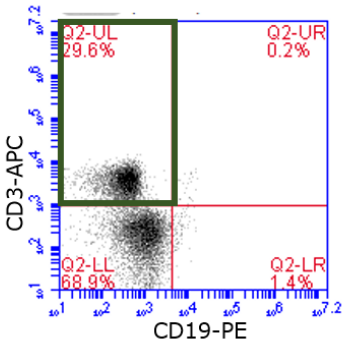
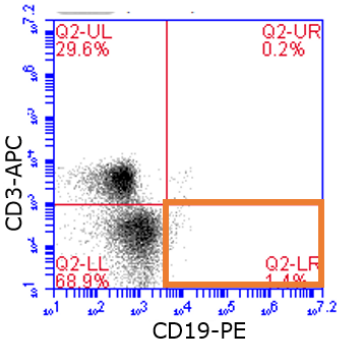
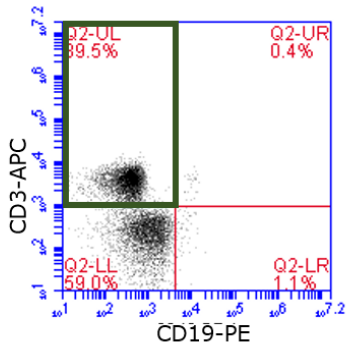
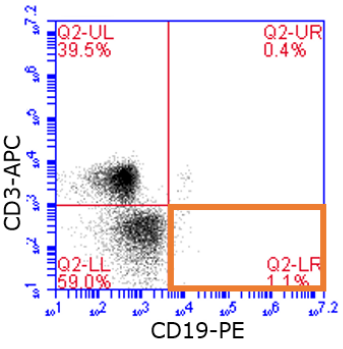
Figure 5.8. Immunophenotyping of lymphocyte population in mice splenocytes. Changes in cell population of T cells (CD3), $CD4^+$ T cells (CD3-CD4) and uncharacterized T cells (CD3-X) were determined using FACS analysis following stimulation with rFIP-fve, CWT-1 and CWT-2 for 48 hr. (a) The plots are representatives of three independent experiments. CD3-stained cells represented T cells; CD3- plus CD4-stained cells represented $CD4^+$ T cells (indicated by dark green box); CD8-stained cells represented $CD8^+$ T cells (indicated by orange box); and CD3-stained cells plus CD4-negatively stained cells represented uncharacterized T cells (indicated by blue arrows). (b) Data were expressed as mean of percentage of cell population (%) ± SD from three independent experiments. There were no significant differences in the cell population of T cells, $CD4^+$ T cells and uncharacterized T cells in rFIP-fve-, CWT-1- and CWT-2-stimulated splenocytes.

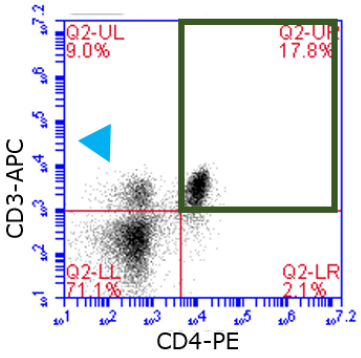
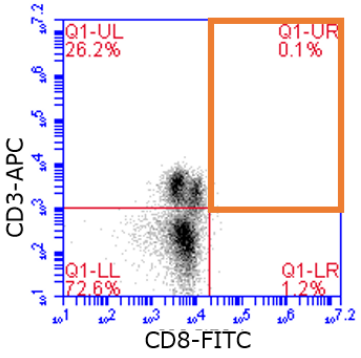
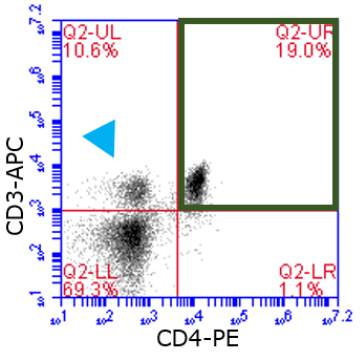
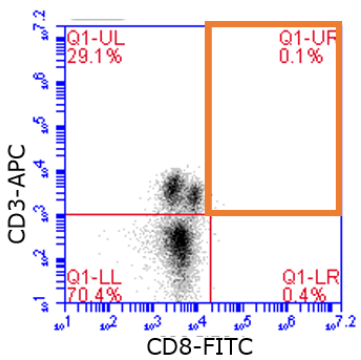
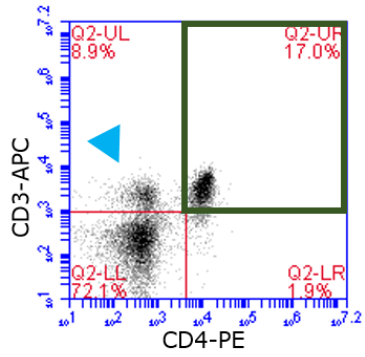
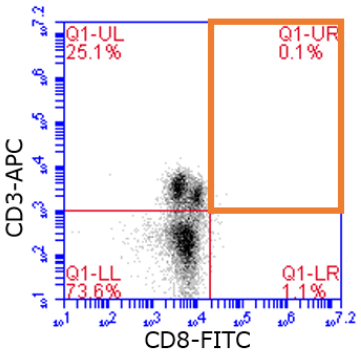
5.3.4.3 Mutants with loops modification

(A) Immunophenotyping of T cells and B cells

Characterization of immune cells was also carried out on mutants CWT-3-, CWT-4-, CWT-6-, CWT-7- and CWT-8-stimulated splenocytes. T cells and B cells are characterized by cells that are stained with CD3- and CD19-antibodies respectively. As shown in **Figure 5.9**, the percentage of T cells (CD3-stained cells) in splenocytes with treatment of 10 µg/ml rFIP-fve, CWT-3, CWT-4, CWT-6, CWT-7 and CWT-8 were 33.67% ± 0.91, 29.9% ± 5.06, 40% ± 0.78, 28.7% ± 5.16, 31.2% ± 3.14, and 27.53% ± 4.91 respectively; whereas the percentage of B cells (CD19-stained cells) in splenocytes with treatment of 10 µg/ml rFIP-fve, CWT-3, CWT-4, CWT-6, CWT-7 and CWT-8 were 1.13% ± 0.23 , 1.13% ± 0.23, 1.03% ± 0.21, 0.97% ± 0.23, 0.9% ± 0.20, and 0.83% ± 0.16 respectively. This implies that rFIP-fve and mutants primarily induced T cells proliferation where only a minimal population of B cells was detected. The percentage of T cells population in rFIP-fve-stimulated splenocytes were not statistically different to CWT-3, CWT-6, CWT-7 and CWT-8. The only significant difference was shown in the percentage of T cells population between CWT-4 and rFIP-fve as well as other mutants. The percentage of T cells population in CWT-4-induced splenocytes were significantly higher than rFIP-fve, CWT-3, CWT-6, CWT-7 and CWT-8. CWT-4 is the mutant that adopts loop FG region from LZ-8.

a)

Treatment	T cells (Dark green box)	B cells (Orange box)
rFIP-fve		
CWT-3		
CWT-4		

Treatment	CD4⁺ T cells (dark green box)	CD8⁺ T cells (orange box)
CWT-6		
CWT-7		
CWT-8		

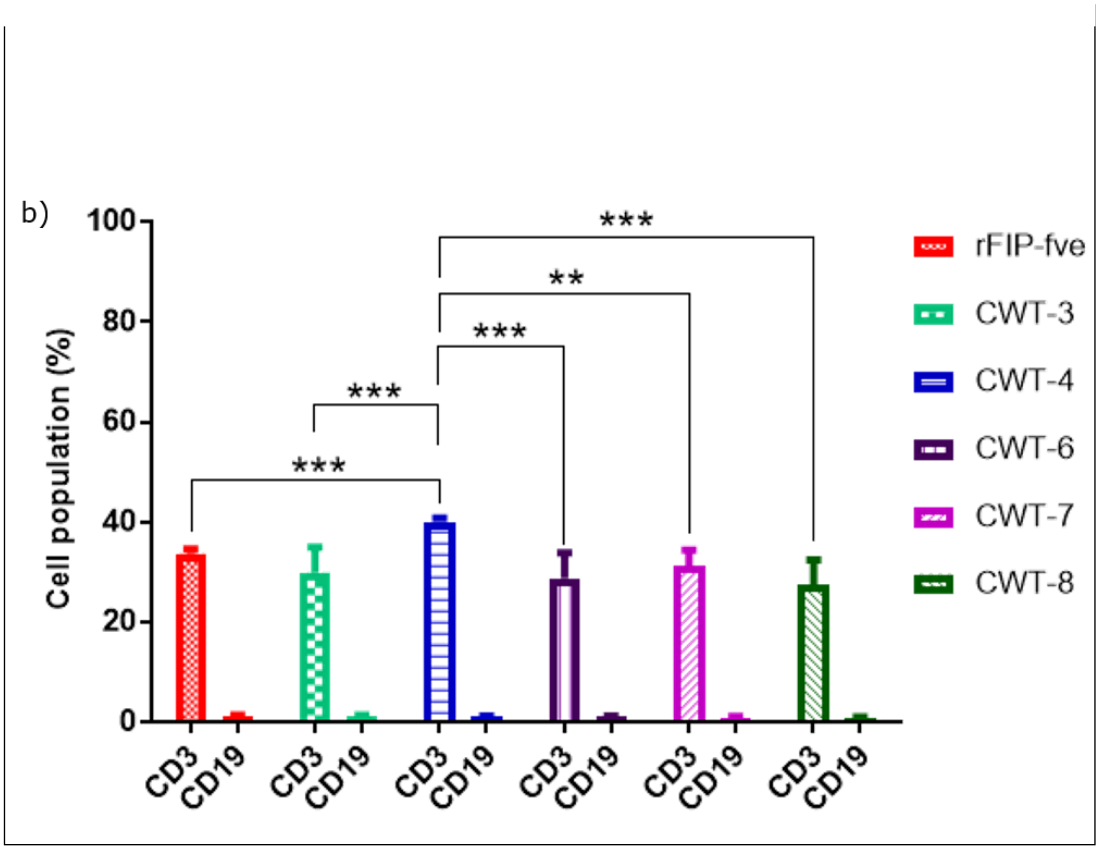
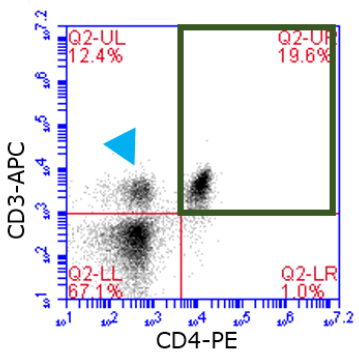
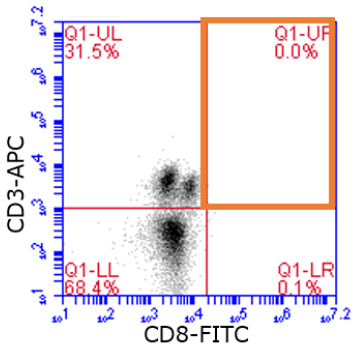
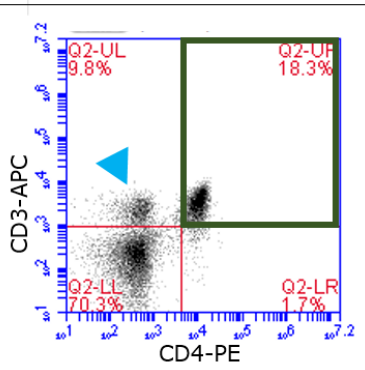
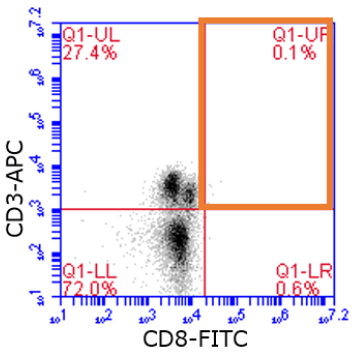
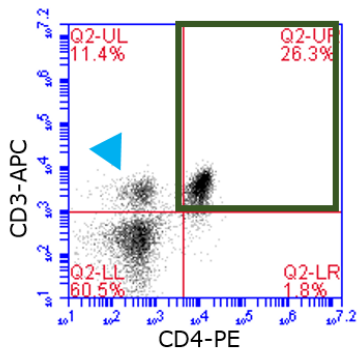
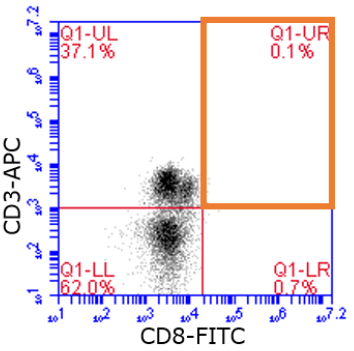


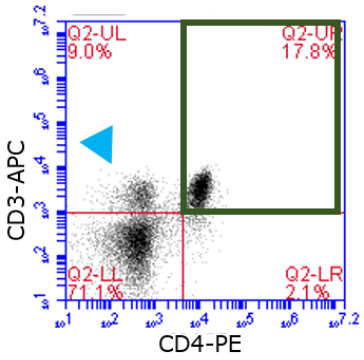
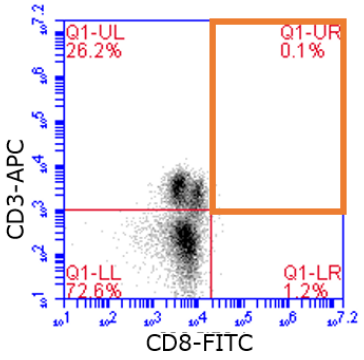
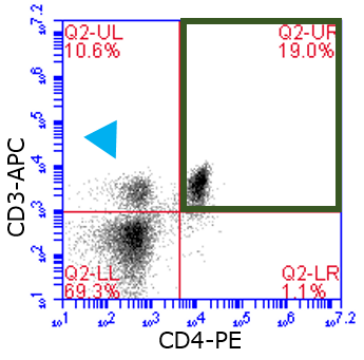
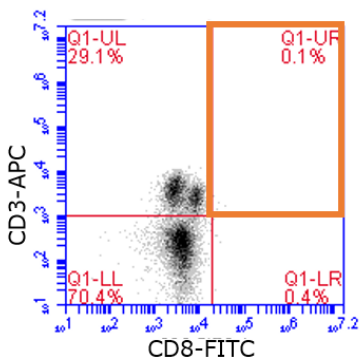
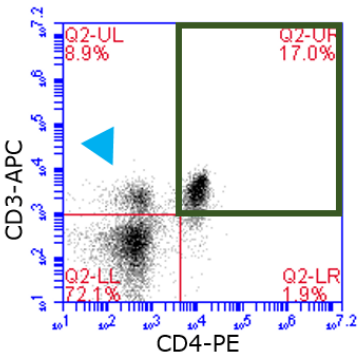
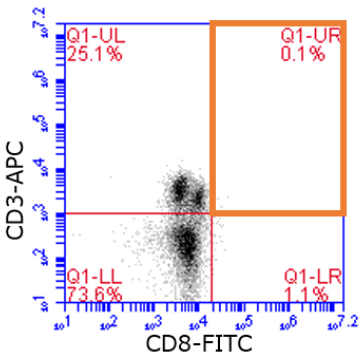
Figure 5.9. Immunophenotyping of lymphocyte population in mice splenocytes. Changes in cell population of T cells (CD3) and B cells (CD19) were determined using FACS analysis following stimulation with rFIP-fve, CWT-3, CWT-4, CWT-6, CWT-7 and CWT-8 for 48 hr. (a) The plots are representatives of three independent experiments. CD3-stained cells represented T cells (indicated by dark green box), whereas CD19-stained cells represented B cells (indicated by orange box). (b) Data were expressed as mean of percentage of cell population (%) ± SD from three independent experiments. The degree of significance in T cells population between CWT-4-induced stimulated splenocytes in comparison to rFIP-fve- and other mutants-induced splenocytes were determined using Tukey multiple comparisons test; $P \leq 0.05$ with *, $P \leq 0.01$ with **, $P \leq 0.001$ with ***, and $P \leq 0.0001$ with ****. CWT-4-induced splenocytes showed apparent higher T cells population in comparison to rFIP-fve and other mutants. There were no significant differences in the T cells population in rFIP-fve-, CWT-3-, CWT-6, CWT-7 and CWT-8-stimulated splenocytes.

(B) Immunophenotyping of T cells, $CD4^+$ T cells, and $CD8^+$ T cells

T cells, $CD4^+$ T cells and $CD8^+$ T cells are characterized by cells that are stained with CD3-, CD4-, and CD8-antibodies respectively. As shown in **Figure 5.10**, the percentage of T cells (CD3-stained cells) in splenocytes with treatment of 10 µg/ml rFIP-fve, CWT-3, CWT-4, CWT-6, CWT-7 and CWT-8 were 32.20% ± 1.04, 28.33% ± 5.75, 38.53% ± 0.80, 28% ± 3.74, 29.87% ± 3.51, and 26.7% ± 3.35 respectively; whereas the percentage of $CD4^+$ T cells (CD4-stained cells) in splenocytes with treatment of 10 µg/ml rFIP-fve, CWT-3, CWT-4, CWT-6, CWT-7 and CWT-8 were 19.40% ± 1.71, 18.33% ± 3.65, 26.5% ± 1.41, 16.87% ± 1.16, 18.93% ± 2.10, and 17.17% ± 1.70 respectively. The $CD4^+$ T cells made up approximately 50% of the T cells that were stimulated by rFIP-fve and mutants, while the $CD8^+$ T cells were not detected in rFIP-fve- and mutants-induced splenocytes. There was a population of cells that stained positively with CD3-antibody yet stained negatively with CD4-antibody as well as CD8-antibody as indicated with blue arrows in **Figure 5.10a**; this implies that the cell population was constituted of uncharacterized T cells as they were neither $CD4^+$ T cells nor $CD8^+$ T cells. The percentage of the uncharacterized T cells in splenocytes with treatment of 10 µg/ml rFIP-fve, CWT-3, CWT-4, CWT-6, CWT-7 and CWT-8 were 12.77% ± 0.81, 10.17% ± 1.00, 11.87% ± 0.57, 9.5% ± 0.78, 10.93% ± 0.85, and 9.53% ± 0.65 respectively. Other than CWT-4, there were no statistically differences in the percentage of $CD4^+$ T cells population in splenocytes that were treated with rFIP-fve, CWT-3, CWT-6, CWT-7 and CWT-8. The percentage of $CD4^+$ T cells population in CWT-4-treated splenocytes was significantly higher than rFIP-fve as well as other mutants with loop modification. Some uncharacterized T cells were also detected in this group of mutants, yet there were no significant differences among rFIP-fve and mutants.

a)

Treatment	CD4⁺ T cells (dark green box)	CD8⁺ T cells (orange box)
rFIP-fve		
CWT-3		
CWT-4		

Treatment	$CD4^+$ T cells (dark green box)	$CD8^+$ T cells (orange box)
CWT-6		
CWT-7		
CWT-8		

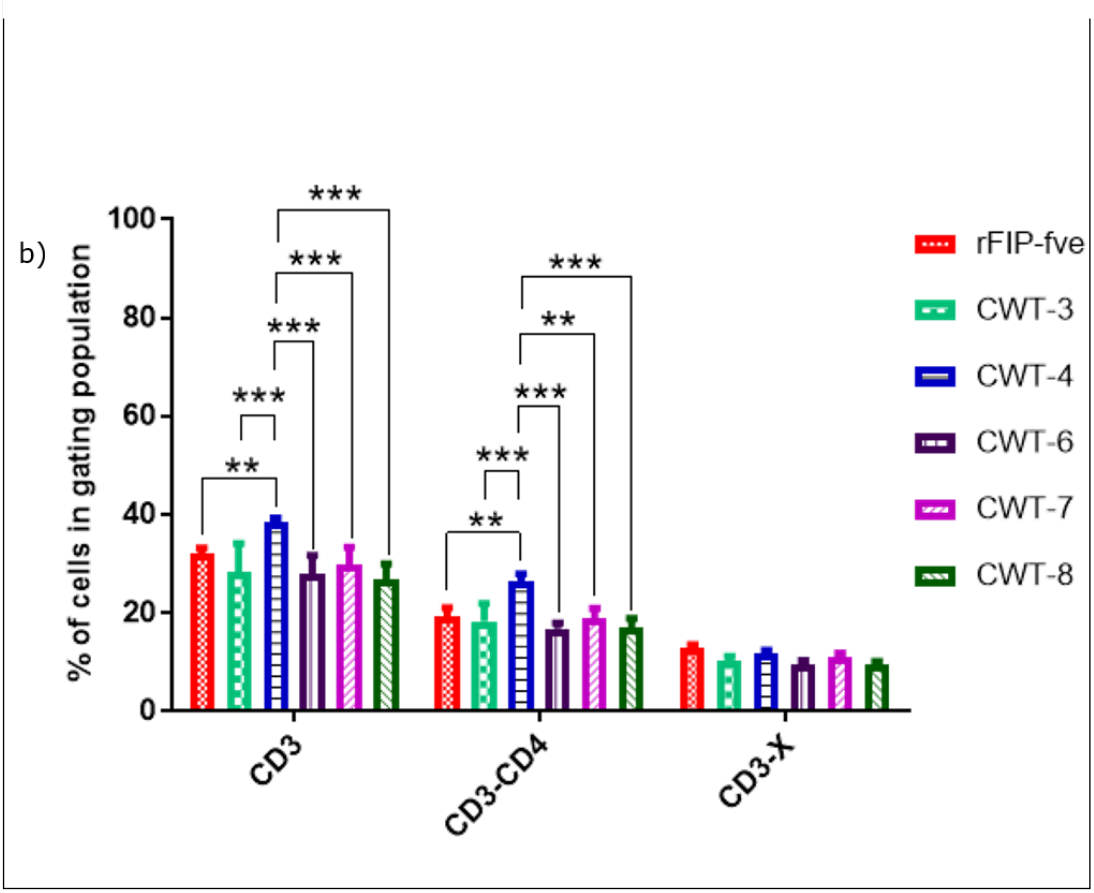
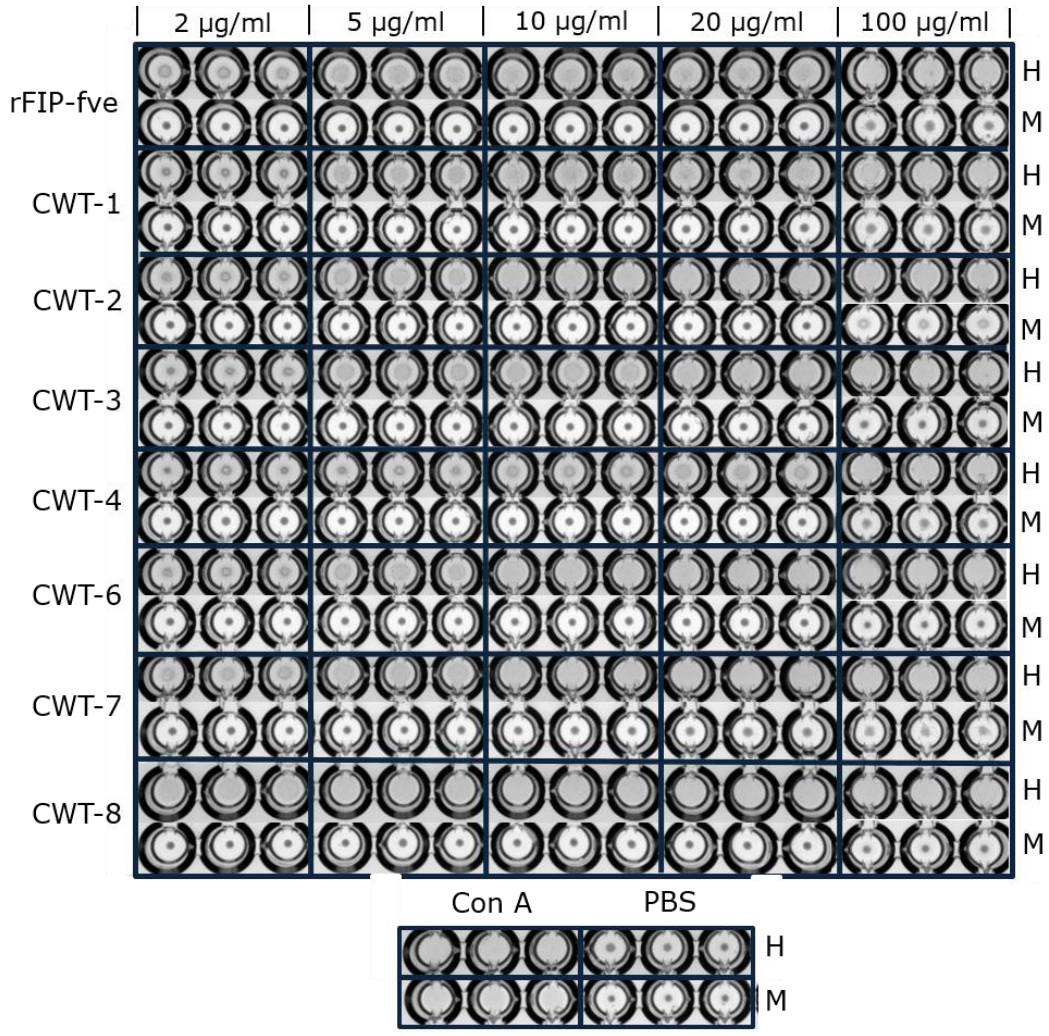


Figure 5.10. Immunophenotyping of lymphocyte population in mice splenocytes. Changes in cell population of T cells (CD3), $CD4^+$ T cells (CD3-CD4) and uncharacterized T cells (CD3-X) were determined using FACS analysis following stimulation with rFIP-fve, CWT-3, CWT-4, CWT-6, CWT-7 and CWT-8 for 48 hr. (a) The plots are representatives of three independent experiments. CD3-stained cells represented T cells; CD3- plus CD4-stained cells represented $CD4^+$ T cells (indicated by dark green box); CD8-stained cells represented $CD8^+$ T cells (indicated by orange box); and CD3-stained cells plus CD4-negatively stained cells represented uncharacterized T cells (indicated by blue arrows). (b) Data were expressed as mean of percentage of cell population (%) ± SD from three independent experiments. The degree of significance in T cells population between CWT-4-induced stimulated splenocytes in comparison to rFIP-fve- and other mutants-induced splenocytes were determined using Tukey multiple comparisons test; $P \leq 0.05$ with *, $P \leq 0.01$ with **, $P \leq 0.001$ with ***, and $P \leq 0.0001$ with ****. There were significant differences in the cell population T cells as well as $CD4^+$ T cells in CWT-4-induced splenocytes in comparison to rFIP-fve-, CWT-3, CWT-6, CWT-7 and CWT-8-stimulated splenocytes.

5.3.5 Haemagglutination activity

Both mice and human RBCs displayed aggregation activities in the presence of 5 µg/ml and 20 µg/ml of Con A respectively, which were used as the positive controls in haemagglutination assay as shown in **Figure 5.11**. In contrast, no haemagglutination activity was seen in PBS, which was used as the negative control. Aggregations of mice RBCs were observed in all of the recombinant proteins. The lowest concentrations of the recombinant proteins that displayed visible agglutination in mice RBCs were 2 µg/ml. On the other hand, distinct haemagglutination activities were displayed in human RBCs. There were no agglutination activities in human RBCs in the presence of rFIP-fve, CWT-1, CWT-2, CWT-4 and CWT-7 at concentrations 2-20 µg/ml; aggregations of human RBCs were observed only at 100 µg/ml. It is important to note that the haemagglutination reactions of human RBCs were not as obvious as the aggregation activities of mice RBCs, in fact the aggregation activities were very mild even at concentration as high as 100 µg/ml of the recombinant proteins. Interestingly, the three mutants CWT-3, CWT-6 and CWT-8 with mutations at loop DE demonstrated no agglutination activities in human RBCs at all of the concentrations tested.



Recombinant proteins	Haemagglutination	
	Mice RBCs	Human RBCs
rFIP-fve	+	+
CWT-1	+	+
CWT-2	+	+
CWT-3	+	-
CWT-4	+	+
CWT-6	+	-
CWT-7	+	+
CWT-8	+	-

Figure 5.11. Haemagglutination activities of rFIP-fve and mutants toward mice red blood cells (M) and human red blood cells of type O (H) were determined by incubating the recombinant proteins with 1.5% red blood cells and 0.2% gelatin. Two concentrations at 5 µg/ml and 20 µg/ml of Con A were included for positive control in haemagglutination toward mice and human red blood cells respectively. PBS was included as negative control. A range of concentrations of rFIP-fve and mutants was assessed for their haemagglutination abilities at 2, 5, 10, 20 and 100 µg/ml in triplicates. Data were representatives of three independent experiments. (+) indicates positive haemagglutination event, whereas (-) indicates negative haemagglutination observation.

5.4 Discussion

Several assays were conducted to investigate the immune-regulating activities of the mutants such as BrdU splenocytes proliferation ELISA, cytokine release ELISA, immune cells characterization flow cytometry analysis, and haemagglutination assay. In the experiments reported herein, the duration of splenocytes stimulation was designated at 48 hours based on the protocols employed in previous studies (Ko *et al.*, 1997; Wu *et al.*, 2008; Lin *et al.*, 2013).

Herein, Balb/c male mice strain was used in the experiments. It is an albino, laboratory-inbred mouse strain that is commonly used for immunological studies as it is very responsive to stimuli (Potter and Boyce, 1962). To ensure result consistency, same sex of mice were utilized in this study. It is noted that male mice have been shown to have tendency to fight with other mice that are house in group and cause physical injury, leading to infection (Nicholson *et al.*, 2009); therefore, there was a possibility of getting discrepancy in experimental results. To minimize result discrepancy, the mice were first examined physically prior to spleen collection to avoid the use of injured mice with wounds. Thus, it is believed that the spleen used in this study were collected from mice that were physically fit.

The first hypothesis examined herein was the supposition regarding to achieving enhanced immunomodulatory ability of FIP-fve via strengthened hydrophobic interaction between α-helices. The positive impacts of the mutation were demonstrated in proliferative responses of CWT-2-stimulated mice splenocytes as well as the concomitant induced secretory of cytokines from the splenocytes. The stimulatory activity of CWT-2 on splenocytes proliferation was approximately one-fold higher as compared to rFIP-fve. Moreover, there were apparent increase in CWT-2-induced cytokines IFN-γ and IL-2 release from mice splenocytes as well. Notably, CWT-2 enhanced as high as five-fold

increase in the secretion of IFN-γ from mice splenocytes. Based on these results, it is suggested that A2L in CWT-2 contributed to the effect of hydrophobicity enhancement within the association of inter-helix, leading to increased stability of dimeric interaction. Potentially, the enhanced stability of homodimer protein then prolonged the half-life of CWT-2, and resulted in increment of immunostimulatory activity on mice splenocytes. Indeed, it is believed that stability of biologic protein drug correlates with their half-life both *in vitro* and *in vivo*. An example of increased protein stability that was associated with improved bioactivity was reported by Whitehead Institute of Biomedical research where modified circular and PEGylated IFN-α2 with higher stability displayed increased cancer cell proliferative-inhibiting activity than wild type linear un-PEGylated form of the protein *in vitro* and *in vivo* (Popp *et al.*, 2011). Considering that one of the key challenges in making therapeutic proteins is to synthesize stable proteins with long half-life, the manufacturing and dosing of therapeutic proteins may be eased by increasing stability of proteins (Osherovich, 2011). Altogether, the finding in this study demonstrated for the first time that reinforcement of the inter-helix hydrophobic interaction via replacement of least hydrophobic residue with higher hydrophobicity residue was able to enhance the *in vitro* immunostimulatory activity of FIP-fve.

Apart from that, the present study also attempts to explore if the addition of highly conserved N-terminal methionine in FIPs family to the N-terminal of FIP-fve would give rise to advantageous effect in immunomodulatory activity of FIP-fve. Methionine is the universal translation start codon in both eukaryotes and prokaryotes. Although the first Met is generally removed in many maturated proteins in both eukaryotes and prokaryotes, some proteins are found to retain their N-terminal Met. The underlying reason of retaining of initiator Met in protein was not clearly known. There was a suggestion that second amino acid adjacent to initial Met serves as the determinant factor on N-terminal protein processing (Flinta *et al.*, 1986). For instance, the first methionine is mostly removed in

the amino acid chain that carries alanine as second amino acid; in the case when second amino acid is lysine, the initial methionine is retained. This deduction on N-terminal Met removal was made after examining on a sample of 120 eukaryotic proteins and 170 prokaryotic proteins (Flinta *et al.*, 1986). Other than that, it is also postulated that protein may require the removal of Met in order to unmask the adjacent amino acid to uncover the biological activities (Meinnel, Mechulam and Blanquet, 1993). For example, unmasked N-terminal Cys was required for the enzymatic activity of *E.coli* glutamine phosphoribosylpyrophosphate amidotransferase (Tso, Hermodson and Zalkin, 1979). The current research showed that there was no significant differences in mice splenocytes stimulation index between rFIP-fve and mutant CWT-1 that harbours N-terminal Met addition. Indeed, it was observed that rFIP-fve induced a higher splenocytes proliferation in comparison to CWT-1 according to the microscopic visualization of splenocytes interactions. Additionally, the secretion level of IL-2 was significantly lower in CWT-1-induced splenocytes as compared to rFIP-fve. Collectively, the results indicated that the N-terminal Met addition did not enhance the immunomodulatory activity of FIP-fve. More importantly, the mutation in CWT-1 resulted in a slight reduction of its immunomodulatory activity. Based on the results, it is surmised that the additional N-terminal Met in CWT-1 possibly affected the interaction of amino acid residues in the N-terminal α-helices that span from residues 2 to 14, diminishing protein stability. In short, the absence of Met residues in FIP-fve appeared necessary to maintain the immunomodulation activity of FIP-fve, which could be the reason why the Met residue is excluded in native FIP-fve.

Another aspect that warrants research attention was the reported distinctive conformations at the two loop regions in FNIII-type domain of FIP-fve and LZ-8. In examination of the effects on loops region modification, some interesting findings were revealed. Results shown that CWT-3 and CWT-6 that harbour only the loop DE (LZ-8) mutation displayed more than one-fold increase in splenocytes stimulatory activities and approximately five-fold increase in IFN-γ releases in comparison to rFIP-fve. There was a significant increase of IL-2 release in mice splenocytes as well but the difference in comparison to rFIP-fve was less profound, unlike IFN-γ release. Provided that LZ-8 has been viewed as a FIP with higher therapeutic status, it was expected that CWT-8 with adoption of both loop DE and FG in LZ-8 would gave the best splenocytes stimulatory activity as the pair of LZ-8-derived loops region was included in the mutant. Contrary to the expectation, treatment of CWT-8 resulted in reduction in splenocytes proliferation as well as decline in cytokines IFN-γ and IL-2 synthesis as compared to CWT-3 and CWT-6. As CWT-8 consists of mutation on both loop DE and FG regions (LZ-8), it thus appeared that the incorporation of loop FG from LZ-8 was responsible for the reduction effects. Another important finding was that E61K hinge residue was not critical in the immune-regulating enhancement of FIP-fve where both CWT-3 and CWT-6 demonstrated similar splenocytes stimulatory activities; CWT-3 is the mutant with loop DE adoption (LZ-8), whereas CWT-6 is the mutant with loop DE and E61K hinge residue adoption (LZ-8). On the other hand, a more apparent effect of hinge residue I97D adoption was observed in loop FG region where CWT-4 that is lacks of mutation I97D demonstrated 35% reduction in splenocytes proliferation assay in comparison to CWT-7 that carries mutation in I97D and loop FG region. All things considered, loop DE mutations that are harboured by CWT-3 and CWT-6 were found to be the main determinant regions that were responsible in enhancing their *in vitro* immune-regulating activities on mice splenocytes.

There is an increasing effort in exploring the application of cytokines to enhance immune system for cancer treatments. In fact, IL-2 was developed as an early candidate for cancer immunotherapy where it was approved for the treatment of renal cell carcinoma in 1992 and metastatic melanoma in 1998 by Food and Drug Administration (FDA) (Rosenberg, 2014). However, the monotherapy of IL-2 is incapable of improving survival of patients even though it displays capability in regressing tumour due to two major factors: (i) dual functional properties of IL-2 on T cells and (ii) toxicity effect of IL-2 in high dose. These have caused limitation in using IL-2 in immunotherapy. Many research are still ongoing to seek for efficient and strategic way of using IL-2 to treat metastatic cancer (Jiang, Zhou and Ren, 2016). Apart from that, IFN-γ was reported to be efficient in impairing tumour angiogenesis via direct inhibition of endothelial cell proliferation (Alshaker and Matalka, 2011). Moreover, IFN-γ was shown to inhibit tumour growth *in vivo* through up-regulation of MHC class I molecules on tumour cells, leading to increased tumour cells immunogenicity that subsequently resulted in tumour cell death (Sengupta *et al.*, 2010). Additionally, IFN-γ also involved in antagonizing the secretion of immunosuppressive cytokines such as TGF-β and IL-10, which may otherwise promote development of highly invasive tumour in metastatic state (Martini *et al.*, 2010). Ding and colleagues also underlined the importance of FIP-fve-stimulated IFN-γ in mediating the cancer-inhibiting effects. They explored the potential of using FIP-fve as adjuvant in cancer immunotherapy by co-administrating human papillomavirus (HPV)-16 E7 oncoproteins and FIP-fve to mice that were challenged with TC-1 cells. It was demonstrated that IFN-γ played a principal role in generating tumour-inhibition effects against TC-1 cell tumour challenge as the effect of FIP-fve plus HPV-16 E7 was greatly weaken in mice with depleted IFN-γ (Ding *et al.*, 2009). Other than that, FIP-fve has been reported to possess anti-inflammatory effect in mice that were sensitized with allergens. The inflammation-inhibition effect was shown to be mainly mediated by the ability of

FIP-fve in inducing the IFN-γ release, which inhibited and neutralized the T_H2-skewed immune response (Hsieh *et al.*, 2003; Lee *et al.*, 2013; Chang *et al.*, 2015; Chu *et al.*, 2017). Collectively, IFN-γ is one of the key players in host immune response that is involved in inhibition of events such as cancer growth or inflammation. With this in view, FIP-fve is regarded as a potential candidate for immunotherapy as it has been demonstrated to be capable of directing immune response towards T_H1 via stimulation of IFN-γ and IL-2 release. Essentially, mutants CWT-2, CWT-3 and CWT-6 that were generated in this research have shown significant enhancement in immune-regulating activities, by which it demonstrated the feasibility in further improving the bioactivities of FIP-fve. In view of this notion, FIP-fve mutants with enhanced immune-modulating abilities offer potential multi-beneficial therapeutic approach by stimulating substantial level of both IFN-γ and IL-2 in the microenvironment of host, which would otherwise require individual synthesis of these two recombinant cytokines proteins.

In order to better understand the immunomodulatory mechanism of FIP-fve, the present research also delved into identifying the specific cell phenotypes that undergo proliferation in mice splenocytes after stimulation with recombinant FIP-fve and mutants proteins. In theory, most lymphocytes are kept at resting states, and the mechanism of initiation requires a step of specific antigen recognition. The clonal expansion of T cells in response to antigen recognition is mediated by a combination of signals from antigen receptor, costimulators, and autocrine growth factors, primarily IL-2 (Abbas, Lichtman and Pillai, 2015). All of the previous studies did not clarify that whether T cells were actually stimulated to proliferate in FIPs-stimulated cultures or whether the FIPs would simply induced effector function without clonal expansion, apart from the study of Ding and research group (2009). Generally, the results of proliferation assays were reported as a representation of whole splenocytes population and the immunostimulatory effect of native FIP-fve or recombinant FIP-fve were assessed by measuring the generation of

induced cytokines IFN-γ and IL-2 (Ko *et al.*, 1997; Wang *et al.*, 2004; Wu *et al.*, 2008; Ding *et al.*, 2009; Ou *et al.*, 2009; Lin *et al.*, 2013). There were no explanation on how FIP-fve activate T cells in the absence of antigen as a step of specific recognition is necessary in T cell initiation.

In this respect, it is of interest to see if rFIP-fve and mutants did stimulate the proliferation of T cells and to compare the differences in T cells proliferation among the generated mutants. Flow cytometry was utilized in this study to examine the changes in types and amounts of immune cells in rFIP-fve- and mutants-stimulated splenocytes; particularly, the T and B cells were targeted. T cells were predominantly detected in the rFIP-fve- and mutants-stimulated cultures where $CD4^+$ T cells made up more than 50% of the total population in detected T cells, while only a minimal amount of B cells was detected in the cultures. This indicates that the recombinant FIP-fve and derivative proteins favoured and directed the kinetic of splenocytes stimulatory responses to T_H1 immune response; this is consistent with the previous research (Ko *et al*., 1995; Lin *et al*., 2013; Lee *et al*., 2013 and Chu *et al.*, 2017). Interestingly, there were no significant differences in the number of induced $CD3^+$ T cells, $CD4^+$ T cells, $CD8^+$ T cells, and uncharacterized T cells among the mutants and rFIP-fve treatment cultures, except CWT-4. In fact, no $CD8^+$ T cells were detected in the rFIP-fve- and mutants-stimulated splenocytes. CWT-4 was found to induce a higher number of T cells (although the induced total splenocytes population was the lowest among the mutants). It is therefore suggested that the mutation (loop FG region (LZ-8)) in CWT-4 might be responsible in stimulating and maintaining T cells but the exact mechanism requires further elucidation. In general, the immunophenotyping results imply that: (i) there were no direct activation of T cells mitogenesis by the rFIP-fve and mutants proteins and (ii) the uncharacterized immune cells were the main populations that contributed to the apparent differences in total splenocytes proliferation index among the rFIP-fve and mutants proteins.

Considering the reasoning as stated above, the differences in IFN-γ- and IL-2-secretions level among the mutants were possibly due to the varied stimulation competency of rFIP-fve and mutants that influenced kinetic of cytokine secretion by immune cells. The role of IFN-γ in mediating survival of unstimulated $CD4^+$ T cells was suggested in balb/c mice (Reed, Branigan and Bamezai, 2008). It was shown that $CD4^+$ T cells pre-exposed with IFN-γ displayed higher proliferation than negative control $CD4^+$ T cells in response to stimulation by antigen $cOVA_{323–339}$, which was a result of enhanced survival of IFN-γ treated $CD4^+$ T cells. Thus, it is postulated that the produced IFN-γ in the splenocytes culture may be involved in the survival of uninduced (antigen)-$CD4^+$ T cells, and maintained the basal amount of $CD4^+$ T cells in this study. This explained the observation where similar amount of T cells were detected in rFIP-fve and mutants-stimulated splenocytes cultures despite having differences in the number of total splenocytes cells. In view of these observations, the results suggested that stimulation with rFIP-fve and the mutants *in vitro* directed the splenocytes stimulatory kinetic toward T_H1 immune response, but T cells mitogenesis were not initiated in the absence of antigen where the recombinant proteins were unable to bypass MHC antigen restriction. The uncharacterized immune cells accounted for the main population that was stimulated by the recombinant proteins where extended study is required to distinguish the stimulated cell population.

Contradictory results were reported by Ding and colleagues (2009), however, who claimed that T cell proliferation was activated when purified $CD90^+$ T cells were co-cultured with mitomycin C-treated bone-marrow dendritic cells (BM-DCs) or splenocytes in the presence of FIP-fve. The BM-DCs and splenocytes was harvested from C57BL/6 mice. It is important to note that they did not utilize any immunophenotyping methods to characterize and measure the activated T cells, rather [^{3}thymidine] incorporation proliferation assay was used in their studies, which demonstrated the proliferation of a total population in the culture without actually characterizing the T cells. Additionally, they did not elaborate further on how FIP-fve bypassed MHC class restriction and activated T cells without the presence of antigen as the T cell activation must include a step of specific recognition. In fact, conflicting results were also demonstrated in the Con A-stimulated splenocytes cultures where one research group showed that there were enhancement in the release of cytokines but proliferation of $CD4^+$ T cells were not detected in Con A-induced cultures (Countiho *et al.*, 1973), whereas another research group presented that there were clonal expansion of $CD8^+$ T cells upon stimulation with Con A (Teh, Phillips and Miller, 1978). The reason of these inconsistent results are unknown. In spite of the inconsistent finding, it is noteworthy to mention that the participation of accessory cells are shown necessary for T cell activation by both FIP-fve (Ding *et al.*, 2009) and Con A (Habu and Raff, 1977). It was found that FIP-fve induced T cell proliferation and IFN-γ production only when T cells were co-cultured with accessory cells such as dendritic cells or splenocytes (Ding *et al.*, 2009). Similarly, there was no proliferation observed in culture of T cells alone with Con A, indicating that Con A does not induce T cell mitogenesis directly (Habu and Raff, 1977). The results from these studies again demonstrated that neither FIP-fve nor Con A was able to carry out direct activation of T cell mitogenesis. This derivation has indeed becomes more apparent when it was shown that the proliferative capacity of Con A-responding cells was lost in

repeated subculture of Con A-stimulated blasts in fresh medium containing Con A (Watanabe, Fathman and Coutinho, 1977). This highlighted the roles of accessory cells that were possibly lost during the repeated subcultures. It was indeed subsequently shown that the proliferating cells can only be initiated upon Con A-dependent interaction among non-proliferating cells such as macrophage type-cells, non-T and other T cells; these cells do not proliferate themselves in ConA-stimulated cultures (Andersson *et al.*, 1979). Notwithstanding the evidences, it is worth noting that the *in vitro* results are likely to differ in *in vivo* setting when the FIP-fve is used as adjuvant and coadministered with specific antigen into a host as clonal expansion of T cells can be stimulated in the presence of antigen recognition. FIP-fve could contribute considerable enhancement in T cell activation *in vivo*, in particular via reinforcement on cytokines release of IFN-γ and IL-2.

Since FIPs possess similar agglutination ability to ConA, haemagglutination assay was often employed in the study of FIPs as one of the assays to analyse their bioactivities. Human RBCs were trypsinized prior to incubation with mutant proteins as no agglutination activities were observed in untrypsinized RBCs. The same observation was reported by Bastiaan-Net and colleagues (2013) as well. Trypsin could uncover and release the binding receptor sites, allowing them to move in the plane of the membrane, and subsequently cross-linking of RBCs take place (Noonan and Burger, 1973). The haemagglutination results were consistent to the previous studies where FIP-fve (Ko *et al.*, 1995) and rFIP-fve (Lin *et al.*, 2013) showed agglutination in human RBCs. Haemagglutination of FIP-fve was not tested in mice previously. This study showed that rFIP-fve and mutants were also capable of agglutinating the mice RBCs. One interesting finding was that mutants CWT-3, CWT-6 and CWT-8 (with adoptions of loop DE (LZ-8)) lost their haemagglutinating abilities, which is the desired feature for the development of safe protein therapeutic drug. Likewise, it was reported that LZ-8 lacks of haemagglutinating activity towards human RBCs as well (Kino *et al.*, 1989). This

indicates that the loop DE region in LZ-8 might be critical in abolishing the haemagglutination ability in FIPs. This feature may not seem necessary in this study as the rest of the mutants induced human RBCs agglutination only at high concentration (100 µg/ml), but the discovered mutation region that could reverse the agglutination feature of FIP-fve may be utilized for protein production in the future study as different expression method or system may yield protein with different haemagglutination competency. The expression system used to produce recombinant FIPs appeared to affect the RBCs epitope specificity of recombinant FIPs as discussed in **Chapter 2 Section 2.2.1**. For instance, both native FIP-fve and rFIP-fve (produced using *P. pastoris* GS115 system) were able to haemagglutinate all four types of human RBC (A, B, AB and O) at 2 µg/ml (Ko *et al*., 1995 and Lin *et al.*, 2013); yet, a contradicting result was noted in rFIP-fve that was expressed using *P. pastoris* X-33 system where no agglutination was observed towards human RBCs (Bastiaan-Net *et al.*, 2013). For this reason, in case if the choice of expression system results in haemagglutination of human RBCs, mutation targeting the loop DE region may be utilized to abolish the agglutination ability of FIPs.

5.5 Conclusion

In summary, the immunomodulatory and haemagglutination effect of N-terminal Met addition (mutant: CWT-1), hydrophobic interaction enhancement (mutant: CWT-2), and loops modification (mutant: CWT-3, CWT-4, CWT-6, CWT-7 and CWT-8) in FIP-fve were investigated in this study. The abilities of mutant group with putative reinforcing N-terminal dimerization and group with loops modification were tabulated in **Table 5.3** respectively. The critical regions that are responsible for immune-regulating activities of FIP-fve were discovered. It was found that adoption of loop DE (LZ-8) was responsible for the considerable enhancement in immunostimulatory activity of FIP-fve derivatives, CWT-3 and CWT-6; particularly the splenocytes proliferative response and secretory IFN-γ and IL-2 cytokine level were greatly elevated. Another very much desired-feature is that the harbouring of loop DE (LZ-8) was capable of abolishing ability of FIP-fve in human RBCs haemagglutination, making it suitable and safe to be developed for protein therapeutic drug use. One of the interesting discoveries was that the adoptions of both loop DE and FG regions from LZ-8 have resulted in a reduction effect to the immune-regulating activity of CWT-8. This has prompt the interest to investigate the immunomodulation effect of substitution of loop FG in LZ-8 in future study. Additionally, it has never been addressed previously that whether FIP-fve is involved in the direct activation of T cells mitogenesis. This study postulated that rFIP-fve and mutants did not stimulate T cell mitogenesis directly in *vitro*, but they generated and directed kinetic of immune responses towards T_H1 and the uncharacterized immune cells accounted for the main population that was stimulated by the recombinant proteins. Momentously, this study represents the first in the FIPs family to demonstrate the enhancement in immunomodulatory activity of FIP-fve by enhancing N-terminal dimerization and modifying loops regions.

Table 5.3. Comparison of immunomodulatory and haemagglutination activities of recombinant FIP-fve and derivatives protein.

Recombinant proteins	Splenocytes proliferative response	Maintenance on T cells population	Secretory IFN-γ production	Secretory IL-2 production	Haemagglutination	
					Human RBCs	Mice RBCs
rFIP-fve	++	+++	+	++	+	+++
CWT-1	++	+++	+	+	+	+++
CWT-2	++++	+++	++	+++	+	+++
CWT-3	++++	+++	++++	++++	-	+++
CWT-4	++	++++	+	++	+	+++
CWT-6	++++	+++	++++	++++	-	+++
CWT-7	+++	+++	++	+++	+	+++
CWT-8	+++	+++	++	+++	-	+++

(+) – indicates level of positive activity
(-) – indicates negative activity

Chapter 6 Evaluation on Anti-Cancer Activities of FIP-fve Mutants

6.1 Introduction

Chapter 6 presents the assessment on the anti-cancer activities of rFIP-fve and mutants against lung cancer and breast cancer cell lines because these two cell lines accounted for amongst the two highest risk in cancer death. Lung cancer is the leading cause of cancer death globally where there was approximately 1.6 million deaths recorded (491,200 deaths in women and 1.1 million deaths in men) in 2012 (American Cancer Society, 2015). Lung cancers are generally classified into two major types: (i) small-cell lung carcinoma (SC) and (ii) non-small-cell lung carcinoma (NSCLC) that comprised of subtypes of adenocarcinoma, large cell carcinoma and squamous cell carcinoma (Watanabe *et al.*, 2010). NSCLC is the most frequently diagnosed lung cancer type where it accounted for an estimation of 85% of all lung cancer cases (Schabath *et al.*, 2014). One commonly used NSCLC cell line is A549 cells, which is an epithelial cell type that was obtained from a pulmonary adenocarcinoma of a 58 year old Caucasian male in 1973. A549 cells possess high migration capability. In 2018, there is an estimation of 234,030 incidences of newly diagnosed lung cancer in US. Cigarette smoking is the highest risk factor for lung cancer thus far, where it responsible for 80% of mortality rate in United States of America (American Cancer Society, 2018). Treatment for lung cancer includes surgery, chemotherapy, radiation, targeted treatment and immunotherapy depending on individual conditions of the patients (Cancer Care, 2018).

Following lung cancer, breast cancer accounted for the second highest mortality rate where it is one of the major causes of cancer death in women in developing countries. Globally, breast cancer accounted for an approximately 521,900 deaths in women in 2012 (American Cancer Society, 2015). In 2018 (US), there is an estimation of 266,120 cases of newly diagnosed breast cancer in women and 2,550 cases of newly diagnosed breast

cancer in men (American Cancer Society, 2018). Based on the expression markers of progesterone receptor (PR), estrogen receptor (ER), and human epidermal growth factor receptor 2 (HER-2)/Neu amplification on breast cancer, the subtypes of breast cancer are classified into hormone receptor positive, amplified HER-2/Neu, and triple-negative breast cancer (lacking of the three expression markers) (Brenton *et al.*, 2005). One of the most commonly used breast cancer cell lines in medical research is MDA-MB-231 cells, which is an epithelial cell type that was obtained from pleural effusion of a 51 year old Caucasian female with metastatic adenocarcinoma (Cailleau, Olivé and Cruciger, 1978). MDA-MB-231 is a triple-negative breast cancer cell line with a highly aggressive and invasive characteristic. Another breast cancer subtype is MCF-7 cells, which was established by Dr Soule research group in 1973 at Michigan Cancer Foundation. MCF-7 was also isolated in pleural effusion of a 69 year old Caucasian woman with metastatic adenocarcinoma (Soule *et al.*, 1973). MCF-7 is both ER- and PR-positive (Shirazi, 2011). It possesses limited motility and metastatic potential (Shirazi, 2011), therefore this cell line is non-aggressive and poorly invasive (Gest *et al.*, 2013). In contrast to MDA-MB-231 that has high migration capability, MCF-7 does not normally migrates as it has a low level of vascular endothelial growth factor (VEGF), which is a key mediator of angiogenesis (Perrot-Applanat and Di Benedetto, 2012). The treatment choices are dependent on the presence of expression markers on the distinct subtypes of breast cancer (Brenton *et al.*, 2005). Amplified HER-2/Neu or triple negative breast cancer usually has a less favourable prognosis than hormone receptor-expressing breast cancer. In general, hormone-inhibition therapy is used to treat breast cancer patient with expression of ER and PR; HER-2/Neu amplification-inhibition is used to treat breast cancer patient with amplified HER-2/Neu; and chemotherapy is used to treat triple negative breast cancer patient (Brenton *et al.*, 2005).

Despite heterogeneity and diversity of tumours, they possess the same ability to survive beyond their normal life span and proliferate continuously that would otherwise be restrained in the normal tissue growth. Generally, suppression of cell apoptosis in addition to the uncontrolled cell proliferation contribute to the initial platform for subsequent occurrence of neoplastic evolution (Evan and Vousden, 2001). The deregulated cell proliferation is associated by two other critical cancer developments, which are invasion and metastasis. Metastasis refers to dissemination of cancer cells from primary cancer site to distant secondary site (Friedl and Wolf, 2003). Metastasis is responsible for the main cause of death in cancer patients. Cancer cell migration and invasion are the two processes involved in cancer metastasis whereby the processes allow invasion into adjacent tissues and intravasation into bloodstream and lymphatic vessels (Friedl and Wolf, 2003).

In recent years, the research in FIPs has been directed to investigation on their anti-cancer abilities. Different research groups have demonstrated the cancer-inhibiting potentials in FIPs such as FIP-fve (Chang *et al.*, 2010, 2013), LZ-8 (Lin *et al.*, 2017), and other newly discovered FIPs, namely FIP-sch3 and FIP-dsq2 (Li *et al.*, 2016, 2017). There is much to be learned and examined to address mechanism and site of action of FIPs utilised in inhibiting cancer cell growth; this knowledge could lay the foundation for future therapeutic development of FIPs. As mentioned earlier, it was shown that LZ-8 possesses much greater anti-cancer ability than FIP-fve in spite of the fact that both of them share highly similar structure. LZ-8 has been reported to have direct toxicity effect against HL60 tumour cells, whereas FIP-fve did not show such activity against the HL60 cells (Huang *et al.*, 2009). Another research group also displayed that FIP-fve contributed to the least cancer-inhibiting ability in comparison to LZ-8, FIP-dsq2 and FIP-sch3 (Li *et al.*, 2016, 2017). It is proposed that the differences in their anti-cancer abilities are due to the variability in the local loops region of each FIPs protein (Huang *et al.*, 2009; Li *et al.*,

2016, 2017). Besides assessment on the immunomodulatory capabilities of rFIP-fve and derivatives, this idea has also intrigued this present research to examine and compare their capabilities in direct inhibition against cancer cells. The list of the generated recombinant proteins of FIP-fve and mutant were presented in **Chapter 5 (Section 5.1, Table 5.1)**. In this chapter, the anti-cancer activities of rFIP-fve and mutants with N-terminal Met addition (mutant: CWT-1), hydrophobic interaction enhancement (mutant: CWT-2), and loops modification (mutant: CWT-3, CWT-4, CWT-6, CWT-7 and CWT-8) were assessed against lung cancer cell line (A549 cell) and breast cancer cell lines (MDA-MB-231 and MCF-7 cells). MTT [3(4,5-dimethyl-thiazoyl-2-yl)2,5diphenyl-tetrazolium bromide] colorimetric assay was utilised to determine the optimal concentration and time point of the respective rFIP-fve and mutants in inhibiting tumour cell viability of all three cell lines. The optimal concentrations determined were then used to investigate the anti-migration activities of rFIP-fve and mutants toward A549 and MDA-MB-231 cells. Lastly, their cancer-inhibiting activities were analysed and compared.

Therefore, the specific objectives for this chapter are: (i) to test a hypothesis that enhancing of dimerization in FIP-fve would further improve its cancer-inhibiting activities; (ii) to investigate the possible mutational benefit of adjoining highly conserved methionine to the N-terminal of FIP-fve; and (iii) to examine the anti-cancer effects of loops modification in FIP-fve, which were adoption of loop DE alone, adoption of loop FG alone, adoption of loop DE and E61K hinge residue, adoption of loop FG and I97D hinge residue, adoption of loop DE and FG, and adoption of loop DE, loop FG, E61K hinge residue, I97D hinge residue.

6.2 Materials and methods

6.2.1 General materials and specialised equipment

6.2.1.1 Cell and cell culture reagents

Human breast cancer cell MDA-MB-231 (American Type Cell Collection (ATCC)® HTB-26™, USA), breast cancer cell MCF-7 (ATCC® HTB-22™, USA), and lung adenocarcinoma epithelial cell A549 (ATCC® CCL 185™, USA) were maintained in RPMI 1640 (Nacalai Tesque, Japan) containing L-glutamine, D-(+)-glucose, and phenol red and supplemented with 10% fetal bovine serum (FBS) (Sigma-aldrich, USA) and 100 unit/mL penicillin and 100 µg/ml streptomycin antibiotic (Gibco™, USA). The supplemented RPMI 1640 was referred as complete RPMI in this context. The cells were incubated at 37˚C in a 5% CO_2 humidified atmosphere. The MDA-MB-231 and MCF-7 breast cancer cell lines were kindly given by Dr Ho Wan Yong from University of Nottingham Malaysia Campus; whereas the lung cancer cell line was obtained from Professor Dr Sandy Loh Hwei San from University of Nottingham Malaysia Campus. PBS (137 mM NaCl, 2.7 mM KCl, 10 mM Na_2HPO_4 and 1.8 mM KH_2PO_4, pH 7.2) was sterilized by autoclaving at 121˚C for 15 min.

6.2.1.2 Specialised equipment

CO_2 incubator (Mermmert, Germany) was used for incubation of cancer cells. The absorbance reading was conducted using Epoch microplate spectrophotometer (BioTek®, USA) and analysed using Gen5 Data Analysis Software (BioTek®, USA). Centrifugation was performed using centrifuge 5810 R (Eppendorf™, USA).

6.2.1.3 Protein samples

Recombinant rFIP-fve and derivatives proteins were prepared as described in **Chapter 4**. All of the two-steps purified recombinant proteins were concentrated to 1 mg/ml using Macrosep® advance centrifugal device (PALL, US) and filter-sterilized using sterile PES 0.22 µM syringe filters (Membrane Solutions, China). Small aliquots of proteins were prepared and stored at -20˚C. Recombinant rFIP-fve and derivatives proteins were prepared freshly for three independent courses of cancer cells treatment.

6.2.2 Cell viability inhibition assay

6.2.2.1 Concentration-dependent cell viability inhibition

The optimum concentrations of recombinant FIP-fve and derivative proteins in inhibiting cancer cell viability was determined using MTT assay according to the protocol as described by Hsin and collegues (2011). The cancer cell lines were prepared for cell viability inhibition assay when the cells reached 70-80% confluence. The spent medium was removed and the cell monolayer was washed with 5 mL sterile PBS, which was subsequently discarded. The cells were trypsinised with 0.25% trypsin-EDTA (Gibco™, USA) at 1 mL per 25 cm^2. The cells in the flask were incubated in CO_2 incubator at 37˚C for 5 min. Then, the cells were resuspended using RPMI-1640 containing 10% FBS to inactivate the trypsin, and the cells were subsequently transferred to a 15 mL falcon tube and centrifuged at 350 x g for 3 min. The media containing trypsin was removed and fresh complete media was added into the tube to resuspend the cells. An aliquot of cells was mixed with trypan blue and counted using haemacytometer. Trypsinised cells were prepared in 5 x 10^3 cells/100 µl and seeded into each well in 96-well plate. The cells were incubated in CO_2 incubator at 37˚C for 24 hr, allowing them to grow and recover. After 24 hr, the media was replaced with fresh complete RPMI media containing 10, 20, and 40 µg/ml of recombinant proteins. Positive and negative controls treatments were also

included with 5 µM of doxorubicin and PBS respectively. After 24 hr of treatment, the inhibition of cell viability was analysed using MTT assay. The media was removed carefully from each well without disturbing the cells, fresh RPMI media containing 0.5 mg/ml of sterile MTT reagent (Sigma-aldrich, USA) was added to each well. The plate was incubated in CO_2 incubator at 37˚C for 4 hr (in dark). During this process, mitochondria dehydrogenase of viable cells convert yellow MTT solution into insoluble formazan with purple colour. In order to solubilize the insoluble formazan, 100 µl of dimethyl sulfoxide (DMSO) was added to each well and incubated for 15 min at 37˚C. The absorbance of solubilized formazan was measured at wavelength of 570 nm. The relative percentage of cell viability was calculated using formula as below:

$$Cell\ viability\ (\%) = \frac{A_{570}\ of\ treated\ cells\ - A_{570}\ of\ blank}{A_{570}\ of\ negative\ control - \ A_{570}\ of\ blank}\ x\ 100$$

Results were expressed as cell inhibition rate (%) calculated by subtracting percentage of cell viability from 100.

6.2.2.2 Time-dependent cell viability inhibition

In time-dependent cell viability inhibition, the cells were subjected to treatments at different time points using optimal concentrations of rFIP-fve and mutants in inhibiting cells determined from concentration-dependent cell viability inhibition experiment. The cells were prepared using the same protocol as described in the **Section 6.2.2.1**. After 24 hr of recovery period, the media for A549 cells was replaced with fresh complete RPMI media containing 20 µg/ml of recombinant proteins; while media for MDA-MB-231 and MCF-7 cells were replaced with fresh complete RPMI media containing 40 µg/ml of recombinant proteins. Positive and negative control treatments were also included with 5 µM of doxorubicin and PBS respectively. The inhibition of cell viability was analysed at 24, 48, and 72 hr using MTT assay with the same protocol as described in **Section 6.2.2.1**.

6.2.3 Cell migration assay

Cell migration assay was used to assess the migration-inhibitory activities of rFIP-fve and mutants. Cells were seeded in 24-well plate at a density that they would reached 90% confluence as a monolayer after 24 hr. A sterile 200 µl yellow pipette tip was used to scratch a line in the centre of the cultured cell monolayer. The cells were washed with sterile PBS to remove the detached cells. Subsequently, complete RPMI media containing 20 µg/ml of recombinant proteins were added to the A549 cells, whereas complete RPMI media containing 40 µg/ml of recombinant proteins were added to MDA-MB-231 cells. PBS was included as negative control. The extents of cell migration in scratched areas were observed and photographed at reference points using Nikon Eclipse TS 100 Inverted microscope (Nikon, Japan) and analysed with imaging software NIS-Elements D 3.0 (Nikon, Japan). The gap distances (in term of area) at the reference points were measured quantitatively using ImageJ software. Results were expressed as percentage of cell migrated, which were calculated by formula as shown below:

$$Cell\ migrated\ (\%) = \frac{Initial\ gap\ distance\ at\ 0\ hr - gap\ distance\ at\ 24\ hr}{Initial\ gap\ distance\ at\ 0\ hr} \quad x \quad 100$$

6.2.4 Statistical analyses

All experiments were performed at least in triplicate in three independent experiments. All values are presented as mean ± SD of three independent experiments. Statistical analysis was performed using GraphPad Prism 7. One-way analysis of variance (ANOVA) was conducted followed by a Tukey multiple comparisons test to determine the significance degree of cancer cell inhibitory rates of rFIP-fve and mutants. In Section 6.3.3.2, two-way ANOVA was carried out followed by a Tukey multiple comparisons test to determine the significance degree of MCF-7 cell inhibitory rates of rFIP-fve and CWT-7 at different time points. The significance levels were denoted at $P \leq 0.05$ with *, $P \leq 0.01$ with **, $P \leq 0.001$ with ***, and $P \leq 0.0001$ with ****.

6.3 Results

6.3.1 Determination of optimal concentration in cancer cell inhibition

6.3.1.1 A549 cells

As shown in **Figure 6.1**, the optimal concentrations that were effective in inhibiting A549 cell viability under treatments of rFIP-fve, CWT-1, CWT-2, CWT-4 and CWT-6 were observed at 20 µg/ml at 30.24% ± 11.20, 25.69% ± 6.81, 28.44% ± 3.00, 27.10% ± 3.44 and 22.01% ± 2.55 respectively. There were no significant differences in A549 cell viability inhibition under treatment of CWT-3 at the three concentrations tested, which were 19.91% ± 4.34 (10 µg/ml), 16.47% ± 2.10 (20 µg/ml), and 17.27% ± 0.96 (40 µg/ml). CWT-7 and CWT-8 demonstrated similar A549 cell inhibition rates at 10 and 20 µg/ml as compared to 40 µg/ml. The percentage of A549 cell inhibition for CWT-7 at 10, 20 and 40 µg/ml were 40.42% ±6.29, 42.21% ± 1.80 and 8.48% ± 1.13 respectively; whereas the percentage of A549 cell inhibition for CWT-8 at 10, 20 and 40 µg/ml were 32.46% ± 2.85, 32.83 % ± 2.04 and 11.08 % ± 1.20 respectively. Based on the results, the optimal concentrations in A549 cell viability inhibition were determined at 20 µg/ml for rFIP-fve, CWT-1, CWT-2, CWT-4 and CWT-6; whereas optimal concentrations in A549 cell viability inhibition were determined at both 10 and 20 µg/ml for CWT-7 and CWT-8. For ease of comparison, concentration of 20 µg/ml of rFIP-fve and mutants were used for the subsequent assays in A549 cells.

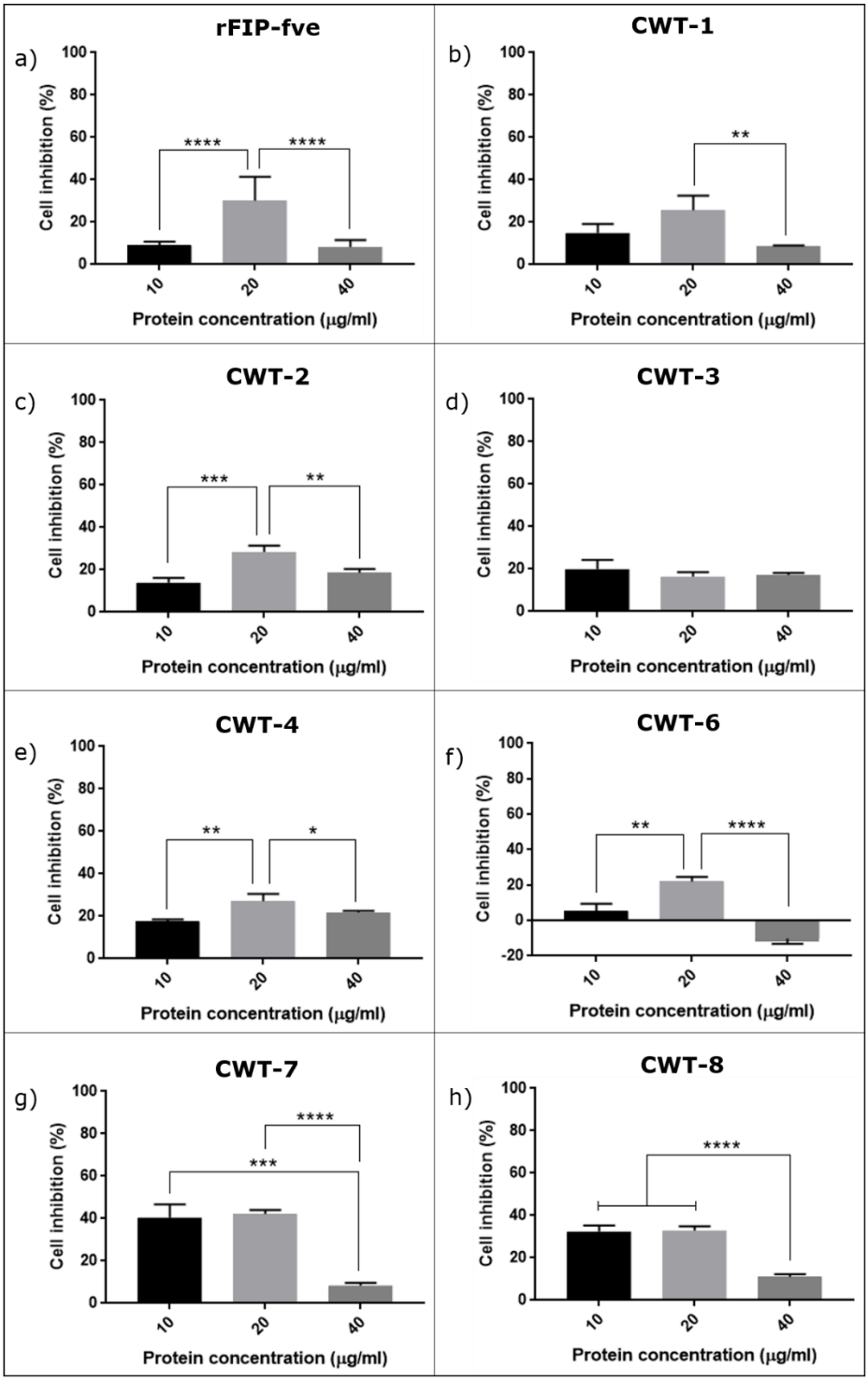


Figure 6.1. Effect of different concentrations of rFIP-fve and mutants in inhibiting lung cancer A549 cell lines. A549 cells were treated with 10, 20 and 40 µg/ml rFIP-fve, CWT-1, CWT-2, CWT-3, CWT-4, CWT-6, CWT-7 and CWT-8. Cell viability was measured using MTT assay. PBS-treated A549 cells was used as negative control. Cell viability was calculated by dividing absorbance of treated cells by absorbance of PBS-treated cells, and times 100 (%). Results were expressed as percentage of cell inhibition, which were calculated by subtracting percentage of cell viability from 100. Data represent mean ± SD of triplicates for three independent experiments. Tukey multiple comparisons test showed degree of significance between different concentrations of the respective rFIP-fve and derivatives treatment; * $P \leq 0.05$, ** $P \leq 0.01$, *** $P \leq 0.001$, **** $P \leq 0.0001$.

6.3.1.2 MDA cells

As demonstrated in **Figure 6.2**, the optimal concentrations that were effective in inhibiting MDA-MB-231 cell viability under treatments of rFIP-fve, CWT-1, CWT-2, CWT-3, CWT-4, CWT-6, CWT-7 and CWT-8 were observed at 40 µg/ml at 27.75% ± 7.18, 24.77% ± 4.64, 26.96% ± 4.27, 21.24% ± 3.03, 18.85% ± 3.12, 34.43% ± 3.12, 16.67% ± 0.78 and 25.08% ± 2.59 respectively. The inhibition rates of MDA-MB-231 cells at treatments of 40 µg/ml were significantly higher than the inhibition rates at treatments of 10 and 20 µg/ml. Based on the results, the optimal concentration 40 µg/ml of rFIP-fve and mutants were used for the subsequent assays in MDA-MB-231 cells.

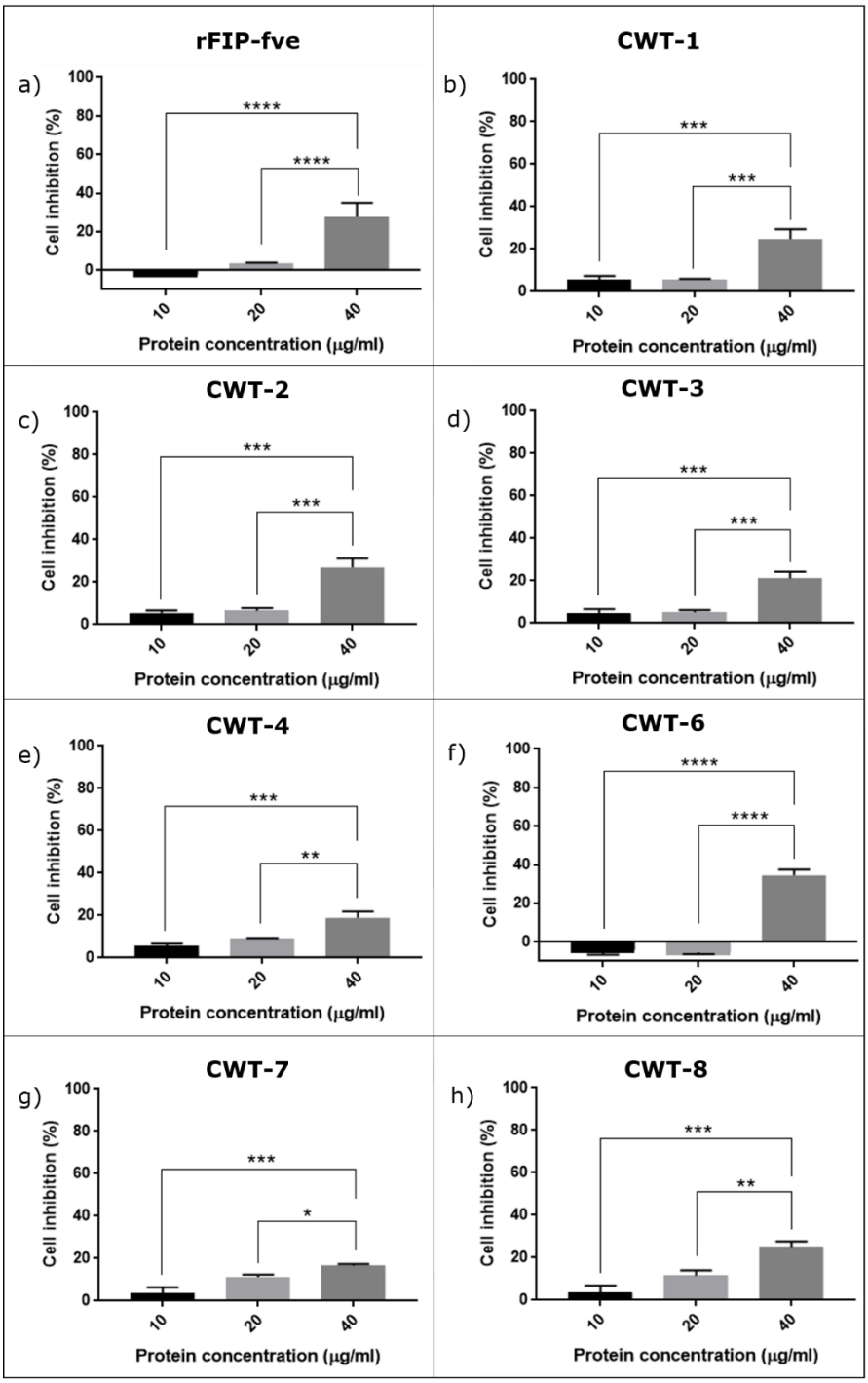


Figure 6.2. Effect of different concentrations of rFIP-fve and mutants in inhibiting breast cancer MDA-MB-231 cell lines. MDA-MB-231 cells were treated with 10, 20 and 40 µg/ml rFIP-fve, CWT-1, CWT-2, CWT-3, CWT-4, CWT-6, CWT-7 and CWT-8. PBS-treated MDA-MB-231 cells was used as negative control. Cell viability was measured using MTT assay. Cell viability was calculated by dividing absorbance of treated cells by absorbance of PBS-treated cells, and times 100 (%). Results were expressed as percentage of cell inhibition, which were calculated by subtracting percentage of cell viability from 100. Data represent mean ± SD of triplicates for three independent experiments. Tukey multiple comparisons test showed degree of significance between different concentrations of the respective rFIP-fve and derivatives treatment; * $P \leq 0.05$, ** $P \leq 0.01$, *** $P \leq 0.001$, **** $P \leq 0.0001$.

6.3.1.3 MCF-7 cells

As shown in **Figure 6.3**, rFIP-fve displayed equally high MCF-7 cell viability inhibitory activities at 20 and 40 µg/ml at 31.15% ± 0.59 and 29.67% ± 5.58 respectively; whereas the optimal concentrations that were effective in inhibiting MCF-7 cell viability under treatments of CWT-1, CWT-2, CWT-3, CWT-7 and CWT-8 were observed at 40 µg/ml at 20.74% ± 1.38, 23.08% ± 4.04, 9.03% ± 2.55, 31.84% ± 2.70 and 13.45% ± 1.47 respectively. On the other hand, treatments of CWT-4 and CWT-6 demonstrated promotion in cell proliferation rather than cell inhibition. Nonetheless, the promotion of cell growth reduced in a dose-dependent manner. The inhibition rates of MCF-7 cell viability for treatment of CWT-4 at 10, 20 and 40 µg/ml were -17.18% ± 4.04, -5.98% ± 0.39 and -2.35% ± 1.91 respectively; while the inhibition rates of MCF-7 cell viability for treatment of CWT-6 at 10, 20 and 40 µg/ml were -21.38% ± 5.17, -10.71% ± 2.19 and 0.43% ± 0.45 respectively. Based on the results, the optimal concentrations in MCF-7 cell viability inhibition were determined at 20 and 40 µg/ml for rFIP-fve and 40 µg/ml for CWT-1, CWT-2, CWT-3, CWT-7 and CWT-8; whereas the optimal concentrations in promoting the least of MCF-7 cell proliferation were determined at 40 µg/ml for CWT-4 and CWT-6. For ease of comparison, concentration of 40 µg/ml of rFIP-fve and mutants were used for the subsequent assays and analyses in MCF-7 cells.

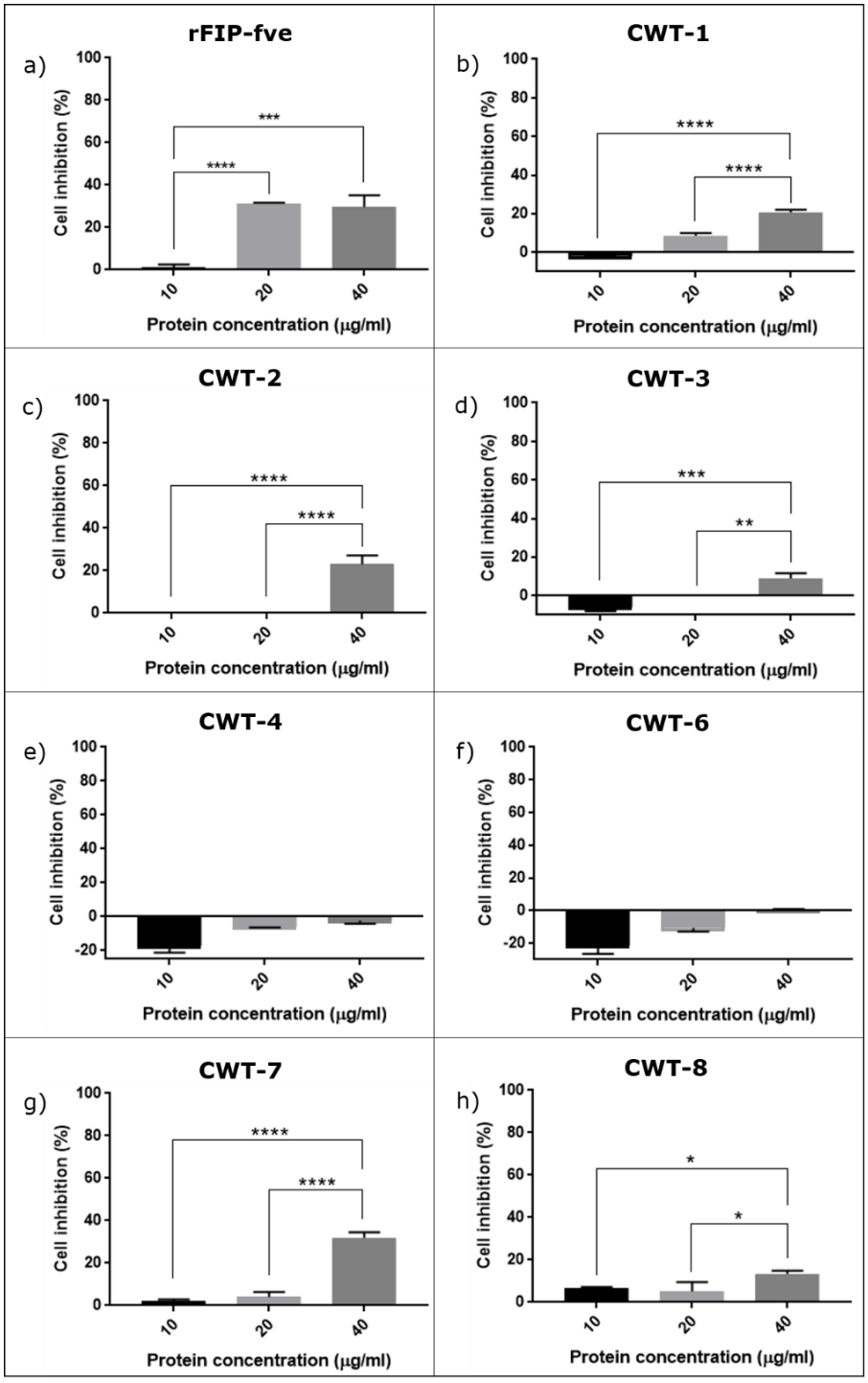


Figure 6.3. Effect of different concentrations of rFIP-fve and mutants in inhibiting breast cancer MCF-7 cell lines. MCF-7 cells were treated with 10, 20 and 40 µg/ml rFIP-fve, CWT-1, CWT-2, CWT-3, CWT-4, CWT-6, CWT-7 and CWT-8. PBS-treated MCF-7 cells was used as negative control. Cell viability was measured using MTT assay. Cell viability was calculated by dividing absorbance of treated cells by absorbance of PBS-treated cells, and times 100 (%). Results were expressed as percentage of cell inhibition, which were calculated by subtracting percentage of cell viability from 100. Data represent mean ± SD of triplicates for three independent experiments. Tukey multiple comparisons test showed degree of significance between different concentrations of the respective rFIP-fve and derivatives treatment; * $P \leq 0.05$, ** $P \leq 0.01$, *** $P \leq 0.001$, **** $P \leq 0.0001$.

6.3.2 Determination of optimal treatment time in cancer cell inhibition

6.3.2.1 A549 cells

The A549 cell inhibition rates of all of the mutants except CWT-3 reduced over time from 24 to 72 hr as demonstrated in **Figure 6.4**. The highest A549 cell inhibitory activities were observed at 24 hr for rFIP-fve, CWT-1, CWT-2, CWT-4, CWT-6, CWT-7 and CWT-8. In comparison to rFIP-fve, CWT-2 exhibited a slower deterioration of A549 cell viability-inhibition effect in time-dependent manner. Although the A549 cell inhibitory activities of CWT-2 and rFIP-fve at 24 hr were not different statistically, CWT-2 displayed higher A549 cell inhibitory activities at 48 and 72 hr as compared to rFIP-fve. The A549 cell inhibition activities of rFIP-fve at 24, 48 and 72 hr were 30.24% ± 11.20, 8.28% ± 3.28 and 0% respectively; whereas the A549 cell inhibition activities of CWT-2 at 24, 48 and 72 hr were 28.44% ± 2.99, 18.63% ± 1.65 and 16.05% ± 2.99 respectively. On the other hand, the A549 cell inhibitory activities of CWT-1 at the three time points were similar to rFIP-fve, which were 25.69% ± 6.81 (24 hr), 8.59% ± 0.44 (48 hr) and 1.56% ± 1.71 (72 hr). The A549 cell inhibitory activities of CWT-3 remained similar at the three time points: 16.47% ± 2.10 (24 hr), 17.27% ± 8.27 (48 hr) and 17.63% ± 0.80 (72 hr).

The A549 cell inhibitory activities for CWT-4 were 27.10% ± 3.44 (24 hr), 21.76% ± 0.75 (48 hr) and 17.23% ± 2.44 (72 hr); for CWT-6 were 22.01% ± 2.55 (24 hr), 5.27% ± 0.71 (48 hr) and 2.43% ± 1.43 (72 hr); for CWT-7 were 42.21% ± 8.80 (24 hr), 7.70% ± 1.12 (48 hr) and 1.84% ± 0.71 (72 hr); and for CWT-8 were 32.83% ± 2.04 (24 hr), 9.38% ± 3/17 (48 hr) and 0 % (72 hr).

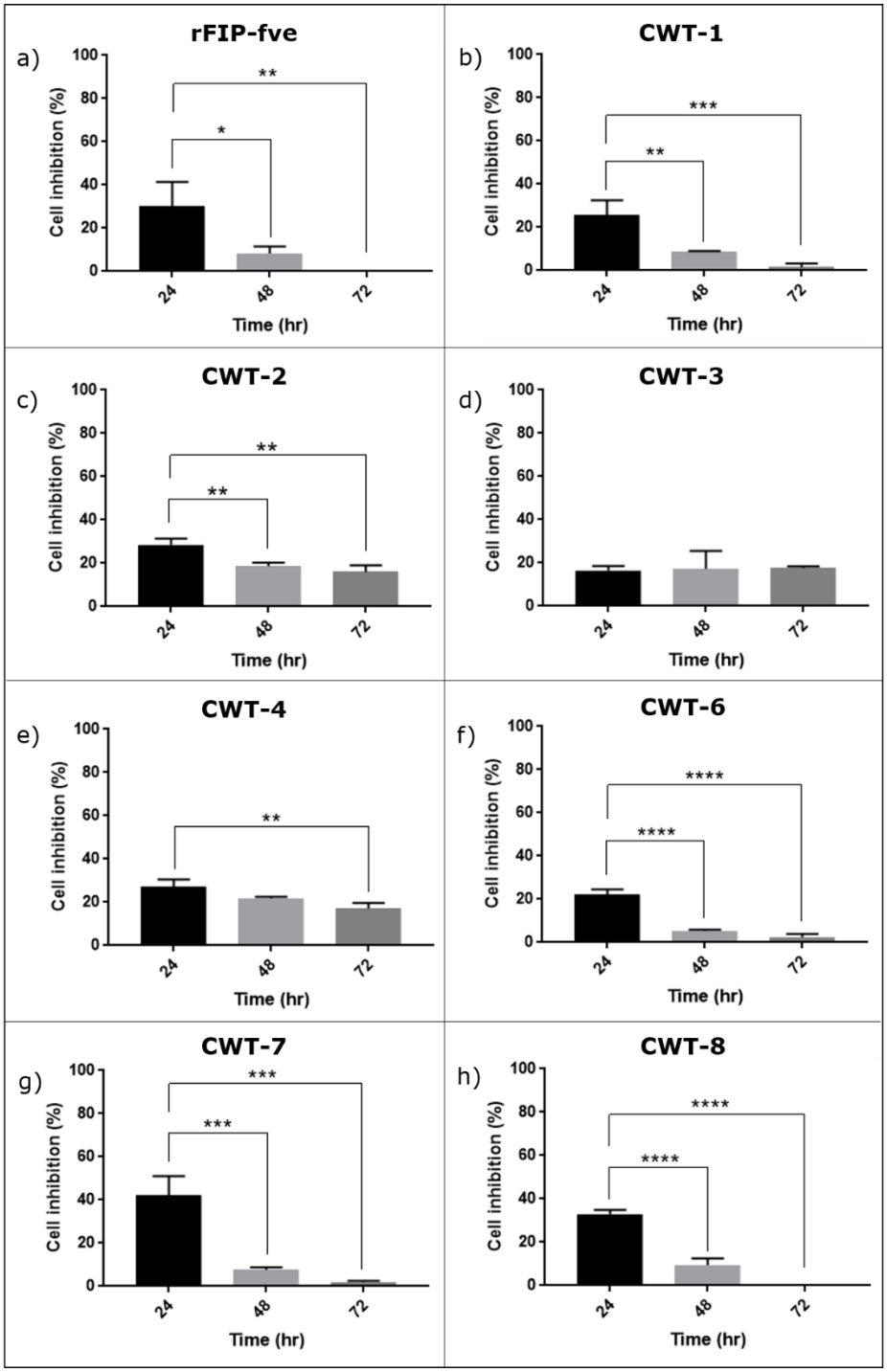


Figure 6.4. Effect of different time treatment of rFIP-fve and mutants in inhibiting lung cancer A549 cell lines. A549 cells were treated with 20 µg/ml rFIP-fve, CWT-1, CWT-2, CWT-3, CWT-4, CWT-6, CWT-7 and CWT-8 for 24, 48, and 72 hr. PBS-treated A549 cells was used as negative control. Cell viability was measured using MTT assay. Cell viability was calculated by dividing absorbance of treated cells by absorbance of PBS-treated cells, and times 100 (%). Results were expressed as percentage of cell inhibition, which were calculated by subtracting percentage of cell viability from 100. Data represent mean ± SD of triplicates for three independent experiments. Tukey multiple comparisons test showed degree of significance between different time points of the respective rFIP-fve and derivatives treatment; * $P \leq 0.05$, ** $P \leq 0.01$, *** $P \leq 0.001$, **** $P \leq 0.0001$.

6.3.2.2 MDA-MB-231 cells

As shown in **Figure 6.5**, treatments of rFIP-fve and CWT-2 maintained the inhibitory of MDA-MB-231 cell viability at similar level from 24 to 48 hr, but diminished at 72 hr. The inhibition rates in MDA-MB-231 cells for treatment of rFIP-fve at 24, 48 and 72 hr were 27.75% ± 7.18, 27.57% ± 7.50 and -5.01% ± 0.71 respectively; while the inhibition rates in MDA-MB-231 cells for treatment of CWT-2 at 24, 48 and 72 hr were 26.96% ± 4.27, 26.36% ± 3.02 and 9.87% ± 1.58 respectively. On the other hand, treatment of CWT-1 failed to maintain its anti-cancer activities where the inhibition activities at 24, 48, and 72 hr were 24.77% ± 4.64, 1.28% ± 1.92 and -3.58% ± 0.25 respectively. Similar to A549 cells, the inhibition effect of CWT-3 were not significantly different at the three time points (24 hr - 21.24% ± 3.03, 48 hr - 14.46% ± 2.98 and 72 hr - 22.36% ± 2.72). Unlike others, CWT-4 displayed a significant increment in inhibitory effect on MDA-MB-231 cells at 72 hr (25.47% ± 1.47) in comparison to the inhibitory activities at 24 hr (18.85% ± 3.12) and 48 hr (13.52% ±7.49). The percentage of MDA-MB-231 cell viability inhibition in treatments of CWT-6, CWT-7 and CWT-8 reduced over time from 24 to 72 hr; the highest cell inhibitory activities were observed at 24 hr for these three mutants. The inhibition rates of MDA-MB-231 cell viability under treatment of CWT-6 at 24, 48 and 72 hr were 33.33% ± 4.39, 16.54% ± 3.61, -5.19% ± 3.74 respectively. The inhibition rates of MDA-MB-231 cell viability under treatment of CWT-7 at 24, 48 and 72 hr were 16.67% ± 0.78, 12.58% ± 3.50, -3.18% ± 1.33 respectively. The inhibition rates of MDA-MB-231 cell viability under treatment of CWT-8 at 24, 48 and 72 hr were 25.08% ± 2.59, 6.98% ± 3.41, -10.82% ± 2.04 respectively.

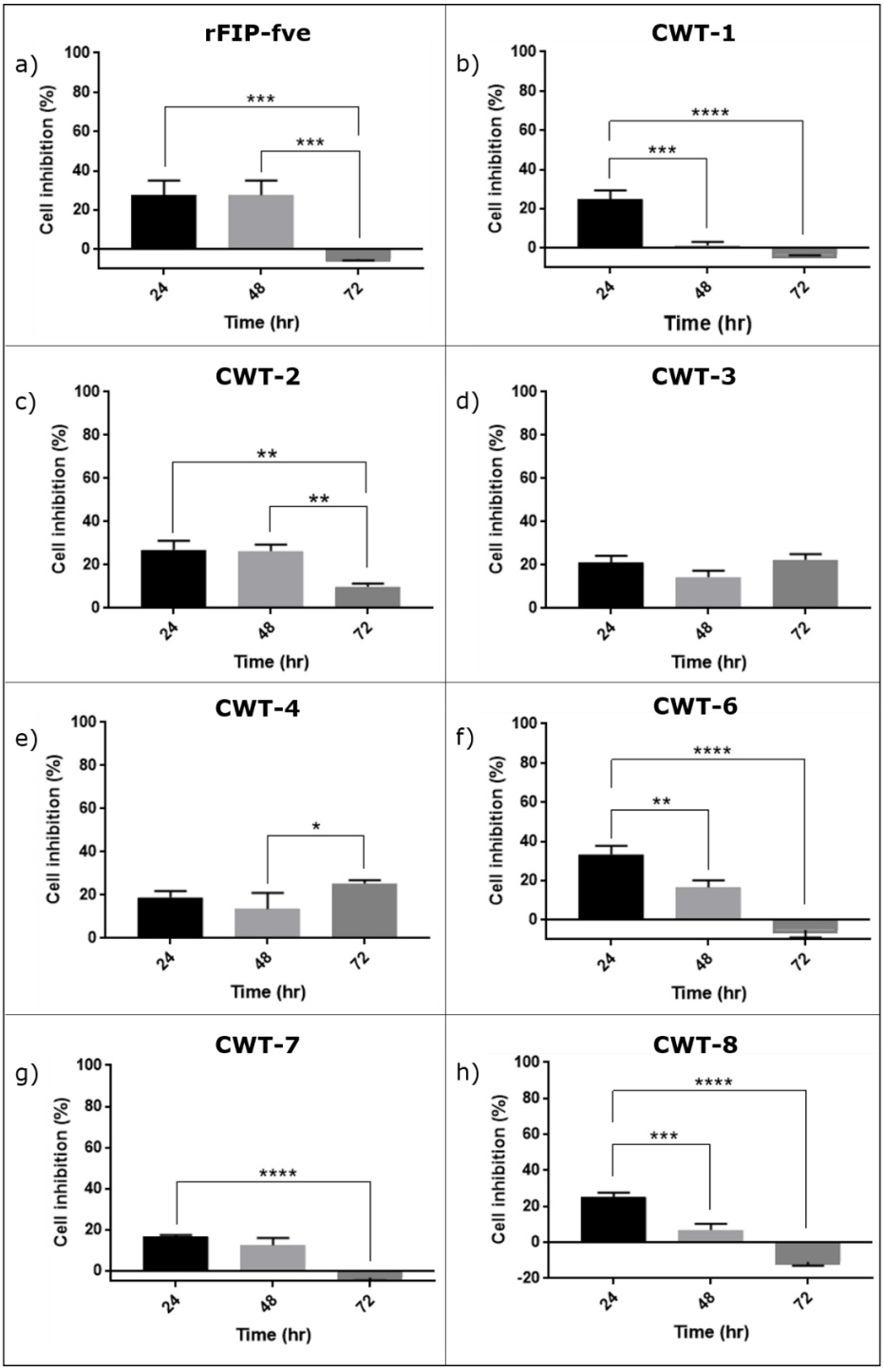


Figure 6.5. Effect of different time treatment of rFIP-fve and mutants in inhibiting breast cancer MDA-MB-231 cell lines. MDA-MB-231 cells were treated with 40 µg/ml rFIP-fve, CWT-1, CWT-2, CWT-3, CWT-4, CWT-6, CWT-7 and CWT-8 for 24, 48 and 72 hr. PBS-treated MDA-MB-231 cells was used as negative control. Cell viability was measured using MTT assay. Cell viability was calculated by dividing absorbance of treated cells by absorbance of PBS-treated cells, and times 100 (%). Results were expressed as percentage of cell inhibition, which were calculated by subtracting percentage of cell viability from 100. Data represent mean ± SD of triplicates for three independent experiments. Tukey multiple comparisons test showed degree of significance between different time points of the respective rFIP-fve and derivatives treatment; ** $P \leq 0.01$, *** $P \leq 0.001$, **** $P \leq 0.0001$.

6.3.2.3 MCF-7 cells

As shown in **Figure 6.6**, the optimal time point of cell viability inhibitory activities in MCF-7 varied among the mutants. The percentage of MCF-7 cell inhibition under treatments of rFIP-fve, CWT-1, CWT-2 and CWT-8 reduced over time from 24 to 72 hr where the highest cell inhibitory activities were observed at 24 hr in these mutants. The MCF-7 inhibition rates for treatment of rFIP-fve were 29.67% ± 5.58 (24 hr), 14.95% ± 0.78 (48 hr) and 10.70% ± 6.09 (72 hr); for CWT-1 were 20.74% ± 1.38 (24 hr), 14.34% ± 4.31 (48 hr) and 12.71% ± 1.17 (72 hr); for CWT-2 were 23.08% ± 4.04 (24 hr), 10.51% ± 1.93 (48 hr) and 7.63% ± 1.14 (72 hr); and for CWT-8 were 13.45% ± 1.47 (24 hr), 12.24% ± 1.44 (48 hr) and 4.57% ± 0.86 (72 hr). Both CWT-1 and CWT-2 did not show enhancement in the MCF-7 cell inhibitory activities. CWT-3 and CWT-4 demonstrated increasing MCF-7 cell viability-inhibitory activities from 24 to 72 hr with peak activities observed at 72 hr. The inhibitory rates of MCF-7 cell viability for CWT-3 at 24, 48 and 72 hr were 9.03% ± 2.55, 12.73% ± 2.14 and 17.24% ± 3.19 respectively; while the inhibitory rates of MCF-7 cell viability for CWT-4 at 24, 48, and 72 hr were -2.35% ± 1.91, 14.16% ± 2.30 and 19.24% ± 3.57 respectively. CWT-7 also displayed an increase of inhibition in MCF-7 cell viability from 24 to 48 hr at 31.84% ± 2.70 and 43.85% ± 10.27 respectively, which was subsequently reduced to 11.43% ± 5.63 at 72 hr. On the other hand, the MCF-7 cell inhibition activities of CWT-6 were rather low as compared to rFIP-fve and other mutants where its inhibition activities at 24, 48 and 72 hr were 0.43% ± 0.45, 6.32% ± 1.08 and 0.36% ± 0.82 respectively.

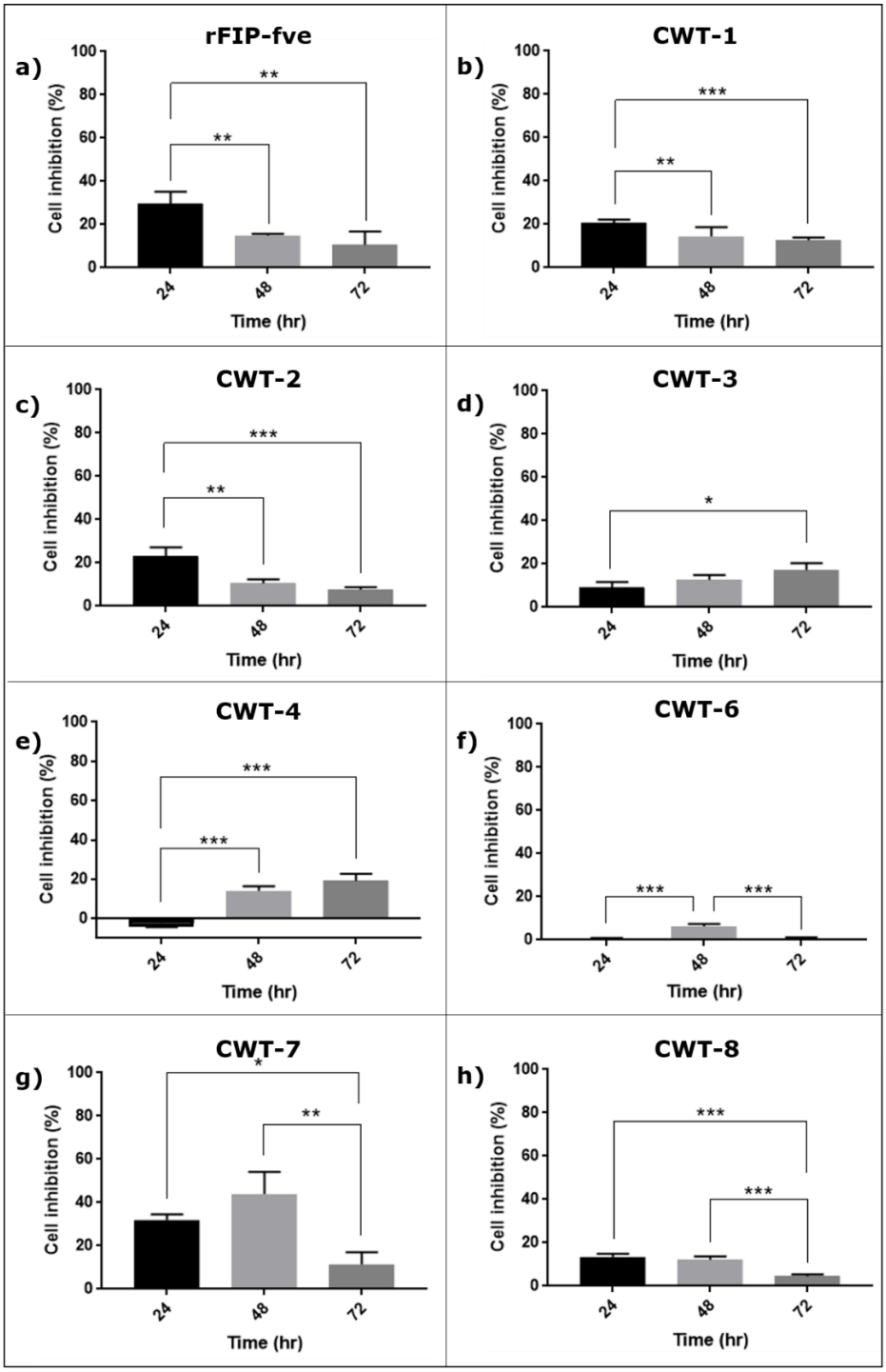


Figure 6.6. Effect of different time treatment of rFIP-fve and mutants in inhibiting breast cancer MCF-7 cell lines. MCF-7 cells were treated with 40 µg/ml rFIP-fve, CWT-1, CWT-2, CWT-3, CWT-4, CWT-6, CWT-7 and CWT-8 for 24, 48, and 72 hr. PBS-treated MCF-7 cells was used as negative control. Cell viability was measured using MTT assay. Cell viability was calculated by dividing absorbance of treated cells by absorbance of PBS-treated cells, and times 100 (%). Results were expressed as percentage of cell inhibition, which were calculated by subtracting percentage of cell viability from 100. Data represent mean ± SD of triplicates for three independent experiments. Tukey multiple comparisons test showed degree of significance between different time points of the respective rFIP-fve and derivatives treatment; $P \leq 0.05$ with *, $P \leq 0.01$ with **, $P \leq 0.001$ with ***, and $P \leq 0.0001$ with ****.

6.3.3 Cell inhibition assessment

The assessment and comparison in terms of differences in cancer cell viability inhibitory activities among rFIP-fve and mutants are classified into two groups: (i) mutant group with putative improved dimerization (**Section 6.3.3.1**) and (ii) mutant group with loops modification (**Section 6.3.3.2**). The cell inhibition assessment was performed using the results at 24 hr as the inhibitory activities at the particular time point were generally the highest.

6.3.3.1 Mutant group with putative enhanced dimerization

A549 cells

As shown in **Figure 6.7**, 20 µg/ml of rFIP-fve, CWT-1 and CWT-2 demonstrated inhibition in A549 cell viability at 30.24% ± 11.20, 25.69% ± 6.81 and 28.44% ± 3 respectively after 24 hr of treatment. Positive control 5 µM doxorubicin showed inhibition in A549 cell viability at 56.69% ± 8.88. There were no significant differences in A549 cell viability inhibition activities between rFIP-fve and mutants at 24 hr of treatment.

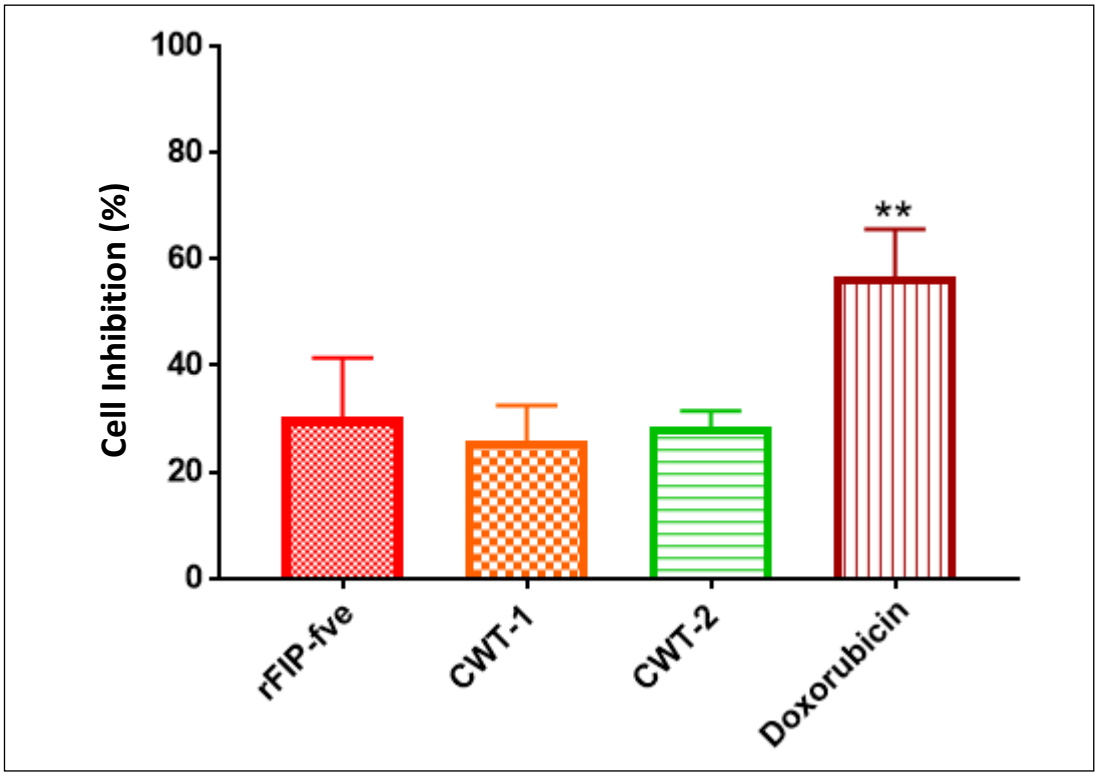


Figure 6.7. Effect of rFIP-fve and mutant group with putative enhanced dimerization on A549 cell viability. A549 cells were treated with 20 µg/ml rFIP-fve, CWT-1, and CWT-2 for 24 hr. PBS-treated A549 cells was used as negative control. Cell viability was measured using MTT assay. Cell viability was calculated by dividing absorbance of treated cells by absorbance of PBS-treated cells, and times 100 (%). Results were expressed as percentage of cell inhibition, which were calculated by subtracting percentage of cell viability from 100. Data represent mean ± SD of triplicates for three independent experiments. Tukey multiple comparisons test showed degree of significance between rFIP-fve and positive control treatment; $P \leq 0.05$ with *, $P \leq 0.01$ with **, $P \leq 0.001$ with ***, and $P \leq 0.0001$ with ****.

MDA-MB-231 cells

As shown in **Figure 6.8**, 20 µg/ml of rFIP-fve, CWT-1 and CWT-2 demonstrated inhibition in MDA-MB-231 cell viability at 27.75% ± 7.18, 24.78% ± 4.64 and 26.97% ± 4.27 respectively after 24 hr of treatment. Positive control 5 µM doxorubicin showed inhibition in MDA-MB-231 cell viability at 50.71% ± 3.56. There were no significant differences in MDA-MB-231 cell viability inhibition activities between rFIP-fve and mutants.

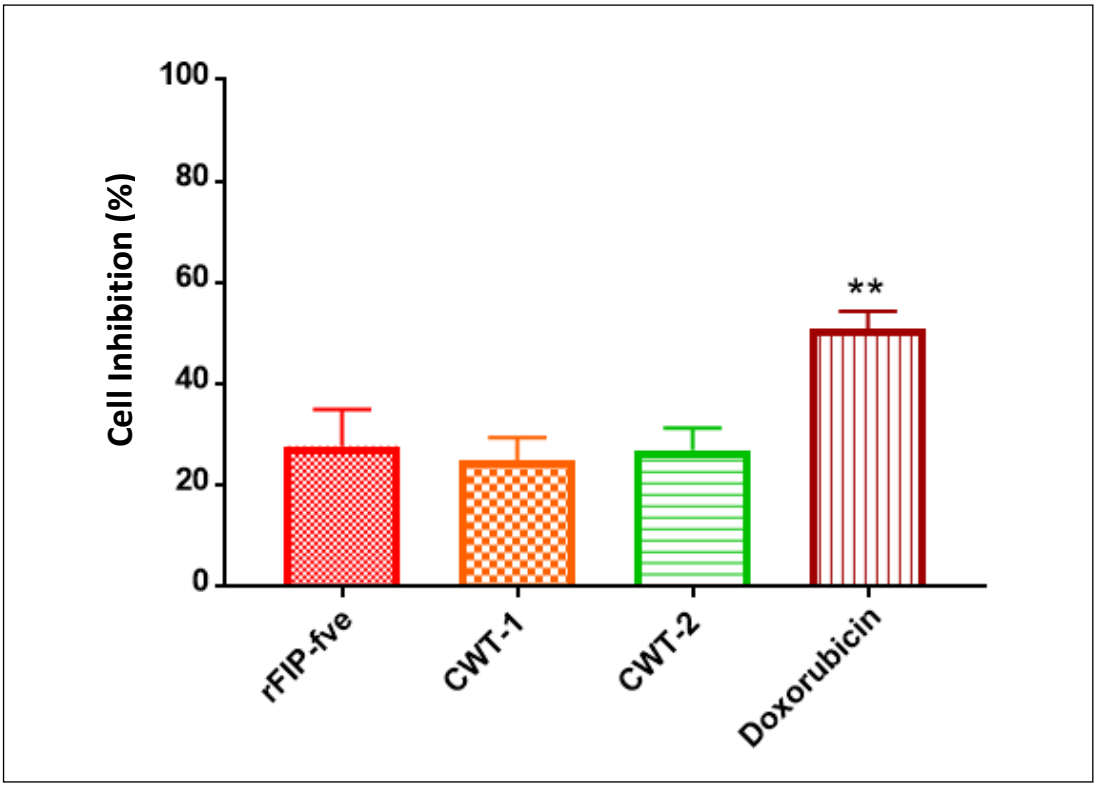


Figure 6.8. Effect of rFIP-fve and mutant group with putative enhanced dimerization on MDA-MB-231 cell viability. MDA-MB-231 cells were treated with 40 µg/ml rFIP-fve, CWT-1, and CWT-2 for 24 hr. PBS-treated MDA-MB-231 cells was used as negative control. Cell viability was measured using MTT assay. Cell viability was calculated by dividing absorbance of treated cells by absorbance of PBS-treated cells, and times 100 (%). Results were expressed as percentage of cell inhibition, which were calculated by subtracting percentage of cell viability from 100. Data represent mean ± SD of triplicates for three independent experiments. Tukey multiple comparisons test showed degree of significance between rFIP-fve and positive control treatment; $P \leq 0.05$ with *, $P \leq 0.01$ with **, $P \leq 0.001$ with ***, and $P \leq 0.0001$ with ****.

MCF-7 cells

As shown in **Figure 6.9**, 40 µg/ml of rFIP-fve, CWT-1 and CWT-2 demonstrated inhibition in MCF-7 cell viability at 29.67% ± 5.58, 20.74% ± 1.38 and 23.08% ± 4.04 respectively after 24 hr of treatment. Positive control 5 µM doxorubicin showed inhibition in MCF-7 cell viability at 76.35% ± 5.62. There were no significant differences in MCF-7 cells-inhibiting activities between rFIP-fve and mutants.

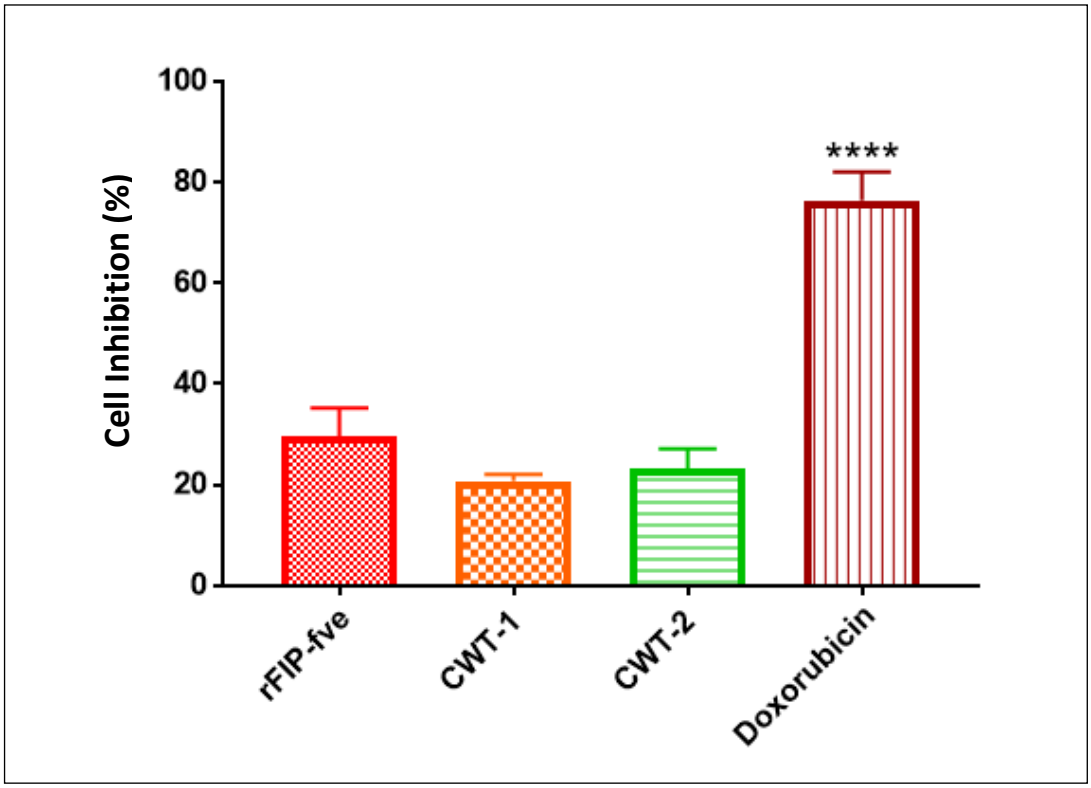


Figure 6.9. Effect of rFIP-fve and mutant group with putative enhanced dimerization on MCF-7 cell viability. MCF-7 cells were treated with 40 µg/ml rFIP-fve, CWT-1, and CWT-2 for 24 hr. PBS-treated MCF-7 cells was used as negative control. Cell viability was measured using MTT assay. Cell viability was calculated by dividing absorbance of treated cells by absorbance of PBS-treated cells, and times 100 (%). Results were expressed as percentage of cell inhibition, which were calculated by subtracting percentage of cell viability from 100. Data represent mean ± SD of triplicates for three independent experiments. Tukey multiple comparisons test showed degree of significance between rFIP-fve and positive control treatment; $P \leq 0.05$ with *, $P \leq 0.01$ with **, $P \leq 0.001$ with ***, and $P \leq 0.0001$ with ****.

6.3.3.2 Mutant group with loops modification

A549 cells

As shown in **Figure 6.10**, 20 µg/ml of rFIP-fve, CWT-3, CWT-4, CWT-6, CWT-7 and CWT-8 demonstrated inhibition rates in A549 cell viability at 30.24% ± 11.20, 16.47% ± 2.10, 27.10% ± 3.44, 22.01% ± 2.55, 42.21% ± 1.80 and 32.83% ± 2.04 respectively. Positive control 5 µM doxorubicin showed inhibition in A549 cell viability at 56.69% ± 8.88. rFIP-fve displayed higher inhibitory activity towards A549 cells in comparison to CWT-3, but there were no significant differences in rFIP-fve as compared to CWT-4, CWT-6 and CWT-8. On the other hand, CWT-7 showed higher A549 cell viability inhibition activity as compared to rFIP-fve and mutants tested in this group except CWT-8. CWT-7 is the mutant that adopts loop FG region and hinge residue I97D from LZ-8, whereas CWT-8 is the mutant that adopts both loop DE and FG regions in LZ-8.

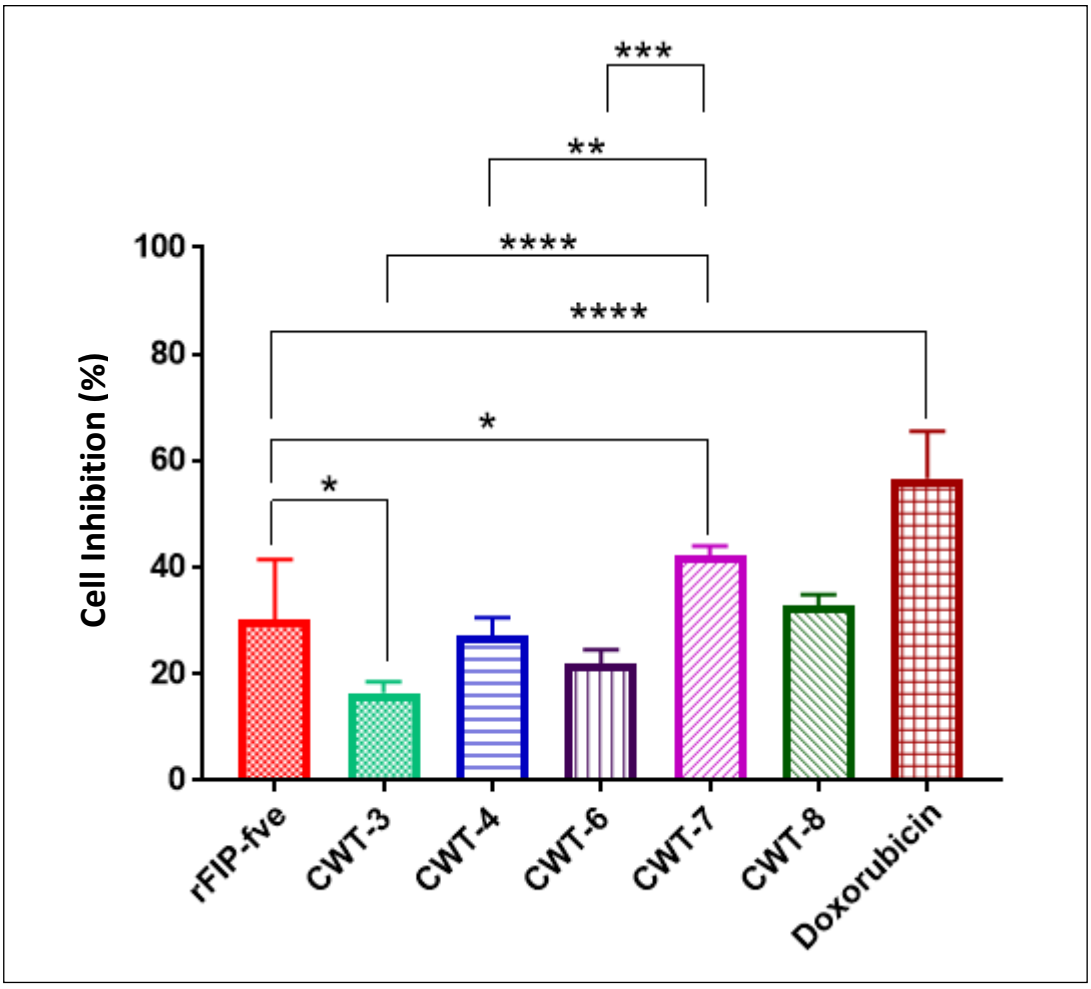


Figure 6.10. Effect of rFIP-fve and mutant group with loop modification on A549 cell viability. A549 cells were treated with 20 µg/ml rFIP-fve, CWT-3, CWT-4, CWT-6, CWT-7 and CWT-8 for 24 hr. PBS-treated A549 cells was used as negative control. Cell viability was measured using MTT assay. Cell viability was calculated by dividing absorbance of treated cells by absorbance of PBS-treated cells, and times 100 (%). Results were expressed as percentage of cell inhibition, which were calculated by subtracting percentage of cell viability from 100. Data represent mean ± SD of triplicates for three independent experiments. Tukey multiple comparisons test showed degree of significance among rFIP-fve, mutants, and positive control treatment; $P \leq 0.05$ with *, $P \leq 0.01$ with **, $P \leq 0.001$ with ***, and $P \leq 0.0001$ with ****.

MDA-MB-231

As shown in **Figure 6.11**, 40 µg/ml of rFIP-fve, CWT-3, CWT-4, CWT-6, CWT-7 and CWT-8 demonstrated inhibition activities in A549 cells at 27.75% ± 7.18, 21.24% ± 3.03, 18.85% ± 3.12, 34.43% ± 3.12, 16.67% ± 0.78 and 25.08% ± 2.59 respectively. Positive control 5 µM doxorubicin showed inhibition in MDA-MB-231 cell viability at 50.71% ± 3.56. rFIP-fve displayed higher inhibitory activity towards MDA-MB-231 cells in comparison to CWT-4 and CWT-7, but rFIP-fve showed lower MDA-MB-231 cell inhibitory activity as compared to CWT-6. rFIP-fve showed no significant differences in MDA-MB-231 cell viability inhibition rates as compared to CWT-3 and CWT-8. Among rFIP-fve and mutants, CWT-6 demonstrated the highest cell viability inhibitory activity in MDA-MB-231 cells; CWT-6 is the mutant that adopts loop DE region and hinge residue E61K in LZ-8.

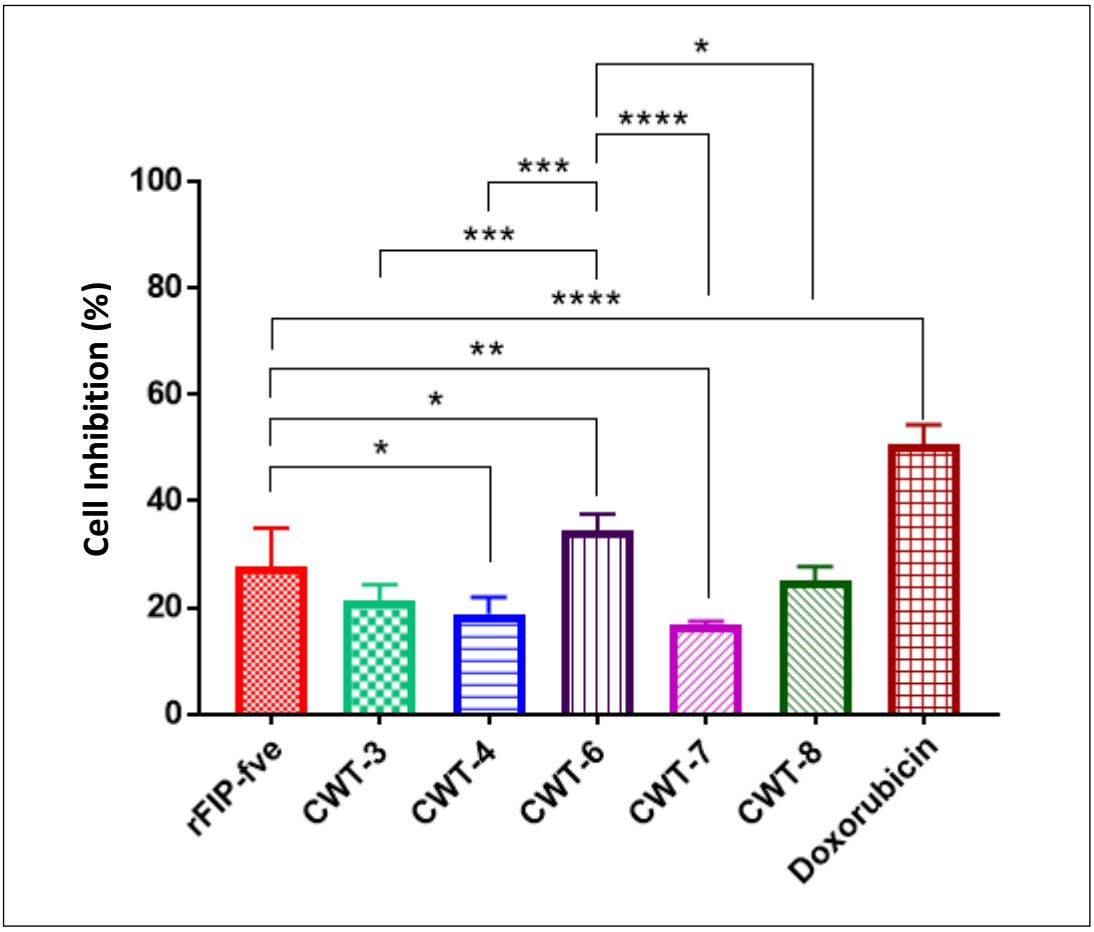


Figure 6.11. Effect of rFIP-fve and mutant group with loop modification on MDA-MB-231 cell viability. MDA-MB-231 cells were treated with 40 µg/ml rFIP-fve, CWT-3, CWT-4, CWT-6, CWT-7 and CWT-8 for 24 hr. PBS-treated MDA-MB-231 cells was used as negative control. Cell viability was measured using MTT assay. Cell viability was calculated by dividing absorbance of treated cells by absorbance of PBS-treated cells, and times 100 (%). Results were expressed as percentage of cell inhibition, which were calculated by subtracting percentage of cell viability from 100. Data represent mean ± SD of triplicates for three independent experiments. Tukey multiple comparisons test showed degree of significance among rFIP-fve, mutants, and positive control treatment; $P \leq 0.05$ with *, $P \leq 0.01$ with **, $P \leq 0.001$ with ***, and $P \leq 0.0001$ with ****.

MCF-7

The comparison in terms of MCF-7 cell viability inhibition activities was unable to be carried out among rFIP-fve and mutants as the time points of highest inhibitory activities for each recombinant proteins were different. For this reason, the comparison of MCF-7 cell viability inhibition activities were performed between rFIP-fve and CWT-7 only by including the inhibitory activities at three time points as these two recombinant proteins demonstrated apparent higher cell viability inhibition activities in comparison to other mutants. As shown in **Figure 6.12**, the percentage of MCF-7 cell viability inhibition of rFIP-fve at 24, 48 and 72 hr were 29.67% ± 5.58, 14.95% ± 0.78 and 10.70% ± 6.09 respectively; whereas the percentage of MCF-7 cell viability inhibition of CWT-7 at 24, 48 and 72 hr were 31.84% ± 2.70, 43.85% ± 10.27 and 11.43% ± 5.63 respectively. Positive control 5 μM doxorubicin showed MCF-7 cell inhibition rates at 76.35% ± 5.62 (24 hr), 92.40% ± 7.55 (48 hr), 100% (72 hr). CWT-7 possesses similar MCF-7 inhibitory activity to rFIP-fve where there were no significant differences between them at 24 hr. Nonetheless, CWT-7 exhibited significantly higher MCF-7 cell inhibition rate as compared to rFIP-fve at 48 hr. Subsequently, both rFIP-fve and CWT-7 displayed reduction of MCF-7 cell inhibitory activities at 72 hr.

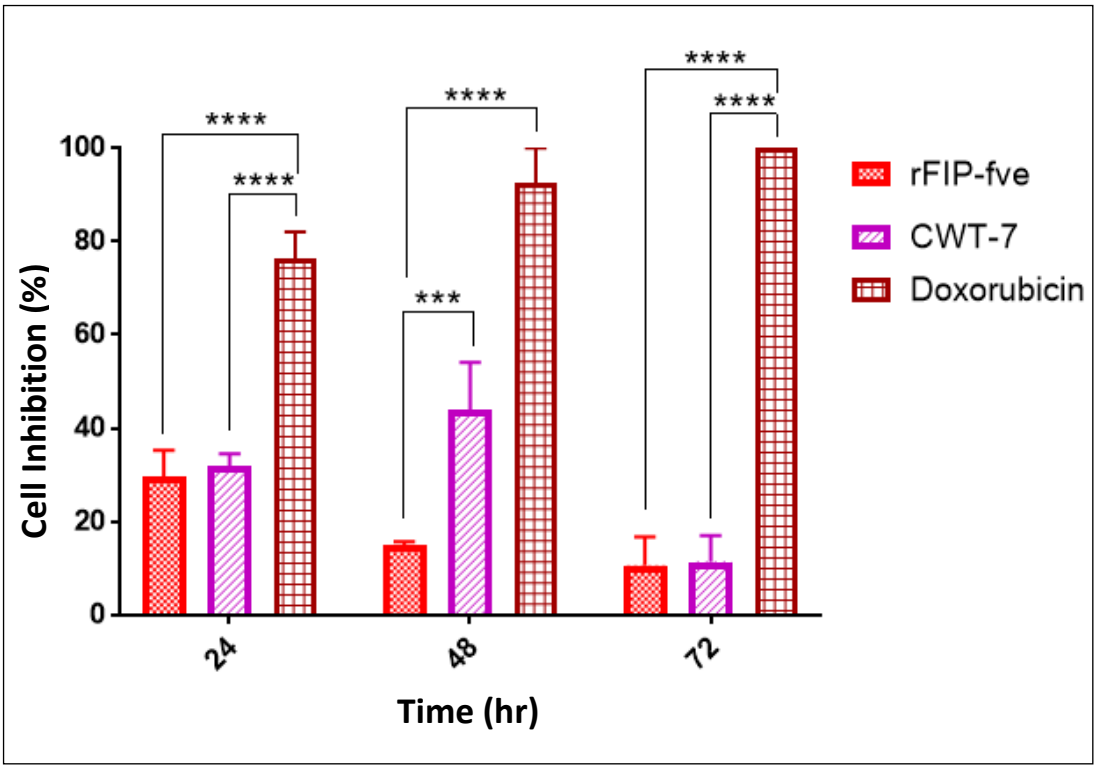


Figure 6.12. Effect of rFIP-fve and mutant group with loop modifications on MCF-7 cell viability. MCF-7 cells were treated with 40 µg/ml rFIP-fve and CWT-7 for 24, 48 and 72 hr. PBS-treated MCF-7 cells was used as negative control. Cell viability was measured using MTT assay. Cell viability was calculated by dividing absorbance of treated cells by absorbance of PBS-treated cells, and times 100 (%). Results were expressed as percentage of cell inhibition, which were calculated by subtracting percentage of cell viability from 100. Data represent mean ± SD of triplicates for three independent experiments. Tukey multiple comparisons test showed degree of significance between rFIP-fve in comparison to mutants and positive control treatment at different time points; $P \leq 0.05$ with *, $P \leq 0.01$ with **, $P \leq 0.001$ with ***, and $P \leq 0.0001$ with ****.

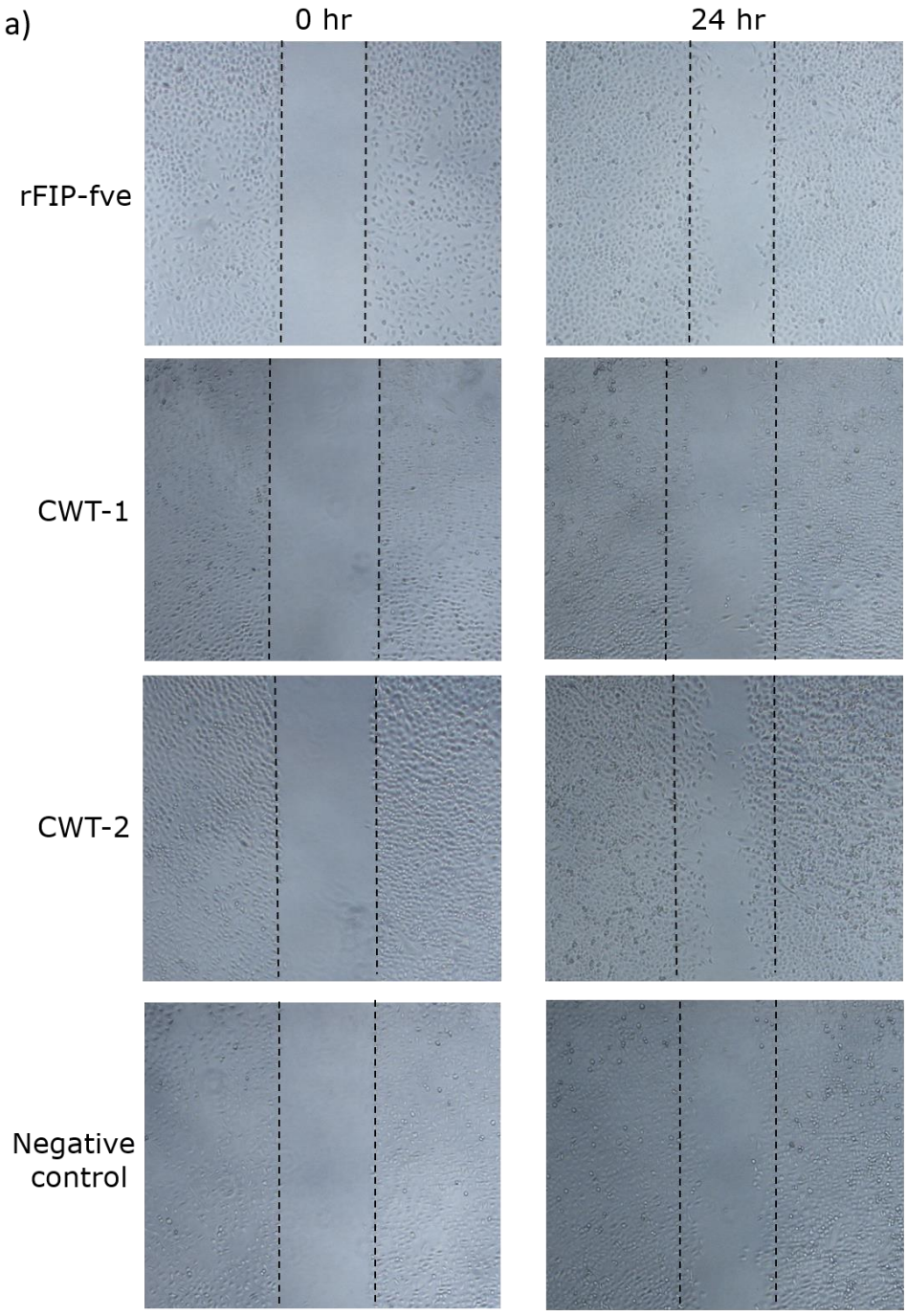
6.3.4 Anti-migration assessment

The ability of rFIP-fve and mutants in inhibiting the migration of A549 and MDA-MB-231 cells were investigated using wound-healing assay. MCF-7 cells were omitted in the anti-migration assessment as it possesses limited motility and metastatic potential (Shirazi, 2011). The migrated cells at the reference points were photographed and the percentage of migrated cells were quantified and presented in this section. The assessment and comparison in terms of differences in cancer cell migratory-inhibition activities among rFIP-fve and mutants are classified into two groups: (i) mutant group with putative improved dimerization (**Section 6.3.4.1**) and (ii) mutant group with loops modification (**Section 6.3.4.2**).

6.3.4.1 Mutant group with putative enhanced dimerization

A549 cells

After incubation with 20 µg/ml of rFIP-fve, CWT-1 and CWT-2 and PBS (negative control) for 24 hr, the cells that migrated in wounded zone were photographed and presented in **Figure 6.13a**. It was found that 20 µg/ml of rFIP-fve, CWT-1, CWT-2 were unable to inhibit A549 cell migration. As shown in **Figure 6.13b**, the percentage of A549 cell migration as a result of treatments with 20 µg/ml rFIP-fve, CWT-1, CWT-2 and negative control were 40.28% ± 7.37, 52.93% ± 4.51, 54.81% ± 12.39 and 46% ± 0.65 respectively. There were no significant differences in the percentage of A549 cell migrations under treatments of 20 µg/ml of rFIP-fve, CWT-1, CWT-2 and negative control.


a)
0 hr
24 hr
rFIP-fve
CWT-1
CWT-2
Negative control

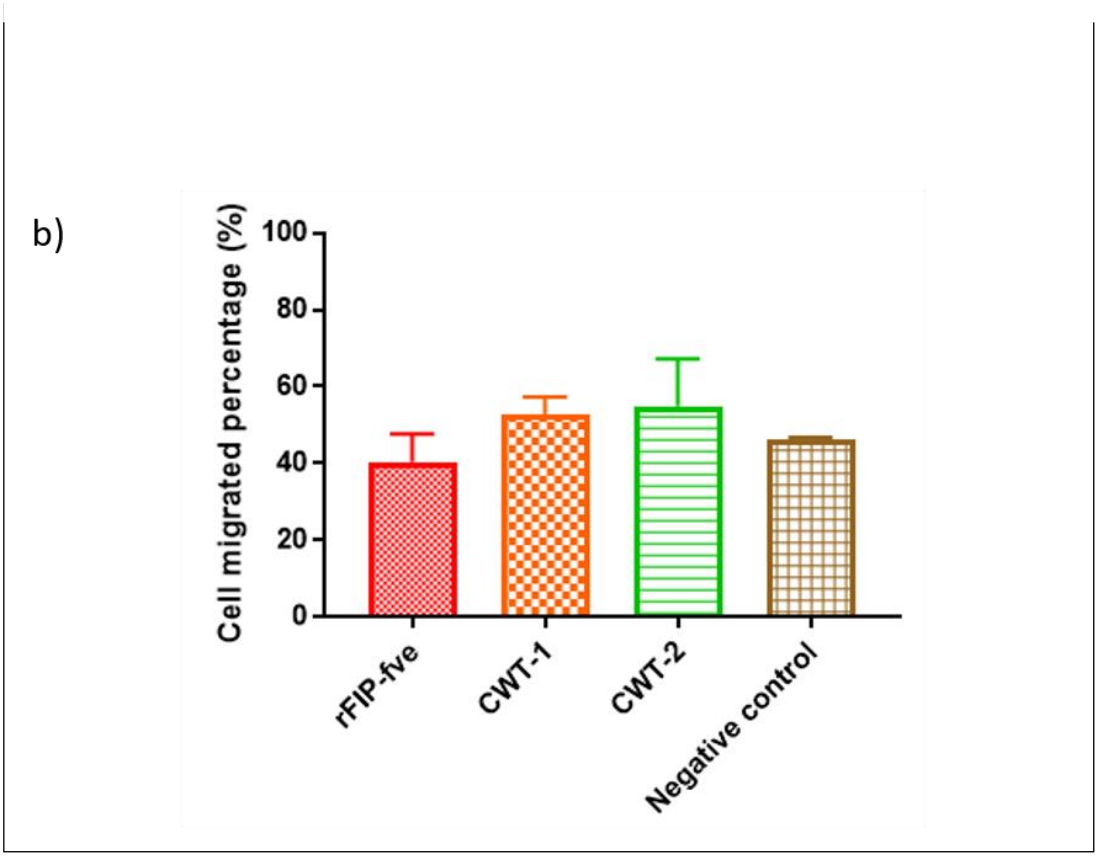
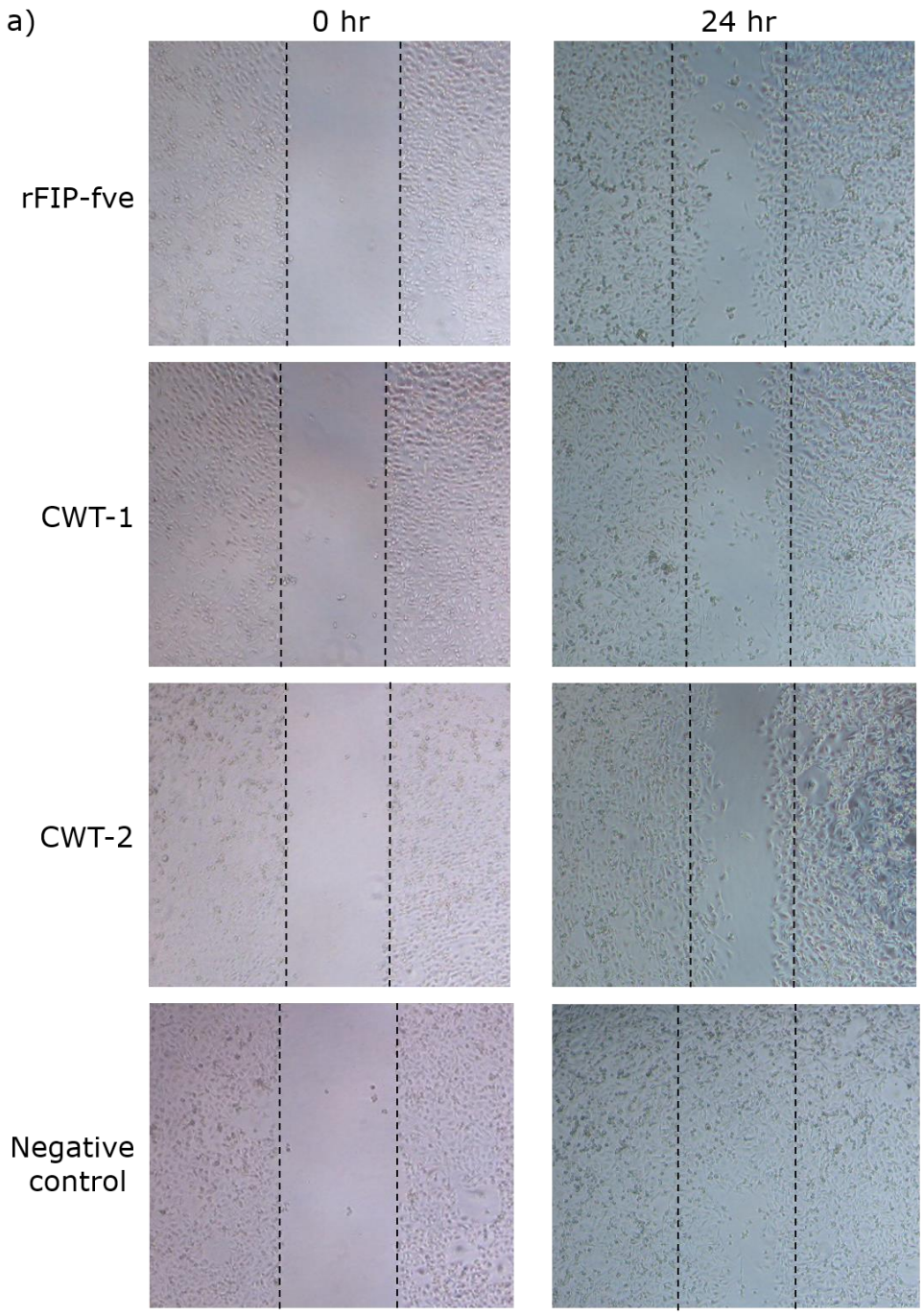


Figure 6.13. Effect of rFIP-fve and mutant group of putative enhanced dimerization on A549 cell migration. A549 cells were treated with 20 µg/ml rFIP-fve, CWT-1 and CWT-2 for 24 hr. PBS-treated A549 cells was used as negative control. (a) After 24 hr incubation, the cell migrations were monitored and photographed by microscopy. (b) The gap distances at the reference points were measured quantitatively using ImageJ software. Results were expressed as percentage of cells migrated, which were calculated by dividing the differences of gap distance between 0 and 24 hr by gap distance at 0 hr, and times 100 (%). Data represent mean ± SD of triplicates for three independent experiments.

MDA-MB-231 cells

After incubation with 40 µg/ml of rFIP-fve, CWT-1 and CWT-2 and PBS (negative control) for 24 hr, the cells that migrated in wounded zone were photographed and presented in **Figure 6.14a**. As shown in **Figure 6.14b**, the percentage of MDA-MB-231 migratory cells of rFIP-fve, CWT-1, CWT-2 and PBS were observed at 61.30% ± 7.56, 58.76% ± 9.54, 59.23% ± 4.43 and 100% respectively. It was found that 40 µg/ml of rFIP-fve, CWT-1, and CWT-2 possess some inhibition towards MDA-MB-231 cell migration in comparison to negative control. Nonetheless, there were no significant differences in the percentage of MDA-MB-231 cell migrations under treatment of 40 µg/ml of rFIP-fve, CWT-1 and CWT-2.


a)
0 hr
24 hr
rFIP-fve
CWT-1
CWT-2
Negative control

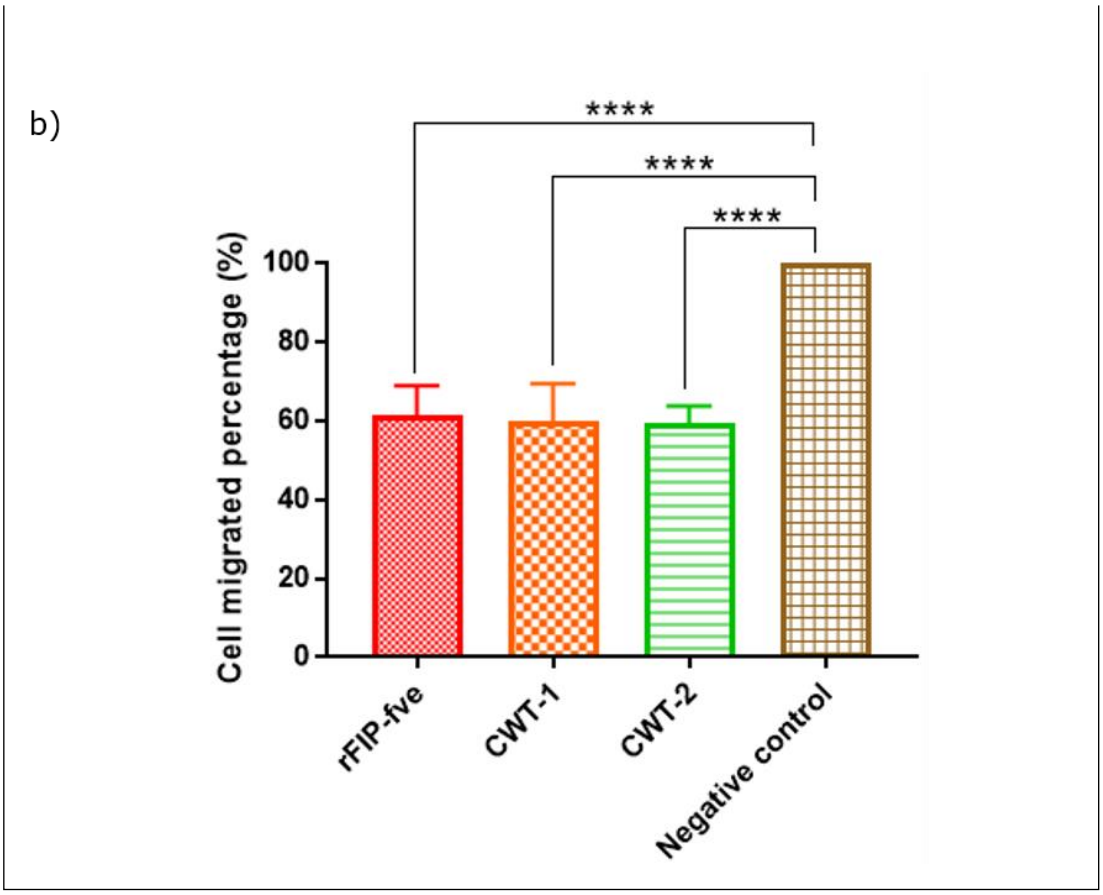
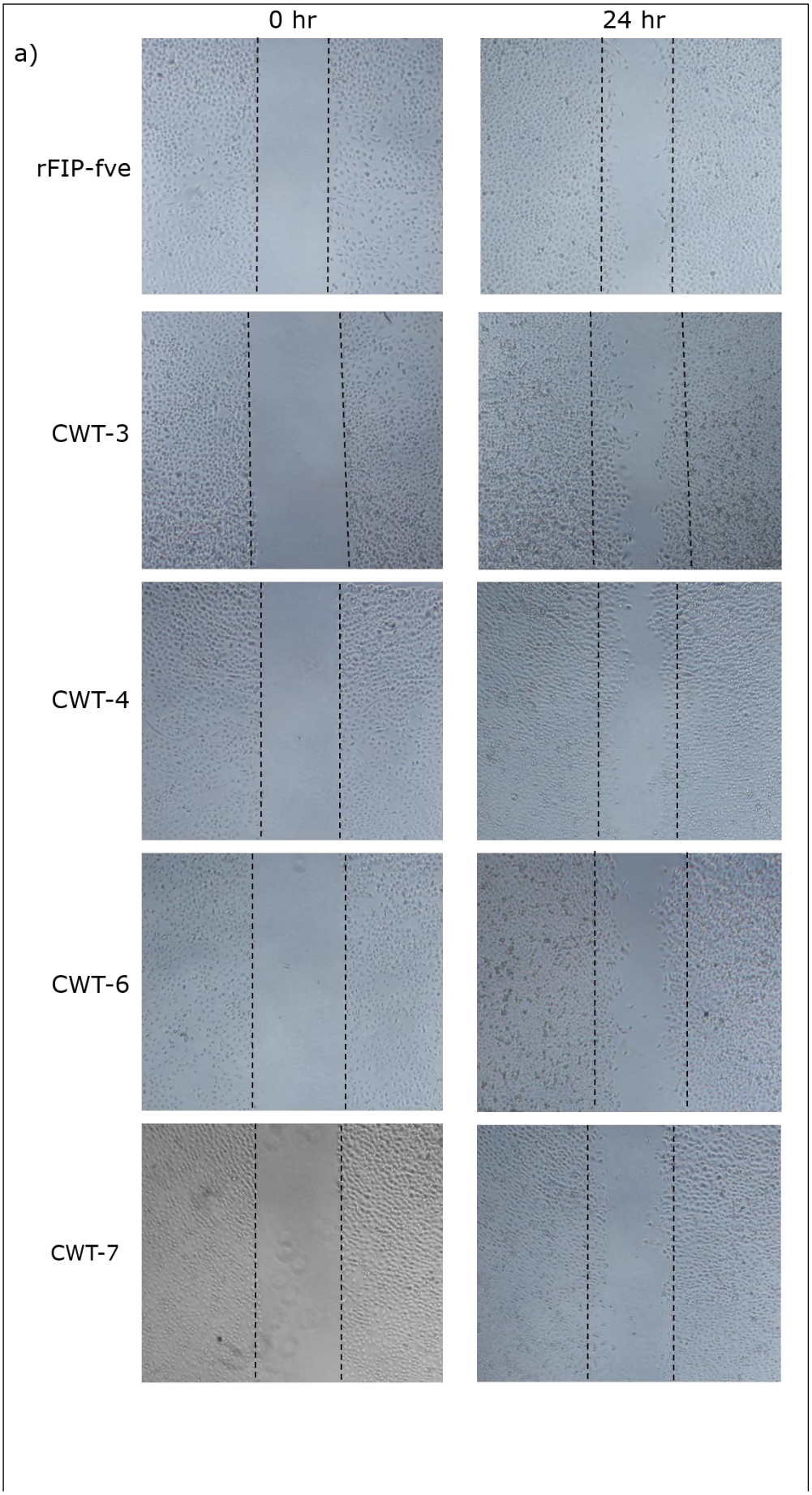


Figure 6.14. Effect of rFIP-fve and mutant group of putative enhanced dimerization on MDA-MB-231 cell migration. MDA-MB-231 cells were treated with 40 µg/ml rFIP-fve, CWT-1 and CWT-2 for 24 hr. PBS-treated MDA-MB-231 cells was used as negative control. (a) After 24 hr incubation, the cell migrations were monitored and photographed by microscopy. (b) The gap distances at the reference points were measured quantitatively using ImageJ software. Results were expressed as percentage of cell migrated, which were calculated by dividing the differences of gap distance between 0 and 24 hr by gap distance at 0 hr, and times 100 (%). Data represent mean ± SD of triplicates for three independent experiments. Tukey multiple comparisons test showed degree of significance among rFIP-fve, mutants, and negative control treatment; $P \leq 0.05$ with *, $P \leq 0.01$ with **, $P \leq 0.001$ with ***, and $P \leq 0.0001$ with ****.

6.3.4.2 Mutant group with loop modification

A549 cells

After incubation with 20 µg/ml of rFIP-fve, CWT-3, CWT-4, CWT-6, CWT-7, CWT-8, and PBS (negative control) for 24 hr, the cells that migrated in wounded zone were photographed and presented in **Figure 6.15a**. It was found that 20 µg/ml of rFIP-fve, CWT-3, CWT-4, CWT-6, CWT-7 and CWT-8 were unable to inhibit A549 cell migration. As shown in **Figure 6.15b**, the percentage of A549 cell migration as a result of treatments with 20 µg/ml rFIP-fve, CWT-3, CWT-4, CWT-6, CWT-7, CWT-8 and PBS were 40.28% ± 7.37, 56.97% ± 4.26, 55.60% ± 3.18, 46.18% ± 2 , 35.47% ± 2.05, 46.68% ± 9.77, and 46.05% ± 0.65 respectively. There were no significant differences in the percentage of A549 cell migrations under treatments of rFIP-fve, mutants and negative control. However, treatment with CWT-7 resulted in the lowest percentage of cell migration among the mutants. CWT-7 also displayed a higher inhibition activity in A549 cell migration in comparison to CWT-3 and CWT-4.


0 hr
24 hr
a)
rFIP-fve
CWT-3
CWT-4
CWT-6
CWT-7

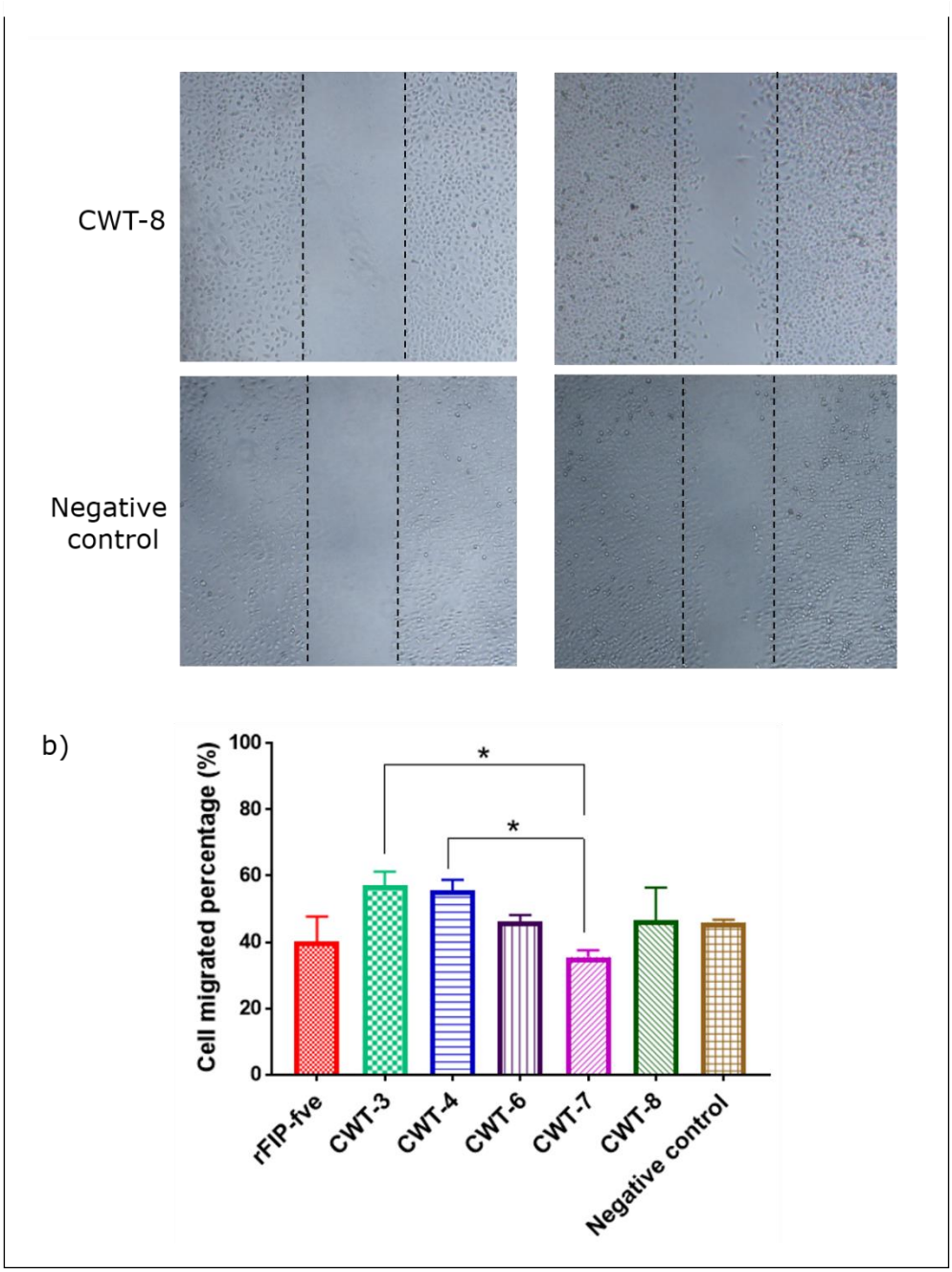
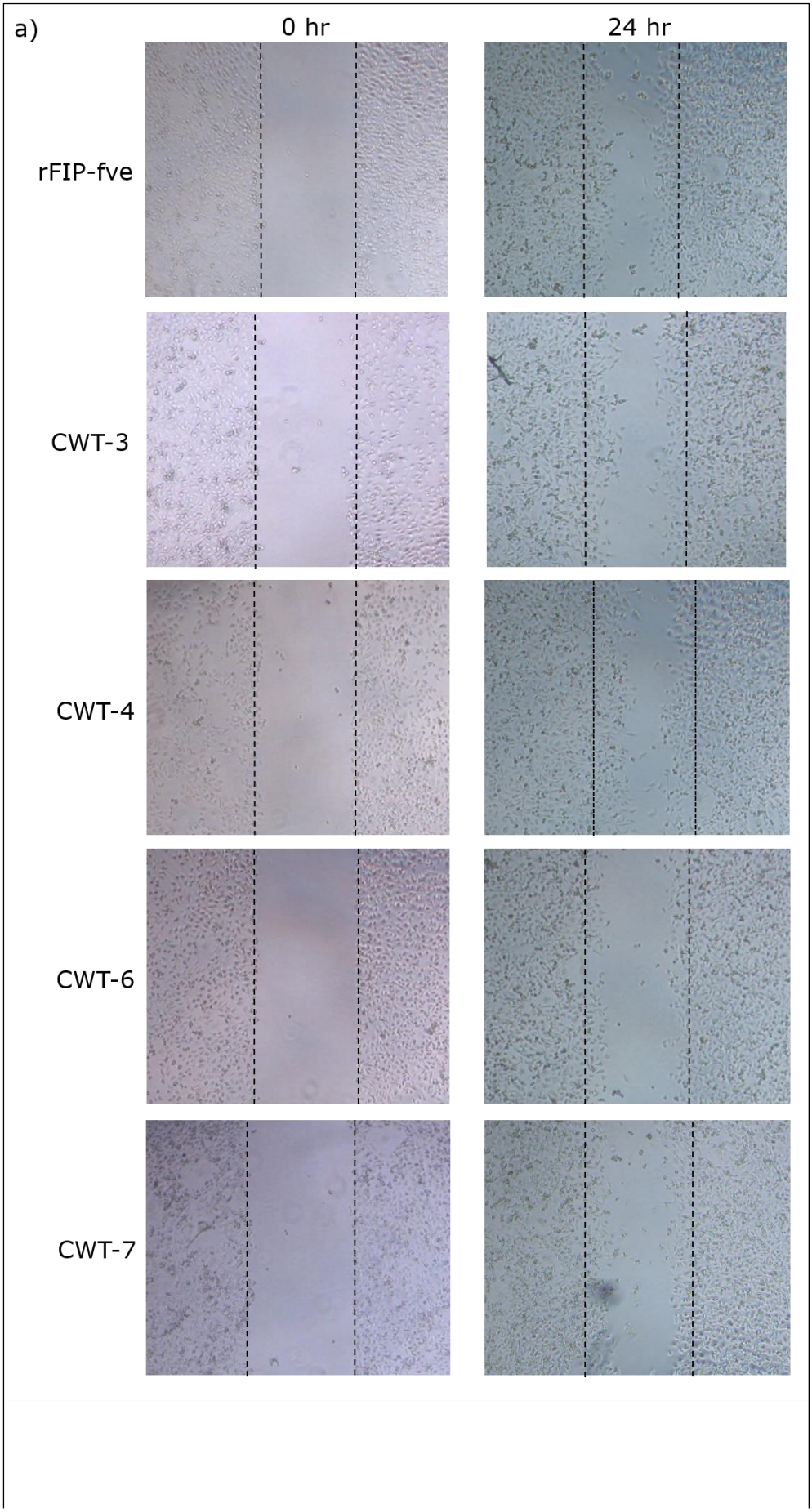


Figure 6.15. Effect of rFIP-fve and mutant group of loops modification on A549 cells migration. A549 cells were treated with 20 µg/ml rFIP-fve, CWT-3, CWT-4, CWT-6, CWT-7 and CWT-8 for 24 hr. PBS-treated A549 cells was used as negative control. (a) After 24 hr incubation, the cell migration was monitored and photographed by microscopy. (b) The gap distances at the reference points were measured quantitatively using ImageJ software. Results were expressed as percentage of cell migrated, which were calculated by dividing the differences of gap distance between 0 and 24 hr by gap distance at 0 hr, and times 100 (%). Data represent mean ± SD of triplicates for three independent experiments. Tukey multiple comparisons test showed degree of significance among rFIP-fve, mutants, and negative control treatment; $P \leq 0.05$ with *, $P \leq 0.01$ with **, $P \leq 0.001$ with ***, and $P \leq 0.0001$ with ****.

MDA-MB-231 cells

After incubation with 40 µg/ml of rFIP-fve, CWT-3, CWT-4, CWT-6, CWT-7, and CWT-8 and PBS (negative control) for 24 hr, the cells that migrated in wounded zone were photographed and presented in **Figure 6.16a**. As shown in **Figure 6.16b**, 40 µg/ml of rFIP-fve, CWT-3, CWT-4, CWT-6, CWT-7 and CWT-8 displayed some inhibition towards MDA-MB-231 cell migration as compared to negative control. The percentage of MDA-MB-231 cell migration as a result of treatments with 40 µg/ml rFIP-fve, CWT-3, CWT-4, CWT-6, CWT-7, CWT-8 and negative control were 61.30% ± 7.56, 64.82% ± 7.01, 61.31% ± 2.19, 39.41% ± 4.50, 64.89% ± 13.57, 66.72% ± 2.89 and 100 % respectively. It was found that CWT-6 demonstrated peak inhibition acitivity in migration of MDA-MB-231 cells among rFIP-fve and mutants.


a)
0 hr
24 hr
rFIP-fve
CWT-3
CWT-4
CWT-6
CWT-7

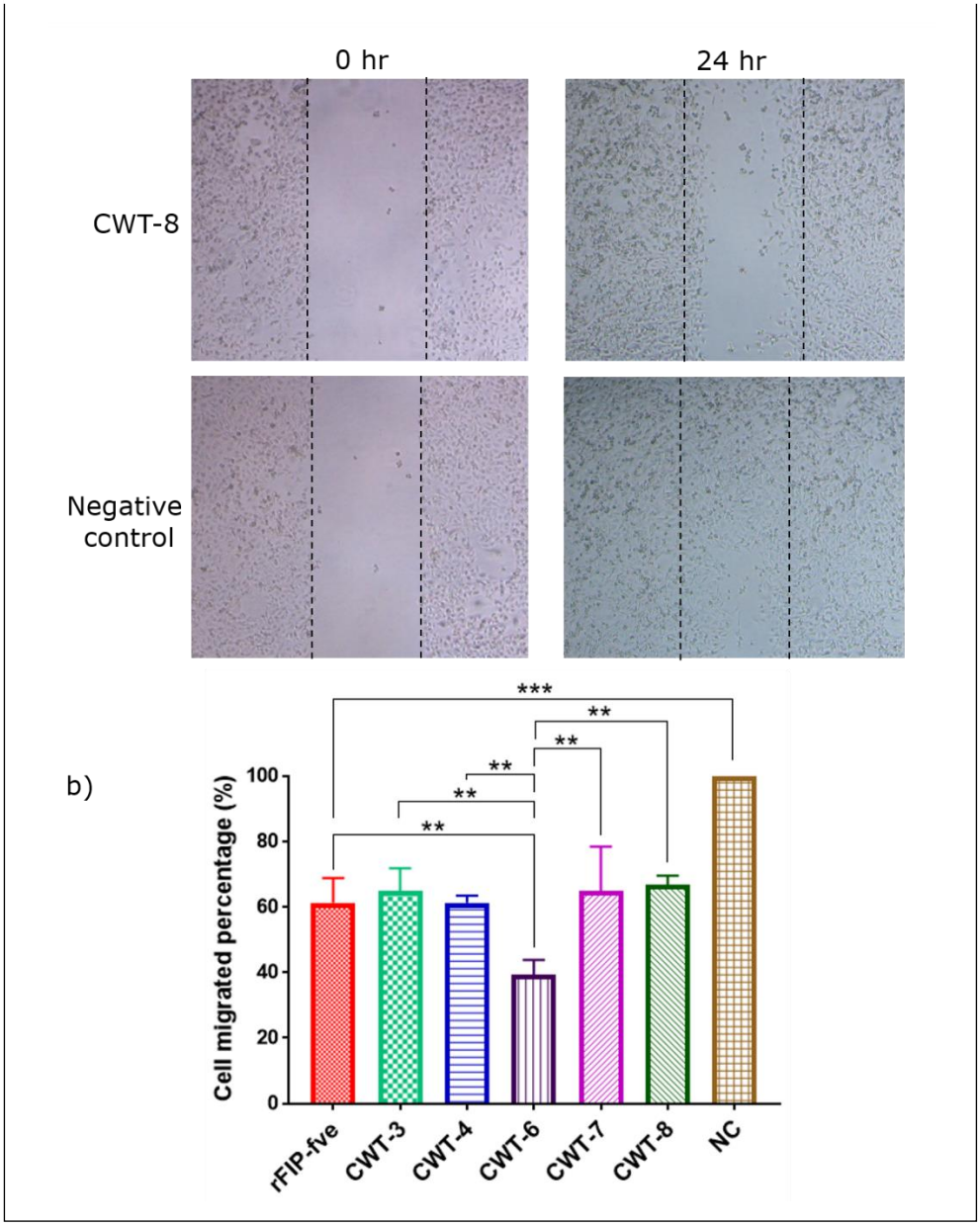


Figure 6.16 Effect of rFIP-fve and mutant group of loops modification on MDA-MB-231 cell migration. MDA-MB-231 cells were treated with 40 µg/ml rFIP-fve, CWT-3, CWT-4, CWT-6, CWT-7 and CWT-8 for 24 hr. PBS-treated MDA-MB-231 cells was used as negative control. (a) After 24 hr incubation, the cell migrations were monitored and photographed by microscopy. (b) The gap distances at the reference points were measured quantitatively using ImageJ software. Results were expressed as percentage of cell migrated, which were calculated by dividing the differences of gap distance between 0 and 24 hr by gap distance at 0 hr, and times 100 (%). Data represent mean ± SD of triplicates for three independent experiments. Tukey multiple comparisons test degree of significance among rFIP-fve, mutants, and negative control treatment; $P \leq 0.05$ with *, $P \leq 0.01$ with **, $P \leq 0.001$ with ***, and $P \leq 0.0001$ with ****.

6.4 Discussion

In this chapter, the anti-cancer activities of rFIP-fve and mutants were investigated and compared using MTT and wound-healing assays. MTT assay was utilised to determine the optimal concentration and time point of the respective rFIP-fve and mutants in inhibiting viability of lung cancer cells A549 and breast cancer cells MDA-MB-231 and MCF-7. Subsequently, the cancer-inhibiting activities of rFIP-fve and derivatives were analysed and compared. The optimal concentrations determined in inhibiting the cell viability of A549 and MDA-MB-231 cells were also used to investigate the anti-migration activities of rFIP-fve and mutants.

For putative enhanced-dimerization group, the optimal concentrations and time points determined for rFIP-fve and mutants were 20 µg/ml at 24 hr in A549 cells. Despite having no significant differences in A549 cell viability- and migration-inhibition activities between rFIP-fve and CWT-2 at 24 hr of treatment, a slower degradation of cell viability inhibition activity in time dependent manner was displayed in CWT-2 as compared to rFIP-fve. The A549 cell inhibitory rates in the treatment of rFIP-fve at 24, 48 and 72 hr were 30.24% ± 11.20, 8.28% ± 3.28 and 0% respectively; whereas the A549 cell inhibitory rates in the treatment of CWT-2 at 24, 48 and 72 hr were 28.44% ± 2.99, 18.63% ± 1.65 and 16.05% ± 2.99 respectively. The results suggested that mutant CWT-2 with putative strengthened inter-helix interaction (A2L) showed potential in prolonging the A549 cell viability inhibition effect, which may be a result of enhanced protein half-life in CWT-2 due to increased stability in maintaining the protein in homodimer state. The dimerization state of FIPs was found necessary for their immunomodulatory function (Lin *et al*., 1997). However, the prolonged cell-inhibitory effect as a result of the hydrophobicity enhancement in CWT-2 was not observed in both MDA-MB-231 and MCF-7 cells. In MCF-7 cells, the cell viability inhibition activities of rFIP-fve and CWT-2 were the highest at 24 hr and gradually diminished in a similar extent as incubation time increased.

Likewise, both rFIP-fve and CWT-2 were similarly able to maintain their cell viability inhibition activities in MDA-MB-231 cells at 24 and 48 hr, but their activities were also degraded at 72 hr. The question arises of why CWT-2 was particularly effective in maintaining its anti-cancer activity in A549 cells but not in MDA-MB-231 and MCF-7 cells. It is postulated that the differences could be possibly due to the different inhibitory mechanisms of CWT-2 possesses in these cell lines, but this proposition required further elucidation in future study. Apart from that, another important finding was that although the cell inhibition activities of CWT-1 against A549 and MCF-7 cells were deemed no difference in comparison to rFIP-fve, it is indeed less effective in inhibiting MDA-MB-231 cells as compared to rFIP-fve. It was observed that the MDA-MB-231 cell-inhibitory activity of CWT-1 degraded rapidly as treatment period increased. This implies that the additional methionine at the N-terminal of FIP-fve was unable to enhance its anti-cancer ability, in fact it deteriorated its anti-cancer activity in MDA-MB-231 cells. Altogether, two important findings are summarized herein based on the cancer-inhibiting activities study on mutant group with putative enhanced dimerization, which are: (i) CWT-1 that harbours additional methionine did not result in enhancement of cell-viability inhibitory activities in all three cell lines tested, moreover it resulted in degradation of cell viability inhibitory activity in MDA-MB-231 cells; and (ii) CWT-2 that carries residue with enhanced hydrophobicity residue demonstrated a slower diminishing of cell viability inhibition activity in A549 cells, which may be a consequence of prolonged protein half-life in CWT-2 due to increased protein stability in homodimer state.

In the mutant group with loops modification, discussion is firstly focused on their inhibitory activities against A549 and MCF-7 cells as the cancer-cell inhibiting activities of recombinant proteins are found similar on these two cell lines. CWT-7 with mutations of loop FG and hinge residue I97D adoption was found to demonstrate the highest cell viability-inhibiting activities in A549 and MCF-7 cells at 42.21% ± 1.80 and 43.85% ±

10.27 respectively. In spite of the fact that rFIP-fve and all of the mutants including CWT-7 were shown incapable of inhibiting the cell migration activity of A549 cell lines, it is noted that CWT-7 demonstrated lowest cell migration percentage in comparison to rFIP-fve, mutants and negative control even though statistically insignificant. Interestingly, it was observed that CWT-4, CWT-7 and CWT-8 with the mutations of loop FG showed higher inhibition rates in A549 cells in comparison to CWT-3 and CWT-6 with mutations of loop DE adoption. It is important to highlight that CWT-8 with both loop DE and FG mutations attributed higher cell viability inhibition activity (although statistically not significant) in A549 cells as compared to CWT-6 that harbours loop DE mutation solely. In this respect, the adoption of loop FG in CWT-8 appeared to increase its inhibitory activity against A549 cell viability. Another interesting observation noted was that CWT-3 with loop DE mutation (without hinge residue E61K) appeared to exhibit great protein stability that gave rise to prolonged protein half-life, which resulted in stable activity throughout 72 hr of treatment period. For instances, it was observed that CWT-3 displayed consistent inhibition activities in A549 cells at 24, 48 and 72 hr (**Figure 6.4**), while CWT-3 showed a gradual increase of inhibition activity in MCF-7 cells along with increased treatment period (**Figure 6.6**). Despite presumably high stability of CWT-3, this mutant showed lower A549 and MCF-7 cell viability inhibition activities as compared to peak inhibitory activity of CWT-7; by which it undermined the putative enhanced stability feature of CWT-3. Besides CWT-3, CWT-4 also displayed lower cell viability-inhibition activities in A549 and MCF-7 cells as compared to CWT-7. More importantly, it is noteworthy to mention that 10 and 20 µg/ml of both CWT-4 and CWT-6 demonstrated promotion in MCF-7 cell proliferation. Although the proliferation promotion effect were gradually reduced as the concentration of treatments of CWT-4 and CWT-6 increased from 20 to 40 µg/ml, the adverse effect as a consequence of treatment using these two mutants have to be taken into consideration in the design of FIPs protein drug for MCF-7

cell line. Both CWT-4 and CWT-7 carry mutations in loop FG region, but CWT-4 lacks of hinge residue I97D, indicating that the adoption of hinge residue together with loop FG from LZ-8 were important for the enhanced cancer-inhibition activities in CWT-7. Above all, the finding in this research suggested that loop FG and hinge residue I97D (LZ-8) in CWT-7 play critical role in strengthening cell viability inhibition effect toward A549 and MCF-7 cell lines.

In MDA-MB-231 cells, CWT-6 with adoption of loop DE and hinge residue E61K was found to demonstrate the highest cell viability- and migration-inhibition activities in comparison to rFIP-fve and all other mutants with loop modification. In contrast to the result of A549 cell-inhibiting assay, CWT-6 displayed apparent higher MDA-MB-231 cell inhibitory activity as compared to CWT-4, CWT-7 and CWT-8 that harbour loop FG (LZ-8) adoption. In fact, CWT-8 with both loop DE and FG resulted in a lower MDA-MB-231 cell inhibitory activity in comparison to CWT-6, albeit possessing the loop DE region. This implies that the presence of loop FG in CWT-8 appeared to decrease its inhibition of cell viability. It is also noteworthy to mention that loop DE together with hinge residue E61K were crucial for enhancing the cell viability-inhibitory activity of the particular mutant against MDA-MB-231 cells. As an example, although CWT-3 displayed stable MDA-MB-231 cell inhibition activities at all three time points, its inhibiting-activity was lower than the peak inhibition activity of CWT-6, which again undermined its putative high stability feature. Taken together, the results herein proposed that loop DE and hinge residues E61K (adoption from LZ-8) in CWT-6 were mainly responsible in the enhanced cell viability-inhibitory and anti-migration abilities against MDA-MB-231 cell lines.

Although it has been mentioned previously that LZ-8 possesses greater cytotoxicity than FIP-fve in HL60 cells, the data was not published in the journal for unknown reason (Huang *et al.*, 2009). Li and colleagues were the first research group that presented the differences of anti-cancer activities in LZ-8, FIP-fve, FIP-sch3 (Li *et al*., 2016) and FIP-dsq2 (Li *et al*., 2017). FIP-sch3 and FIP-dsq2 are novel FIPs that were recently discovered from *Stachybotrys chartarum* and *Dichomitus squalens* respectively. Lung cancer A549 cell line was used frequently in the anti-cancer research of FIPs. Recombinant FIP-dsq2 and FIP-sch3 proteins were compared to recombinant FIP-fve and LZ-8 proteins in terms of their anti-cancer activities by subjecting treatment of 8 µg/ml of these FIPs to A549 cells; these recombinant FIPs were generated using *E.coli* system (Li *et al.*, 2016, 2017). In these two studies, the cancer cell-inhibitory activities of LZ-8 were the highest among the FIPs tested, whereas treatment with FIP-fve resulted in the lowest inhibitory rate among the FIPs tested. The inhibitory rates of FIP-fve, LZ-8, FIP-dsq2, and FIP-sch3 were 7.03 %, 59.99%, 33.43 %, and 46.23 % respectively. Complementary to this, it was shown that the treatments of recombinant LZ-8, FIP-dsq2 and FIP-sch3 proteins exerted A549 cell cytotoxic effects via apoptosis induction (Li *et al.*, 2016, 2017). The author then explored on the possible structural differences in FIP-dsq2 in comparison to known 3D proteins structures of FIP-fve and LZ-8. The structure of FIP-dsq2 was modelled based on the resolved protein structures of FIP-fve and LZ-8, and the model structure of FIP-dsq2 was subsequently aligned against FIP-fve and LZ-8. As shown in **Figure 6.17**, FIP-dsq2 superimposed nearly perfectly to LZ-8 including loop DE and FG regions; in contrast, the two loop regions are distinctive to FIP-fve (Li *et al.*, 2017). This could be the reason why FIP-dsq2 possessed considerably higher A549 cell-inhibiting activity as compared to FIP-fve. Considering of the observation that FIP-dsq2 exhibited lower A549 cell inhibitory activity than LZ-8 despite sharing high structural similarity in both of the loop regions, this might indicate that other factors such as: (i) the properties of

the amino acid in the loop regions and/or (ii) other regions of proteins might possibly play a role in the higher cytotoxic activity in LZ-8 among the FIPs. There are four amino acid residues differences in loop DE region and three amino acid residues differences in loop FG region between FIP-dsq2 and LZ-8 (Li *et al.*, 2017). Herein, the critical regions that enhance the cancer-inhibiting ability of FIP-fve mutants against all three cancer cell lines were determined. Surprisingly, the adoption of both loop DE and FG regions (LZ-8) did not result in the optimal anti-cancer activities in MDA-MB-231, A549 and MCF-7 cell lines. It was expected that the adoption of these two loops would yield cancer-inhibiting activities similar in strength to LZ-8 that possesses both of the loops (Li *et al.*, 2017). Besides the loop regions, it has not been taken into account on impact (in term of protein bioactivity) of this inconspicuous divergence in the N-terminal dimerization of FIP-fve and LZ-8 (as shown in **Figure 6.17**). In other words, it has not been thought that N-terminal dimerization might involve in determining the bioactivities variation of these FIPs protein. It was reported that the process of dimerization is crucial for insulin and epidermal growth factor to bind to their receptors on cell surface and exert their activity (Shai, 1995). Therefore, it is possible that the structural differences in N-terminal dimerization site of FIPs could be critical for cell surface recognition, which is important to exert their cancer-inhibitory activity (Lin *et al*., 1997). Based on the finding in this study, it is now speculated that the less apparent variation in local region of N-terminal dimerization between FIP-fve and LZ-8 might also contribute to the superior cancer-inhibiting ability of LZ-8. Further research on the differences of N-terminal dimerization region might provide insight into revealing their possible roles in attributing to the variation in bioactivities in FIPs proteins.

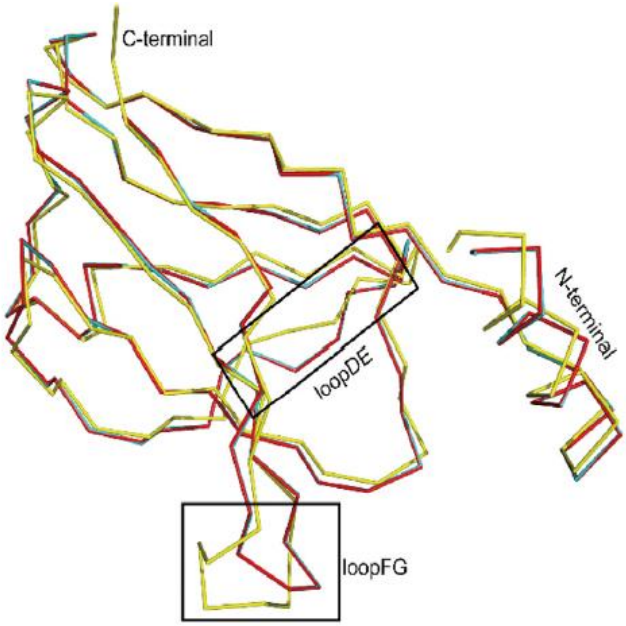


Figure 6.17. (A) Superposition of 3D protein structure of the monomers of FIP-fve (yellow), LZ-8 (cyan), and FIP-dsq2 (red). The differences in loop DE and FG regions are indicated in the black boxes. Image adopted from Li *et al.* (2017).

Most of the research on FIP-fve have been focused on its immunomodulatory activities, hence there were limited references on the study of anti-cancer activities of FIP-fve. It was reported that native FIP-fve was able to inhibit *in vitro* A549 cell viability and migration in concentration-dependent manner previously (Chang *et al.*, 2013). Their results showed that 92.5, 187.5 and 375 µg/ml of FIP-fve treatment resulted in inhibitory rates of 20, 35 and 40% respectively. Simialr to their finding, treatment of rFIP-fve and mutants in A549 cells also showed reduction in cell viability; nonetheless it is important to note that the concentrations of FIP-fve used in study of Chang and colleagues (2013) were very much higher than the concentrations of recombinant proteins utilised in the current study, yet the percentage of cell viability shown in their study were approximately similar to this research. It was demonstrated that FIP-fve inhibited A549 cell viability through initiation of cell cycle arrest instead of induction of cell apoptosis as there was less than 7% of the apoptotic cells detected in FIP-fve-treated cells. The result of which was consistent to the finding of Li and research group (2017) where 10.88% of apoptotic

cells were detected in 8 µg/ml of FIP-fve treatment (no difference to negative control). The FIP-fve treatment resulted in an increase of G1 cells and accompanied with an increase of p53, p21 and p27 population (Chang *et al.*, 2013), which were the main signals that involved in cell cycle arrest (Sharma *et al.*, 2006). Therefore, FIP-fve was suggested to suppress the proliferation of A549 cells through p53 activation pathway. Likewise, prior research by Wu and colleagues (2011) displayed that recombinant LZ-8 inhibited A549 cell proliferation by initiating G1 cell cycle arrest via p53 induction pathway as well. Furthermore, it was also shown that FIP-fve inhibited migratory ability of A549 cells by diminishing expression of Rac GTPase-activating protein 1 (RacGAP1) and Rac1 and inhibiting filopodia fiber formation. Overexpression of RacGAP1 has been identified as one of the genes to predict risk of early recurrence of human hepatocellular carcinoma (Wang, Ooi and Hui, 2007). Altogether, it was concluded in their research that FIP-fve induced anti-growth effect on lung cancer A549 cells through p53 activation pathway and inhibited A549 cell migration via RacGAP1 (Chang *et al.*, 2013). While that was the case, 20 µg/ml of rFIP-fve as well as mutants generated in this study were ineffective in impeding the A549 cell migration; but, the use of 92.5 and 187.5 µg/ml of FIP-fve were shown to exhibit complete inhibition on A549 cell migration (Chang *et al.*, 2013). This suggests that a high concentration of FIP-fve might be required to inhibit A549 cell migration effectively. The contrasting results were likely due to the high concentration of FIP-fve used in the study of research group of Chang (2013). With that knowledge in mind, rFIP-fve and mutants are postulated to suppress the cell growth through p53 activation pathway, and higher concentration of FIP-fve might be necessary in order to inhibit A549 cell migration.

As the mechanistic study of FIP-fve on its anti-cancer ability is limited, the mechanism study on cancer-inhibiting effect of LZ-8 is presented as example herein. In correlation to the previous studies (Wu *et al.*, 2011; Li *et al.*, 2016; Li *et al.*, 2017),

recombinant LZ-8 at concentrations of 2.5, 5, and 10 μg/ml were found effective in inhibiting proliferation and inducing apoptosis in lung cancer cells including NSCLC adenocarcinoma cells (A549, H1975, CL1-5, and PC9 cells) and NSCLC squamous cells (H226 cells); the LZ-8 in the study was synthesized using *Pichia Pastoris* system (Lin *et al.*, 2017). The mechanism underlying the inhibition was examined by targeting on epidermal growth factor receptor (EGFR), which is validated to be one of the therapeutic-target for some types of cancer. For instance, aberrant EGFR expression has been found in most of the lung cancer patients, in which the highly expressed EGFR is usually associated with abnormal downstream signalling of EGFR (Sharma *et al.*, 2007). Inhibitors and antibodies for EGFR are available for lung cancer inhibition, nonetheless they are accompanied with problems such as secondary mutations and drug resistance (Bardelli and Jänne, 2012). It was shown that LZ-8 initiated cell cycle arrest and cell apoptosis in wild type EGFR-expressing A549, H226 and CL1-5 cells as well as mutated EGFR-expressing PC9 and H1975 cells by (i) downregulating the EGFR expression and (ii) triggering signalling pathway, which resulted in EGFR degradation. The LZ-8-induced degradation of EGFR is mediated through stimulation of ubiquitin E3 ligase, c-Cbl binding to EGFR, which is followed by endocytosis of EGFR into clathrin-coated pits and resulted in ubiquitination and break down of EGFR. Besides lung cancer cells, LZ-8 also induced cell viability inhibition and reduced EGFR expression in other cancer cell lines such as breast (MDA-MB-231 and MDA-MB-468), cervical cancer (HeLa), and colon cancer (SW480 and HT29). Notably, this study was the first study that displayed interaction of LZ-8 with EGFR that was found on the A549 cell surface, leading to degradation of EGFR (Lin *et al.*, 2017). From this perspective, it is postulated that the inhibition of A549, MDA-MB-231 and MCF-7 cell viability demonstrated by rFIP-fve and mutants in this study might be mediated by the same pathway as well but will need experiment to verify this suggestion.

Generally, rFIP-fve and mutants showed diminishing of cell inhibitory activities in time dependent manner. The assessment on *in vitro* cancer-inhibiting activities of FIPs in previous studies were carried out for 24 hr only (Chang *et al*., 2013; Li *et al*., 2016; Li *et al*., 2017), therefore the data of subsequent inhibitory rates that pass 24 hr were not available as a reference for current research. To explain the gradual loss of cancer-inhibiting activities of rFIP-fve and mutants, the rationale derived from study of Lin and colleagues (2017) that showed binding of LZ-8 on cell surface receptor is discussed herein. Based on the related literature, it is believed that the FIPs proteins (including rFIP-fve and mutants) might act by binding onto the specific receptors on the cancer cell surface and trigger subsequent signalling pathways that deliver signals for cell cycle arrest and/or apoptosis; and these pathways rely on the stability (in term of maintaining homodimer state) and availability of the FIPs – without which it may results in degradation of cancer-inhibiting abilities. For instance in cell cycle arrest induction, FIPs might be effective in arresting cell cycle while the proteins are still in bound to the receptor but the activity would be slowly diminished as FIPs lose its stability, and the interaction would be disestablished and results in reduction of cancer-inhibiting ability. Whereas in cell apoptosis initiation, FIPs protein may be internalized during cell apoptosis process as FIPs are still in bound with the cell surface receptor; this renders insufficient of functional FIPs in the treatment condition to interact with cell surface receptors of other viable cancer cells, and results in diminishing of anti-cancer ability. The speculation will need to be verified using methods such as SDS-PAGE and western blot where they can be used to assess the presence and integrity of protein in culture over time by identifying and semi-quantifying the protein of interest at several time points. Additionally, differential scanning calorimetry (DSC) can be used to characterize protein stability of rFIP-fve and mutants by measuring the heat change associated with the thermal denaturation of molecule. The current research serves as a preliminary study that showed differences of

anti-cancer abilities in the mutants as compared to rFIP-fve without clarifying the underlying mechanism. Extended study is required to dictate and address the mechanism of the cancer-inhibiting effect in these mutants, which may include: (i) co-immunoprecipitation to investigate the binding partners of the rFIP-fve mutants in different cancer cell lines; (ii) cell cycle arrest evaluation to examine if rFIP-fve mutants induce cancer cell-inhibition via cell cycle arrest; and (iii) cell apoptosis assay to determine if rFIP-fve mutants trigger cancer cell-inhibition through apoptosis pathway.

6.5 Conclusion

To sum up, the cancer-inhibiting effect of N-terminal methionine addition (mutant: CWT-1), hydrophobic interaction enhancement (mutant: CWT-2), and loops modification (mutant: CWT-3, CWT-4, CWT-6, CWT-7 and CWT-8) in FIP-fve were investigated in this study. The anti-cancer abilities of these mutants were tabulated in **Table 6.1**. rFIP-fve and mutant proteins exhibited different anti-cancer activities and efficiencies in A549, MDA-MB-231 and MCF-7 cell lines. The methionine residue should be excluded from the design and generation of rFIP-fve protein as CWT-1 with additional methionine was incapable of enhancing cell-viability inhibitory activities in all three cell lines tested, indeed it degraded the cancer-inhibitory activity in MDA-MB-231 cells. CWT-2 with hydrophobicity enhancement in dimerization showed potential in prolonging the inhibition of cell viability in A549 cell lines, supposedly via enhanced protein stability. CWT-6 consisting of adoption of loop DE and hinge residue E61K from LZ-8 demonstrated highest cell viability-inhibition and anti-migration activities in MDA-MB-231; whereas CWT-7 comprising of adoption of loop FG and hinge residue I97D from LZ-8 exhibited optimal cell inhibition activities in A549 and MCF-7 cell lines. The difference of activities in these mutants were resulted from changes in amino acid residues in the loop regions – to which the mechanism involved in exerting cancer-inhibiting activities required further elucidation. This study laid a preliminary foundation displaying for the first time that optimal functionality of FIP-fve in inhibiting different types of cancer cell lines can be modified by introducing mutations in the loop regions.

Table 6.1. Comparison of cell viability inhibition and anti-migration activities of rFIP-fve and mutants

Recombinant protein	Cell viability-inhibition activity			Anti-migration activity		Putative protein stability in time-dependent manner		
	A549 cells	MDA-MB-231 cells	MCF-7 cells	A549 cells	MDA-MB-231 cells	A549 cells	MDA-MB-231 cells	MCF-7 cells
rFIP-fve	+++	+++	+++	-	++	+	++	+
CWT-1	+++	+++	+++	-	++	+	+	+
CWT-2	+++	+++	+++	-	++	++	++	+
CWT-3	++	++	++	-	++	+++	+++	+++
CWT-4	++++	++	++	-	++	++	++++	++++
CWT-6	++	++++	+	-	++++	+	+	+
CWT-7	++++	++	++++	-	++	+	+	++
CWT-8	+++	+++	++	-	++	+	+	++

(+) – indicates level of positive activity
(-) – indicates negative activity

Chapter 7 X-ray Crystallography

7.1 Introduction

The application of structural biology is important to research in biomedical and biotechnology industries as well as to drug discovery in pharmaceutical industry. The structure of protein is required to fully depict the function and mechanism of a protein (Dale, Oefner and D'Arcy, 2003). Two of the most commonly used techniques in determining the three-dimensional structure of protein are X-ray crystallography and Nuclear Magnetic Resonance (NMR) spectroscopy. Currently, X-ray crystallography is the only method that can generates highly precise atomic level structural image of biological macromolecules, whereas NMR offers information such as structural and dynamic data (McPherson and Gavira, 2014). In fact, there are more than 100000 protein structures deposited in Protein Data Bank in which most of them were resolved using X-ray crystallography (Calero *et al.*, 2014). High quality crystal growth is a prerequisite in X-ray crystallography study, and very often it has becomes a major bottleneck in the process (Dale, Oefner and D'Arcy, 2003; McPherson and Gavira, 2014). The quality of protein crystal that is defined by its size and physical properties has a direct impact on the quality of diffraction intensity produced, which ultimately determines the quality of protein structural image at the final stage (McPherson 1989). It was suggested that the ordered formation of stable and large crystal (dimension greater than 0.1 mm along each axis) with sufficient long-range order is required for effective X-ray diffraction (Whitford, 2005).

Establishment of supersaturation state in mother liquor is required for macromolecule crystallization. Supersaturation is a non-equilibrium condition created under specific physical and chemical condition where the amount of macromolecule is beyond limitation of solubility (McPherson and Gavira, 2014). The association between

protein and solvent is perturbed by reagent in mother liquor, shifting equilibrium in favour of protein-protein interaction. Nucleation site is developed as a result of further concentration of solution; this process is critical for crystal growth. It is followed by expansion and then cessation as crystal reaches a limiting size (Whitford, 2005). Therefore, protein crystallization relies on the promotion of supersaturation state, which leads to the generation of solid state macromolecule. The properties of undersaturated solution must be altered to limit the solubility of macromolecules in the solution in order to establish supersaturation state in solution. Several approaches that may be performed to achieve supersaturation state are described as followed: (i) by changing pH of solution to alter degree of attraction in between macromolecules; (ii) by adding salt to modify chemical activity of water; and (iii) by adding ion or polymer to modify interaction between solvent and macromolecule (McPherson and Gavira, 2014). In general, protein crystallization is initiated with systematic screening on parameters such as protein concentration, solution condition, and incubation temperature to search for optimal condition in growing crystal (Whitford, 2005).

The growth of protein crystal can be carried out using methods such as vapour diffusion methods (sitting-drop and hanging-drop), microdialysis button, and free-interface diffusion. Sitting-drop and hanging-drop techniques are described herein as these two techniques were utilized for the crystallization experiment in this research. The sitting drop method is illustrated in **Figure 7.1a**. Specific reservoir solution is placed in the well bottom, while protein drop consisting of protein sample and reservoir solution is placed on the elevated platform. Coverslip or sealing tape with grease is subsequently used to seal over the well before incubation for protein growth (McPherson and Gavira, 2014). The water is equilibrated via vapour diffusion against reservoir solution in sealing chamber, and the equilibration leads to an increase in concentration in both protein and precipitant in drop, which eventually induces protein crystallization in the drop (Whitford,

2005). The hanging-drop method is illustrated in **Figure 7.1b**; this method is only differs to sitting drop method in the set-up of protein drop. In hanging-drop method, the protein drop is suspended from a coverslip over the reservoir solution (McPherson and Gavira, 2014).

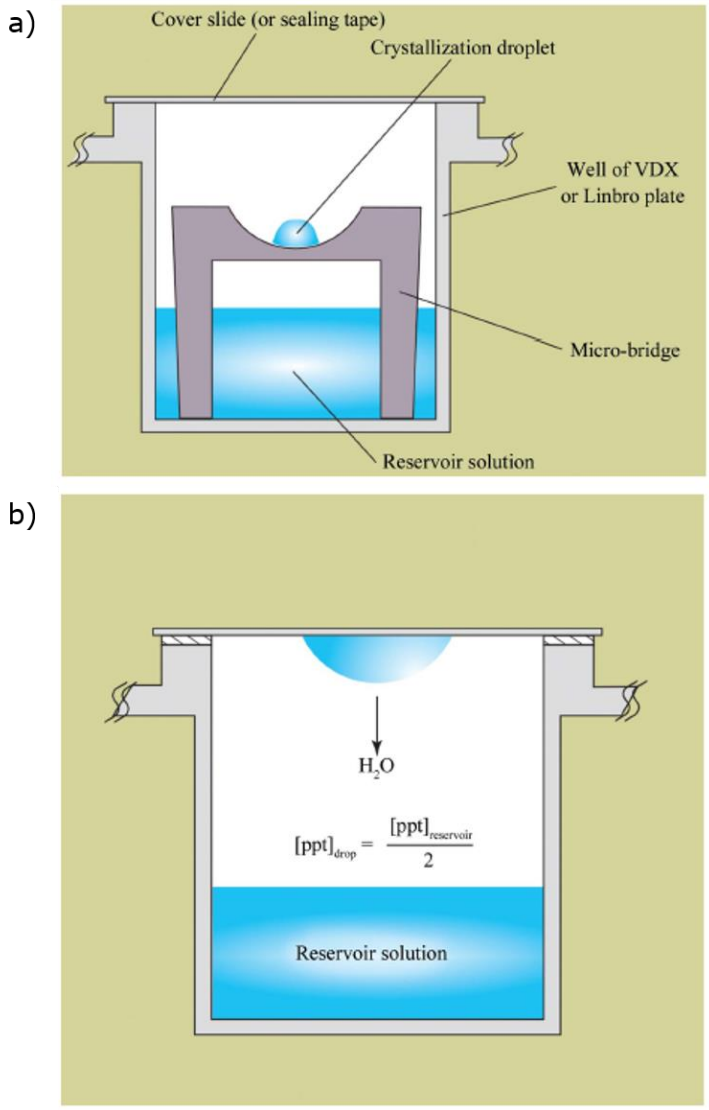


Figure 7.1. Two vapour diffusion methods, sitting-drop and hanging-drop are illustrated in this schematic diagram. Both of the methods are performed using the same element of protein drop and reservoir as well as physical equilibrium process.(a) Sitting-drop vapour diffusion method involves placing the protein drop at elevated platform and adding reservoir solution to the bottom of well. The well is then sealed using sealing tape with grease. (b) Hanging-drop vapour diffusion technique involves suspending the protein drop from coverslip over reservoir solution and adding reservoir solution to the bottom of the well. The well is then sealed using grease. Image adopted from McPherson and Gavira (2014).

X-ray diffraction experiment gives rise to a map of electron distribution in the macromolecule. The electron density map is used to estimate the position of atoms within a molecule as electrons are located closely around the nucleus of atoms. Since X-ray diffraction from a single molecule consisting of only a few electrons would be too weak to be measurable, crystal with immense numbers of molecules that are organized in order is required to ensure result with a considerable good electron density map. The intensity of scattered signals is enhanced as a result of molecular ordering in crystal. The atomic structure is obtained from the electron density distribution of the macromolecular crystal, which is the Fourier transform of the waves diffracted by the crystal (Whitford, 2005).

Chapter 7 presents attempt on determination of the three-dimensional structure of H-CWT6-EK-GFP (annotation as "CWT-6" in **Chapter 5 and 6**) as it demonstrated highest *in vitro* immune-regulating activity in mice splenocytes (as discussed in **Chapter 5**) as well as effective cell viability-inhibiting activity in MDA-MB-231 cells (as discussed in **Chapter 6**) among the mutants generated in this study. CWT-6 is the mutant that adopts and carries both loop DE and hinge residue E61K from LZ-8. Given its effective functional activities, it is therefore of interest to determine if the mutation on both loop DE and hinge residue E61K in CWT-6 would alter the conformation of loop DE to position in a similar way as the loop DE in LZ-8, and that loop conformation is crucial to the immunoregulatory and anti-cancer activities of CWT-6. Thus, the delineated three-dimensional structure of CWT-6 will give an insight into the conformational change in loop region.

To achieve the aim of this chapter, the crystallization experiment was conducted using (i) fusion protein H-CWT6-Ek-GFP and (ii) cleaved protein H-CWT6 (fusion protein was cleaved using enterokinase). The rationale underlying this strategy is based on prior research that showed respective successful crystallization using either fusion protein or cleaved protein. The large fusion tag is normally removed from the fusion protein in order to grow crystal as the fusion tag may interrupt the formation of well-ordered diffracting crystal (Bucher, Evdokimov and Waugh, 2002). Protease is used to remove fusion tag by acting specifically at

engineered-proteolysis region, which is followed by further purification to purify target protein from fusion tag and protease (Smyth *et al.*, 2003). On the other hand, large fusion tags such as maltose binding protein (MBP) (Li, Manna, Dai, Cheung, & Zhang, 2003), glutathione S transferase (GST) (Kuge *et al.*, 1997) or thioredoxin (Stoll *et al.*, 1998) may be essential for enhancing protein stability and solubility, which contribute and facilitate the crystallization of the protein of interest. In this respect, large fusion tags were retained intentionally in order to expedite target protein crystallization. The condition that favour protein crystallization is mainly dependent on the nature of protein itself, hence different strategies have to be explored for successful protein crystallization (Smyth *et al.*, 2003).

Hence, the specific objectives for this chapter are: (i) to produce recombinant proteins H-CWT6-Ek-GFP in large scale for protein crystallization experiment; (ii) to obtain cleaved H-CWT6 by digesting fusion protein H-CWT6-Ek-GFP using enterokinase; (iii) to purify target recombinant fusion proteins H-CWT6-Ek-GFP using three successive rounds of purification including immobilized metal affinity chromatography (IMAC), size exclusion chromatography (SEC), and ion exchange chromatography (IEX) purification methods; (iv) to purify target cleaved proteins H-CWT6 using four successive rounds of purification including IMAC, SEC, IMAC, and IEX purification techniques; (v) to achieve high protein yield by concentrating the purified proteins; (vi) to determine the optimal condition for protein crystallization by performing crystallization screening and optimizing crystallization condition; (vii) to obtain X-ray diffraction pattern by subjecting the grown crystals to X-ray analysis.

7.2 Methods and material

Recombinant protein H-CWT6-EK-GFP was first produced in the lab of University of Nottingham Malaysia Campus. Further proteins purification work, crystallization and X-ray analysis were performed with assistance and guidance from Dr Mohd Anuar Jonet in Comparative Genomics and Genetics Research Centre, Malaysia Genome Institute.

The fusion protein was further purified using ion exchange chromatography. The purified H-CWT6-EK-GFP protein was subjected to initial crystallization screening. The crystal generated were subjected to X-ray analysis.

For cleaved H-CWT6 protein, fusion protein H-CWT6-EK-GFP was digested using enterokinase to eradicate GFP. Subsequently, H-CWT6 was further purified using IMAC and IEX to retrieve H-CWT6. The purified H-CWT6 was subjected to crystallization screening and optimization. The crystals formed were then analysed using X-ray analysis. The schematic diagram of workflow conducted in this experiment is presented in **Figure 7.2**.

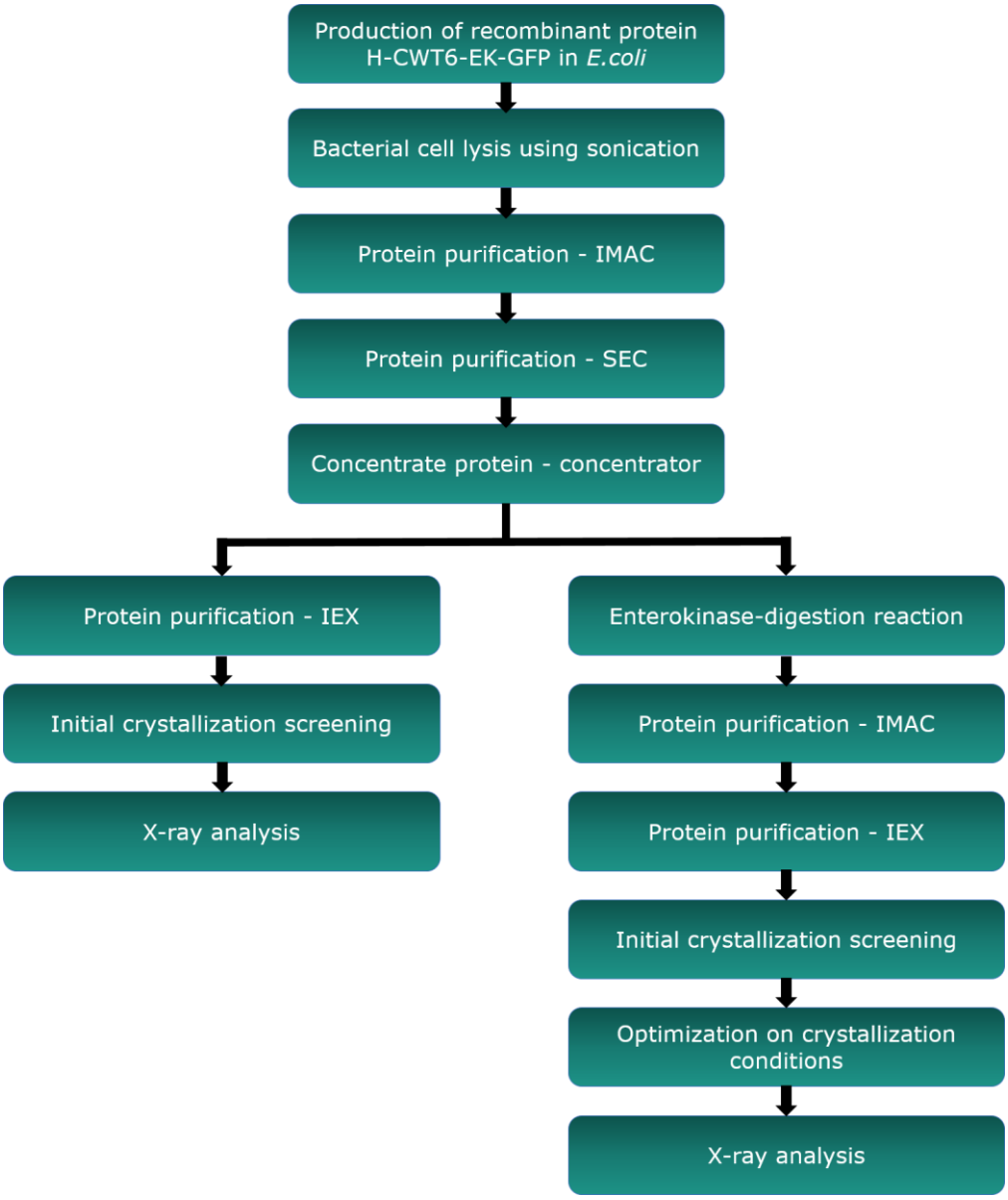


Figure 7.2. Schematic representation of workflow conducted for X-ray crystallography study of recombinant protein CWT-6 in two different states: (i) fusion protein H-CWT6-Ek-GFP and (ii) cleaved protein H-CWT6.

7.2.1 General materials and equipments

7.2.1.1 Protein sample preparation

Recombinant protein H-CWT6-EK-GFP was synthesized and purified using the same method as described in **Chapter 4**. After protein purification via IMAC and SEC, the recombinant protein was concentrated to 25 mg/ml using Macrosep® advance centrifugal device (PALL, US). For each round of crystallization screening, approximately 1 mL of 25 mg/ml H-CWT6-EK-GFP was yielded from 2L of bacterial culture.

7.2.1.2 Specialized equipment

AKTA Avant chromatography system (GE Healthcare, USA) was used to conduct further protein purification after the initial protein purification (manually) using IMAC and SEC as described in **Chapter 4**.

7.2.2 Further purification of fusion protein H-CWT6-Ek-GFP

7.2.2.1 Ion exchange chromatography

Further purification was carried out in ion exchange chromatography using 1 mL HiTrap Q FF (packed with Q Sepharose Fast Flow strong anion exchange resin) (GE Healthcare, US) connected to AKTA Avant chromatography system to remove impurities. The 1 mL HiTrap Q FF column was equilibrated with 25 mM Tris buffer (pH 8.0). After equilibration, the protein were loaded into the column. Subsequently, the bound proteins were eluted stepwise using 1M Tris Buffer of increasing salt molarity at flow rate of 1 mL/min. Fractions were collected at 1 mL per fraction. The collected fractions with protein of interest were pooled and concentrated to 100 µl at 4000 x g (4˚C) using Macrosep® advance centrifugal device.

7.2.3 Further purification of H-CWT6

7.2.3.1 Enterokinase digestion

Enterokinase digestion for recombinant protein H-CWT6-EK-GFP was prepared using 7.5 mg fusion protein, reaction buffer (20 mM Tris-HCl, 50 mM NaCl, 2 mM $CaCl_2$ pH 8.0), 112 unit enterokinase (NEB®, UK). The reaction tube was incubated at 25˚C for 24 hr.

7.2.3.2 IMAC purification

The enterokinase-digested protein reaction was subjected to IMAC purification to isolate protein of interest containing hexahistidine tag from cleaved GFP. IMAC purification was performed using HisTrap 1 mL column connected to AKTA Avant chromatography system. The resin was equilibrated with equilibrium buffer (25 mM Tris pH 8.0, 150 mM NaCl and 25 mM imidazole). After equilibration, the digested reaction was loaded into column and washed with five volume of equilibration buffer. Subsequently, the bound protein was eluted using a linear gradient of 0 to 300 mM imidazole buffered with 25 mM Tris (pH 8.0) and 150 mM NaCl. Fractions were collected at 1 mL per fraction.

7.2.3.3 Ion exchange chromatography

The fractions with protein of interest were subjected to IEX purification to remove impurities prior to protein crystallization set up. The protocol is described in **Section 7.2.2.1**.

7.2.4 Crystallization

Initial crystallization screening of purified H-CWT6-Ek-GFP and H-CWT6 were performed using screening solutions Crystal Screen 1 (Hampton Research, USA), Crystal Screen 2 (Hampton Research, USA), Index HT (Hampton Research, USA), Polyethylene glycol (PEG)/Ion Screen ((Hampton Research, USA) and JCSG screen (Molecular Dimensions, USA). The screening plates were set up using Crystal Gryphon, an automated crystallization drop set up instrument (Art Robbins Instrument, USA). All crystallization screening trials were conducted using vapour diffusion method with 100 nL of mother liquor sitting drop consisting of half volume of proteins drop (three different protein concentration at 3, 5 and 10 mg/ml) and half volume of reagent on customized microtiter plates (Greiner) at 4˚C and 20˚C. The set up plates were evaluated at 0, 1, 2, 7 and 28 days after setup using light microscope.

To optimize crystallization condition, crystals were regrown using buffered precipitant solution of different combinations of pH (5.5, 6.0, 6.5, 7.0, 7.5 and 8.0) and PEG concentration (23%, 25%, 27% and 30%) based on the determined condition that resulted in crystal growth. The optimization plate was set up using hanging drop vapour diffusion in 24-wells plate. Each well was first filled with 1 mL of buffered precipitant solution. Subsequently, 1 µl of 5 mg/ml protein sample was placed onto a coverslip and followed by addition of 1 µl of buffered precipitant solution. Triplicate droplets were included for each condition. The coverslip was inverted over the well and sealed using grease. The plates were then incubated at 20˚C. The set up plates were evaluated at 0, 1, 2, 7, 14, 21 and 28 days after setup using light microscope. The crystallization condition was further optimized using additive screen from Hampton Research containing 96 unique reagents.

As the resultant formation of crystals may be either protein crystal (macromolecule) or salt crystal (small molecule), crush test was used to identify potential protein crystal (with insufficient size or irregular shape that was not suitable to be analysed using X-ray) by using a micro-probe to crush the crystal. Salt crystal is hard, whereas a protein crystal is crumble and break apart easily (Hampton Research, 2016). On the other hand, the formed crystals with appropriate size were subjected to X-ray analysis.

7.2.5 X-ray analysis

Diffraction data was measured using a Rigaku Micromax-007 rotating-anode X-ray generator (Cu Kα, λ = 1.5418 Å) operating at 30 mA and 40 kV, coupled to Pilatus 200-K detection (as shown in **Figure 7.3**). The crystals were flash cooled directly in a stream of gaseous nitrogen at 100 K. Data were analysed using HKL 3000.

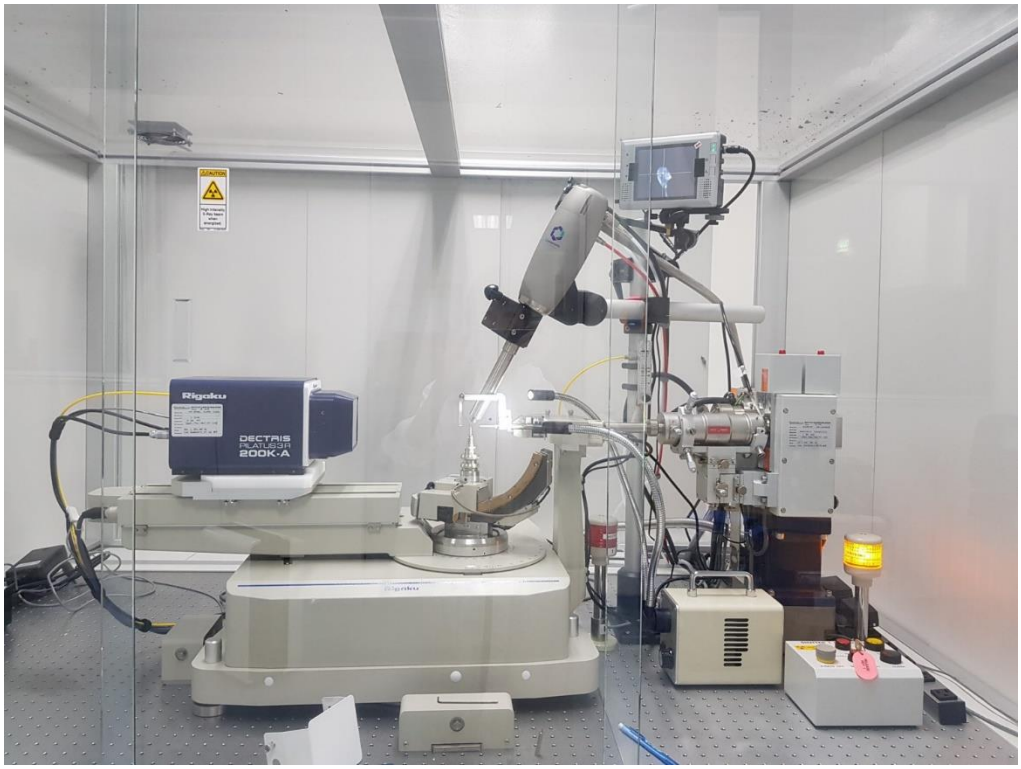
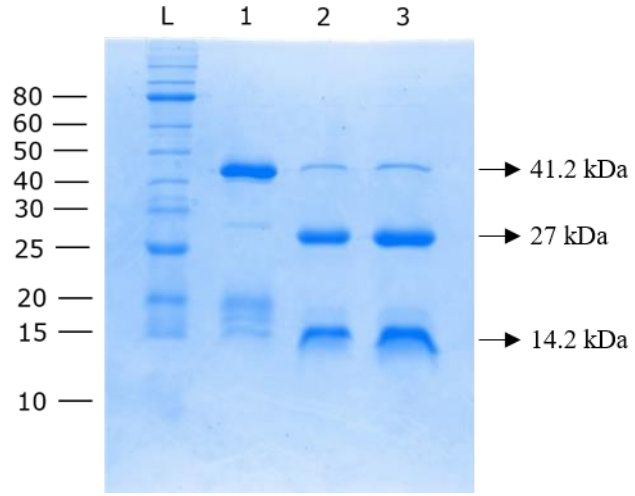


Figure 7.3. Rigaku Micromax-007 rotating-anode X-ray generator coupled to Pilatus 200-K detector that was used to collect diffraction data is shown in this image.

7.3 Results

7.3.1 Enterokinase-digestion reaction

Result of enterokinase-digestion reaction is presented in **Figure 7.4**. The undigested protein reaction showed an intense protein band with an approximate size of 41.2 kDa. The digested protein reaction consisted of three protein bands at estimated sizes of 41.2 kDa, 27 kDa and 14.2 kDa, which represented undigested fusion protein H-CWT6-Ek-GFP, GFP and H-CWT6 respectively. This result indicated that most of the fusion proteins were successfully cleaved, releasing GFP proteins from H-CWT6.



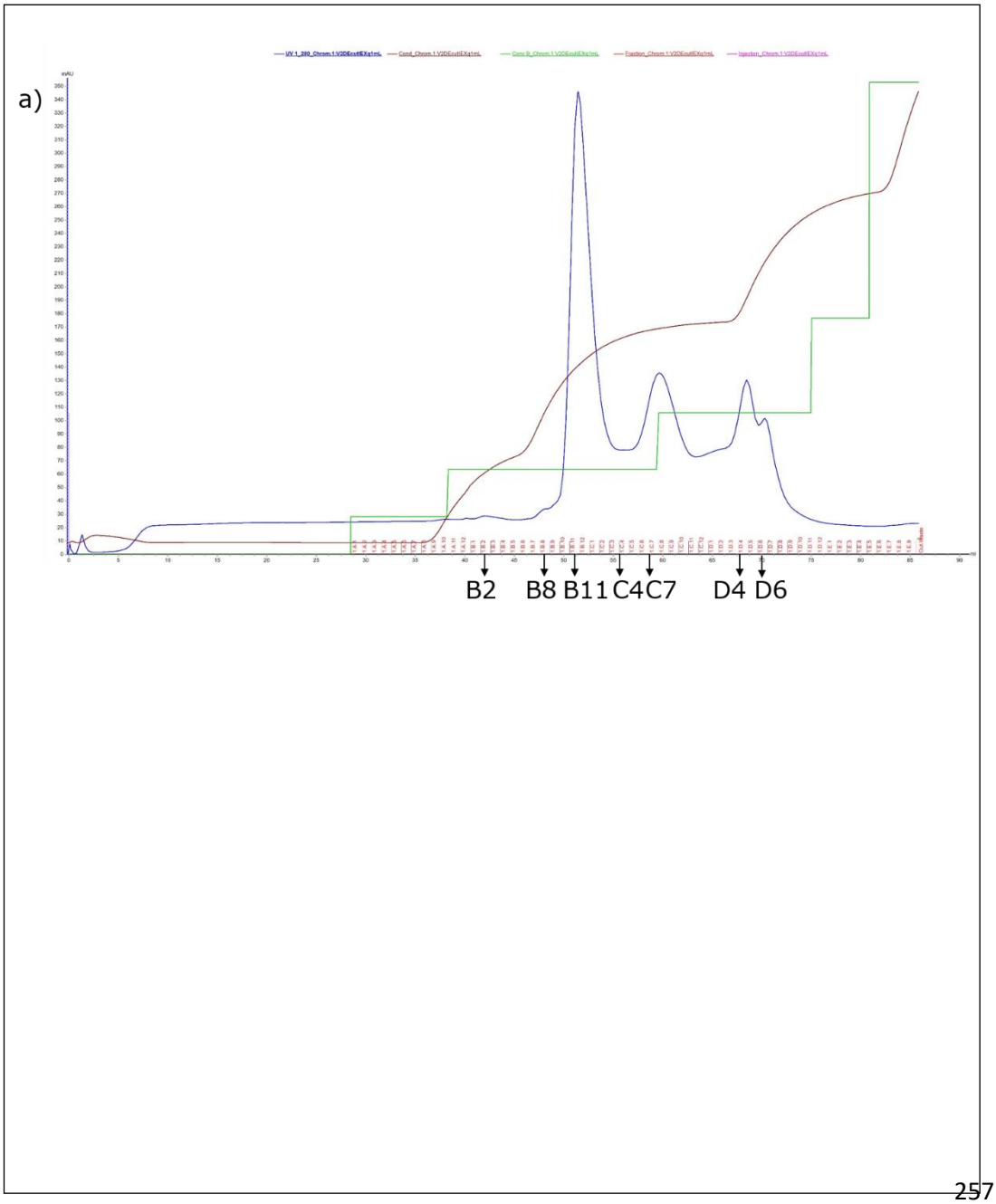
Lane	Sample		Estimated size (kDa)
L	Unstained Protein Standard, Broad Range (10-200 kDa)		-
1	Fusion protein H-CWT6-EK-GFP (undigested)		41.2
2 & 3	Digested protein reaction	Fusion H-CWT6-EK-GFP	41.2
		GFP	27
		H-CWT6	14.2

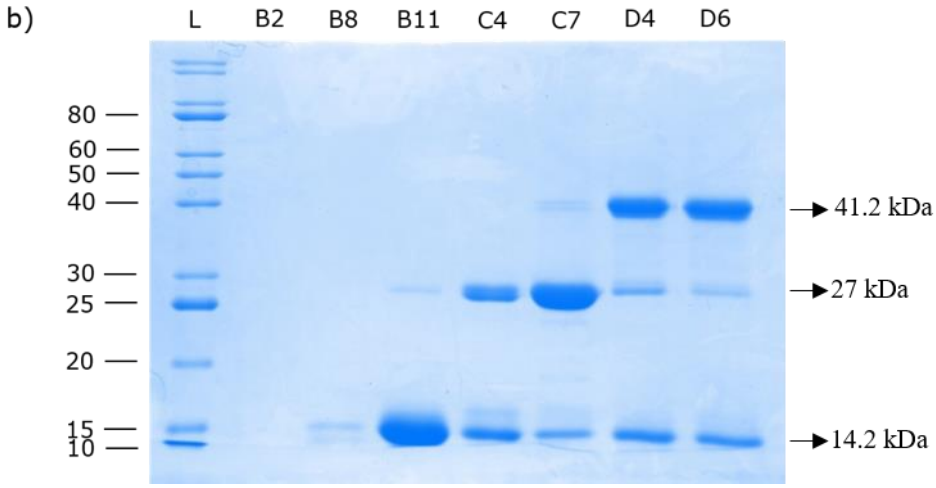
Figure 7.4. SDS-PAGE profile of coomassie blue-stained protein samples from enterokinase-digested reaction of fusion protein H-CWT6-EK-GFP. Result showed that majority of fusion protein was successfully digested, yielding three protein bands at 41.2 kDa, 27 kDa and 14.2 kDa that represented fusion protein H-CWT6-EK-GFP, GFP, and H-CWT6 respectively.

7.3.2 Purification of H-CWT6

7.3.2.1 Further purification using IEX

As shown in **Figure 7.5a**, IEX chromatogram showed the highest peak was eluted at step gradient value of 18% (v/v), followed by elution of GFP and fusion protein H-CWT6-EK-GFP. Although most of the H-CWT6 protein was eluted at step gradient value of 18% (v/v), some GFP was eluted together with the protein of interest in the fraction B11 (**Figure 7.5b**).



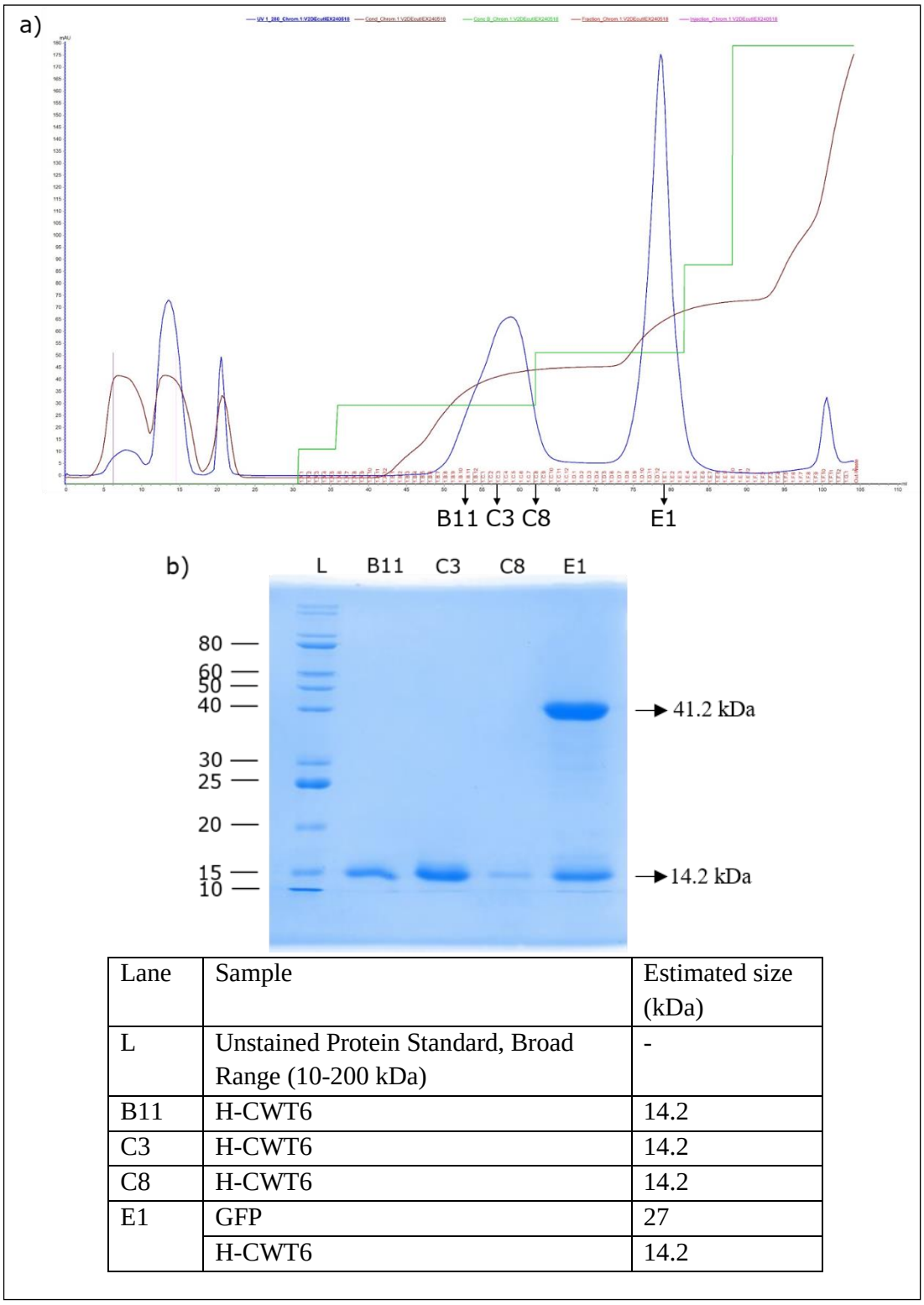


Lane	Sample	Estimated size (kDa)
L	Unstained Protein Standard, Broad Range (10-200 kDa)	-
B2	-	-
B8	H-CWT6	14.2
B11	GFP	27
	H-CWT6	14.2
C4	GFP	27
	H-CWT6	14.2
C7	Fusion H-CWT6-EK-GFP	41.2
	GFP	27
	H-CWT6	14.2
D4	Fusion H-CWT6-EK-GFP	41.2
	GFP	27
	H-CWT6	14.2
D6	Fusion H-CWT6-EK-GFP	41.2
	GFP	27
	H-CWT6	14.2

Figure 7.5. Further purification of digested fusion protein H-CWT6-EK-GFP using ion exchange chromatography. (a) IEX chromatogram of protein samples from enterokinase-digested fusion protein H-CWT6-EK-GFP. (b) SDS-PAGE profile of coomassie blue-stained protein fractions from IEX purification. Result showed that majority of H-CWT6 was eluted in fraction B11 at step gradient value of 18% (v/v), but some GFP was eluted together with the protein of interest in the fraction B11.

7.3.2.2 Further purification using IMAC and IEX

To eradicate trace of GFP completely, enterokinase-digested fusion protein H-CWT6-EK-GFP reaction was first performed using IMAC purification to remove GFP. IEX was then carried out to purify H-CWT6 and to remove undigested fusion protein H-CWT6-EK-GFP. As shown in **Figure 7.6a**, it was observed that some of the samples were eluted before salt gradient begin. This was due to the high ionic strength of the IMAC-purified protein sample. Therefore, the remaining protein sample was diluted with 25 mM Tris buffer (pH 8.0) before loading into column. IEX chromatogram showed several peaks detected at different values of step gradient. Second higher peak was detected at step gradient value of 18% (v/v), while the highest peak was observed at step gradient value of 30% (v/v). As demonstrated in **Figure 7.6b**, majority of the target protein H-CWT6 was eluted at fraction C3, whereas most of the fusion protein H-CWT6-EK-GFP was eluted at fraction E1. Based on the SDS PAGE, fractions B11, C3 and C8 consisted only protein of interest H-CWT6, implying that GFP was successfully removed from the target protein.



Lane	Sample	Estimated size (kDa)
L	Unstained Protein Standard, Broad Range (10-200 kDa)	-
B11	H-CWT6	14.2
C3	H-CWT6	14.2
C8	H-CWT6	14.2
E1	GFP	27
	H-CWT6	14.2

Figure 7.6. Further purification of digested fusion protein H-CWT6-EK-GFP using IMAC and followed by IEX. (a) IEX chromatogram of protein samples from IMAC-purified protein sample consisting of H-CWT6 and GFP proteins displayed several peaks at different values of step gradient. (b) SDS-PAGE profile of coomassie blue-stained protein fractions from IEX purification. Result showed that majority of target protein H-CWT6 was eluted at fraction C3, whereas most of the fusion H-CWT6-EK-GFP was eluted at fraction E1. Fractions B11, C3 and C8 consisted only protein of interest H-CWT6, implying that GFP was successfully removed from the target protein.

7.3.3 Crystallization

7.3.3.1 Initial extensive crystallization

Purified fusion protein H-CWT6-Ek-GFP

Crystal formation was not observed in all of the initial extensive crystallization screening plates using purified fusion protein H-CWT6-Ek-GFP except one set up condition. As shown in **Figure 7.7**, three crystals of appropriate shapes were discovered in well condition with D10 Index HT (0.1 M BIS-TRIS pH 6.5, 20% PEG monomethyl ether 5,000) that was set up with 10 mg/ml fusion protein H-CWT6-EK-GFP after 6 months of incubation at 20˚C. The tetragonal-like crystal as indicated with red arrow was selected for X-ray analysis. As purified fusion protein H-CWT6-Ek-GFP does not seem to favour crystallization, H-CWT6-Ek-GFP was not subjected to further crystallization optimization.

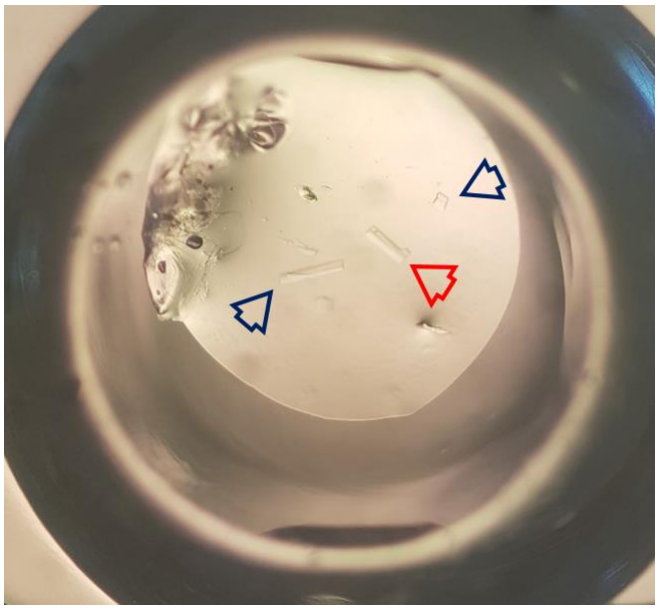


Figure 7.7. Crystals grown from initial screening condition of D10 Index HT (0.1 M BIS-TRIS pH 6.5, 20% PEG monomethyl ether 5,000) with fusion protein H-CWT6-EK-GFP after incubation at 20˚C for 6 months. The crystal as indicated with red colour arrow was subjected to crystallization.

Purified cleaved protein H-CWT6

As demonstrated in **Figure 7.8**, initial extensive crystallization screening using purified H-CWT6 has resulted in formation of crystals at a concentration of 5 mg/ml under four conditions after 14 days of incubation at 20˚C. Needle-like crystals (**Figure 7.8a**) were formed under condition of (i) C3 NEXTAL JCSG (0.2 M NaCl, 0.1 M phosphate citrate pH 4.2, 20% PEG 8000). Plate-like crystals (**Figure 7.8b**) were grown under condition of (ii) D5 NEXTAL JCSG (0.1 M HEPES pH 7.5, 70% (v/v) 2,4-methyl pentanediol (MPD). Needle cluster crystals (**Figure 7.8c**) were grown under condition of (iii) D8 index HT (0.1 M HEPES pH 7.5, 25% PEG 3350). Another plate-like crystals (**Figure 7.8d**) were formed under condition of (iv) F11 Index HT (0.2 M NaCl, 0.1 M Tris pH 6.5, 25% PEG 4000). Out of the four crystals formed from the screening, three of the crystals grew at pH 6.5 and 7.5.

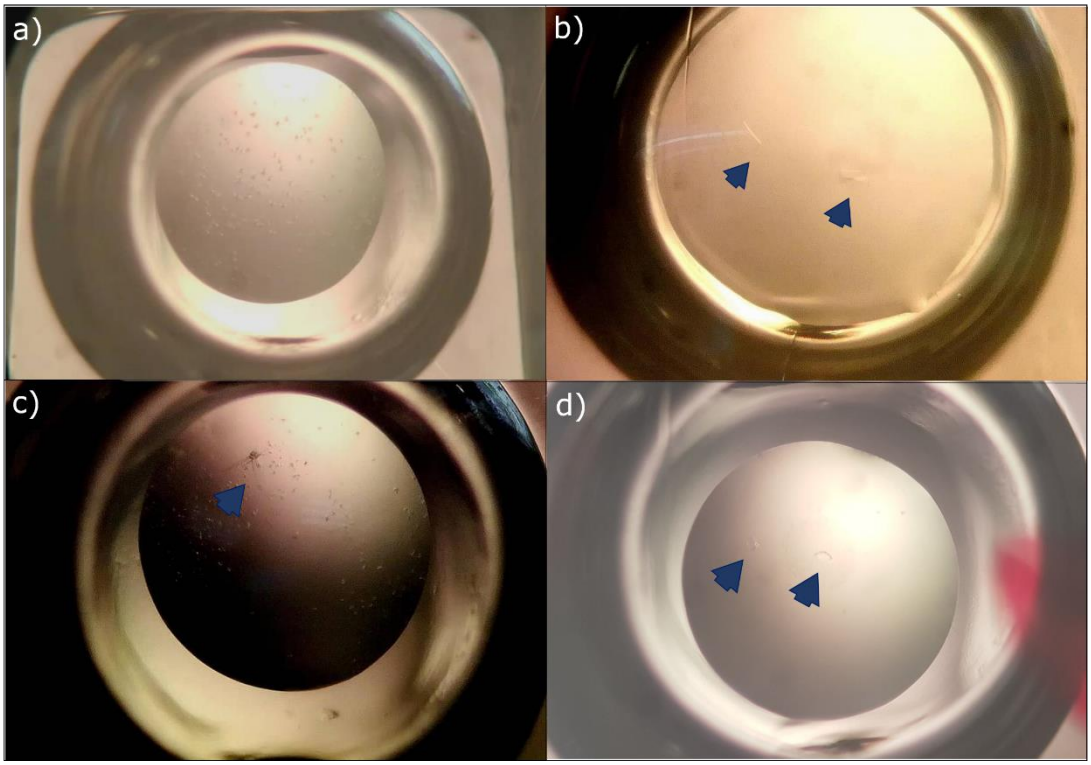


Figure 7.8. Crystals grown from the initial crystallization screening (using purified H-CWT6 as protein drop) after 14 days of incubation at 20˚C. (a) The needle-like crystals were formed under conditions of C3 NEXTAL JCSG (0.2 M NaCl, 0.1 M phosphate citrate pH 4.2, 20% PEG 8000). (b) The plate-like crystals were grown under conditions of D5 NEXTAL JCSG (0.1 M HEPES pH 7.5, 70% (v/v) MPD. (c) The needle cluster crystals were formed under condition of D8 index HT (0.1 M HEPES pH 7.5, 25% PEG 3350). (d) The plate-like crystals were grown under condition of F11 Index HT (0.2 M NaCl, 0.1 M Tris pH 6.5, 25% PEG 4000).

7.3.3.2 Optimization (modification of conditions)

As shown in **Figure 7.9a and b**, the crystals were able to be regrown using 5 mg/ml of protein under optimized condition of C3 NEXTAL JCSG at: (i) 0.2 M NaCl, 0.1 M phosphate citrate pH 4.2, 25% PEG 8000 and (ii) 0.2 M NaCl, 0.1 M phosphate citrate pH 4.2, 27% PEG 8000 respectively. Besides that, crystals were also reformed using 5 mg/ml of protein under optimized condition of F11 index HT (0.2 M NaCl, 0.1 M Tris pH 7.0, 27% PEG 4000) as displayed in **Figure 7.9c**.

7.3.3.3 Optimization (additive screen)

Subsequently, additive screen was used in extended optimization protocol as additives have been shown previously to be able to improve the size and quality of crystals (Cudney *et al.*, 1994). Under modified condition of C3 NEXTAL JCSG (0.2 M NaCl, 0.1 M phosphate citrate pH 4.2, 25% PEG 8000), addition of additive 22 (0.1 M potassium sodium tartrate tetrahydrate) has resulted in development of a larger orthorhombic-like crystal after 14 days of incubation as shown in **Figure 7.9d**. Besides that, addition of additive 22 in modified condition of C3 NEXTAL JCSG (0.2 M NaCl, 0.1 M phosphate citrate pH 4.2, 27% PEG 8000) also resulted in establishment of rod-like crystals as demonstrated in **Figure 7.9e**. Other than that, addition of additive 49 (0.01 M ethylenediaminetetraacetic acid disodium salt dihydrate) in modified condition of F11 Index HT (0.2 M NaCl, 0.1 M Tris pH 7.0, 27% PEG 4000 pH 7.0) has resulted in formation of plate-like crystals (**Figure 7.9f**).

Based on the crush test, the rod-like crystals (**Figure 7.9e**) were deduced to be salt crystals, while the plate-like crystals (**Figure 7.9f**) appeared to be protein crystals. The bigger size orthorhombic-like single crystal (**Figure 7.9d**) was subjected to X-ray analysis.

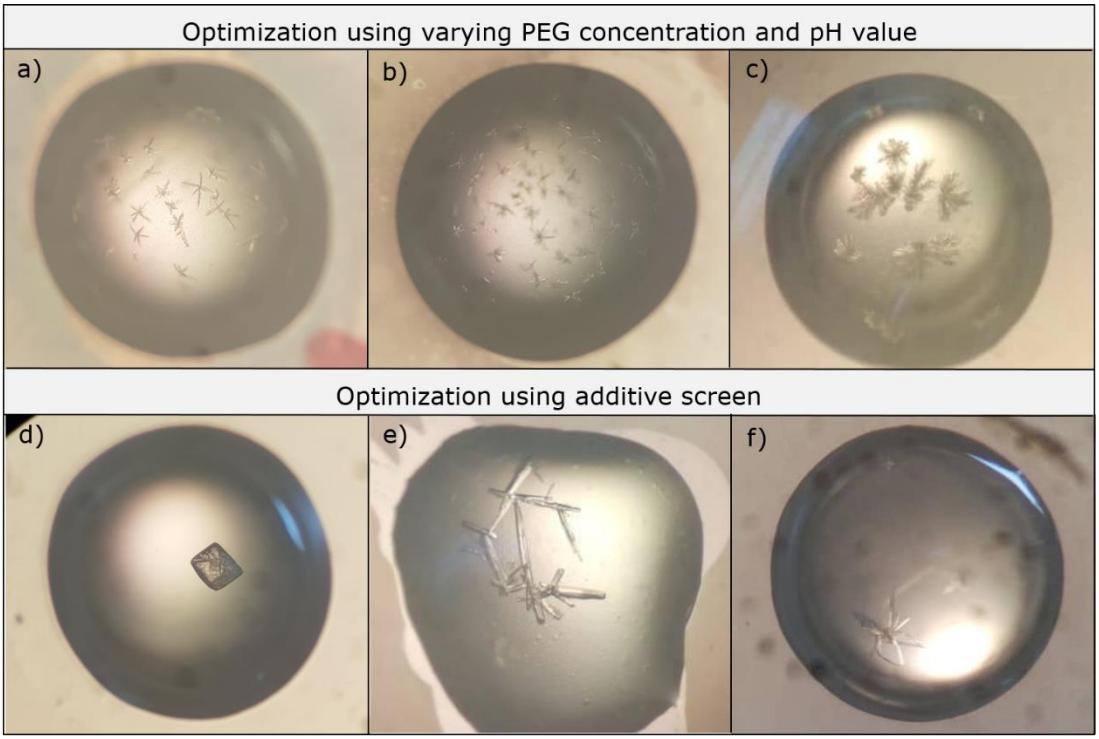


Figure 7.9. Crystals formed from the optimization by varying PEG concentration, pH value and additive addition. The crystals were regrown under the optimized conditions of C3 NEXTAL JCSG at (a) 0.2 M NaCl, 0.1 M phosphate citrate pH 4.2, 25% PEG 8000 and (b) 0.2 M NaCl, 0.1 M phosphate citrate pH 4.2, 27% PEG 8000. (c) Crystals were also reformed under optimized condition of F11 index HT at 0.2 M NaCl, 0.1 M Tris pH 7.0, 27% PEG 4000. (d) Addition of additive 22 (0.1 M potassium sodium tartrate tetrahydrate) to modified condition of C3 NEXTAL JCSG (0.2 M NaCl, 0.1 M phosphate citrate pH 4.2, 25% PEG 8000) resulted in development of a larger orthorhombic-like crystal. (e) Addition of additive 22 in modified condition of C3 NEXTAL JCSG (0.2 M NaCl, 0.1 M phosphate citrate pH 4.2, 27% PEG 8000) also resulted in establishment of rod-like crystals. (f) Addition of additive 49 (0.01 M ethylenediaminetetraacetic acid disodium salt dihydrate) in modified condition of F11 Index HT (0.2 M NaCl, 0.1 M Tris pH 7.0, 27% PEG 4000 pH 7.0) has resulted in formation of plate-like crystals.

7.3.4 X-ray analysis

Diffraction patterns of protein crystal (macromolecule) and salt crystal (small molecule) are different, therefore the results of which can be also used to distinguish protein crystal from salt crystal (Whitford, 2005). As shown in **Figure 7.10**, diffraction spots of bigger size orthorhombic-like crystal (**Figure 7.9d**) were widely dispersed and not focused, indicating that the crystal was a salt crystal. Salt crystal consists of small unit cells, which resulted in reflection that are far apart. On the other hand, the diffraction pattern of protein crystal normally appeared like a lattice of spots, which give rise to the visible ring of spots in protein crystals as only spherical section of the lattice is apparent. As demonstrated in **Figure 7.11**, diffraction spots of the tetragonal-shape crystals (**Figure 7.8**) were closely spaced and formed intense and sharp spots; this implied that the crystal was a protein crystal. However, the generated data herein was unable to be utilised for further analysis as the resolution of generated diffraction spots in the protein crystal was limited.

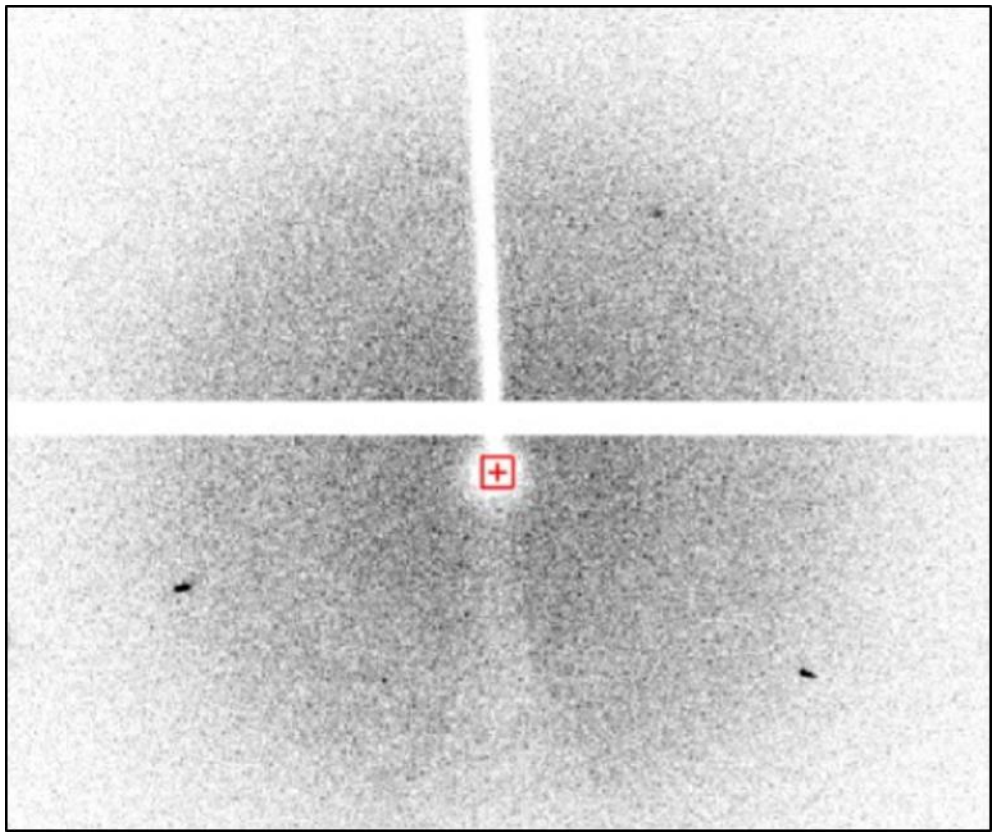


Figure 7.10. X-ray diffraction pattern of orthorhombic-like crystal. The diffraction spots were widely dispersed and not focused, indicating that the crystal was a salt crystal.

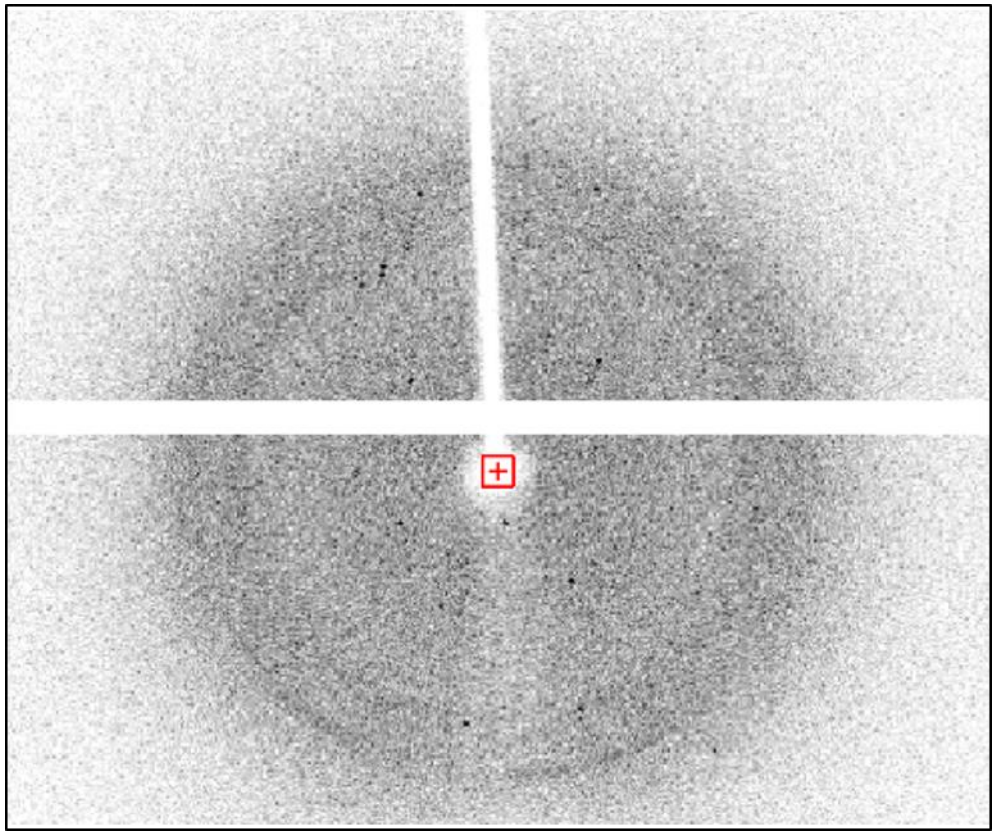


Figure 7.11. X-ray diffraction pattern of the tetragonal-like crystals. The diffraction spots were closely spaced and formed intense and sharp spots, implying that the crystal was a protein crystal.

7.4 Discussion

In this chapter, recombinant protein H-CWT6-Ek-GFP was subjected to crystallization process with the aim to obtain detail visualization of its structure at atomic resolution. The proteins were produced in large scale to ensure sufficient protein for extensive crystallization screening that required protein sample with high concentration. Several crystals were obtained from the crystallization set up, unfortunately most of the shapes of crystals were needle-like and plate-like. There were only two crystals that were grown into bigger sizes with regular shape. The two crystals were then analysed using X-ray diffraction to determine their crystal structures.

In order to achieve the specific aim of **Chapter 7**, two strategies were employed herein to crystallize the protein of interest by using two protein conditions, which were fusion protein H-CWT6-Ek-GFP and cleaved protein H-CWT6. All of the initial crystallization screening set up for fusion protein H-CWT6-Ek-GFP have failed to grow protein crystal except one that was formed only after six months of incubation. Nonetheless, result of X-ray diffraction pattern of the fusion protein crystal was deemed inconclusive due to limited resolution of generated diffraction spots in the protein crystal. Given this circumstance, modification via genetic engineering approach may be needed to facilitate the protein crystallization of the fusion proteins in future study. For example, fusion protein of gp21 ectodomain segment of human T cell leukemia virus type 1 transmembrane protein with MBP fusion tag was successfully crystallized after engineering a rigid linkage to reduce flexibility of the linker. It is noteworthy to mention that they have failed to obtain crystal when flexible linker was used to link MBP to gp21 (Kobe *et al.*, 1999). It is suggested that the flexible linker region (connecting the fusion proteins) may cause conformational heterogeneity, which impedes the protein molecules from arranging into well-ordered formation (Smyth *et al.*, 2003). In connection therewith, it is thought that the enterokinase cleavage site linker that lies between H-CWT6 and GFP

might introduce flexibility to the fusion protein, interrupting the protein molecule from getting into order in crystal growth. This may explain why the protein crystals formed only in one set up conditions out of the extensively set up conditions. Indeed, the X-ray diffraction pattern of the only one fusion protein crystal revealed that the molecules arrangement in the crystal was poor, therefore the resolution generated from the diffraction spots were limited. It was observed that while it appeared difficult to crystallize fusion protein H-CWT6-Ek-GFP, crystal growth was obtained two weeks after crystallization plate set up using digested and purified H-CWT6 proteins. Despite the fact that shape and size of the H-CWT6 protein crystals were inappropriate to be applicable for X-ray analysis, the study herein identified that condition F11 index HT with modification of parameters as well as addition of additive screen 49 have improved the growth and quality of protein crystal structure. This indicates that the determined condition can be delved into and further optimized as it appeared promising in contributing to successful crystallization of higher quality crystals in future study. Taken together, the results herein suggested that H-CWT6 protein is regarded as a suitable candidate rather than fusion protein H-CWT6-GFP to be applied in protein crystallization study as the crystallization results are encouraging.

Besides modification on parameters such as pH, temperature and PEG concentration, additive screen was also utilised herein to assist with formation of crystals during crystallization set up. It has been previously demonstrated that additive contributes to the success of crystallization in some proteins by guiding and securing lattice formation and by making critical interaction between molecules in crystal via cross-linking of molecules (McPherson & Cudney, 2006 & McPherson & Gavira, 2014). It is important to highlight that the use of additive screen has indeed helped to improve protein crystal formation, but it also facilitated the growth of salt crystals in this study. For example, the addition of additive 22 has caused formation of salt crystals instead of protein crystal

under modified conditions of C3 NEXTAL JCSG: (i) 0.2 M NaCl, 0.1 M phosphate citrate pH 4.2, 25% PEG 8000 and (ii) 0.2 M NaCl, 0.1 M phosphate citrate pH 4.2, 27% PEG 8000. In this respect, it is important to note that additive 22 together with the above mentioned conditions are likely to give rise to salt crystal. On the other hand, the addition of additive 49 in modified condition of F11 Index HT (0.2 M NaCl, 0.1 M Tris pH 7.0, 27% PEG 4000 pH 7.0) has improved the crystal structure growth from needle cluster protein crystals to plate-like protein crystals. Due to time constraint, further work to improve the growth of the protein crystal was unable to be performed. Hence, it is proposed that extended optimizations on parameters used such as pH, temperature, precipitant concentration, incubation duration as well as increasing protein homogeneity and quality should be included in future study to obtain good quality crystals.

Protein crystal growth required patience and perseverance to search for the optimal parameters and factors that contribute to the formation of well-ordered crystal, which would give rise to measurable diffraction with high resolution. Normally, extensive and successive rounds of trials are required to achieve the desired results in the field of protein crystallization (McPherson and Gavira, 2014). Every protein has distinctive crystallization endeavour as different proteins possess different propensities in crystal growth, making the protein itself the most influential variable in crystallization. In fact, it was suggested that protein quality should be optimized rather than relying on increasing the crystallization screening conditions as the expected number of crystallization hit is not necessarily proportional to the number of crystallization screening applied (Dale, Oefner and D'Arcy, 2003).

When every other crystallization approaches in modifying the parameters of protein droplet fail, two options are left to be explored, which are: (i) enhance protein quality by further purifying to increase sample homogeneity and (ii) modify protein by mutagenesis using recombinant DNA techniques. Generally, high homogeneity of protein

sample can greatly increased possibility of success in crystal formation. Further purification is therefore considered as an important steps to be invested in terms of effort and cost to improve the success rate in crystallization (McPherson and Gavira, 2014). One of the important features that determine natural tendency of a protein to crystallize is stability of protein. In fact, majority of the proteins being crystallized successfully in the very beginning of crystallography development were remarkably stable molecules (McPherson and Gavira, 2014). In order to obtain H-CWT6, the fusion protein was subjected to enterokinase digestion for 24 hr at 25˚C to eliminate the GFP molecule. This additional step increased the exposure of protein to higher temperature for a period of time, which may therefore reduced the protein stability before it was subjected to crystallization set up. With that consideration in mind, genetic recombinant technique can be used in future study to exclude GFP coding sequence at DNA level, allowing the proteins to be purified in a straightforward manner without the need to remove GFP. The modification may be useful in improving the stability of protein.

Apart from X-ray crystallography, other methods such as NMR may also be applied in 3D structure determination of protein as NMR provides direct and quick measurement on the protein structure in its native environment, allowing collection on its dynamic data (Kessel and Ben-Tal, 2018). However, NMR technique is not applicable in this study due to two reason. Firstly, it is known that secondary structure elements rather than the linking loops are better delineated by NMR method due to the relaxed conformations in loops (Kessel and Ben-Tal, 2018). Therefore, NMR is not appropriate as it was planned to define the conformation structure of loop DE in CWT-6. Secondly, NMR is limited for measurement of proteins with molecular weight that are lesser than 25 kDa only (Navarro, Wu and Wang, 2009). For this reason, the NMR technique is not applicable herein as the molecular weight for both undigested fusion protein H-CWT6-EK-GFP (82.4 kDa) and digested H-CWT6 (28.4 kDa) were definitely more than 25 kDa.

7.5 Conclusion

In conclusion, the current research has failed to obtain well-diffracting crystal of CWT-6 with adoption of loop DE and hinge residue E61K (LZ-8) that showed enhanced *in vitro* immunomodulatory capability and breast cancer MDA-MB-231 cell viability-inhibiting activity. Nonetheless, the current study revealed that H-CWT6 served as a better protein candidate than fusion protein H-CWT6-Ek-GFP to be used for protein crystallization. Following the extensive screening on the conditions that are suitable for H-CWT-6 protein growth, the search has been narrowed down to one condition, F11 index HT (0.2 M NaCl, 0.1 M Tris pH 7.0, 27% PEG 4000) with additive screen 49 that appeared promising to be explored further in future study for protein crystal formation. Further optimization and modification are necessary to generate high quality crystal in order to determine the three-dimensional structure of CWT-6 protein. It is anticipated that three-dimensional structure will extend understanding and knowledge of the FIPs in terms of functional and structural relationship.

Chapter 8 General Discussion

The primary aim of this study was to identify the functional sites in FIP-fve that contribute to its immunomodulatory and anti-cancer activities, allowing exploration of possibility to further enhance the feasibility of FIP-fve to be developed as a potential candidate for immunotherapy. Several research groups have reported the medicinal properties of FIP-fve in which it is capable of stimulating human peripheral blood mononuclear cells to generate various cytokines that are effective in alleviating allergy reaction and inhibiting tumor. For instance, oral administrations of FIP-fve were shown to alleviate the allergic symptoms in mice that were challenged with allergens. FIP-fve is capable of skewing and directing immune response towards T_H1 response, suppressing allergic airway inflammation that is triggered by T_H2 cytokines, T_H17 cytokines or IgE (Ko *et al.*, 1995; Hsieh *et al.*, 2003; Lee *et al.*, 2013; Chang *et al.*, 2015 and Chu *et al.*, 2017). Apart from that, oral-treatment of FIP-fve has significantly slowed down the tumour development of hepatoma-bearing mice as well as prolonged the survival period of hepatoma-bearing mice in relative to control group by inhibiting tumour cell proliferation via strengthening of both innate and adaptive immunity (Chang *et al.*, 2010). Besides that, FIP-fve was also demonstrated to be effective in inhibiting A549 lung cancer cell proliferation and migration directly (Chang *et al.*, 2013). Hence, FIP-fve is said to possess both direct and indirect inhibition against cancer cell growth. With the demonstration of success of FIP-fve treatment *in vitro* and in animal models, further understanding on the structure of FIP-fve is viewed as one of the prerequisite for the advancement of FIP-fve to be applied in pharmaceutical use. The research question for this study originated from the unclear structural-functional relationship of FIP-fve as well as other FIPs member in spite of the fact that many research have been conducted to examine their bioactivities. Hence, this research aimed to investigate the structural and functional relationship of FIP-fve.

There are three hypothesis proposed in this research: (i) immunomodulatory and anti-cancer abilities of FIP-fve could be further enhanced by strengthening the hydrophobic interaction between the α-helices, which could potentially results in improvement of protein stability; (ii) probable mutational benefits could be attained by adding the highly conserved N-terminal Met to the beginning of α-helices of FIP-fve; and (iii) immunomodulation and cancer-inhibiting activities of FIP-fve could be strengthened by adopting the loop regions from LZ-8 that might be mainly responsible for determining its bioactivities.

To achieve the research aim, eight derivatives of FIP-fve that targeted on N-terminal alpha-helices and loops regions were engineered using site-directed mutagenesis, and the recombinant FIP-fve and mutants proteins were synthesized using *E. coli* expression system. Two-steps protein purification was performed using IMAC and SEC. All of the recombinant proteins were successfully expressed and purified except recombinant protein H-CWT5-EK-GFP. Subsequently, the functional activities of purified proteins were evaluated based on their immunomodulation and anti-cancer abilities.

The first hypothesis of this research builds on existing knowledge that was presented in previous studies by research group of Lin (1997) and Paaventhan (2003). The sustention of the hydrophobic interaction in between of the helices is regarded imperative to maintain the homodimer state of FIP-fve, which is crucial for its immunomodulatory ability (Lin *et al*, 1997 and Paaventhan, 2003). Hence, the current study developed a hypothesis that immunomodulatory and cancer-inhibiting activities of FIP-fve could be further improved by enhancing the inter-helix hydrophobic interaction of FIP-fve. Results demonstrated that strengthening of hydrophobic interaction between the N-terminal alpha-helices dimerization sites have successfully enhanced the *in vitro* immune-regulating and anti-cancer activities of CWT-2. One of the most notable examples was that the mice

splenocytes proliferation response under treatment of CWT-2 was approximately one-fold higher as compared to rFIP-fve. Other than enhancement in immunomodulatory activity, the stronger hydrophobic interaction in CWT-2 also displayed potential in prolonging its cell viability inhibition effect in lung cancer A549 cells. Although there were no significant differences in A549 cell viability- and migration-inhibition activities between rFIP-fve and CWT-2 after 24 hr of cells treatment, CWT-2 did display a slower degradation of cell viability inhibition activity in time dependent manner as compared to rFIP-fve. Unlike A549 cells, CWT-2 showed no significant differences in cancer-inhibiting activity in comparison to rFIP-fve in MDA-MB-231 and MCF-7. Nonetheless, the reason that caused the absence of prolonging cell viability-inhibition activities in MCF-7 and MDA-MB-231 under the treatment of CWT-2 is unclear. All of the improved bioactivities of CWT-2 reported herein were attributed to the single amino acid substitution, A2L in N-terminal alpha helical region (amino acid residues 1-13). Based on the results in this study, it is deduced that the enhanced immunomodulation and cancer-inhibition effect were resulted from increased stability (in term of homodimer state) of recombinant CWT-2 protein, leading to prolonged protein half-life. In fact, protein engineering techniques are commonly used to facilitate the development of novel protein therapeutics and to promote compliance of patient through optimizing of protein half-life and functionality (Podust *et al.*, 2016). One notable exemplary strategy applied to extend protein half-life is protein derivatization and conjugation that includes PEGlyation, albumin-fusion and FC-fusion (Lagassé *et al.*, 2017). Longer *in vivo* protein half-life is important in enabling the application of protein therapeutic drug with minimal efficacious dose. Conversely, proteins with short half-life requires repetitive intake or injection during the course of treatment (Gunaydin *et al.*, 2018). In essence, the insights drawn from this research substantiates the finding presented in previous literatures, which highlighted the importance of N-terminal alpha helices in the FIP-fve dimerization. Given these points,

the first hypothesis developed herein – reinforcement of N-terminal dimerization could contribute to enhancement of functional activities of FIP-fve is generally accepted.

Present study also attempts to explore the covert mutational effect derived from incorporation of the highly conserved N-terminal methionine in FIPs family. An examination into primary structures of the proteins revealed that all of the 16 discovered FIPs consist of N-terminal methionine residue except FIP-fve, FIP-vvo and FIP-ppl. It is uncertain of the reason why most of the native FIPs retained methionine in their amino acid chains, therefore the effect of addition of methionine to N-terminal of FIP-fve was examined in this study. While a reinforcement to the functional activities of FIP-fve was anticipated, the finding suggested otherwise where it was found that the addition of N-terminal Met has failed to enhance the bioactivities of FIP-fve. In the immunomodulatory study, there was no significant differences in mice splenocytes stimulation index between rFIP-fve and mutant CWT-1 that harboured N-terminal methionine addition. Notwithstanding the insignificant differences in splenocytes stimulation index, it was observed that cell-cell interaction in CWT-1-induced splenocytes culture was indeed lesser in comparison to rFIP-fve based on microscopic visualization of splenocytes interaction at 24 hr. Furthermore, the secretion level of IL-2 was significantly lower in CWT-1 as compared to rFIP-fve. Likewise, a similar event was observed in the investigation on anti-cancer activities of CWT-1. CWT-1 and rFIP-fve displayed nearly equal cell viability-inhibiting activities on both A549 and MCF-7 cells. On the other hand, CWT-1 showed comparatively lower anti-cancer activity on MDA-MB-231 cells in comparison to rFIP-fve as the functional activity of CWT-1 quickly degraded after 24 hr of treatment. The results therefore imply not only that the addition of methionine at N-terminal of FIP-fve was unable to improve its cancer-inhibiting ability, but also deteriorates its anti-cancer activity in MDA-MB-231 cells. In this respect, it appeared that the additional N-terminal methionine in CWT-1 could have affected the hydrophobic

interaction in the N-terminal α-helices, which span from residues 2 to 14. As noted earlier, the inter-helix interaction represents one of the most important subunit-subunit interaction between the FIP-fve dimer whereby it functions to bind and stabilize the two monomers of FIP-fve. In summation, disengagement of methionine residues as the first codon in FIP-fve is suggested as necessary to ensure and maintain the functional activities of FIP-fve. This could be the reason why methionine residue is excluded in native FIP-fve. Importantly, the topic of N-terminal methionine in FIP-fve warrants research attention for some reason. It is noticed that the coding sequence of FIP-fve that was deposited in National Center for Biotechnology Information (NCBI) database as Genbank: GU388420.1 includes methionine as the first amino acid. Furthermore, a review paper that discussed on the status and prospect of FIPs family also falls short of addressing the accurate amino acid sequence of native FIP-fve in which they presented the coding sequence for FIP-fve in the same way as Genbank: GU388420.1 (Li, Wang and Zhou, 2011). These misleading information on the basic coding sequence of FIP-fve may impose undesirable effect on the functional activities of FIP-fve in future study. To answer if the presence of methionine influences the bioactivities of FIP-fve, the current research sought to address the uncertainty. On the whole, the conclusive evidences shown herein emphasized a need to exclude Met as the starting codon of FIP-fve in order to sustain the immunomodulatory and anti-cancer activities of FIP-fve.

Last but not least, it is worthwhile to delve into the central enigma reported by prior studies, which recognized the divergences that occurred predominantly in loop regions of the FIPs (Huang *et al*., 2009 and Li *et al*., 2017). In order to better understand the impact imposed by the distinctive loops, FIP-fve derivatives were generated to adopt the loop DE and FG regions from LZ-8, and subjected to immune-regulating and cancer-inhibiting analyses. According to the immunomodulation results, loop DE region in CWT-3 and CWT-6 appeared to play a crucial role in enhancing the mice splenocytes

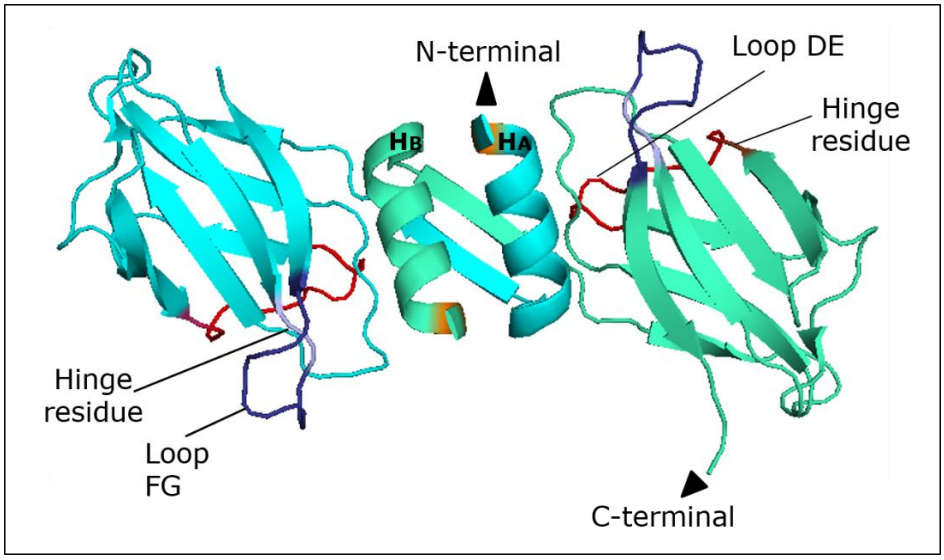
immunomodulatory activities. While adoption of loop FG and hinge residue I97D in CWT-7 also contributed partly to elevation of immune-regulating activities, the induction of splenocytes stimulatory response was approximately 40% lesser than CWT-3 and CWT-6. Coupled with this result, the stimulation of IFN-γ release in CWT-7-treated splenocytes was about 50% lower in comparison to CWT-3 and CWT-6. Accordingly, these results suggested that loop DE is the principal determinant region that is responsible in regulating immunomodulatory capability of FIP-fve. In the evaluation of anti-cancer capability, the cancer-inhibiting abilities of rFIP-fve and derivatives were considered suboptimal as not only that cell viability-inhibition effect attained in general were lesser than 45%, but also diminished over time. One interesting observation noted was that different FIP-fve mutants with engineered loop possess distinctive optimum cancer-inhibiting activities on all three cancer cell lines examined. As an example, CWT-6 comprisig of loop DE and hinge residues E61K exhibited the highest cell viability-inhibitory and anti-migration effect in breast cancer cell line MDA-MB-231. By contrast, CWT-7 consisting of loop FG and hinge residue mutation I97D demonstrated the most effective cell viability-inhibition towards lung cancer cell line A549 and breast cancer cell line MCF-7. Interestingly, rather than inhibiting cell growth, cancer-inhibition treatment using CWT-6 has caused MCF-7 cells to proliferate. In this respect, it appeared that contribution of loop region in FIPs in determining their specificity in cancer-inhibiting abilities of FIPs is comparatively high, which could be engineered by modifying the loop region. Surprisingly, it was noted that adoption of both loop DE and loop FG regions in CWT-8 resulted in lower immunomodulatory and cancer-inhibitory activities as compared to mutant containing only loop DE or FG alone. In spite of lack of evidences in comparison of immunoregulatory abilities between LZ-8 and FIP-fve, it is believed that LZ-8 that originated from medicinal mushroom *Ganoderma lucidum* with well-known curative status possesses higher immunomodulation capability as compared to FIP-fve that isolated

from an edible mushroom *Flammulina velutipes*. Indeed, previous literature has shown that anti-cancer capabilities of LZ-8 were very much higher than FIP-fve (Huang *et al.*, 2009; Li *et al*., 2016; Li *et al*., 2017). From this perspective, it was postulated that the FIP-fve mutant that harboured both loop DE and FG regions from LZ-8 could generate the optimal immunomodulatory as well as cancer-inhibiting activities. Nevertheless, the results from this study were unexpected and contrasted to initial belief. Based on these *in vitro* results shown herein, it is believed that modified FIP-fve with improved *in vitro* immunomodulatory and cancer-inhibitory activities have shown great potential to be further developed for application in immunotherapy. Taking into account of all points discussed, it is therefore suggested that future immuno-therapeutic application of recombinant FIP-fve mutant proteins might have to be tailored specially for each patient with distinctive prolife of diseases. For instance, mutant carrying mutation of loop DE and hinge residues E61K can be administered as therapeutic application to patient with MDA-MB-231 breast cancer as it is effective in enhancing the immunomodulatory as well as in breast cancer cell growth-inhibition capability of the particular patient. On the other hand, derivative harbouring loop FG and hinge residue I97D can be assigned to patient with A549 lung cancer or MCF-7 breast cancer as it is capable of reinforcing immunomodulatory (although suboptimal) and inhibiting cancer cell viability. To sum up, these *in vitro* data presented herein demonstrated that: (i) immunomodulation capability of FIP-fve can be enhanced by adopting loop DE region from LZ-8 and (ii) anti-cancer capability of FIP-fve can be reinforced by adopting either loop DE plus hinge residue E61K or loop FG region plus hinge residue I91D depending on the cancer cell types.

Following introduction of use of chemotherapy in 1940 and targeted therapy in late 1990, immunotherapy serves as the third significant progress in systemic treatment of cancer (Ascierto *et al.*, 2018). The success of immunotherapy was first seen in clinical application of immune checkpoint inhibitors such as anti-programmed death (PD)-1 or PD-ligand 1 agent and anti-cytotoxic T-lymphocyte-associated antigen (CTLA)-4 in melanoma as well as other cancer types. Indeed, this accomplishment of clinical success has largely encouraged the growth and advancement of more options of immunotherapies. There are approximately 3000 cancer-immunotherapy trials, covering hundreds of diseases that are in progress currently. With increasing numbers of immunotherapeutic available, many potential schemes of therapeutic options arise either by combining different types of immunotherapeutic candidates or by associating immunotherapy with other treatment approaches (Ascierto *et al.*, 2018). Owing to the fact that FIP-fve has been repeatedly reported for its immunomodulatory capability, it emerges as one of the potential candidates for immunotherapy. Most importantly, it is noteworthy to mention that FIP-fve demonstrated stable activity when it was delivered orally (Hsieh *et al.*, 2003; Chang *et al.*, 2010, 2015; Lee *et al.*, 2013; Chu *et al.*, 2017). In fact, oral administration is the preferred route of therapeutic drug delivery as it is generally regarded as the most comfort way for drug intake, which largely improves patient compliance (Bruno, Miller and Lim, 2015). For this reason, the convenience method of administration and stability makes FIP-fve a great potential to be developed for pharmaceutical use.

Above all, the central theme of this study is the determination of the structural and functional relationship of FIP-fve with regards to its immunomodulation and cancer-inhibition abilities. It is important to emphasize that the results generated from this research represent a preliminary conclusion to identifying of structural-functional relationship of FIP-fve. This study lays a foundation and paves the way to a holistic elucidation for other FIPs. Further investigation is necessary to identify remaining sites

that are responsible for functional activities of FIP-fve both *in vitro* and *in vivo*; and the yielded information of which could be utilized to engineer, fine tune, and introduce novel functional activities to FIP-fve as well as other FIPs in the family. Worthwhile to mention, this is the first study that reported on the successful enhancement of functional activities of FIP-fve by reinforcing the inter-helix hydrophobic interaction and by modifying the loops region. In summary, a tabulation of importance of the amino acids sites that are crucial in determining the immunoregulatory and cancer-inhibitory activities of FIP-fve is laid out in **Figure 8.1**.



Amino acid residues site	Mutation	Functional activities
N-terminal alpha helices	Increased residues hydrophobicity	Postulated to stabilize the inter-helix dimerization of FIP-fve that led to: • Enhancement in immune-regulating activity in mice splenocytes • Slower degradation of anti-cancer activity in lung cancer A549 cells
Loop DE	Adoption (LZ-8)	• Reinforcement of immune-modulatory activity in mice splenocytes • Abolishment of haemagglutination ability towards human RBCs
Loop DE & putative hinge residue	Adoption (LZ-8)	• Strengthening of immune-regulatory activity in mice splenocytes • Enhancement of inhibitory activity in breast cancer MDA-MB-231 cells • Abolishment of haemagglutination ability towards human RBCs
Loop FG & putative hinge residue	Adoption (LZ-8)	• Enhancement of inhibitory activity in lung cancer A549 cells • Enhancement of inhibitory activity in breast cancer MCF-7 cells

Figure 8.1. Tabulation of importance of the amino acids sites in determining the immunoregulatory and cancer-inhibitory activities of FIP-fve. The major regions of FIP-fve that were targeted for examination are highlighted as followed: orange colour indicated residue for enhanced hydrophobicity (A2L); red colour indicated loop DE region (S62P, N63S, F64Y, T67E, P68S, S69D, G71S); dark blue colour indicated loop FG region (G101N, S103Del, E104Del, E105D, Y106F); pink colour indicated putative hinge residue for loop DE (E61K); light blue colour indicated hinge residue for loop FG (I97D).

Limitations of current study and suggestions for improvement

Despite the ultimate objective of the research has been accomplished, there were some inevitable constraints in this study and are addressed herein. Firstly, one of the aspects that required research attention is the design of protein tagging to FIP-fve. As mentioned in Chapter 3, GFP was included in the C-terminal of FIP-fve and mutants as GFP allows visualization of fluorescent GFP-tagged target protein during protein expression and purification. Due to lacking of automated chromatography system, size exclusion chromatography was conducted manually without the use of automated chromatography system, in such manner information such as chromatogram was not available for protein peak detection. GFP tag has became particularly necessary to be utilised as a reporter fluorescent protein for collection of the GFP-tagged recombinant proteins during manual size-exclusion chromatography. Additionally, the study required expression and purification of eight different recombinant proteins, making purification work tedious and therefore there is a need to process the purification procedure more efficiently. Size exclusion chromatography applied in this study allowed the purification procedure to be processed more effectively than dialysis. Although it appeared that the inclusion of GFP at the C-terminal of FIP-fve did not cause undesired consequences to the protein of interest based on the functional activities result, expression of recombinant proteins without GFP tag at C-terminal could be performed in future study with the involvement of automated purification system to ensure as minimal protein interference as possible. While the GFP tag did not seem to interfere the functional activities of rFIP-fve and mutants, the fusion protein H-CWT6-Ek-GFP appeared to cause conformational heterogeneity during crystallization process, and resulted in difficulty in protein crystallization (Chapter 7). Cleaved protein H-CWT6 with removal of GFP was shown to favour protein crystallization rather than fusion protein H-CWT6-Ek GFP, hence it appeared necessary to use H-CWT-6 without GFP tag as a protein candidate for future

crystallography study. Having said that, the fluorescent characteristics of GFP protein can be utilised to identify and localize interaction of the target protein fused to GFP at cellular level in protein localization experiment. GFP enables *in situ* monitoring of protein localization and visualization of dynamic cellular events. This is especially important in the research of FIP-fve as it has been shown to interact with the cell surface receptor of human peripheral mononuclear cells (Liu *et al.*, 2012), thus localization of FIP-fve with GFP tag could contribute knowledge on its mechanism of action in relation to its immunomodulatory and ant-cancer activities. In fact, the current research has shown the feasibility of using recombinant fusion protein of rFIP-fve with GFP tag in stimulating effective immunomodulatory response in mice splenocytes as well as inducing cell-viability inhibiting activity in cancer cells. Nonetheless, this protein localization experimental plan was unable to be carried out in this research because of time constraint. In this respect, both of the concerns discussed above may be addressed in the future study.

Secondly, optimization on protein production could be regarded as another aspect to be improved in future. Instead of optimizing the generation of protein in a comprehensive manner, the optimization of protein synthesis was performed by varying only two parameters - cultivation temperature and duration in a general manner. In the interest of achieving the ultimate goal, the current research focused on determining the functional activities of recombinant FIP-fve and mutant proteins rather than achieving the highest yield possible. Hence, parameters such as expression system, vectors choice, inducer concentration, codon optimization, cultivation temperature and cultivation duration could be modified to obtain the optimal recombinant protein yield for extended study.

Lastly, immunomodulatory analysis is an additional aspect to be considered for further refinement (Chapter 5). The concentration of recombinant FIP-fve and mutant proteins (10 µg/ml) and duration of splenocyte stimulation (48 hr) used in the experiment were designated based on the previous literatures (Wu *et al.*, 2008; Wu *et al.*, 2013 and Lin *et al.*, 2013). The finding yielded from previous studies served as a great benchmark for the current research. For this reason, there was only one of each parameter that was included in the examination. As our principal objective was to compare the mice splenocytes immuno-stimulatory level among the recombinant mutant proteins, the determination of the peak immune response was therefore deemed unnecessary. Considering that the results shown herein may not be the optimal stimulatory level, an improvement to this experimental design may be to encompass several time points of splenocytes stimulation and different concentrations of target recombinant mutant proteins for the immune-regulating analysis. The results of which will be able to demonstrate the optimum immunomodulatory level that is achievable by the particular recombinant mutant proteins.

Conclusion

The present study represents an exploratory understanding to structural and functional relationship of FIP-fve with respect to its immunomodulatory and cancer-inhibitory abilities. This is especially important to contribute to the enigma in distinctive bioactivities discovered among the members of FIPs family. Understanding the functional-structural association of FIPs could unleash immense benefits to the field of immunotherapy as well as allergy treatment. It is of no doubt that modified FIP-fve protein with reinforced N-terminal dimerization or derivative FIP-fve proteins with adoption of a certain loop region from LZ-8 confer significant enhancement of *in vitro* immunomodulation and *in vitro* cancer-inhibition capabilities. With reference to these, several important findings in the mutagenesis study of FIP-fve are recapitulated herein: (i) reinforcement of N-terminal dimerization has shown possibility to improve its immunomodulatory and lung cancer cells A549-inhibitory activities, presumably via increasing protein stability that leads to prolong protein half-life; (ii) N-terminal methionine should be excluded in construction of recombinant FIP-fve protein as mutant with additional methionine has failed to enhance its bioactivities and deteriorated the functional activities at some instances; (iii) adoption of loop DE and hinge residue E61K (LZ-8) are mainly responsible in enhancing its immune-regulating capability as well as in exerting peak cell viability inhibiting activity in breast cancer cells MDA-MB-231; (iv) adoption of loop DE (LZ-8) could abolish haemagglutination ability on human red blood cells; and (v) adoptions of loop FG and hinge residue I97D (LZ-8) play a critical role in strengthening its cancer-inhibiting capabilities in breast cancer cells MCF-7 and lung cancer cells A549. The research lays a groundwork and serves as a crucial step in paving way for other FIPs towards advancing into immuno-therapeutic candidate in future. To conclude, this research is practicable and displayed potential in directing FIP-fve to

achieve a prominent impact in the field of cancer-immunotherapy with further knowledge on its structural-functional relationship.

References

Abbas, A. K., Lichtman, A. H. and Pillai, S. (2015) *Cellular and Molecular Immunology,* 8th edn. Canada: Saunder.

Adamová, L., Malinovská, L. and Wimmerová, M. (2014) 'New sensitive detection method for lectin hemagglutination using microscopy', *Microscopy Research and Technique*, 77(10), pp. 841–849.

Alshaker, H. A. and Matalka, K. Z. (2011) 'IFN-gamma, IL-17 and TGF-beta involvement in shaping the tumor microenvironment: The significance of modulating such cytokines in treating malignant solid tumors', *Cancer Cell International*, 11, pp. 1–12.

American Cancer Society (2018) *Cancer facts and figures 2018*. Atlanta: American Cancer Society.

American Cancer Society (2015) *Global cancer facts & figures.* 3rd Edition. Atlanta: American Cancer Society.

Andersson, J., Grönvik, K. O., Larsson, E. L. and Coutinho, A. (1979) 'Studies on T lymphocyte activation. I. Requirements for the mitogen-dependent production of T cell growth factors.', *European journal of immunology*, 9(8), pp. 581–587.

Andrew, S. M., Titus, J. A. and Zumstein, L. (2001) 'Dialysis and concentration of protein solutions', *Current protocols in immunology*, Appendix 3, pp. 1–5.

Ascierto, P. A., Brugarolas, J., Buonaguro, L., Butterfield, L. H., Carbone, D., Daniele, B e*t al*. (2018) 'Perspectives in immunotherapy: Meeting report from the Immunotherapy Bridge (29-30 November, 2017, Naples, Italy)', *Journal for ImmunoTherapy of Cancer*. Journal for ImmunoTherapy of Cancer, 6(69), pp. 1–14.

Bachmann, B. J.. (1990) 'Linkage map of *Escherichia coli* K-12, Edition 8.', *Microbiological Reviews*, 54(2), pp. 130–197.

Baeshen, N., Baeshen, M. N., Sheikh, A., Bora, R. S., Ahmed, M. M., Ramadan, H. A., Saini, K. S. *et al.* (2014) 'Cell factories for insulin production.', *Microbial cell factories*, 13, pp. 1-9.

Bai, J. Y., Li, Y. F., Liu, Y. and Lin, Z. P. (2005). *Isolation and sequence analysis of immunomodulatory protein gene from Ganoderma japonicum* [online]. Available at: UniProtKB - Q52PH4 (Q52PH4_9APHY)

Baneyx, F. and Mujacic, M. (2004) 'Recombinant protein folding and misfolding in *Escherichia coli*', *Nature Biotechnology*, 22(11), pp. 1399–1407.

Bardelli, A. and Jänne, P. A. (2012) 'The road to resistance: EGFR mutation and cetuximab', *Nature Medicine*. Nature Publishing Group, 18(2), pp. 199–200.

Barrett, N. A. and Austen, K. F. (2009) 'Innate immunity in T_H2-type airway inflammation', *NIH Public Access*, 31(3), pp. 425–437.

Bastiaan-Net, S., Chanput, W., Hertz, A., Zwittink, R. D., Mes, J. J. and Wichers, H. J. (2013) 'Biochemical and functional characterization of recombinant fungal immunomodulatory proteins (rFIPs)', *International immunopharmacology*, 15, pp. 167–175.

Becker, R. H. A. (2007) 'Insulin glulisine complementing basal insulins: A review of structure and activity', *Diabetes Technology & Therapeutics*, 9(1), pp. 109–121.

Bennett, M. J., Schlunegger, M. P. and Eisenberg, D. (1995) '3D domain swapping: A mechanism for oligomer assembly', *Protein Science*, 4(12), pp. 2455–2468.

Bergdoll, M., Remy, M. H., Cagnon, C., Masson, J. M. and Dumas, P. (1997) 'Proline-dependent oligomerization with arm exchange.', *Structure*, 5(3), pp. 391–401.

Berlec, A. and Štrukelj, B. (2013) 'Current state and recent advances in biopharmaceutical production in *Escherichia coli*, yeasts and mammalian cells', *Journal of Industrial Microbiology and Biotechnology*, 40(3–4), pp. 257–274.

Bio-Rad Laboratories (2014) *Biotechnology explorer™ pGLO ™ bacterial transformation kit* [Online]. Available at: http://www.bio-rad.com/webroot/web/pdf/lse/literature/1660033.pdf

Boraston, A. B., Bolam, D. N., Gilbert, H. J. and Davies, G. J. (2004) 'Carbohydrate-binding modules: fine-tuning polysaccharide recognition', *Biochem. J*, 382(Pt 3), pp. 769–781.

Bornhorst, J. and Falke, J. (2000) 'Purification of proteins using polyhistidine affinity tags', *Methods Enzymol.*, 326, pp. 245–254.

Bosnjak, B., Stelzmueller, B., Erb, K. J. and Epstein, M. M. (2011) 'Treatment of allergic asthma: Modulation of Th2 cells and their responses', *Respiratory Research*., 12(114), pp. 1-12.

Brenton, J. D., Carey, L. A., Ahmed, A. A. and Caldas, C. (2005) 'Molecular classification and molecular forecasting of breast cancer: ready for clinical application?', *Journal of Clinical Oncology*, 23(29), pp. 7350–7360.

Bruno, B. J., Miller, G. D. and Lim, C. S. (2013) 'Basics and recent advances in peptide and protein drug delivery', *Therapeutic delivery*, 4(11), pp. 1443–1467.

Bucher, M. H., Evdokimov, A. G. and Waugh, D. S. (2002) 'Differential effects of short affinity tags on the crystallization of *Pyrococcus furiosus* maltodextrin-binding protein', *Acta Crystallographica Section D: Biological Crystallography*, 58(Pt 3), pp. 392–397.

Cailleau, R., Olivé, M. and Cruciger, Q. V. (1978) 'Long-term human breast carcinoma cell lines of metastatic origin: preliminary characterization.', *In vitro*, 14(11), pp. 911–5.

Calero, G., Cohen, A. E., Luft, J. R., Newman, J. and Snell, E. H. (2014) 'Identifying, studying and making good use of macromolecular crystals', *Acta Crystallographica Section F:Structural Biology Communications*, 70(8), pp. 993–1008.

Cancer Care. (2018) *Non-small cell lung cancer treatment* [online]. Available at: https://www.lungcancer.org/find_information/publications/163-lung_cancer_101/269-non-small_cell_lung_cancer_treatment.

Chalfie, M., Tu, Y., Euskirchen, G., Ward, W. W. and Prasher, D. C. (1994) 'Green fluorescent protein as a marker gene expression.', *Science*, 263, pp. 802–806.

Chang, H. H., Hsieh, K. Y., Yeh, C. H., Tu, Y. P. and Sheu, F. (2010) 'Oral administration of an Enoki mushroom protein FVE activates innate and adaptive immunity and induces anti-tumor activity against murine hepatocellular carcinoma', *International immunopharmacology*, 10(2), pp. 239–246.

Chang, Y. C., Hsiao, Y. M., Wu, M. F., Ou, C. C., Lin, Y. W., Lue, K. H. and Ko, J. L. (2013) 'Interruption of lung cancer cell migration and proliferation by fungal immunomodulatory protein FIP-fve from *Flammulina velutipes*.', *Journal of agricultural and food chemistry*, 61(49), pp. 12044–52.

Chang, Y. C., Chow, Y. H., Sun, H. L., Liu, Y. G., Lee, Y. T., Lue, K. H. and Ko, J. L. (2014) 'Alleviation of respiratory syncytial virus replication and inflammation by fungal immunomodulatory protein FIP-fve from *Flammulina velutipes*', *Antiviral Research*, 110, pp. 124–131.

Chang, Y. C., Hsiao, Y. M., Hung, S. C., Chen, Y. W., Ou, C. C., Chang, W. T., Lue, K. H. and Ko, J. L. (2015) 'Alleviation of *Dermatophagoides microceras*-induced allergy by an immunomodulatory protein, FIP-fve, from *Flammulina velutipes* in mice', *Bioscience, Biotechnology and Biochemistry*, 79(1), pp. 88–96.

Chu, P. Y., Sun, H. L., Ko, J. L., Ku, M. S., Lin, L. J., Lee, Y. T., Liao, P. F., Pan, H. H., Lu, H. L. and Lue, K. H. (2017) 'Oral fungal immunomodulatory protein-*Flammulina velutipes* has influence on pulmonary inflammatory process and potential treatment for allergic airway disease: A mouse model', *Journal of Microbiology, Immunology and Infection*, 50(3), pp. 297–306.

Chung, K. F., Wenzel, S. E., Brozel, J. L., Bush, A., Castro, M., Sterk, P. J. *et al*. (2014) 'International ERS/ATS guidelines on definition, evaluation and treatment of severe asthma', *European Respiratory Journal*, 43(2), pp. 343–373.

Cline, J., Braman, J. C. and Hogrefe, H. H. (1996) 'PCR fidelity of pfu DNA polymerase and other thermostable DNA polymerases', *Nucleic Acids Research*, 24(18), pp. 3546–3551.

Cooper, M. A., Fehniger, T. A., Fuchs, A., Colonna, M. and Caligiuri, M. A. (2004) 'NK cell and DC interactions', *Trends in Immunology*, 25(1), pp. 47–52.

Costa, S., Almeida, A., Castro, A. and Domingues, L. (2014) 'Fusion tags for protein solubility, purification, and immunogenicity in *Escherichia coli*: The novel Fh8 system', *Frontiers in Microbiology*, 5(63), pp. 1–20.

Cota, E. and Clarke, J. (2000) 'Folding of beta-sandwich proteins: Three-state transition of a fibronectin type III module', *Protein Science*, 9(1), pp. 112–120.

Countiho, A., Moller, G., Anderson, J and Bullock, W. W. (1973) '*In vtiro* activation of mouse lymphocytes in serum-free medium: effect of T and B cell mitogens on proliferation and antibody synthesis', *Eur. J. Immunol.*, 3(5), pp. 299–306.

Crowe, J., Döbeli, H., Gentz, R., Hochuli, E., Stüber, D. and Henco, K. (1994) '6xHis-Ni-NTA chromatography as a superior technique in recombinant protein expression/purification', *Methods Molecular Biology*, 31(37), pp. 371–388.

Cudney, R., Patel, S., Weisgraber, K., Newhouse, Y. and McPherson A. (1994) 'Screening and optimization strategies for macromolecular crystal growth', *Acta Crystallographica Section D Biological Crystallography*, 50, pp. 414–423.

Dale, G. E., Oefner, C. and D'Arcy, A. (2003) 'The protein as a variable in protein crystallization', *Journal of Structural Biology*, 142(1), pp. 88–97.

Ding, Y., Seow, S. V., Huang, C. H., Liew, L. M., Lim, Y. C., Kuo, I. C. and Chua, K. Y. (2009) 'Coadministration of the fungal immunomodulatory protein FIP-Fve and a tumour-associated antigen enhanced antitumour immunity', *Immunology*, 128(1 Suppl), pp. e881-894.

Dong, H., Nilsson, L. and Kurland, C. G. (1995) 'Gratuitous overexpression of genes in *Escherichia coli* leads to growth inhibition and ribosome destruction', *Journal of Bacteriology*, 177(6), pp. 1497–1504.

Englesberg, E. (1961) 'Enzymatic characterization of 17 L-arabinose negative mutants of *Escherichia coli*.', *Journal of bacteriology*, 81, pp. 996–1006.

Evan, G. I. and Vousden, K. H. (2001) 'Proliferation, cell cycle and apoptosis in cancer', *Nature*, 411(6835), pp. 342–348.

Flinta, C., Persson, B., Jörnvall, H. and Heijne, G. V. (1986) 'Sequence determinants of cytosolic N-terminal protein processing', *European Journal of Biochemistry*, 154(1), pp. 193–196.

Friedl, P. and Wolf, K. (2003) 'Tumour-cell invasion and migration: Diversity and escape mechanisms', *Nature Reviews Cancer*, 3(5), pp. 362–374.

GE Healthcare. (2010) *Strategies for protein purification handbook* [online]. Available at: https://www.sigmaaldrich.com/content/dam/sigma-aldrich/docs/Sigma-Aldrich/General_Information/1/ge-strategies-for-protein-purification.pdf

Genentech. (1978) *First successful laboratory production of human insulin announced* [Online]. Available at: http://www.gene.com/media/press-releases/4160/1978-09-06/first-successful-laboratory-production-o.

Gest, C., Joimel, U., Huang, L., Pritchard, L. L., Petit, A., Dulong, C., Buquet, C. *et al*. (2013) 'Rac3 induces a molecular pathway triggering breast cancer cell aggressiveness: Differences in MDA-MB-231 and MCF-7 breast cancer cell lines', *BMC Cancer*, 13(63).

Structural Genomics Consortium. (2008) 'Protein production and purification', *Nature methods*, 5(2), pp. 135–146.

Gross, J. and Englesberg, E. (1959) 'Determination of the order of mutational sites governing L-arabinose utilization in *Escherichia coli*Br by transduction with phage Plbt', *Virology*, 9(3), pp. 314–331.

Gunaydin, H., Altman, M. D., Ellis, M., Fuller, P., Johnson, S. A., Lahue, B. and Lapointe, B. (2018) 'Strategy for extending half-life in drug design and its significance', *ACS Medicinal Chemistry Letters*, 9(6), pp. 528–533.

Guzman, L. M., Belin, D., Carson, M. J. and Beckwith, J. (1995) 'Tight regulation, modulation, and high-level expression by vectors containing the arabinose p(BAD) promoter', *Journal of Bacteriology*, 177(14), pp. 4121–4130.

Haak-Frendscho, M., Kino, K., Sone, T. and Jardieu, P. (1993) 'Ling Zhi-8: A novel T cell mitogen induces cytokine production and upregulation of ICAM-1 expression', *Cellular Immunology*, 150(1), pp. 101–113.

Habu, S. and Raff, M. C. (1977) 'Accessory cell dependence of lectin-induced proliferation of mouse T lymphocytes', *European Journal of Immunology*, 7(7), pp. 451–457.

Hampton Research (2016) *Salt or Protein Crystals ?* [Online]. Available at: https://hamptonresearch.com/documents/product/hr007641_cg101_salt_or_protein_crystals.pdf

Hellman, L. and Fried, M. (2007) 'Electrophoretic mobility shift assay (EMSA) for detecting protein-nucleic acid interactions', *Nature protocols*, 2(8), pp. 1849–1861.

Hosfield, T. and Lu, Q. (1999) 'Influence of the amino acid residue downstream of (Asp)4Lys on enterokinase cleavage of a fusion protein', *Analytical Biochemistry*, 269(1), pp. 10–16..

Howey, D. C., Bowsher, R. R., Brunelle, R. L. and Woodworth, J. R. (1994) '[Lys(B28), Pro(B29)]-human insulin: A rapidly absorbed analogue of human insulin', *Diabetes*, 43(3), pp. 396–402.

Hsieh, K. Y., Hsu, C. L., Lin, J. Y., Tsai, C. C. and Lin, R. H. (2003) 'Oral administration of an edible-mushroom-derived protein inhibits the development of food-allergic reactions in mice', *Clinical Experimental Allergy*, 33(11), pp. 1595–1602.

Hsin, I. L., Ou, C. C., Wu, T. C., Jan, M. S., Wu, M., F., Chiu, L. Y., Lue, K. H. and Ko, J. L. (2003) 'GMI, an immunomodulatory protein from *Ganoderma microsporum*, induces autophagy in non-small cell lung cancer cells', *Autophagy*, 7(8), pp. 873–882.

Hsu, H., Hsu, C. L., Lin, R. H., Kao, C. L. and Lin, J. Y. (1997) 'Fip-vvo, a new fungal immunomodulatory protein isolated from *Volvariella volvacea*', *Biochemical Journal*, 323(Pt 2), pp. 557–565.

Huang, L., Sun, F., Liang, C., He, Y. X., Bao, R., Liu, L and Zhou, C. Z. (2009) 'Crystal structure of LZ-8 from the medicinal fungus *Ganoderma lucidium*', *Proteins*, 75(2), pp. 524–527.

Jiang, T., Zhou, C. and Ren, S. (2016) 'Role of IL-2 in cancer immunotherapy', *Oncoimmunology*, 5(6), pp. 1–10.

Kessel, A. and Ben-Tal, N. (2018) *Introduction To Proteins: Structure, Function, And Motion*. 2nd edn. Boca Raton: Chapman & Hall/CRC.

Kimple, M. E., Brill, A. L. and Pasker, R. L. (2013) 'Overview of affinity tags for protein purification', *Current Protocols in Protein Science*, (73), pp. 608–616.

Kindt, T. J., Goldsby, R. A. and Osborne, B. A. (2007) *Kuby Immunology*. 6th edn. New York: W. H. Freeman.

Kino, K., Yamashita, A., Yamaoka, K., Watanabe, J., Tanaka S., Ko, K., Shimizu, K. and Tsunoo, H. (1989) 'Isolation and characterization of a new immunomodulatory protein, from *Ganoderma lucidium*', *The Journal of Biological Chemistry*, 264(1), pp. 472–478.

Ko, J. L., Hsu, C. L., Lin, R. H., Kao, C. L and Lin, J. Y. (1995) 'A new fungal immunomodulatory protein, FIP-fve isolated from the edible mushroom, *Flammulina velutipes* and its complete amino acid sequence', *European Journal of Biochemistry*, 228(2), pp. 244–249.

Ko, K. L., Lin, S. J., Hsu, C. L., Kao, C. L. and Lin J. Y. (1997) 'Molecular cloning and expression of a fungal immunomodulatory protein, FIP-fve from *Flammulina velutipes*', *J Formos Med Assoc*, 96(7), pp. 517–524.

Kobe, B., Center, R. J., Kemp, B. E. and Poumbourios, P. (1999) 'Crystal structure of human T cell leukemia virus type 1 gp21 ectodomain crystallized as a maltose-binding protein chimera reveals structural evolution of retroviral transmembrane proteins', *Proc Natl Acad Sci U S A*, 96(8), pp. 4319–4324.

Kolodrubetz, D. and Schleif, R. (1981) 'Regulation of the L-Arabinose transport operon in *Escherichia coli*', *J. Mol. Biol.*, 151(2), pp. 215–227.

Kong, X., Zhang, J., Han, X., Zhang, P., Dai, X., Liu, J., Zhang, X., Lee, I and Liu, S. (2013) 'High-yield production in *Escherichia coli* of fungal immunomodulatory protein isolated from *Flammulina velutipes* and its bioactivity assay *in vivo*', *International Journal of Molecular Sciences*, 14(2), pp. 2230–2241.

Kuge, M., Fujii, Y., Shimizu, T., Hirose, F., Matsukage, A. and Hakoshima, T. (1997) 'Use of a fusion protein to obtain crystals suitable for X-ray analysis: Crystallization of a GST-fused protein containing the DNA-binding domain of DNA replication-related element-binding factor, DREF', *Protein Science*, 6(8), pp. 1783–1786.

Kurlander, R. J., Ellison, D. M. and Hall, J. (1984) 'The blockade of Fc receptor-mediated clearance of immune complexes *in vivo* by a monoclonal antibody (2.4G2) directed against Fc receptors on murine leukocytes', *The Journal of Immunology*, 133(2), pp. 855–862.

Lagassé, H. A. D., Alexak, A., Simhadri, V. L., Katagiri, N. H., Jankowski, W., Sauna, Z. E. and Kimchi-Sarfaty, C. (2017) 'Recent advances in (therapeutic protein) drug development', *F1000Research*, 6(113).

Lee, Y. T., Lee, S. S., Sun, H. L., Lu, K. H., Ku, M. S., Sheu, J. N., Ko, J. L. and Lue, K. H. (2013) 'Effect of the fungal immunomodulatory protein FIP-fve on airway inflammation and cytokine production in mouse asthma model', *Cytokine*, 61(1), pp. 237–244.

Lee, Y., Wu, C. T., Sun, H. L., Ko, J. L. and Lue, K. H. (2017) 'Fungal immunomodulatory protein-fve could modulate airway remodel through by affect IL-17 cytokine', *Journal of Microbiology, Immunology and Infection*, 51(5), pp. 598–607.

Li, F., Wen, H., Liu, X., Zhou, F. and Chen, G. (2012) 'Gene cloning and recombinant expression of a novel fungal immunomodulatory protein from *Trametes versicolor*', *Protein Expression and Purification*, 82(2), pp. 339–344.

Li, Q. Z., Wang, X. F. and Zhou, X. W. (2011) 'Recent status and prospects of the fungal immunomodulatory protein family', *Critical Reviews in Biotechnology*, 31(4), pp. 365–375.

Li, R, Manna, A. C., Dai, S. D., Cheung, A. L. and Zhang, G. Y. (2003) 'Crystal structure of the SarS protein from *Staphylococcus aureus*', *Journal of Bacteriology*, 185(14), pp. 4219–4225.

Li, S., Nie, Y., Ding, Y., Shi, L. and Tang, X. (2014) 'Recombinant expression of a novel fungal immunomodulatory protein with human tumor cell antiproliferative activity from *Nectria haematococca*', *International Journal of Molecular Sciences*, 15(10), pp. 17751–17764.

Li, S., Zhao, L., Xu, W., Jiang, Z., Kang, J., Wang, F. and Xin, F. (2016) 'Identification and characterisation of a novel protein FIP-sch3 from *Stachybotrys chartarum*', *PLoS ONE*, 11(12), pp. 1–17.

Li, S., Jiang, Z., Sun, L., Liu, X., Huang, Y., Wang F. and Xin, F. (2017) 'Characterization of a new fungal immunomodulatory protein, FIP-dsq2 from *Dichomitus squalens*', *Journal of Biotechnology*, 246, pp. 45–51.

Li, S. Y., Shi, L. J., Ding, Y., Nie, Y. and Tang X. M. (2015) 'Identification and functional characterization of a novel fungal immunomodulatory protein from *Postia placenta*', *Food and Chemical Toxicology*, 78, pp. 64–70.

Lin, J. (2011). *Molecular cloning of a fungal immunomodulatory gene, FIP-gap from Ganoderma applanatum* [online]. Available at: UniProtKB - G5CJT8 (G5CJT8_9APHY)

Lin, J. W, Jia, J., Shen, Y. H., Zhong, M., Chen, L. J., Li, H. G. *et al.* (2013) 'Functional expression of FIP-fve, a fungal immunomodulatory protein from the edible mushroom *Flammulina velutipes* in *Pichia pastoris* GS115', *Journal of biotechnology*, 168(4), pp. 527–533.

Lin, J. Y. and Chou, T. B. (1984) 'Isolation and characterization of a lectin from edible mushroom, *Volvariella vovacea*', *J. Biochem.*, 96(1), pp. 35–40.

Lin, J. W., Guan, S. Y., Duan, Z. W., Shen, Y. H., Fan, W. L., Chen, L. J. and Zhang, L. (2016) 'Gene cloning of a novel fungal immunomodulatory protein from *Chroogomphis rutilus* and its expression in *Pichia pastoris*', *Journal of Chemical Technology and Biotechnology*, 91(11), pp. 2761–2768.

Lin, T. Y., Hsu, H. Y., Sun, W. H., Wu, T. H. and Tsao, S. M. (2017) 'Induction of Cbl-dependent epidermal growth factor receptor degradation in Ling Zhi-8 suppressed lung cancer', *International Journal of Cancer*, 140(11), pp. 2596–2607.

Lin, W. H, Hung, C. H., Hsu, C. L. and Lin, J. Y. (1997) 'Dimerization of the N-terminal amphipathic α-Helix domain of the fungal immunomodulatory protein from *Ganoderma tsugae* (Fip-gts) defined by a yeast two-hybrid system and site-directed mutagenesis', *Journal of Biological Chemistry*, 272(32), pp. 20044–20048.

Ling, M. M. and Robinson, B. H. (1997) 'Approaches to DNA mutagenesis: An overview', *Analytical Biochemistry*, 254(2), pp. 157–178.

Liu, H. and Naismith, J. H. (2008) 'An efficient one-step site-directed deletion, insertion, single and multiple-site plasmid mutagenesis protocol.', *BMC biotechnology*, 8(91).

Liu, Y. F., Chang, S. H., Sun, H. L., Chang, Y. C., Hsin, I. L., Lue, K. H. and Ko, J. L. (2012) 'IFN-γ induction on carbohydrate binding module of fungal immunomodulatory protein in human peripheral mononuclear cells', *Journal of agricultural and food chemistry*, 60(19), pp. 4914–4922,

Liu, Y. and Eisenberg, D. (2002) '3D domain swapping: As domains continue to swap', *Protein Science*, 11(6), pp. 1285–1299.

Martini, M., Testi, M. G., Pasetto, M., Picchio, M. C., Innamorati, G., Mazzocco, M. *et al.* (2010) 'IFN-γ-mediated upmodulation of MHC class I expression activates tumor-specific immune response in a mouse model of prostate cancer', *Vaccine*, 28(20), pp. 3548–3557.

McPherson, A. and Cudney, B. (2006) 'Searching for silver bullets: An alternative strategy for crystallizing macromolecules', *Journal of Structural Biology*, 156(3), pp. 387–406.

McPherson, A. and Gavira, J. A. (2014) 'Introduction to protein crystallization', *Acta Crystallographica Section F:Structural Biology Communications*, 70(1), pp. 2–20.

Meinnel, T., Mechulam, Y. and Blanquet, S. (1993) 'Methionine as translation start signal: A review of the enzymes of the pathway in *Escherichia coli*', *Biochimie*, 75(12), pp. 1061–1075.

Messenger, L. J. and Zalkin, H. (1979) 'Glutamine phosphoribosylpyrophosphate amidotransferase from *Escherichia coli*. Purification and properties', *Journal of Biological Chemistry*, 254(9), pp. 3382–3392.

Munoz, N., Bosch, F. X., Sanjosé, S. D., Herrero, R., Castellsagué, X, Shah, K. V. *et al.* (2003) 'Epidemiologic classification of human papillomavirus types associated with cervical cancer', *The New England Journal of Medicine*, 348, pp. 518–527.

Navarro, A., Wu, H. S. and Wang, S. S. (2009) 'Engineering problems in protein crystallization', *Separation and Purification Technology*, 68(2), pp. 129–137.

Nettleship, J. E., Assenberg, R., Diprose, J. M., Rahman-Hug, N. and Owens, R. J. (2010) 'Recent advances in the production of proteins in insect and mammalian cells for structural biology', *Journal of Structural Biology*, 172(1), pp. 55–65.

Nicholson, A., Malcolm, R. D., Russ, P. L., Cough, K., Touma, C., Palme, R. and Wiles, M. V. (2009) 'The response of C57BL/6J and BALB/cJ mice to increased housing density.', *Journal of the American Association for Laboratory Animal Science : JAALAS*, 48(6), pp. 740–753.

Noonan, K. D. and Burger, M. M. (1973) 'The relationship of concanavalin a binding to lectin-initiated cell agglutination', *Journal of Cell Biology*, 59(1), pp. 134–142.

Osherovich, L. (2011) 'Engineering Protein Stability', *Science-Business eXchange*, 4(7), pp. 1–3.

Ou, C. C., Hsiao, Y. M., Wu, W. J., Tasy, G. J., Ko, J. L. and Lin, M. Y. (2009) 'FIP-fve stimulates interferon-gamma production via modulation of calcium release and PKC-alpha activation', *Journal of agricultural and food chemistry*, 57(22), pp. 11008–13.

Owens, D. R., Coates, P. A., Luzio, S. D., Tinbergen, J. P. and Kurzhals, R. (2000) 'Pharmacokinetics of 125 I-labeled insulin glargine (HOE 901) in healthy men: comparison with NPH insulin and the influence of different subcutaneous injection sites', *Diabetes Care*, 23(6), pp. 813–819.

Paaventhan, P., Joseph, J. S., Seow, S. V., Vaday, S., Robinson, H., Chua, K. Y. and Kolatkar, P. R. (2003) 'A 1.7 Å structure of Fve, a member of the new fungal immunomodulatory protein family', *Journal of Molecular Biology*, 332(2), pp. 461–470.

Pal, R., Dahal, S. and Pal, S. (2009) 'Prevalence of bronchial asthma in Indian children', *Indian Journal of Community Medicine*, 34(4), pp. 310-316

Parham, P. (2009) *The immune system*. 3rd edn. London & New York: Taylor & Francis Group.

Pasut, G., Sergi, M. and Veronese, F. M. (2008) 'Anti-cancer PEG-enzymes: 30 years old, but still a current approach', *Advanced Drug Delivery Reviews*, 60(1), pp. 69–78.

Perrot-Applanat, M. and Di Benedetto, M. (2012) 'Autocrine functions of VEGF in breast tumor cells: Adhesion, survival, migration and invasion', *Cell Adhesion and Migration*, 6(6), pp. 547–553.

Perry, C. M. and Jarvis, B. (2001) 'Peginterferon-alpha-2a (40 kD): a review of its use in the management of chronic hepatitis C', *Drugs*, 61(15), pp. 2263–2288.

Phillips, N. B., Wan, Z. L., Whittaker, L., Hu, S. Q., Huang, K., Hua, Q. X. *et al*. (2010) 'Supramolecular protein engineering: Design of zinc-stapled insulin hexamers as a long acting depot', *Journal of Biological Chemistry*, 285(16), pp. 11755–11759.

Podust, V. N., Balan, S., Sim, B. C., Coyle, M. P., Ernst, U. Peters, R. T. and Shellenberger, V. (2016) 'Extension of *in vivo* half-life of biologically active molecules by XTEN protein polymers', *Journal of Controlled Release*, 28(240), pp. 52–66.

Pogulis, R. J., Vallejo, A, N. and Pease, L. R. (1996) '*In vitro* recombination and mutagenesis by overlap extension PCR.', *Methods in molecular biology*, 57, pp. 167–176.

Poluri, K. M. and Gulati, K. (2017) *Protein engineering techniques: Gateways to synthetic protein universe*. Singapore: Springer.

Popp, M. W., Dougan, S. K., Chuang, T. Y., Spooner, E. and Ploegh, H. L. (2011) 'Sortase-catalyzed transformations that improve the properties of cytokines', *Proceedings of the National Academy of Sciences*, 108(8), pp. 3169–3174.

Potter, M. and Boyce, C. R. (1962) 'Induction of plasma-cell neoplasms in strain BALB/c mice with mineral oil and mineral oil adjuvants', *Nature*, 193(4820), pp. 1086–1087.

Promega Corporation (2015) *pGEM®- T and pGEM®- T Easy Vector Systems* [Online]. Available at: https://www.promega.co.uk/~/media/files/resources/protocols/technical manuals/0/pgem-t and pgem-t easy vector systems protocol.pdf.

Pushparajah, V., Fatima, A., Chong, C. H., Gambule, T. Z., Chan, C. J., Ng, S. T. *et al*. (2016) 'Characterisation of a new fungal immunomodulatory protein from tiger milk mushroom, *Lignosus rhinocerotis*', *Scientific Reports*, 6(30010), pp. 1–12.

Reed, J. M., Branigan, P. J. and Bamezai, A. (2008) 'Interferon Gamma Enhances Clonal Expansion and Survival of CD4 $^{+}$ T Cells', *Journal of Interferon & Cytokine Research*, 28(10), pp. 611–622.

Roche (2010) *Cell Proliferation ELISA , BrdU (colorimetric)* [Online]. Available at: https://cssportal.roche.com/LFR_PublicDocs/ras/11647229001_en_14.pdf.

Rosano, G. L. and Ceccarelli, E. A. (2014) 'Recombinant protein expression in *Escherichia coli*: Advances and challenges', *Frontiers in Microbiology*, 5(172), pp. 1–17.

Rosenberg, S. A. (2014) 'IL-2: the first effective immunotherapy for human cancer', *The Journal of Immunology*, 192(12), pp. 5451–5458.

Sajid, M., Ahmad, M. U., Khan, M. A., Anjum, M. A. and Mushtaq, M. H. (2012) 'Investigation of equine influenza virus in two geographical regions of Pakistan', *Tropical Animal Health and Production*, 45(2), pp. 693–694.

Sanchez-Garcia, L., Martin, L., Mangues, R., Ferrer-Miralles, N., Vázquez, E. and Villaverde, A. (2016) 'Recombinant pharmaceuticals from microbial cells: A 2015 update', *Microbial Cell Factories*, 15(33), pp. 1–7.

Sano, K. and Ogawa, H. (2014) ‘Hemagglutination (inhibition) assay’, *Methods Molecular Biology*, 1200, pp. 47–52.

Schabath, M. B. *et al.* (2014) ‘Temporal trends from 1986 to 2008 in overall survival of small cell lung cancer patients’, *Lung Cancer*, 86(1), pp. 14–21.

Schumann, W. and Ferreira, L. C. S. (2004) ‘Production of recombinant proteins in *Escherichia coli*’, *Genetics and Molecular Biology*, 27(3), pp. 442–453.

Sengupta, N., MacFie, T. S., MacDonald, T. T., Pennington, D. and Silver, A. R. (2010) ‘Cancer immunoediting and “spontaneous” tumor regression’, *Pathology Research and Practice*, 206(1), pp. 1–8.

Seow, S. V., Kuo, I. C., Paaventhan, P., Kolatkar, P. R. and Chua, K. Y. (2003) ‘Crystallization and preliminary X-ray crystallographic studies on the fungal immunomodulatory protein Fve from the golden needle mushroom (*Flammulina velutipes*)’, *Acta Crystallographica - Section D Biological Crystallography*, 59(8), pp. 1487–1489.

Shai, Y. (1995) ‘Molecular recognition between membrane-spanning polypeptides.’, *Trends Biochemical Science*, 20(11), pp. 460–464.

Sharma, N., Timmers, C., Trikha, P., Saavedra, H. I., Obery, A. and Leone, G. (2006) ‘Control of the p53-p21CIP1 Axis by E2f1, E2f2, and E2f3 is essential for G1/S progression and cellular transformation.’, *The Journal of biological chemistry*, 281(47), pp. 36124–31.

Sharma, S. V., Bell, D. W., Settleman, J. and Haber, D. A. (2007) ‘Epidermal growth factor receptor mutations in lung cancer’, *Nature Reviews Cancer*, 7(3), pp. 169–181.

Sharon, N. and Lis, H. (1989) ‘Lectins as cell recognition molecules’, *Science*, 246(4927), pp. 227–234.

Sheu, F., Chien, P. J., Chien, A. L., Chen, Y. F. and Chin, K. L. (2004) 'Isolation and characterization of an immunomodulatory protein (APP) from the Jew's Ear mushroom *Auricularia polytricha*', *Food Chemistry*, 87(4), pp. 593–600.

Shirazi, F. H., Zarghi, A., Kobarfard, F., Zendehdel, R., Nakhjavani, M. and Arfaiee, S. (2011) 'Remarks in successful cellular investigations for fighting breast cancer using novel synthetic ompounds' in Gundus, M. *Breast cancer – focusing tumor microenvironment, stem cells and metastasis* [Online]. Available at: http://www.intechopen.com/books/breast-cancer-focusingtumor-microenvironment-stem-cells-and-metastasis/remarks-in-successful-cellular-investigations-for-fightingbreast-cancer-using-novel-synthetic-compo

Simpson, K. L. and Spencer, C. M. (1999) 'Insulin aspart.', *Drugs*, 57(5), pp. discussion 766-767.

Smyth, D. R., Mrozkiewicz, M. K., McGrath, W. J., Listwan, P. and Kobe, B. (2003) 'Crystal structures of fusion proteins with large-affinity tags', *Protein Science*, 12(7), pp. 1313–1322.

Soisson, S. M., MacDougall-Shackleton, B., Schleif, R and Wolberger, C. (1997) 'Structural basis for ligand-regulated oligomerization of AraC', *Science*, 276(5311), pp. 421–425.

Soule, H. D., Vazguez, J., Long, A., Albert, S. and Brennan, M. (1973) 'A human cell line from a pleural effusion derived from a breast carcinoma', *J Natl Cancer Inst*, 51(5), pp. 1409–1416.

Stoll, V. S., Manohar, A. V., Gillon, W., MacFarlane, E. L., Hynes, R. C. and Pai, E. F. (1998) 'A thioredoxin fusion protein of VanH, a D-lactate dehydrogenase from *Enterococcus faecium*: Cloning, expression, purification, kinetic analysis, and crystallization', *Protein Science*, 7(5), pp. 1147–1155.

Swanson, K. A., Settembre, E. C., Shaw, C. A., Dey, A. K., Rappuoli, R., Mandl, C. W. *et al.* (2011) 'Structural basis for immunization with postfusion respiratory syncytial virus fusion F glycoprotein (RSV F) to elicit high neutralizing antibody titers', *Proceedings of the National Academy of Sciences*, 108(23), pp. 9619–9624.

Teh, H. S., Phillips, R. A. and Miller, R. G. (1978) 'Quantitative studies on the precursors of cytotoxic lymphocytes. IV. Specificity and cross-reactivity of cytotoxic clones', *Journal of Immunology*, 120(2), pp. 425–428.

Tong, M. H., Chien, P. J., Chang, H. H., Tsai, M. J. and Sheu, F. (2008) 'High processing tolerances of immunomodulatory proteins in Enoki and Reishi mushrooms', *Journal of Agricultural and Food Chemistry*, 56(9), pp. 3160–3166.

Turanli-Yildiz, B., Alkim, C. and Cakar, Z. P. (2012) 'Protein engineering methods and applications', *Protein Engineering*, pp. 33–58.

Tu Z. M., He, G. Y., Li, K. X., Chen, M. J., Chang, J. L, Chen, L. *et al*. (2005) 'An improved system for competent cell preparation and high efficiency plasmid transformation using different *Escherichia coli* strains', *Electronic Journal of Biotechnology*, 8(1).

Unkeless, J. C. (1979) 'Characterization of a monoclonal antibody directed against macrophage and lymphocyte', *The Journal of Experimental Medicine*, 150(3), pp. 580–596.

Vazquez-Lombardi, R., Roome, B. and Christ, D. (2013) 'Molecular engineering of therapeutic cytokines', *Antibodies*, 2(3), pp. 426–451.

Wada, T., Azegami, M., Sugiyama, M., Tsuneki, H. and Sasaoka, T. (2008) 'Characteristics of signalling properties mediated by long-acting insulin analogue glargine and detemir in target cells of insulin', *Diabetes Research and Clinical Practice*, 81(3), pp. 269–277.

Wands, J. R., Podolsky, D. K. and Isselbacher, K. J. (1976) 'Mechanism of human lymphocyte stimulation by concanavalin A: role of valence and surface binding sites.', *Proceedings of the National Academy of Sciences of the United States of America*, 73(6), pp. 2118–22.

Wang, P. H., Hsu, C. L., Tang, S. C., Huang, Y. L., Lin, J. Y. and Ko, J. L. (2004) 'Fungal immunomodulatory protein from *Flammulina velutipes* induces interferon-γ production through p38 mitogen-activated protein kinase signaling pathway', *Journal of Agricultural and Food Chemistry*, 52(9), pp. 2721–2725.

Wang, S. M., Ooi, L. L., and Hui, K. M. (2007) 'Identification and validation of a novel gene signature associated with the recurrence of human hepatocellular carcinoma', *Clinical Cancer Research*, 13(21), pp. 6275–6283.

Watanabe, T., Miura, T., Degawa, Y., Fujita, Y., Inoue, M., Kawaguchi, M. and Furihata, C. (2010) 'Comparison of lung cancer cell lines representing four histopathological subtypes with gene expression profiling using quantitative real-time PCR', *Cancer Cell Int*, 10(2), pp. 1–12

Watanabe, T., Fathman, C. G. and Coutinho, A. (1977) 'Clonal growth of T cells *in vitro*: preliminary attempts to a quantitative approach', *Immunological Reviews*, 35, pp. 3–37.

Wermerskirchen, A. S., LaTocha, D. H. and Clarke, B. L. (2000) 'Adrenocorticotropic hormone controls Concanavalin A activation of rat lymphocytes by modulating IL-2 production', *Life Sciences*, 67(18), pp. 2177–2187.

Whitford, D. (2005) *Proteins structure and function*. England: John Wiley & Sons Ltd.

Wilcox, G., Meuris, P., Bass, R. and Englesberg, E. (1974) 'Regulation of the L-arabinose operon BAD *in vitro*.', *The Journal of biological chemistry*, 249(9), pp. 2946–2952.

Wood, P. (2006) *Unverstanding Immunology*. 2nd edn. England: Pearson Education Ltd.

Wu, C. T., Lin, T. Y., Hsu, H. Y., Sheu, F., Ho, C. M. and Chen, E. (2011) 'Ling Zhi-8 mediates p53-dependent growth arrest of lung cancer cells proliferation via the ribosomal protein S7-MDM2-p53 pathway.', *Carcinogenesis*, 32(12), pp. 1890–6.

Wu, C. M., Wu, T. Y., Kao, S. S., Ko, J. L. and Jinn, T. R. (2008) 'Expression and purification of a recombinant Fip-fve protein from *Flammulina velutipes* in baculovirus-infected insect cells', *Journal of Applied Microbiology*, 104(5), pp. 1354–1362.

Wu, M. Y., Hsu, M. F., Huang, C. S., Fu, H. Y., Huang, C. T. and Yang, C. S. (2007) 'A 2.0 Å Structure of GMI , a member of the fungal immunomodulatory protein family from *Ganoderma microsporum*, *Protein crystallography*, II, p. 132.

Wu, T. Y., Chen, H. A., Li, F. Y., Lin, C. T., Wu, C. W., Heish, F. C. *et al.* (2013) 'High-level expression, purification and production of the fungal immunomodulatory protein-gts in baculovirus-infected insect larva', *Applied Biochemistry and Biotechnology*, 169(3), pp. 976–989.

Zheng, L., Baumann, U. and Reymond, J. L. (2004) 'An efficient one-step site-directed and site-saturation mutagenesis protocol.', *Nucleic acids research*, 32(14). p.e115

Zhou, X. W., Xie, M., Hong, F. and Li, Q. Z. (2009) 'Genomic cloning and characterization of a FIP-gsi gene encoding a fungal immunomodulatory protein from *Ganoderma sinense* Zhao *et al*. (Aphyllophoromycetideae)', *International Journal of Medicinal Mushrooms*, 11(1), pp. 77–86.

Appendices

Appendices for Chapter 3

A3.1 Hydrophobicity index for common amino acids

Table A3.1. Hydrophobicity index for common amino acids. Hydrophobicity index is a measure of relative hydrophobicity of an amino acid. The values are normalized relative to glycine that is neutral (value: 0). Table adopted from Monera *et al.* (1995).

Amino acid residues	Hydrophobicity index (pH 7)
Very hydrophobic	
Phe	100
Ile	99
Trp	97
Leu	97
Val	76
Met	74
Hydrophobic	
Tyr	63
Cys	49
Ala	41
Neutral	
Thr	13
His	8
Gly	0
Ser	-5
Gln	-10
Hydrophilic	
Arg	-14
Lys	-23
Asn	-28
Glu	-31
Pro	-46
Asp	-55

A3.2 Nucleotide and amino acid sequences of FIP-fve cDNA

Nucleotide sequence

```
  1 ATC TCC GCC ACG TCG CTC ACC TTC CAG CTT GCC TAC TTG
 40 GTG AAG AAG ATC GAT TTC GAC TAC ACC CCC AAC TGG GGC
 79 CGT GGT ACC CCA AGC AGC TAC ATC GAC AAC CTT ACC TTC
118 CCC AAG GTT CTC ACC GAC AAA AAA TAC TCG TAC CGC GTC
157 GTG GTC AAT GGC TCT GAC CTT GGC GTC GAG TCC AAC TTC
196 GCA GTG ACA CCG TCC GGT GGG CAG ACC ATC AAC TTC CTC
235 CAG TAC AAC AAG GGG TAT GGT GTC GCG GAC ACC AAA ACG
274 ATT CAA GTT TTC GTT GTC ATT CCA GAT ACC GGC AAC TCG
313 GAG GAG TAC ATC ATC GCT GAG TGG AAG AAG ACT
```

Amino acid sequence

```
  1 MSATSLTFQL AYLVKKIDFD YTPNWGRGTP SSYIDNLTFP KVLTDKKYSY
 51 RVVVNGSDLG VESNFAVTPS GGQTINFLQY NKGYGVADTK TIQVFVVIPD
101 TGNSEEYIIA EWKKT
```

Feature

FIP-fve	:Nucleotide (1…345)	:Amino acid (1…115)

A3.3 Protocol of RNeasy Plant Mini Kit for RNA purification

A combination of 450 µl Buffer RLT and 4.5 µl of β-mercaptoethanol (Sigma, Germany) was added to the ground tissue powder. The mixture was vortexed vigorously and followed by incubation at 56˚C for 3 min in order to lyse the tissue. The lysate was transferred to a QIAshredder spin column with 2 ml collection tube, and centrifuged for 2 min at 13000 x g. In the centrifugation step, the lysate was homogenized, while cell debris was removed at the same time. The supernatant of flow-through was transferred to a new microcentrifuge tube. An amount of 0.5 volume 95% ethanol was added to the cleared lysate. The mixture was mixed immediately by pipetting and transferred to an RNeasy spin column with a 2 ml collection tube. The spin column was centrifuged for 15 s at 8,000 x g and the flow through was discarded.

During RNA isolation, an on-column DNase digestion was performed by using RNase-Free DNase Set (QIAGEN®, Germany) to eliminate genomic DNA contamination. To wash spin column membrane before proceeding to DNase digestion, 350 µl Buffer RW1 was added to RNeasy spin column and centrifuged for 15 s at 8000 x g. The flow-through was discarded. Prior to using DNase I, the stock solution was prepared by dissolving lyophilized DNase I (1500 Kunitz units) in 550 µl of RNase-free water. A combination of 10 µl DNase I stock solution (0.37 Kunitz units) and 70 µl Buffer RDD was added directly to the RNeasy spin column membrane and incubated at 25˚C for 15 min. Wash steps were performed by adding (i) 350 µl Buffer RW1 to the RNeasy spin column and centrifuged for 15 s at 8000 x g; (ii) 500 µl Buffer RPE to the RNeasy spin column and centrifuged for 15 s at 8000 x g; and (iii) 500 µl of Buffer RPE to the RNeasy spin column and centrifuged for 2 min at 8000 x g. The third washing step with longer time of centrifugation ensured that ethanol was not carried over during RNA elution, which may otherwise affect downstream reactions. The Buffer RPE was first diluted with 4 volumes of 95% ethanol.

A new 1.5 ml collection tube was attached to RNeasy spin column. To elute the RNA, 50 µl RNase-free water was added directly to spin column membrane and centrifuged for 1 min at 8000 x g. The isolated RNA was kept at -20˚C for further use.

A3.4 Protocol of Gel/PCR DNA Fragments Extraction kit for PCR clean up

The reaction product was transferred to a 1.5 ml microcentrifuge tube. Five volumes of DF buffer was added to 1 volume of the reaction product and mixed by vortex. The sample mixture was transferred to a DF Column with 2 mL collection tube and centrifuged at 15000 x g for 30 s. The flow through was discarded. A combination of 600 µl of Wash Buffer and ethanol was added into the center of the DF Column, and placed at room temperature for 1 min. The DF Column was then centrifuged at 15000 x g for 30s. The flow-through was discarded. The DF Column was again centrifuged at 15000 x g for 3 min to dry the column matrix. The dried DF Column was transferred to a new 1.5 ml microcentrifuge tube. An amount of 50 µl Elution Buffer was added into the center of column matrix, and placed at room temperature for 3 min to ensure that Elution Buffer was absorbed thoroughly. The DF Column was then centrifuged at 15000 x g for 2 min in order to elute the purified DNA. The concentration of purified *FIP-fve* cDNA was determined and sent for DNA sequencing service using forward primer FIPfve-FP and reverse primer FIPfve-RP.

A3.5 Protocol of calcium chloride competent cells preparation

TOP10 bacterial cells were streaked over LB agar surface using 4-ways streaking technique, and incubated at 37˚C for 16 hr to isolate individual clonal population from the mixed population. A single bacteria colony was randomly picked from the bacterial plate using sterile pipette tip and inoculated in 20 ml of LB media in 250 ml of erlemenyer flask. The procedure was conducted within sterile field created by Bunsen burner flame. The flask was incubated at 37˚C for 16 hr. After 16 hr of incubation, 200 µl of the bacterial culture was transferred into a new conical flask containing 20 ml of LB broth and incubated at 37˚C until the OD_{600} of the culture reached 0.4-0.5. The flask with the bacterial cells was chilled on ice for 20 min. Subsequently, the bacterial cells were centrifuged at 4500 x g for 5 min at 4˚C. The supernatant was decanted. The cell pellet was resuspended in 2 ml of 50 mM sterile ice-cold calcium chloride (0.1 volume of initial culture volume). The resuspended cells were incubated on ice for 10 min. The cells were centrifuged at 4500 x g for 5 min at 4˚C. The supernatant was discarded. The pellet was resuspended gently in 2 ml of 50 mM sterile ice-cold calcium chloride with 15% glycerol solution. The cells were incubated on ice for 1 hr. The competent cells were distributed into single-aliquot tubes and kept at -80˚C.

A3.6 Protocol of High-Speed Plasmid Mini Kit for plasmid extraction

Cultured bacterial cells (4 ml) were harvested in 1.5 mL microcentrifuge tubes with three rounds of centrifugation at 15000 x g for 1 min. A combination of 200 µl PD1 Buffer and RNase A was added to the tube, and the pellet was resuspended by vortexing. Subsequently, 200 µl of PD2 Buffer was added to the sample mixture and mixed gently via tube inversion. To ensure the lysate is homogenous, the sample mixture was placed at room temperature for 3 min. An amount of 300 µl of PD3 Buffer was added to the sample mixture and mixed immediately via tube inversion for 10 times. The tube was centrifuged at 15000 x g for 3 min, and the supernatant was transferred to a PD Column with a 2 ml Collection Tube. The PD Column tube was centrifuged at 15000 x g for 30 s. The flow-through was discarded. A combination of 600 µl of Wash Buffer and ethanol was added into the PD Column and centrifuged at 15000 x g for 30 s. The flow-through was discarded. The PD Column was centrifuged again at 15000 x g for 3 min in order to dry the column matrix. In plasmid DNA elution step, 50 µl Elution Buffer was added into the center of PD Column matrix and placed at room temperature for 3 min to ensure that the Elution Buffer was fully absorbed. Lastly, the PD Column was centrifuged at 15000 x g for 2 min to elute the purified DNA. The extracted plasmid DNA was then subjected to DNA sequencing service by using M13/pUC forward and reverse primers to verify *FIP-fve* cDNA sequences.

A3.7 Nucleotide and amino acid sequences of rFIP-fve gene cassettes

Nucleotide sequence

```
  1 GCT AGC CAC CAT CAC CAT CAC CAT TCC GCC ACG TCG CTC
 40 ACC TTC CAG CTT GCC TAC TTG GTG AAG AAG ATC GAT TTC
 79 GAC TAC ACC CCC AAC TGG GGC CGT GGT ACC CCA AGC AGC
118 TAC ATC GAC AAC CTT ACC TTC CCC AAG GTT CTC ACC GAC
157 AAA AAA TAC TCG TAC CGC GTC GTG GTC AAT GGC TCT GAC
196 CTT GGC GTC GAG TCC AAC TTC GCA GTG ACA CCG TCC GGT
235 GGG CAG ACC ATC AAC TTC CTC CAG TAC AAC AAG GGG TAT
274 GGT GTC GCG GAC ACC AAA ACG ATT CAA GTT TTC GTT GTC
313 ATT CCA GAT ACC GGC AAC TCG GAG GAG TAC ATC ATC GCT
352 GAG TGG AAG AAG ACT GAC GAC GAC GAC AAG ATC GCT AGC
```

Amino acid sequence

```
  1 ASHHHHHHSA TSLTFQLAYL VKKIDFDYTP NWGRGTPSSY IDNLTFPKVL
 51 TDKKYSYRVV VNGSDLGVES NFAVTPSGGQ TINFLQYNKG YGVADTKTIQ
101 VFVVIPDTGN SEEYIIAEWK KTDDDDKIAS
```

Feature

NheI RE site	:Nucleotide (1…6)	:Amino acid (1…2)
Hexahistidine tag	:Nucleotide (7…24)	:Amino acid (3…8)
FIP-fve	:Nucleotide (25…366)	:Amino acid (9…122)
Enterokinase	:Nucleotide (367…384)	:Amino acid (123…128)
NheI RE site	:Nucleotide (385…390)	:Amino acid (129…130)

A3.8 Nucleotide and amino acid sequences of CWT-1 gene cassettes

Nucleotide sequence

```
  1 GCT AGC CAC CAT CAC CAT CAC CAT ATG TCC GCC ACG TCG

 40 CTC ACC TTC CAG CTT GCC TAC TTG GTG AAG AAG ATC GAT

 79 TTC GAC TAC ACC CCC AAC TGG GGC CGT GGT ACC CCA AGC

118 AGC TAC ATC GAC AAC CTT ACC TTC CCC AAG GTT CTC ACC

157 GAC AAA AAA TAC TCG TAC CGC GTC GTG GTC AAT GGC TCT

196 GAC CTT GGC GTC GAG TCC AAC TTC GCA GTG ACA CCG TCC

235 GGT GGG CAG ACC ATC AAC TTC CTC CAG TAC AAC AAG GGG

274 TAT GGT GTC GCG GAC ACC AAA ACG ATT CAA GTT TTC GTT

313 GTC ATT CCA GAT ACC GGC AAC TCG GAG GAG TAC ATC ATC

352 GCT GAG TGG AAG AAG ACT GAC GAC GAC GAC AAG ATC GCT

391 AGC
```

Amino acid sequence

```
  1 ASHHHHHHMS ATSLTFQLAY LVKKIDFDYT PNWGRGTPSS YIDNLTFPKV
 51 LTDKKYSYRV VVNGSDLGVE SNFAVTPSGG QTINFLQYNK GYGVADTKTI
101 QVFVVIPDTG NSEEYIIAEW KKTDDDDKIA S
```

Annotation:
Dark green wording - inserted methionine (S1InsM)

Feature

NheI RE site	:Nucleotide (1…6)	:Amino acid (1…2)
Hexahistidine tag	:Nucleotide (7…24)	:Amino acid (3…8)
CWT-1	:Nucleotide (25…369)	:Amino acid (9…125)
Enterokinase	:Nucleotide (370…385)	:Amino acid (126…130)
NheI RE site	:Nucleotide (386…391)	:Amino acid (130…131)

A3.9 Nucleotide and amino acid sequences of CWT-2 gene cassettes

Nucleotide sequence

```
  1 GCT AGC CAC CAT CAC CAT CAC CAT TCC CTC ACG TCG CTC

 40 ACC TTC CAG CTT GCC TAC TTG GTG AAG AAG ATC GAT TTC

 79 GAC TAC ACC CCC AAC TGG GGC CGT GGT ACC CCA AGC AGC

118 TAC ATC GAC AAC CTT ACC TTC CCC AAG GTT CTC ACC GAC

157 AAA AAA TAC TCG TAC CGC GTC GTG GTC AAT GGC TCT GAC

196 CTT GGC GTC GAG TCC AAC TTC GCA GTG ACA CCG TCC GGT

235 GGG CAG ACC ATC AAC TTC CTC CAG TAC AAC AAG GGG TAT

274 GGT GTC GCG GAC ACC AAA ACG ATT CAA GTT TTC GTT GTC

313 ATT CCA GAT ACC GGC AAC TCG GAG GAG TAC ATC ATC GCT

352 GAG TGG AAG AAG ACT GAC GAC GAC GAC AAG ATC GCT AGC
```

Amino acid sequence

```
  1 ASHHHHHHSL TSLTFQLAYL VKKIDFDYTP NWGRGTPSSY IDNLTFPKVL
 51 TDKKYSYRVV VNGSDLGVES NFAVTPSGGQ TINFLQYNKG YGVADTKTIQ
101 VFVVIPDTGN SEEYIIAEWK KTDDDDKIAS
```

Annotation:
Orange wording – Substituted amino acid residue for enhanced hydrophobicity (A2L)

Feature

NheI RE site	:Nucleotide (1…6)	:Amino acid (1…2)
Hexahistidine tag	:Nucleotide (7…24)	:Amino acid (3…8)
CWT-2	:Nucleotide (25…366)	:Amino acid (9…122)
Enterokinase	:Nucleotide (367…384)	:Amino acid (123…128)
NheI RE site	:Nucleotide (385…390)	:Amino acid (129…130)

A3.10 Nucleotide and amino acid sequences of CWT-3 gene cassettes

Nucleotide sequence

```
  1 GCT AGC CAC CAT CAC CAT CAC CAT TCC GCC ACG TCG CTC

 40 ACC TTC CAG CTT GCC TAC TTG GTG AAG AAG ATC GAT TTC

 79 GAC TAC ACC CCC AAC TGG GGC CGT GGT ACC CCA AGC AGC

118 TAC ATC GAC AAC CTT ACC TTC CCC AAG GTT CTC ACC GAC

157 AAA AAA TAC TCG TAC CGC GTC GTG GTC AAT GGC TCT GAC

196 CTT GGC GTC GAG CCC AGC TAC GCA GTG GAA TCG GAC GGT

235 TCG CAG ACC ATC AAC TTC CTC CAG TAC AAC AAG GGG TAT

274 GGT GTC GCG GAC ACC AAA ACG ATT CAA GTT TTC GTT GTC

313 ATT CCA GAT ACC GGC AAC TCG GAG GAG TAC ATC ATC GCT

352 GAG TGG AAG AAG ACT GAC GAC GAC GAC AAG ATC GCT AGC
```

Amino acid sequence

```
  1 ASHHHHHHSA TSLTFQLAYL VKKIDFDYTP NWGRGTPSSY IDNLTFPKVL
 51 TDKKYSYRVV VNGSDLGVEP SYAVESDGSQ TINFLQYNKG YGVADTKTIQ
101 VFVVIPDTGN SEEYIIAEWK KTDDDDKIAS
```

Annotation:
Red wording - loop DE region (S62P, N63S, F64Y, T67E, P68S, S69D, G71S)

Feature

NheI RE site	:Nucleotide (1…6)	:Amino acid (1…2)
Hexahistidine tag	:Nucleotide (7…24)	:Amino acid (3…8)
CWT-3	:Nucleotide (25…366)	:Amino acid (9…122)
Enterokinase	:Nucleotide (367…384)	:Amino acid (123…128)
NheI RE site	:Nucleotide (385…390)	:Amino acid (129…130)

A3.11 Nucleotide and amino acid sequences of CWT-4 gene cassettes

Nucleotide sequence

```
  1 GCT AGC CAC CAT CAC CAT CAC CAT TCC GCC ACG TCG CTC

 40 ACC TTC CAG CTT GCC TAC TTG GTG AAG AAG ATC GAT TTC

 79 GAC TAC ACC CCC AAC TGG GGC CGT GGT ACC CCA AGC AGC

118 TAC ATC GAC AAC CTT ACC TTC CCC AAG GTT CTC ACC GAC

157 AAA AAA TAC TCG TAC CGC GTC GTG GTC AAT GGC TCT GAC

196 CTT GGC GTC GAG TCC AAC TTC GCA GTG ACA CCG TCC GGT

235 GGG CAG ACC ATC AAC TTC CTC CAG TAC AAC AAG GGG TAT

274 GGT GTC GCG GAC ACC AAA ACG ATT CAA GTT TTC GTT GTC

313 ATT CCA GAT ACC AAC AAC DEL DEL GAC TTC ATC ATC GCT

352 GAG TGG AAG AAG ACT GAC GAC GAC GAC AAG ATC GCT AGC
```

Amino acid sequence

```
  1 ASHHHHHHSA TSLTFQLAYL VKKIDFDYTP NWGRGTPSSY IDNLTFPKVL

 51 TDKKYSYRVV VNGSDLGVES NFAVTPSGGQ TINFLQYNKG YGVADTKTIQ

101 VFVVIPDTNN DFIIAEWKKT DDDDKIAS
```

Annotation:
Dark blue wording - loop FG region (G101N, S103Del, E104Del, E105D, Y106F)

Feature

NheI RE site	:Nucleotide (1…6)	:Amino acid (1…2)
Hexahistidine tag	:Nucleotide (7…24)	:Amino acid (3…8)
CWT-4	:Nucleotide (25…360)	:Amino acid (9…120)
Enterokinase	:Nucleotide (361…378)	:Amino acid (121…126)
NheI RE site	:Nucleotide (379…384)	:Amino acid (127…128)

A3.12 Nucleotide and amino acid sequences of CWT-5 gene cassettes

Nucleotide sequence

```
  1 GCT AGC CAC CAT CAC CAT CAC CAT TCC GCC ACG TCG CTC

 40 ACC TTC CAG CTT GCC TAC TTG GTG AAG AAG ATC GAT TTC

 79 GAC TAC ACC CCC AAC TGG GGC CGT GGT ACC CCA AGC AGC

118 TAC ATC GAC AAC CTT ACC TTC CCC AAG GTT CTC ACC GAC

157 AAA AAA TAC TCG TAC CGC GTC GTG GTC AAT GGC TCT GAC

196 CTT GGC GTC GAG CCC AGC TAC GCA GTG GAA TCG GAC GGT

235 TCG CAG ACC ATC AAC TTC CTC CAG TAC AAC AAG GGG TAT

274 GGT GTC GCG GAC ACC AAA ACG ATT CAA GTT TTC GTT GTC

313 ATT CCA GAT ACC AAC AAC DEL DEL GAC TTC ATC ATC GCT

352 GAG TGG AAG AAG ACT GAC GAC GAC GAC AAG ATC GCT AGC
```

Amino acid sequence

```
  1 ASHHHHHHSA TSLTFQLAYL VKKIDFDYTP NWGRGTPSSY IDNLTFPKVL

 51 TDKKYSYRVV VNGSDLGVEP SYAVESDGSQ TINFLQYNKG YGVADTKTIQ

101 VFVVIPDTNN DFIIAEWKKT DDDDKIAS
```

Annotation:
Red wording - loop DE region (S62P, N63S, F64Y, T67E, P68S, S69D, G71S)
Dark blue wording - loop FG region (G101N, S103Del, E104Del, E105D, Y106F)

Feature

NheI RE site	:Nucleotide (1…6)	:Amino acid (1…2)
Hexahistidine tag	:Nucleotide (7…24)	:Amino acid (3…8)
CWT-5	:Nucleotide (25…360)	:Amino acid (9…120)
Enterokinase	:Nucleotide (361…378)	:Amino acid (121…126)
NheI RE site	:Nucleotide (379…384)	:Amino acid (127…128)

A3.13 Nucleotide and amino acid sequences of CWT-6 gene cassettes

Nucleotide sequence

```
  1 GCT AGC CAC CAT CAC CAT CAC CAT TCC GCC ACG TCG CTC

 40 ACC TTC CAG CTT GCC TAC TTG GTG AAG AAG ATC GAT TTC

 79 GAC TAC ACC CCC AAC TGG GGC CGT GGT ACC CCA AGC AGC

118 TAC ATC GAC AAC CTT ACC TTC CCC AAG GTT CTC ACC GAC

157 AAA AAA TAC TCG TAC CGC GTC GTG GTC AAT GGC TCT GAC

196 CTT GGC GTC AAG CCC AGC TAC GCA GTG GAA TCG GAC GGT

235 TCG CAG ACC ATC AAC TTC CTC CAG TAC AAC AAG GGG TAT

274 GGT GTC GCG GAC ACC AAA ACG ATT CAA GTT TTC GTT GTC

313 ATT CCA GAT ACC GGC AAC TCG GAG GAG TAC ATC ATC GCT

352 GAG TGG AAG AAG ACT GAC GAC GAC GAC AAG ATC GCT AGC
```

Amino acid sequence

```
  1 ASHHHHHHSA TSLTFQLAYL VKKIDFDYTP NWGRGTPSSY IDNLTFPKVL

 51 TDKKYSYRVV VNGSDLGVKP SYAVESDGSQ TINFLQYNKG YGVADTKTIQ

101 VFVVIPDTGN SEEYIIAEWK KTDDDDKIAS
```

Annotation:
Yellow wording - putative hinge residue for loop DE (E61K)
Red wording - loop DE region (S62P, N63S, F64Y, T67E, P68S, S69D, G71S)

Feature

NheI RE site	:Nucleotide (1…6)	:Amino acid (1…2)
Hexahistidine tag	:Nucleotide (7…24)	:Amino acid (3…8)
CWT-6	:Nucleotide (25…366)	:Amino acid (9…122)
Enterokinase	:Nucleotide (367…384)	:Amino acid (123…128)
NheI RE site	:Nucleotide (385…390)	:Amino acid (129…130)

A3.14 Nucleotide and amino acid sequences of CWT-7 gene cassettes

Nucleotide sequence

```
  1 GCT AGC CAC CAT CAC CAT CAC CAT TCC GCC ACG TCG CTC

 40 ACC TTC CAG CTT GCC TAC TTG GTG AAG AAG ATC GAT TTC

 79 GAC TAC ACC CCC AAC TGG GGC CGT GGT ACC CCA AGC AGC

118 TAC ATC GAC AAC CTT ACC TTC CCC AAG GTT CTC ACC GAC

157 AAA AAA TAC TCG TAC CGC GTC GTG GTC AAT GGC TCT GAC

196 CTT GGC GTC GAG TCC AAC TTC GCA GTG ACA CCG TCC GGT

235 GGG CAG ACC ATC AAC TTC CTC CAG TAC AAC AAG GGG TAT

274 GGT GTC GCG GAC ACC AAA ACG ATT CAA GTT TTC GTT GTC

313 GAT CCA GAT ACC AAC AAC DEL DEL GAC TTC ATC ATC GCT

352 GAG TGG AAG AAG ACT GAC GAC GAC GAC AAG ATC GCT AGC
```

Amino acid sequence

```
  1 ASHHHHHHSA TSLTFQLAYL VKKIDFDYTP NWGRGTPSSY IDNLTFPKVL
 51 TDKKYSYRVV VNGSDLGVES NFAVTPSGGQ TINFLQYNKG YGVADTKTIQ
101 VFVVDPDTNN DFIIAEWKKT DDDDKIAS
```

Annotation:
Purple wording - hinge residue for loop FG (I97D)
Dark blue wording - loop FG region (G101N, S103Del, E104Del, E105D, Y106F)

Feature

NheI RE site	:Nucleotide (1…6)	:Amino acid (1…2)
Hexahistidine tag	:Nucleotide (7…24)	:Amino acid (3…8)
CWT-7	:Nucleotide (25…360)	:Amino acid (9…120)
Enterokinase	:Nucleotide (361…378)	:Amino acid (121…126)
NheI RE site	:Nucleotide (379…384)	:Amino acid (127…128)

A3.15 Nucleotide and amino acid sequences of CWT-8 gene cassettes

Nucleotide sequence

```
  1 GCT AGC CAC CAT CAC CAT CAC CAT TCC GCC ACG TCG CTC

 40 ACC TTC CAG CTT GCC TAC TTG GTG AAG AAG ATC GAT TTC

 79 GAC TAC ACC CCC AAC TGG GGC CGT GGT ACC CCA AGC AGC

118 TAC ATC GAC AAC CTT ACC TTC CCC AAG GTT CTC ACC GAC

157 AAA AAA TAC TCG TAC CGC GTC GTG GTC AAT GGC TCT GAC

196 CTT GGC GTC AAG CCC AGC TAC GCA GTG GAA TCG GAC GGT

235 TCG CAG ACC ATC AAC TTC CTC CAG TAC AAC AAG GGG TAT

274 GGT GTC GCG GAC ACC AAA ACG ATT CAA GTT TTC GTT GTC

313 GAT CCA GAT ACC AAC AAC DEL DEL GAC TTC ATC ATC GCT

352 GAG TGG AAG AAG ACT GAC GAC GAC GAC AAG ATC GCT AGC
```

Amino acid sequence

```
  1 ASHHHHHHSA TSLTFQLAYL VKKIDFDYTP NWGRGTPSSY IDNLTFPKVL

 51 TDKKYSYRVV VNGSDLGVKP SYAVESDGSQ TINFLQYNKG YGVADTKTIQ

101 VFVVDPDTNN DFIIAEWKKT DDDDKIAS
```

Annotation:
Yellow wording - putative hinge residue for loop DE (E61K)
Red wording - loop DE region (S62P, N63S, F64Y, T67E, P68S, S69D, G71S)
Purple wording - hinge residue for loop FG (I97D)
Dark blue wording - loop FG region (G101N, S103Del, E104Del, E105D, Y106F)

Feature

NheI RE site	:Nucleotide (1…6)	:Amino acid (1…2)
Hexahistidine tag	:Nucleotide (7…24)	:Amino acid (3…8)
CWT-7	:Nucleotide (25…360)	:Amino acid (9…120)
Enterokinase	:Nucleotide (361…378)	:Amino acid (121…126)
NheI RE site	:Nucleotide (379…384)	:Amino acid (127…128)

A3.16 Protocol of Gel/PCR DNA fragment kits for purification of DNA from electrophoresed gel

Gel/PCR DNA fragments kit (Geneaid, Taiwan) was used to extract DNA from electrophoresed gel during the generation of gene cassettes. DNA fragments on agarose gel were excised and the extra agarose gel was trimmed off. The retrieved agarose gel with DNA fragment was transferred to the respective 1.5 ml microcentrifuge tubes, and followed by the addition of 500 µl of DF buffer and vortexing. The tube was incubated at 55˚C for 15 min to ensure that the gel slices were completely dissolved. The dissolved mixture was left to cool at room temperature. All of the sample mixture was transferred into DF column with a 2 ml collection tube. The DF Columns was then centrifuged at 15000 x g for 30 s. The flow through was discarded. W1 Buffer (400 µl) was added into the DF Column and centrifuged at 15000 x g for 30 s. The flow through was decanted. An amount of 600 µl of Wash Buffer was added into the DF Column; the Wash Buffer was mixed with 95% ethanol prior to use. The DF Column was left at room temperature for 1 min and centrifuged at 15000 x g for 30 s. The flow through was discarded. The DF Column was again centrifuged at 15000 x g for 3 min in order to dry the column matrix. The dried columns were then transferred to new microcentrifuge tubes, and followed with DNA elution step with the addition of 50 µl Elution Buffer into the center of the column matrix. The DF Columns were left stand for 3 min so that the Elution Buffer was completely absorbed. After 3 min, the DF Columns were centrifuged at 15000 x g for 2 min to elute the purified DNA.

A3.17 Sequencing results of FIP-fve cDNA

Forward primer (FIPfve-FP)

GNCCTCCCTGGTGAGAGTCGATTTCGACTACACCCCCAACTGGGGCCGTGGTAC
CCCAAGCAGCTACATCGACAACCTTACCTTCCCCAAGGTTCTCACCGACAAAAA
ATACTCGTACCGCGTCGTGGTCAATGGCTCTGACCTTGGCGTCGAGTCCAACTTC
GCAGTGACACCGTCCGGTGGGCAGACCATCAACTTCCTCCAGTACAACAAGGGG
TATGGTGTCGCGGACACCAAAACGATTCAAGTTTTCGTTGTCATTCCAGATACCG
GCAACTCGGAGGAGTACATCATCGCTGAGTGGAAGAAGANN

Reverse primer (FIPfve-RP)

ANNCNCCGGGAGGGCGGCCTCGGCACTGGAAACAGCGAAAACTTGAATCGTTT
TGGTGTCCGCGACACCATACCCCTTGTTGTACTGGAGGAAGTTGATGGTCTGCCC
ACCGGACGGTGTCACTGCGAAGTTGGACTCGACGCCAAGGTCAGAGCCATTGAC
CACGACGCGGTACGAGTATTTTTTGTCGGTGAGAACCTTGGGGAAGGTAAGGTT
GTCGATGTAGCTGCTTGGGGTACCACGGCCCCAGTTGGGGGTGTAGTCGAAATC
GATCTTCTTCACCAAGTAGGCAAGCTGGAAGGTGAGCGACGTGGCGGACATAA

Compiled DNA sequence

ATGTCCGCNCAGTCGCTCACCTTCCAGCTTGCCTACTTGGTGAAGAAGATCGATT
TCGACTACACCCCCAACTGGGGCCGTGGTACCCCAAGCAGCTACATCGACAACC
TTACCTTCCCCAAGGTTCTCACCGACAAAAAATACTCGTACCGCGTCGTGGTCA
ATGGCTCTGACCTTGGCGTCGAGTCCAACTTCGCAGTGACACCGTCCGGTGGGC
AGACCATCAACTTCCTCCAGTACAACAAGGGGTATGGTGTCGCGGACACCAAAA
CGATTCAAGTTTTCGTTGTCATTCCAGATACCGGCAACTCGGAGGAGTACATCAT
CGCTGAGTGGAAGAAG

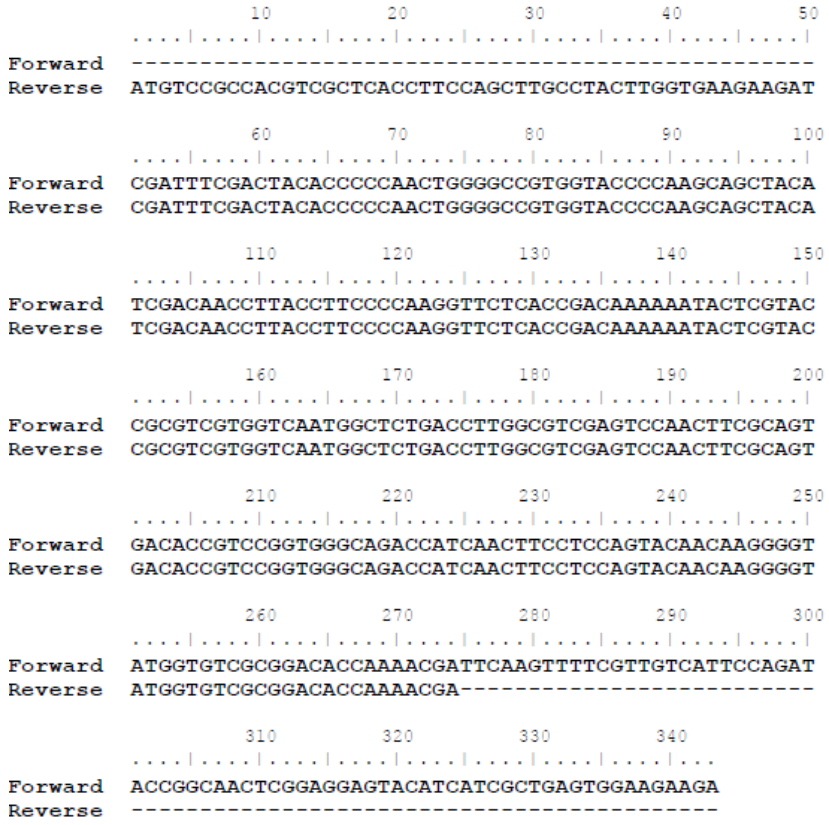


Figure A3.1. Alignment of sequencing results for FIP-fve cDNA using forward (FIPfve-FP) and reverse primers (FIPfve-RP). The diagram serves as an example for the forward and reverse sequences alignment generated during sequencing analyses in this study.

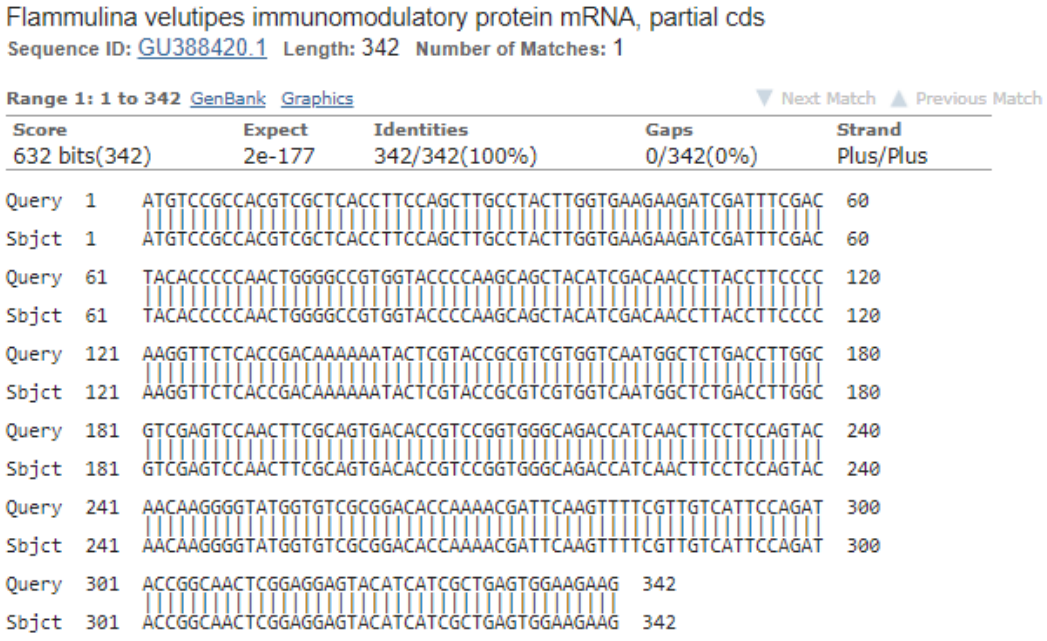


Figure A3.2. Alignment between FIP-fve cDNA and FIP-fve mRNA (GU388420.1) in sequence database using BLAST®. The diagram serves as an example for analysis of the compiled sequences against FIP-fve template.

A3.18 Sequencing results of FIP-fve cDNA in pGEM-FIPfve

Forward primer (M13F/pUC)

NNNNNNNCGGGGATGTATACGACTCACTATAGGGCGAATTGGGCCCGACGTCGCATG
CTCCCGGCCGCCATGGCGGCCGCGGGAATTCGATTCTTCTTCCACTCAGCGATGATGT
ACTCCTCCGAGTCGCCGGTATCTGGAATGACAACGAAAACTTGAATCGTTTTGGTGTCC
GCGACACCATACCCCTTGTTGTACTGGAGGAAGTTGATGGTCTGCCCACCGGACGGTG
TCACTGCGAGGTTGGACTCGACGCCAAGGTCAGAGCCATTGACCACGACGCGGTACGA
GTATTTTTTGTCGGTGAGAACCTTGGGGAAGGTAAGGTTGTCGATGTAGCTGCTTGGG
GTACCACGGCCCCAGTTGGGGGTGTAGTCGAAATCGATCTTCTTCACCAAGTAGGCAA
GCTGGAAGGTGAGCGACGTGGCGGACATAATCACTAGTGAATTCGCGGCCGCCTGCA
GGTCGACCATATGGGAGAGCTCCCAACGCGTTGGATGCATAGCTTGAGTATTCTATAG
TGTCACCTAAATAGCTTGGCGTAATCATGGTCATAGCTGTTTCCTGTGTGAAATTGTTAT
CCGCTCACAATTCCACACAACATACGAGCCGGAAGCATAAAGTGTAAAGCCTGGGGTG
CCTAATGAGTGAGCTAACTCACATTAATTGCGTTGCGCTCACTGCCCGCTTTCCAGTCG
GGAAACCTGTCGTGCCAGCTGCATTAATGAATCGGCCAACGCGCGGGGAGAGGCGGT
TTGCGTATTGGGCGCTCTTCCGCTTCCTCGCTCACTGACTCGCTGCGCTCGGTCGTTCG
GCTGCGGCGAGCGGTATCAGCTCACTCAAAGGCGGTAATACGGTTATCCACAGAATCA
GGGGATAACGCAGGAAAGAACATGTGAGCAAAAGGCCAGCAAAAGGCCAGGAACCGT
AAAAAGGCCGCGTTGCTGGCGTTTTTCCATAGGCTCCGCCCCCCTGACGAGCATCACA
AAAATCGACGCTCAAGTCAGAGGTGGCGAAACCCGACAGGACTATAAAGATACCAGGC
GTTTCCCCCTGGAAGCTCCCTCGTGCGCTCTCCTGTTCCGACCCTGCCGCTTACCGGAT
ACCTGTCCGCCTTTCTCCTTTCGGGAAGCGTGGCGCTTTTCTCATAGCTTCACGCTGGA
AGGTATCTCCAGTTCCGGGGTAAGTCCGTTCGGTTCCAAGCTTGGGCTTGGGTGGCAC
GAAACCCCCCCGTTTAAGCCCGAACCCGTTGGGCCCTTTAATCGGNGAAACTATTCGG
CTTTGAGTTCCACACCCGGTAAA

Forward primer (M13R/pUC)

NNNCNNACTTTAGGTGACTATAGAATACTCAAGCTATGCATCCAACGCGTTGGGAGCT
CTCCCATATGGTCGACCTGCAGGCGGCCGCGAATTCACTAGTGATTATGTCCGCCACG
TCGCTCACCTTCCAGCTTGCCTACTTGGTGAAGAAGATCGATTTCGACTACACCCCCAA
CTGGGGCCGTGGTACCCCAAGCAGCTACATCGACAACCTTACCTTCCCCAAGGTTCTCA
CCGACAAAAAATACTCGTACCGCGTCGTGGTCAATGGCTCTGACCTTGGCGTCGAGTC
CAACCTCGCAGTGACACCGTCCGGTGGGCAGACCATCAACTTCCTCCAGTACAACAAG
GGGTATGGTGTCGCGGACACCAAAACGATTCAAGTTTTCGTTGTCATTCCAGATACCGG
CGACTCGGAGGAGTACATCATCGCTGAGTGGAAGAAGAATCGAATTCCCGCGGCCGCC
ATGGCGGCCGGGAGCATGCGACGTCGGGCCCAATTCGCCCTATAGTGAGTCGTATTAC
AATTCACTGGCCGTCGTTTTACAACGTCGTGACTGGGAAAACCCTGGCGTTACCCAACT
TAATCGCCTTGCAGCACATCCCCCTTTCGCCAGCTGGCGTAATAGCGAAGAGGCCCGC
ACCGATCGCCCTTCCCAACAGTTGCGCAGCCTGAATGGCGAATGGACGCGCCCTGTAG
CGGCGCATTAAGCGCGGCGGGTGTGGTGGTTACGCGCAGCGTGACCGCTACACTTGC
CAGCGCCCTAGCGCCCGCTCCTTTCGCTTTCTTCCCTTCCTTTCTCGCCACGTTCGCCG
GCTTTCCCCGTCAAGCTCTAAATCGGGGGCTCCCTTTAGGGTTCCGATTTAGTGCTTTA
CGGCACCTCGACCCCAAAAAACTTGATTAGGGTGATGGTTCACGTAGTGGGCCATCGC
CCTGATAGACGGTTTTTCGCCCTTTGACGTTGGAGTCCACGTTCTTTAATAGTGGACTC
TTGTTCCAAACTGGAACAACACTCAACCCTATCTCGGTCTATTCTTTTGATTTATAAGGG
ATTTTGCCGATTTCGGCCTATTGGTTAAAAAATGAGCTGATTTAACAAAAATTTAACGCG
AATTTTAACAAAATATTAACGCTTACAATTTCCTGATGCGGGATTTTCTCCTTACGCATCT
GTGCGGGTATTTCACACCGCATCAGGGGGGCCTTTTTCGGGGAAATTGGCGCGGAAAC
CCCTATTTTGGTTATTTTTCCAAAAAACATTCAAAAAATGGTATCCCGCTCCTGGAAACA
TATACCCCGGG

A3.19 Sequencing results of H-FIPfve-Ek sequence in pGLO:: H-rFIPFVE-EK-GFP

Forward primer (pBAD-FP)

AGGATTCGGACTCCTGACGCTTTTTATCGCAACTCTCTACTGTTTCTCCATACCCGTTTTTTTGGGC
TAGAAATAATTTTGTTTAACTTTAAGAAGGAGATATACATATGGCTAGCCACCATCACCATCACCAT
TCCGCCACGTCGCTCACCTTCCAGCTTGCCTACTTGGTGAAGAAGATCGATTTCGACTACACCCCC
AACTGGGGCCGTGGTACCCCAAGCAGCTACATCGACAACCTTACCTTCCCCAAGGTTCTCACCGA
CAAAAAATACTCGTACCGCGTCGTGGTCAATGGCTCTGACCTTGGCGTCGAGTCCAACTTCGCAG
TGACACCGTCCGGTGGGCAGACCATCAACTTCCTCCAGTACAACAAGGGGTATGGTGTCGCGGA
CACCAAAACGATTCAAGTTTTCGTTGTCATTCCAGATACCGGCAACTCGGAGGAGTACATCATCGC
TGAGTGGAAGAAGACTGACGACGACGACAAGATCGCTAGCAAAGGAGAAGAACTTTTCACTGGA
GTTGTCCCAATTCTTGTTGAATTAGATGGTGATGTTAATGGGCACAAATTTTCTGTCAGTGGAGAG
GGTGAAGGTGATGCTACATACGGAAAGCTTACCCTTAAATTTATTTGCACTACTGGAAAACTACCT
GTTCCATGGCCAACACTTGTCACTACTTTCTCTTATGGTGTTCAATGCTTTTCCCGTTATCCGGATC
ATATGAAACGGCATGACTTTTTCAAGAGTGCCATGCCCGAAGGTTATGTACAGGAACGCACTATAT
CTTTCAAAGATGACGGGAACTACAAGACGCGTGCTGAAGTCAAGTTTGAAGGTGATACCCTTGTT
AATCGTATCGAGTTAAAAGGTATTGATTTTAAAGAAGATGGAAACATTCTCGGACACAAACTCGAG
TACAACTATAACTCACACAATGTATACATCACGGCAGACAAACAAAAGAATGGAATCAAAGCTAAC
TTCAAAATTCGCCACAACATTGAAGATGGATCCGTTCAACTAGCAGACCATTATCAACAAAATACT
CCAATTGGCGATGGCCCTGTCCTTTTACCAGAAAACCATTACTGGTCGAACAATCTGCCTTTTCAA
AGATTCCAACGAAAAGCGGGACCAATGGTCCTTCTGGATTTGGAACGGCGGTGGGATACCATGG
GCTTGTAGGATCTCTAAATAAGGAATTCCATCCGGCACCGGGGAATCCCTAAATCCAACCAGAGG
GTTCAAATTTGGTCGTTTTGCGGCGAAAACAAATATCTATCCTCGGAATTACATTAACTTAACCAAC
AACAGTGTGTATAAAACTAATTTCCTTGGGCACTTGTACGGGGGCTTCCCAGGTGCCCTGAGAAA
TATCAAGAAGCGCCCTGGCCAGAAGTGTGTAGGCCCCCTCTTTA

Reverse primer (FIPfve-FP)

GCGCATGTACTCCTCCGAGTTGCCGGTATCTGGAATGACAACGAAAACTTGAATCGTTTTGGTGT
CCGCGACACCATACCCCTTGTTGTACTGGAGGAAGTTGATGGTCTGCCCACCGGACGGTGTCACT
GCGAAGTTGGACTCGACGCCAAGGTCAGAGCCATTGACCACGACGCGGTACGAGTATTTTTTGTC
GGTGAGAACCTTGGGGAAGGTAAGGTTGTCGATGTAGCTGCTTGGGGTACCACGGCCCCAGTTG
GGGGTGTAGTCGAAATCGATCTTCTTCACCAAGTAGGCAAGCTGGAAGGTGAGCGACGTGGCGG
AATGGTGATGGTGATGGTGGCTAGCCATATGTATATCTCCTTCTTAAAGTTAAACAAAATTATTTCT
AGCCCAAAAAAACGGGTATGGAGAAACAGTAGAGAGTTGCGATAAAAAGCGTCAGGTAGGATCC
GCTAATCTTATGGATAAAAATGCTATGGCATAGCAAAGTGTGACGCCGTGCAAATAATCAATGTG
GACTTTTCTGCCGTGATTATAGACACTTTTGTTACGCGTTTTTGTCATGGCTTTGGTCCCGCTTTGT
TACAGAATGCTTTTAATAAGCGGGGTTACCGGTTTGGTTAGCGAGAAGAGCCAGTAAAAGACGCA
GTGACGGCAATGTCTGATGCAATATGGACAATTGGTTTCTTCTCTGAATGGCGGGAGTATGAAAA
GTATGGCTGAAGCGCAAAATGATCCCCTGCTGCCGGGATACTCGTTTAATGCCCATCTGGTGGCG
GGTTTAACGCCGATTGAGGCCAACGGTTATCTCGATTTTTTTATCGACCGACCGCTGGGAATGAA
AGGTTATATTCTCAATCTCACCATTCGCGGTCAGGGGGTGGTGAAAAATCAGGGACGAGAATTTG
TTTGCCGACCGGGTGATATTTTGCTGTTCCCGCCAGGAGAGATTCATCACTACGGTCGTCATCCG
GAGGCTCGCGAATGGTATCACCAGTGGGTTTACTTTCGTCCGCGCGCCTACTGGCATGAATGGCT
TAACTGGGCCGTCAAAATTTGCCAATACGGGGTTCTTTCCCCCCGGATGAAACCGCACCAGCCCG
CATTTCAGCGACCTGGTTTGGGCAAATCATTAACGCCGGGGCAAGGGGAAAGGGCGCTATTTCG
GAACTGCGGGGCAATAAATCGGCTTGGAACAATTGTTACTGGCGGCCCAGGGAAACCAATTAACC
GAGTCCCTTCTATCCACCCGAAGGAAAAATTCGGGGTAACCCGAGGTTTTGTTCAAAAAATCCCG
GGGATTACCTGGGGAGAAACGCCAATTTTTGAATTCCGCGACGGGTCCCACAGCTAAGGTTTGTC
TTTTGCCCCCTCTCA

A3.20 Sequencing results of H-CWT1-Ek sequence in pGLO:: H-CWT1-EK-GFP

Forward primer (pBAD-FP)

NNNGAATGGGATCTACTGACGCTTTTTATCGCACTCTCTACTGTTTCTCCATACCCGTTTTTTTGG
GCTAGAAATAATTTTGTTTAACTTTAAGAAGGAGATATACATATGGCTAGCCACCATCACCATCAC
CATATGTCCGCCACGTCGCTCACCTTCCAGCTTGCCTACTTGGTGAAGAAGATCGATTTCGACTAC
ACCCCCAACTGGGGCCGTGGTACCCCAAGCAGCTACATCGACAACCTTACCTTCCCCAAGGTTCT
CACCGACAAAAAATACTCGTACCGCGTCGTGGTCAATGGCTCTGACCTTGGCGTCGAGTCCAACT
TCGCAGTGACACCGTCCGGTGGGCAGACCATCAACTTCCTCCAGTACAACAAGGGGTATGGTGTC
GCGGACACCAAAACGATTCAAGTTTTCGTTGTCATTCCAGATACCGGCAACTCGGAGGAGTACAT
CATCGCTGAGTGGAAGAAGACTGACGACGACGACAAGATCGCTAGCAAAGGAGAAGAACTTTTC
ACTGGAGTTGTCCCAATTCTTGTTGAATTAGATGGTGATGTTAATGGGCACAAATTTTCTGTCAGT
GGAGAGGGTGAAGGTGATGCTACATACGGAAAGCTTACCCTTAAATTTATTTGCACTACTGGAAA
ACTACCTGTTCCATGGCCAACACTTGTCACTACTTTCTCTTATGGTGTTCAATGCTTTTCCCGTTAT
CCGGATCATATGAAACGGCATGACTTTTTCAAGAGTGCCATGCCCGAAGGTTATGTACAGGAACG
CACTATATCTTTCAAAGATGACGGGAACTACAAGACGCGTGCTGAAGTCAAGTTTGAAGGTGATA
CCCTTGTTAATCGTATCGAGTTAAAAGGTATTGATTTTAAAGAAGATGGAAACATTCTCGGACACA
AACTCGAGTACAACTATTACTCACACAAGGTATACATCACGGGCAGACAAACAAAAGAATGGGAA
TCCAAGCTAACTTCAAAATTCGCCCACAACATTGAAAGAGGGATCCCGTTCAACTAGGCAGACCAT
TATTCAACCAAATACCTCCAATTGGGCGATGGCTCCTGGTCCTTTATA

Forward primer (FIPfve-FP)

NNNNNNNNNNNNNNANANNGCCAGCTTGCATGCCTGCAGGTCGACTCTAGAGGATCCCCGGG
TACCGAGCTCGAATTCATTATTTGTAGAGCTCATCCATGCCATGTGTAATCCCAGCAGCAGTTACA
AACTCAAGAAGGACCATGTGGTCACGCTTTTCGTTGGGATCTTTCGAAAGGGCAGATTGTGTCGA
CAGGTAATGGTTGTCTGGTAAAAGGACAGGGCCATCGCCAATTGGAGTATTTTGTTGATAATGGT
CTGCTAGTTGAACGGATCCATCTTCAATGTTGTGGCGAATTTTGAAGTTAGCTTTGATTCCATTCTT
TTGTTTGTCTGCCGTGATGTATACATTGTGTGAGTTATAGTTGTACTCGAGTTTGTGTCCGAGAAT
GTTTCCATCTTCTTTAAAATCAATACCTTTTAACTCGATACGATTAACAAGGGTATCACCTTCAAAC
TTGACTTCAGCACGCGTCTTGTAGTTCCCGTCATCTTTGAAAGATATAGTGCGTTCCTGTACATAA
CCTTCGGGCATGGCACTCTTGAAAAAGTCATGCCGTTTCATATGATCCGGATAACGGGAAAAGCA
TTGAACACCATAAGAGAAAGTAGTGACAAGTGTTGGCCATGGAACAGGTAGTTTTCCAGTAGTGC
AAATAAATTTAAGGGTAAGCTTTCCGTATGTAGCATCACCTTCACCCTCTCCACTGACAGAAAATTT
GTGCCCATTAACATCACCATCTAATTCAACAAGAATTGGGACAACTCCAGTGAAAAGTTCTTCTCC
TTTGCTAGCGATCTTGTCGTCGTCGTCAGTCTTCTTCCACTCAGCGATGATGTACTCCTCCGAGTT
GCCGGTATCTGGAATGACAACGAAAACTTGAATCGTTTTGGNGTCCGCGACACCATTACCCCTTG
TTTGTCTGGAAGGAAGTTGANGGTCTGCCCACCGGACGGTGTCACTGCGAAGTTGGATT

A3.21 Sequencing results of H-CWT2-Ek sequence in pGLO:: H-CWT2-EK-GFP

Forward primer (pBAD-FP)

AAGGGAATCTTCCTGACGCTTTTTATCGCAACTCTCTACTGTTTCTCCATACCCGTTTTTTTGGGCT
AGAAATAATTTTGTTTAACTTTAAGAAGGAGATATACATATGGCTAGCCACCATCACCATCACCATT
CCCTCACGTCGCTCACCTTCCAGCTTGCCTACTTGGTGAAGAAGATCGATTTCGACTACACCCCCA
ACTGGGGCCGTGGTACCCCAAGCAGCTACATCGACAACCTTACCTTCCCCAAGGTTCTCACCGAC
AAAAAATACTCGTACCGCGTCGTGGTCAATGGCTCTGACCTTGGCGTCGAGTCCAACTTCGCAGT
GACACCGTCCGGTGGGCAGACCATCAACTTCCTCCAGTACAACAAGGGGTATGGTGTCGCGGAC
ACCAAAACGATTCAAGTTTTCGTTGTCATTCCAGATACCGGCAACTCGGAGGAGTACATCATCGCT
GAGTGGAAGAAGACTGACGACGACGACAAGATCGCTAGCAAAGGAGAAGAACTTTTCACTGGAG
TTGTCCCAATTCTTGTTGAATTAGATGGTGATGTTAATGGGCACAAATTTTCTGTCAGTGGAGAGG
GTGAAGGTGATGCTACATACGGAAAGCTTACCCTTAAATTTATTTGCACTACTGGAAAACTACCTG
TTCCATGGCCAACACTTGTCACTACTTTCTCTTATGGTGTTCAATGCTTTTCCCGTTATCCGGATCA
TATGAAACGGCATGACTTTTTCAAGAGTGCCATGCCCGAAGGTTATGTACAGGAACGCACTATAT
CTTTCAAAGATGACGGGAACTACAAGACGCGTGCTGAAGTCAAGTTTGAAGGTGATACCCTTGTT
AATCGTATCGAGTTAAAAGGTATTGATTTTAAAGAAGATGGAAACATTCTCGGACACAAACTCGAG
TACAACTATAACTCACACAATGTATACATCACGGCAGACAAACAAAAGAATGGAATCAAAGCTAAC
TTCAAAATTCGCCACAACATTGAAGATGGATCCGTTCAACTAGCAGACCATTATCAACAAAATACT
CCAATTGGCGATGGCCCTGTCCTTTTACCAAAAAACCATTACCTGCCGAACAAATCTGTCCTTTTC
AAAAGATCCCAACGAAAAGGTGGGACCCAATGGTTCCTTCTGGAGTTGGTAACGGCTGCGGGGA
TAACACGTGGTATGGAATAATCCTCCCAATACAGGAATTCCATCCCGGTACCCGGGGAATCCCTA
AAGCTTACCTGATGGTGTTCAATCTTGGTGTGTTTGGCGGACTGACAGAATTTCCCCCCGCATTTG
ATTAACTCGAATCAGAACATGTTGCAATACACGAATTTCCCGTGGGGCATTAGCGCGGGTTCTTCT
TTACCCTTTGCTATACACATTTAAACCTTTCTAACTTTGATTTTGGGGGCTTCCCTAATCCTAAATG
GGATCTCTCCTTTACATATAAAAAGGTCTTCTAGAAATGTGCCCTCCTCACCCGCTTGTGTTTAGG
TACC

Reverse primer (FIPfve-RP)

GTGCATCGTACTCCTCCGAGTTGCCGGTATCTGGAATGACAACGAAAACTTGAATCGTTTTGGTGT
CCGCGACACCATACCCCTTGTTGTACTGGAGGAAGTTGATGGTCTGCCCACCGGACGGTGTCACT
GCGAAGTTGGACTCGACGCCAAGGTCAGAGCCATTGACCACGACGCGGTACGAGTATTTTTTGTC
GGTGAGAACCTTGGGGAAGGTAAGGTTGTCGATGTAGCTGCTTGGGGTACCACGGCCCCAGTTG
GGGGTGTAGTCGAAATCGATCTTCTTCACCAAGTAGGCAAGCTGGAAGGTGAGCGACGTGAGGG
AATGGTGATGGTGATGGTGGCTAGCCATATGTATATCTCCTTCTTAAAGTTAAACAAAATTATTTCT
AGCCCAAAAAAACGGGTATGGAGAAACAGTAGAGAGTTGCGATAAAAAGCGTCAGGTAGGATCC
GCTAATCTTATGGATAAAAATGCTATGGCATAGCAAAGTGTGACGCCGTGCAAATAATCAATGTG
GACTTTTCTGCCGTGATTATAGACACTTTTGTTACGCGTTTTTGTCATGGCTTTGGTCCCGCTTTGT
TACAGAATGCTTTTAATAAGCGGGGTTACCGGTTTGGTTAGCGAGAAGAGCCAGTAAAAGACGCA
GTGACGGCAATGTCTGATGCAATATGGACAATTGGTTTCTTCTCTGAATGGCGGGAGTATGAAAA
GTATGGCTGAAGCGCAAAATGATCCCCTGCTGCCGGGATACTCGTTTAATGCCCATCTGGTGGCG
GGTTTAACGCCGATTGAGGCCAACGGTTATCTCGATTTTTTTATCGACCGACCGCTGGGAATGAA
AGGTTATATTCTCAATCTCACCATTCGCGGTCAGGGGGTGGTGAAAAATCAGGGACGAGAATTTG
TTTGCCGACCGGGTGATATTTTGCTGTTCCCGCCAGGAGAGATTCATCACTACGGGTCGTCATCC
GGGAGGCTCGCGAATGGTATCACCAGTGGGGTTTACTTTTCGTCCGCCGCGCCTACTGGGCATG
AATGGGCTTTAACTGGGCCGGTCAATATTTTGCCCATTACGGGGGTTTCTTTTCCCCCCGGAATGA
AAGCGCAACCAGCCCGCATTTTCAGCGAACCTGGTTTGGGCCAAATCATTAAACGCCCGGGGCAA
GGGGAAAGGGGCGCTATTTCCGGAACCTGCCTGGGCAATAAAATCTGGCCTTTGAACAATTTGA

A3.22 Sequencing results of H-CWT3-Ek sequence in pGLO:: H-CWT3-EK-GFP

Forward primer (pBAD-FP)

AAGGGGTTCTACTGACGCTTTTTATCGCAACTCTCTACTGTTTCTCCATACCCGTTTTTTTGGGCTA
GAAATAATTTTGTTTAACTTTAAGAAGGAGATATACATATGGCTAGCCACCATCACCATCACCATTC
CGCCACGTCGCTCACCTTCCAGCTTGCCTACTTGGTGAAGAAGATCGATTTCGACTACACCCCCA
ACTGGGGCCGTGGTACCCCAAGCAGCTACATCGACAACCTTACCTTCCCCAAGGTTCTCACCGAC
AAAAAATACTCGTACCGCGTCGTGGTCAATGGCTCTGACCTTGGCGTCGAGCCCAGCTACGCAGT
GGAATCGGACGGTTCGCAGACCATCAACTTCCTCCAGTACAACAAGGGGTATGGTGTCGCGGAC
ACCAAAACGATTCAAGTTTTCGTTGTCATTCCAGATACCGGCAACTCGGAGGAGTACATCATCGCT
GAGTGGAAGAAGACTGACGACGACGACAAGATCGCTAGCAAAGGAGAAGAACTTTTCACTGGAG
TTGTCCCAATTCTTGTTGAATTAGATGGTGATGTTAATGGGCACAAATTTTCTGTCAGTGGAGAGG
GTGAAGGTGATGCTACATACGGAAAGCTTACCCTTAAATTTATTTGCACTACTGGAAAACTACCTG
TTCCATGGCCAACACTTGTCACTACTTTCTCTTATGGTGTTCAATGCTTTTCCCGTTATCCGGATCA
TATGAAACGGCATGACTTTTTCAAGAGTGCCATGCCCGAAGGTTATGTACAGGAACGCACTATAT
CTTTCAAAGATGACGGGAACTACAAGACGCGTGCTGAAGTCAAGTTTGAAGGTGATACCCTTGTT
AATCGTATCGAGTTAAAAGGTATTGATTTTAAAGAAGATGGAAACATTCTCGGACACAAACTCGAG
TACAACTATAACTCACACAATGTATACATCACGGCAGACAAACAAAAGAATGGAATCAAAGCTAAC
TTCAAAATTCGCCACAACATTGAAGATGGATCCGTTCAACTAGCAGACCATTATCAACAAAATACT
CCAATTGGCGAAGGGCCCTGTCCTTTTACCAGAAAACCATTACCTGTCGAACCAATCTGCCCTTTC
CAAAGATCCCAACGAAAAGCTTGACCACTGGGTCCTTCTTGAATTTGGAACGGCCGCTGGGAATA
CCACGGGCAGGGAAGAGCCTCACAAATAAGGAATTCCAAGCTCGGTACCCGGGGGATCCCTTAA
AATCCAACTCGAACGGATGGAAACTTGGGCTGTTTTGGCGCAGAAGAAAGAAATTTTCACCCCTG
TAACCATTTTACTCCAAACCCCGAAACGGGTTTGTATATAATACTAATTTGCCGGGGCCGTATAAA
GCGGGGGTGTCCCCCCGCAACCTTCGCCAAACTCAAAATGGAATCCCTCTCGACCCTCGGAGAGT
GAGGGGGCGCCCCCACGGAAAAATAGAGAAAAGGCTTCGTCTAATAATAAGAAATGTGGCTCTAC
AAACAGGGGGCCTTTGTTTATCGTATTCTCTCTTCA

Reverse primer (FIPfve-RP)

TCGGATGTACTCCTCCGAGTTGCCGGTATCTGGAATGACAACGAAAACTTGAATCGTTTTGGTGTC
CGCGACACCATACCCCTTGTTGTACTGGAGGAAGTTGATGGTCTGCGAACCGTCCGATTCCACTG
CGTAGCTGGGCTCGACGCCAAGGTCAGAGCCATTGACCACGACGCGGTACGAGTATTTTTTGTCG
GTGAGAACCTTGGGGAAGGTAAGGTTGTCGATGTAGCTGCTTGGGGTACCACGGCCCCAGTTGG
GGGTGTAGTCGAAATCGATCTTCTTCACCAAGTAGGCAAGCTGGAAGGTGAGCGACGTGGCGGA
ATGGTGATGGTGATGGTGGCTAGCCATATGTATATCTCCTTCTTAAAGTTAAACAAAATTATTTCTA
GCCCAAAAAAACGGGTATGGAGAAACAGTAGAGAGTTGCGATAAAAAGCGTCAGGTAGGATCCG
CTAATCTTATGGATAAAAATGCTATGGCATAGCAAAGTGTGACGCCGTGCAAATAATCAATGTGGA
CTTTTCTGCCGTGATTATAGACACTTTTGTTACGCGTTTTTGTCATGGCTTTGGTCCCGCTTTGTTA
CAGAATGCTTTTAATAAGCGGGGTTACCGGTTTGGTTAGCGAGAAGAGCCAGTAAAAGACGCAGT
GACGGCAATGTCTGATGCAATATGGACAATTGGTTTCTTCTCTGAATGGCGGGAGTATGAAAAGT
ATGGCTGAAGCGCAAAATGATCCCCTGCTGCCGGGATACTCGTTTAATGCCCATCTGGTGGCGGG
TTTAACGCCGATTGAGGCCAACGGTTATCTCGATTTTTTTATCGACCGACCGCTGGGAATGAAAG
GTTATATTCTCAATCTCACCATTCGCGGTCAGGGGGTGGTGAAAAATCAGGGACGAGAATTTGTT
TGCCGACCGGGTGATATTTTGCTGTTCCCGCCAGGAGAGATTCATCACTACGGTCGTCATCCGAA
GGCTCGCGAATGGTATCACCAGTGGGGTTTACTTTCGTCCGCGCGCCTACTGGCATGAATGGCTT
AACTGGGCCGTCAATATTTGCCAATACGGGGGTTCTTTCGCCCGGGATGAAGCCGCACCAGCCC
GCATTTTCAGCCACCCGGTTTGGGGCAATTCATTAACCGCCGGGCAAAGGGGAAAGGGCCCTATT
TCGGAACTTGCTGGGCAAATAATTCTGCTTTGAAACAATTGTTAACTGGCGGCCCCATGGGAAGC
CGTTAA

A3.23 Sequencing results of H-CWT4-Ek sequence in pGLO:: H-CWT4-EK-GFP

Forward primer (pBAD-FP)

NNNNNNNNNANNNNACCTTGNCGCTTTTTATCGCAACTCTCTACTGTTTCTCCATACCCGTTTTTT
TGGGCTAGAAATAATTTTGTTTAACTTTAAGAAGGAGATATACATATGGCTAGCCACCATCACCAT
CACCATTCCGCCACGTCGCTCACCTTCCAGCTTGCCTACTTGGTGAAGAAGATCGATTTCGACTAC
ACCCCCAACTGGGGCCGTGGTACCCCAAGCAGCTACATCGACAACCTTACCTTCCCCAAGGTTCT
CACCGACAAAAAATACTCGTACCGCGTCGTGGTCAATGGCTCTGACCTTGGCGTCGAGTCCAACT
TCGCAGTGACACCGTCCGGTGGGCGGACCATCAACTTCCTCCAGTACAACAAGGGGTATGGTGT
CGCGGACACCAAAACGATTCAAGTTTTCGTTGTCATTCCAGATACCAACAACGACTTCATCATCGC
TGAGTGGAAGAAAACTGACGACGACGACAAGATCGCTAGCAAAGGAGAAGAACTTTTCACTGGA
GTTGTCCCAATTCTTGTTGAATTAGATGGTGATGTTAATGGGCACAAATTTTCTGTCAGTGGAGAG
GGTGAAGGTGATGCTACATACGGAAAAGCTTACCCTTTAATTTATTTGCACTACTGGAAAACTACC
TGTTCCATGGCCCAACACTTGTCACTACTTTTCTCTTATGGTGTTCAATGCTTTTTCCCGTATCCCG
GATCATATGAAACGGCATGACTTTTTCAAGAGTGCCNTGNCCGAAAGTTATGTAAGGAACGCACT
ATATCTTTCAAAATGAC

Reverse primer (FIPfve-RP)

AAGGTTCTTTTGTCAAGCTGTATGTCTATAGCGAGATGAGTCGTTGTTGGTATCTGGAATGACAAC
GAAAACTTGAATCGTTTTGGTGTCCGCGACACCATACCCCTTGTTGTACTGGAGGAAGTTGATGG
TCCGCCCACCGGACGGTGTCACTGCGAAGTTGGACTCGACGCCAAGGTCAGAGCCATTGACCAC
GACGCGGTACGAGTATTTTTTGTCGGTGAGAACCTTGGGGAAGGTAAGGTTGTCGATGTAGCTGC
TTGGGGTACCACGGCCCCAGTTGGGGGTGTAGTCGAAATCGATCTTCTTCACCAAGTAGGCAAGC
TGGAAGGTGAGCGACGTGGCGGAATGGTGATGGTGATGGTGGCTAGCCATATGTATATCTCCTT
CTTAAAGTTAAACAAAATTATTTCTAGCCCAAAAAAACGGGTATGGAGAAACAGTAGAGAGTTGCG
ATAAAAAGCGTCAGGTAGGATCCGCTAATCTTATGGATAAAAATGCTATGGCATAGCAAAGTGTG
ACGCCGTGCAAATAATCAATGTGGACTTTTCTGCCGTGATTATAGACACTTTTGTTACGCGTTTTT
GTCATGGCTTTGGTCCCGCTTTGTTACAGAATGCTTTTAATAAGCGGGGTTACCGGTTTGGTTAGC
GAGAAGAGCCAGTAAAAGACGCAGTGACGGCAATGTCTGATGCAATATGGACAATTGGTTTCTTC
TCTGAATGGCGGGAGTATGAAAAGTATGGCTGAAGCGCAAAATGATCCCCTGCTGCCGGGATACT
CGTTTAATGCCCATCTGGTGGCGGGTTTAACGCCGATTGAGGCCAACGGTTATCTCGATTTTTTTA
TCGACCGACCGCTGGGAATGAAAGGTTATATTCTCAATCTCACCATTCGCGGTCAGGGGGTGGTG
AAAAAATCAGGGACGAGAATTTGTTTGGCCGACCGGGTGATATTTTGCTGGTTCCCGCCAGGAAA
AGATTCATCACTACCGGTCGTCATCCGGGAGGCTCCGCGAATGGTATCACCCGTGGGGGTTTACT
TTTCGTCCGCGCGGCCTAACGGCCATGAAAGGGCTTAACTGGGCCGCCAAAATTTGGCCAAAACC
GGGGGTTCTTTCCACCCGGAAGGAAACGCACCAACCCGCATTTTCATCCGACCTGGTTTGGGGCA
AAACCTTTAAACGCCCGGGCCAAGGGGGAAAGGGTGCCTTTTTCTCGAATCTGCCGTGATTAAAA
AATTCGGCTTTGAACAAATTGTATACGCGGCTGGCCTATGGGAGAGCCTATTACAGTGATTACGA
CACTGACACTTCACGAGTATGATTAACTACTGGGGATACCCATATGTGGTCTAGACAACACCATCA
TATAATACTTTCCTCTCTATACAAACCTTTCTAATTTTGAAGACCTTCGCCAAGAGACGCTACAAAA
CGTAGTATTATCGATGATTACCACGAGAAGATCGATTTGTAGAAACCAGATTTTCATTCCACCCGT
ATGACATGTACAGAAATCGCAAATAACCTA

A3.24 Sequencing results of H-CWT5-Ek sequence in pGLO:: H-CWT5-EK-GFP

Compiled DNA sequence

AAAAACGGATCCTACCTGACGCTTTTTATCGCAACTCTCTACTGTTTCTCCATACCCGTTTTTTTGG
GCTAGAAATAATTTTGTTTAACTTTAAGAAGGAGATATACATATGGCTAGCCACCATCACCATCAC
CATTCCGCCACGTCGCTCACCTTCCAGCTTGCCTACTTGGTGAAGAAGATCGATTTCGACTACACC
CCCAACTGGGGCCGTGGTACCCCAAGCAGCTACATCGACAACCTTACCTTCCCCAAGGTTCTCAC
CGACAAAAAATACTCGTACCGCGTCGTGGTCAATGGCTCTGACCTTGGCGTCGAGCCCAGCTACG
CAGTGGAATCGGACGGTTCGCAGACCATCAACTTCCTCCAGTACAACAAGGGGTATGGTGTCGC
GGACACCAAAACGATTCAAGTTTTCGTTGTCATTCCAGATACCAACAACGACTTCATCATCGCTGA
GTGGAAGAAGACTGACGACGACGACAAGATCGCTAGCAAAGGAGAAGAACTTTTCACTGGAGTT
GTCCCAATTCTTGTTGAATTAGATGGTGATGTTAATGGGCACAAATTTTCTGTCAGTGGAGAGGGT
GAAGGTGATGCTACATACGGAAAGCTTACCCTTAAATTTATTTGCACTACTGGAAAACTACCTGTT
CCATGGCCAACACTTGTCACTACTTTCTCTTATGGTGTTCAATGCTTTTCCCGTTATCCGGATCATA
TGAAACGGCATGACTTTTTCAAGAGTGCCATGCCCGAAGGTTATGTACAGGAACGCACTATATCTT
TCAAAGATGACGGGAACTACAAGACGCGTGCTGAAGTCAAGTTTGAAGGTGATACCCTTGTTAAT
CGTATCGAGTTAAAAGGTATTGATTTTAAAGAAGATGGAAACATTCTCGGACACAAACTCGAGTAC
AACTATAACTCACACAATGTATACATCACGGCAGACAAACAAAAGAATGGAATCAAAGCTAACTTC
AAAATTCGCCACTACATTGAAGATGGATCCGTTCAACTAGCTGACCTTTATCACCAAATACTCCAA
TTGGCGATGGCCCTGTCCTTTTACCGAATACCTTTACCTGGCGAACCAATCTGCCCTTTCGAAAGA
TCCCAACCAAAATTCGGACCCTTGGTCCTTCTGGATTTTGAACGGTAGTCGGATATTCCTAGGAAT
TGGATTAATCTTCTATTAATGATTATACTTCTTGGTCCCGTGGTAACTCATTATACGA

Reverse primer (FIPfve-RP)

AAAAGTAGTTTTTGCTTTGCTGTGCTATATCAGCGATGATGAAGTCGTTGTTGGTATCTGGAATGA
CAACGAAAACTTGAATCGTTTTGGTGTCCGCGACACCATACCCCTTGTTGTACTGGAGGAAGTTG
ATGGTCTGCGAACCGTCCGATTCCACTGCGTAGCTGGGCTCGACGCCAAGGTCAGAGCCATTGA
CCACGACGCGGTACGAGTATTTTTTGTCGGTGAGAACCTTGGGGAAGGTAAGGTTGTCGATGTAG
CTGCTTGGGGTACCACGGCCCCAGTTGGGGGTGTAGTCGAAATCGATCTTCTTCACCAAGTAGGC
AAGCTGGAAGGTGAGCGACGTGGCGGAATGGTGATGGTGATGGTGGCTAGCCATATGTATATCT
CCTTCTTAAAGTTAAACAAAATTATTTCTAGCCCAAAAAAACGGGTATGGAGAAACAGTAGAGAGT
TGCGATAAAAAGCGTCAGGTAGGATCCGCTAATCTTATGGATAAAAATGCTATGGCATAGCAAAG
TGTGACGCCGTGCAAATAATCAATGTGGACTTTTCTGCCGTGATTATAGACACTTTTGTTACGCGT
TTTTGTCATGGCTTTGGTCCCGCTTTGTTACAGAATGCTTTTAATAAGCGGGGTTACCGGTTTGGT
TAGCGAGAAGAGCCAGTAAAAGACGCAGTGACGGCAATGTCTGATGCAATATGGACAATTGGTTT
CTTCTCTGAATGGCGGGAGTATGAAAAGTATGGCTGAAGCGCAAAATGATCCCCTGCTGCCGGGA
TACTCGTTTAATGCCCATCTGGTGGCGGGTTTAACGCCGATTGAGGCCAACGGTTATCTCGATTTT
TTTATCGACCGACCGCTGGGAATGAAAGGTTATATTCTCAATCTCACCATTCGCGGTCAGGGGGT
GGTGAAAAATCAGGGACGAGAATTTGTTTGCCGACCGGGTGATATTTTGCTGTTCCCGCCAGGAA
AAGATTCATCACTACGGTCGTCATCCGGAGGCTCCCGAATGGTATCACCAGGGGGTTTACTTTCG
TCCGCCCGCCTACTGGCATGAAGGGCTTAACGGGCCGCCAAAATTTGCCAATACGGGGGTTCTTT
CCCCCGGAAGAAAGCCCCCCATGCCCCTTTTCACGGACCTGGTTGGGGCAAATCATTAACGCCGG
GCAATGGGAAAGGGGCCTTTCTCGAAATTGCTTGGCAAAAAATCGGGTTGGATAATTGTTTTCCG
TGGGCTCTGTGAAGCTTATAAATGCTTGCGCCTCCTCCACCTTTGGGTATATTCGCTACTCCTTGG
GTTGTCCAACGAATATGATTCTTCCGATGATTAGAGCGATCTATGCAACCTCCGCCTTTGATCCCA
CTATGGTTTGCACGCTTCCAGAAGGCACCTACACATCATTCTTACCGT

A3.25 Sequencing results of H-CWT6-Ek sequence in pGLO:: H-CWT6-EK-GFP

Forward primer (pBAD-FP)

AAAAAACGGACTACTGACGCTTTTTATCGCACTCTCTACTGTTTCTCCATACCCGTTTTTTTGGGCT
AGAAATAATTTTGTTTAACTTTAAGAAGGAGATATACATATGGCTAGCCACCATCACCATCACCATT
CCGCCACGTCGCTCACCTTCCAGCTTGCCTACTTGGTGAAGAAGATCGATTTCGACTACACCCCC
AACTGGGGCCGTGGTACCCCAAGCAGCTACATCGACAACCTTACCTTCCCCAAGGTTCTCACCGA
CAAAAAATACTCGTACCGCGTCGTGGTCAATGGCTCTGACCTTGGCGTCAAGCCCAGCTACGCAG
TGGAATCGGACGGTTCGCAGACCATCAACTTCCTCCAGTACAACAAGGGGTATGGTGTCGCGGA
CACCAAAACGATTCAAGTTTTCGTTGTCATTCCAGATACCGGCAACTCGGAGGAGTACATCATCGC
TGAGTGGAAGAAGACTGACGACGACGACAAGATCGCTAGCAAAGGAGAAGAACTTTTCACTGGA
GTTGTCCCAATTCTTGTTGAATTAGATGGTGATGTTAATGGGCACAAATTTTCTGTCAGTGGAGAG
GGTGAAGGTGATGCTACATACGGAAAGCTTACCCTTAAATTTATTTGCACTACTGGAAAACTACCT
GTTCCATGGCCAACACTTGTCACTACTTTCTCTTATGGTGTTCAATGCTTTTCCCGTTATCCGGATC
ATATGAAACGGCATGACTTTTTCAAGAGTGCCATGCCCGAAGGTTATGTACAGGAACGCACTATAT
CTTTCAAAGATGACGGGAACTACAAGACGCGTGCTGAAGTCAAGTTTGAAGGTGATACCCTTGTT
AATCGTATCGAGTTAAAAGGTATTGATTTTAAAGAAGATGGAAACATTCTCGGACACAAACTCGAG
TACAACTATAACTCACACAATGTATACATCACGGCAGACAAACAAAAGAATGGAATCAAAGCTAAC
TTCAAAATTCGCCACAACATTGAAGATGGATCCGTTCAACTAGCAGACCATTATCAACAAAATACT
CCAATTGGCGATGGCCCTGTCCTTTTACCAAACAACCATTACCTGTCGACCAATCTGCCCTTTCGA
AAGTCCCAACGAAAAGCGTGACCAATGGTCCTTCTGGATTTGAAACGCTGCGGGGATACCAGGTC
CTGGAGGAGCCTCCAATAAGGAATCCGACCTGGTACCGGGGAATCCTTAG

Forward primer (FIPfve-RP)

GGGGATGTACTCCTCCGAGTTGCCGGTATCTGGAATGACAACGAAAACTTGAATCGTTTTGGTGT
CCGCGACACCATACCCCTTGTTGTACTGGAGGAAGTTGATGGTCTGCGAACCGTCCGATTCCACT
GCGTAGCTGGGCTTGACGCCAAGGTCAGAGCCATTGACCACGACGCGGTACGAGTATTTTTTGTC
GGTGAGAACCTTGGGGAAGGTAAGGTTGTCGATGTAGCTGCTTGGGGTACCACGGCCCCAGTTG
GGGGTGTAGTCGAAATCGATCTTCTTCACCAAGTAGGCAAGCTGGAAGGTGAGCGACGTGGCGG
AATGGTGATGGTGATGGTGGCTAGCCATATGTATATCTCCTTCTTAAAGTTAAACAAAATTATTTCT
AGCCCAAAAAAACGGGTATGGAGAAACAGTAGAGAGTTGCGATAAAAAGCGTCAGGTAGGATCC
GCTAATCTTATGGATAAAAATGCTATGGCATAGCAAAGTGTGACGCCGTGCAAATAATCAATGTG
GACTTTTCTGCCGTGATTATAGACACTTTTGTTACGCGTTTTTGTCATGGCTTTGGTCCCGCTTTGT
TACAGAATGCTTTTAATAAGCGGGGTTACCGGTTTGGTTAGCGAGAAGAGCCAGTAAAAGACGCA
GTGACGGCAATGTCTGATGCAATATGGACAATTGGTTTCTTCTCTGAATGGCGGGAGTATGAAAA
GTATGGCTGAAGCGCAAAATGATCCCCTGCTGCCGGGATACTCGTTTAATGCCCATCTGGTGGCG
GGTTTAACGCCGATTGAGGCCAACGGTTATCTCGATTTTTTTATCGACCGACCGCTGGGAATGAA
AGGTTATATTCTCAATCTCACCATTCGCGGTCAGGGGGTGGTGAAAAATCAGGGACGAGAATTTG
TTTGCCGACCGGGTGATATTTTGCTGTTCCCGCCAGGAGAGATTCATCACTACGGTCGTCATCCG
GAGGCTCGCGAATGGTATCACCAGTGGGTTTACTTTCGTCCGCGCGCCTACTGGCATGAATGGCT
TAACTGGGCCGTCAATATTTTGCCATACGGGGGTTCTTTCCCCCGGATGAAGCCGCACCAACCCG
CATTTCAGCCAACCTGTTTGGGGCAAATCATTAAACGCCGGGGCAAGGGGAAAGGGCGCTATTCC
GGAACTGGCTGGCGAATAAATCTGGCTTGAACCAATTGTTTACTGGCGGGCCCATGGAAGT
CCATTAAACAAATCCCCTCCCTTCCCGCTAAAGGTAAACTCGGGGTACCCCAAGGGGTT
GGGAGGGTA

A3.26 Sequencing results of H-CWT7-Ek sequence in pGLO:: H-CWT7-EK-GFP

Forward primer (pBAD-FP)

GGGATGCGGGATCTACTGACGCTTTTTATCGCAACTCTCTACTGTTTCTCCATACCCGTTTTTTTG
GGCTAGAAATAATTTTGTTTAACTTTAAGAAGGAGATATACATATGGCTAGCCACCATCACCATCA
CCATTCCGCCACGTCGCTCACCTTCCAGCTTGCCTACTTGGTGAAGAAGATCGATTTCGACTACAC
CCCCAACTGGGGCCGTGGTACCCCAAGCAGCTACATCGACAACCTTACCTTCCCCAAGGTTCTCA
CCGACAAAAAATACTCGTACCGCGTCGTGGTCAATGGCTCTGACCTTGGCGTCGAGTCCAACTTC
GCAGTGACACCGTCCGGTGGGCAGACCATCAACTTCCTCCAGTACAACAAGGGGTATGGTGTCG
CGGACACCAAAACGATTCAAGTTTTCGTTGTCGATCCAGATACCAACAACGACTTCATCATCGCTG
AGTGGAAGAAGACTGACGACGACGACAAGATCGCTAGCAAAGGAGAAGAACTTTTCACTGGAGT
TGTCCCAATTCTTGTTGAATTAGATGGTGATGTTAATGGGCACAAATTTTCTGTCAGTGGAGAGGG
TGAAGGTGATGCTTC

Forward primer (FIPfve-RP)

ACGCATGACGTCGTTGTTGGTATCTGGATCGACAACGAAAACTTGAATCGTTTTGGTGTCCGCGA
CACCATACCCCTTGTTGTACTGGAGGAAGTTGATGGTCTGCCCACCGGACGGTGTCACTGCGAAG
TTGGACTCGACGCCAAGGTCAGAGCCATTGACCACGACGCGGTACGAGTATTTTTTGTCGGTGAG
AACCTTGGGGAAGGTAAGGTTGTCGATGTAGCTGCTTGGGGTACCACGGCCCCAGTTGGGGGTG
TAGTCGAAATCGATCTTCTTCACCAAGTAGGCAAGCTGGAAGGTGAGCGACGTGGCGGAATGGT
GATGGTGATGGTGGCTAGCCATATGTATATCTCCTTCTTAAAGTTAAACAAAATTATTTCTAGCCCA
AAAAAACGGGTATGGAGAAACAGTAGAGAGTTGCGATAAAAAGCGTCAGGTAGGATCCGCTAAT
CTTATGGATAAAAATGCTATGGCATAGCAAAGTGTGACGCCGTGCAAATAATCAATGTGGACTTTT
CTGCCGTGATTATAGACACTTTTGTTACGCGTTTTTGTCATGGCTTTGGTCCCGCTTTGTTACAGA
ATGCTTTTAATAAGCGGGGTTACCGGTTTGGTTAGCGAGAAGAGCCAGTAAAAGACGCAGTGACG
GCAATGTCTGATGCAATATGGACAATTGGTTTCTTCTCTGAATGGCGGGAGTATGAAAAGTATGG
CTGAAGCGCAAAATGATCCCCTGCTGCCGGGATACTCGTTTAATGCCCATCTGGTGGCGGGTTTA
ACGCCGATTGAGGCCAACGGTTATCTCGATTTTTTTATCGACCGACCGCTGGGAATGAAAGGTTA
TATTCTCAATCTCACCATTCGCGGTCAGGGGGTGGTGAAAAATCAGGGACGAGAATTTGTTTGCC
GACCGGGTGATATTTTGCTGTTCCCGCCAGGAGAGATTCATCACTACGGTCGTCATCCGGAGGCT
CGCGAATGGTATCACCAGTGGGTTTACTTTCGTCCGCGCGCCTACTGGCATGAATGGCTTAACTG
GGCCGTCAATATTTGCCAATACCGGGGTTCTTTTCGCCCGGATGAAGCCGAACCAGCCCGCATTT
CACCGACCTGGTTGGGGCAAATCATTAACCCCCGGGCAAAGGGGAAAGGGCGCCTATTCGGAAC
TGCTGGCCGATAAATCTGGCTTGAGCAATTGTTACTGCGGGGCCATGGAAACGAATTAACGGATT
CCTTCCATCCACCGAAGGGAATATCCGGGTACCCCAAGGCTTGGCCAAAAACTTCCCCGAATCCC
CTGGGCAAAAAACCAATTTTGGAAATCCCCCACGTTTCCCCAACGAG

A3.27 Sequencing results of H-CWT8-Ek sequence in pGLO:: H-CWT8-EK-GFP

Forward primer (pBAD-FP)

GGATTCGGATCTACCTGACGCTTTTTATCGCACTCTCTACTGTTTCTCCATACCCGTTTTTTTGGGC
TAGAAATAATTTTGTTTAACTTTAAGAAGGAGATATACATATGGCTAGCCACCATCACCATCACCAT
TCCGCCACGTCGCTCACCTTCCAGCTTGCCTACTTGGTGAAGAAGATCGATTTCGACTACACCCCC
AACTGGGGCCGTGGTACCCCAAGCAGCTACATCGACAACCTTACCTTCCCCAAGGTTCTCACCGA
CAAAAAATACTCGTACCGCGTCGTGGTCAATGGCTCTGACCTTGGCGTCAAGCCCAGCTACGCAG
TGGAATCGGACGGTTCGCAGACCATCAACTTCCTCCAGTACAACAAGGGGTATGGTGTCGCGGA
CACCAAAACGATTCAAGTTTTCGTTGTCGATCCAGATACCAACAACGACTTCATCATCGCTGAGTG
GAAGAAGACTGACGACGACGACAAGATCGCTAGCAAAGGAGAAGAACTTTTCACTGGAGTTGTCC
CAATTCTTGTTGAATTAGATGGTGATGTTAATGGGCACAAATTTTCTGTCAGTGGAGAGGGTGAA
GGTGATGCTACATACGGAAAGCTTACCCTTAAATTTATTTGCACTACTGGAAAACTACCTGTTCCA
TGGCCAACACTTGTCACTACTTTCTCTTATGGTGTTCAATGCTTTTCCCGTTATCCGGATCATATGA
AACGGCATGACTTTTTCAAGAGTGCCATGCCCGAAGGTTATGTACAGGAACGCACTATATCTTTCA
AAGATGACGGGAACTACAAGACGCGTGCTGAAGTCAAGTTTGAAGGTGATACCCTTGTTAATCGT
ATCGAGTTAAAAGGTATTGATTTTAAAGAAGATGGAAACATTCTCGGACACAAACTCGAGTACAAC
TATAACTCACACAATGTATACATCACGGCAGACAAACAAAAGAATGGAATCAAAGCTAACTTCAAA
ATTCGCCACAACATTGAAGATGGATCCGTTCAACTAGCCGACCATTATCAACAAAATACTCCAATT
GGCGAAGGCCCTGTCCTTTTACCAGAAAACCATTACCTGTCGACACAATCTGCCCTTTCGAAAGAT
CCCAACGAAAAGCGGGACCCATGGACCTTTCTGATTTTGTACTGCTGGGGGGAATACCTCGGCCA
GGGAGGATCCTACAAAATAATGAATTTAAATTCCTGATCCCGGGTAATCCACCTATAGCCGTCCGC
AGGCTCGTCCGATTGGCAGTTTTGTGGGATAAACAAAGATTTCCTGCGCGCGCAACGTTAACCGC
AAGCACCTATACTGTTTAGAAAACAGGAATTTCCTGGCGTACTTTTCCGGGGGCCTCCCTGCAGC
CTCCGCCTATCATTAGTTGACAATCAACACCTAGTGAGACTGTCGGC

Reverse primer (FIPfve-RP)

GCGGCATGGATGTCGTTGTTGGTATCTGGATCGACAACGAAAACTTGAATCGTTTTGGTGTCCGC
GACACCATACCCCTTGTTGTACTGGAGGAAGTTGATGGTCTGCGAACCGTCCGATTCCACTGCGT
AGCTGGGCTTGACGCCAAGGTCAGAGCCATTGACCACGACGCGGTACGAGTATTTTTTGTCGGTG
AGAACCTTGGGGAAGGTAAGGTTGTCGATGTAGCTGCTTGGGGTACCACGGCCCCAGTTGGGGG
TGTAGTCGAAATCGATCTTCTTCACCAAGTAGGCAAGCTGGAAGGTGAGCGACGTGGCGGAATG
GTGATGGTGATGGTGGCTAGCCATATGTATATCTCCTTCTTAAAGTTAAACAAAATTATTTCTAGCC
CAAAAAAACGGGTATGGAGAAACAGTAGAGAGTTGCGATAAAAAGCGTCAGGTAGGATCCGCTA
ATCTTATGGATAAAAATGCTATGGCATAGCAAAGTGTGACGCCGTGCAAATAATCAATGTGGACTT
TTCTGCCGTGATTATAGACACTTTTGTTACGCGTTTTTGTCATGGCTTTGGTCCCGCTTTGTTACAG
AATGCTTTTAATAAGCGGGGTTACCGGTTTGGTTAGCGAGAAGAGCCAGTAAAAGACGCAGTGAC
GGCAATGTCTGATGCAATATGGACAATTGGTTTCTTCTCTGAATGGCGGGAGTATGAAAAGTATG
GCTGAAGCGCAAAATGATCCCCTGCTGCCGGGATACTCGTTTAATGCCCATCTGGTGGCGGGTTT
AACGCCGATTGAGGCCAACGGTTATCTCGATTTTTTTATCGACCGACCGCTGGGAATGAAAGGTT
ATATTCTCAATCTCACCATTCGCGGTCAGGGGGTGGTGAAAAATCAGGGACGAGAATTTGTTTGC
CGACCGGGTGATATTTTGCTGTTCCCGCCAGGAGAGATTCATCACTACGGTCGTCATCCGGAGGC
TCGCGAATGGTATCACCAGTGGGTTTACTTTCGTCCGCGCGCCTACTGGCATGAATGGCTTAACT
GGCCGTCAATATTTGCCAATACGGGGGTTCTTTCCGCCCGGATGAAAGCGCACCCAGCCGCATTT
CAGCGACCTGTTTGGGGCAAATCATTAACGCCGGGCAAGGGAAAGGGCGCTATTCGGAACTGCT
GGGGAAAAAATCTGCTTGGAGCAATTGTTACTGGCGGCCCAGGGGAACCTATTAACGAATCCCTT
CAATCCACCGAAGGGAAATCCGGGTAACGCAGAGGTTTGGCAGTAAATCACCCGATACCCTGGG
CAAAACGCAATTTTTGTATTTCCCCCGGTTTCCAAAACAAGTTTA

Appendices for Chapter 4

A4.1 Example on fluorescence visualization of collected fractions from protein purification using IMAC

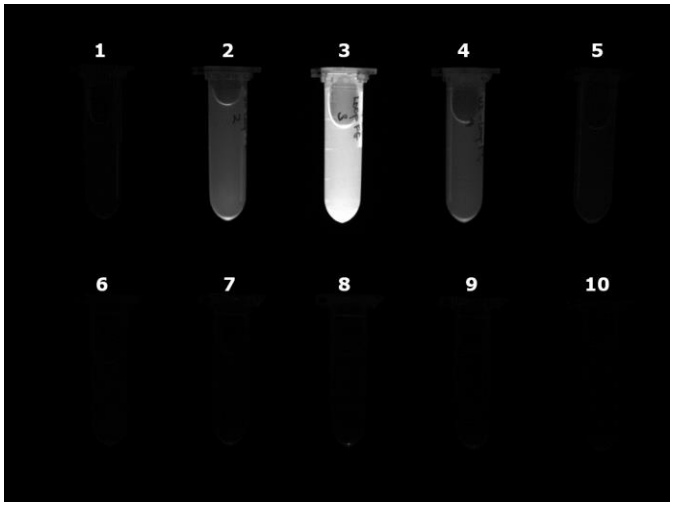


Figure A4.1. Fluorescence visualization of collected protein fractions containing GFP tag in tubes (labelled 1-10) from protein purification using IMAC.

A4.2 Example on fluorescence visualization of collected fractions from protein purification using SEC

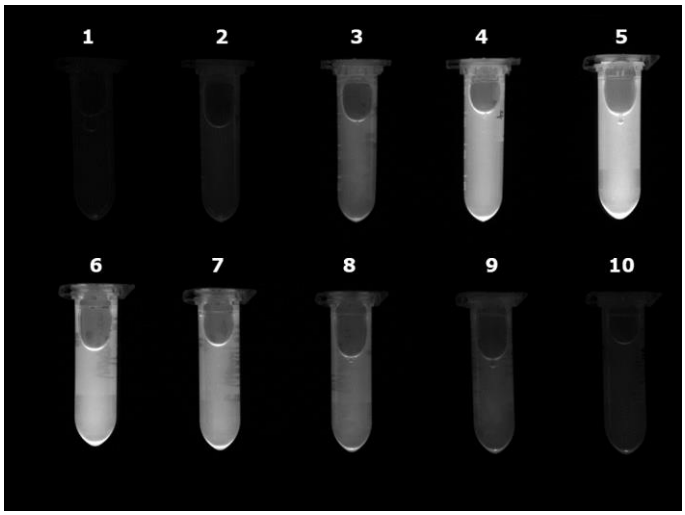


Figure A4.2. Fluorescence visualization of collected protein fractions containing GFP tag in tubes (labelled 1-10) from protein purification using SEC.

A4.3 Protein molecular weight determination

Molecular weight = 41104.98 Residues = 366
Average Residue Weight = 112.309 Charge = -2.0
Isoelectric Point = 6.2975
A280 Molar Extinction Coefficients = 44810 (reduced) 44935 (cystine bridges)
A280 Extinction Coefficients 1mg/ml = 1.090 (reduced) 1.093 (cystine bridges)
Improbability of expression in inclusion bodies = 0.574

Residue	Number	Mole%	DayhoffStat
A = Ala	16	4.372	0.508
B = Asx	0	0.000	0.000
C = Cys	2	0.546	0.188
D = Asp	29	7.923	1.441
E = Glu	20	5.464	0.911
F = Phe	18	4.918	1.366
G = Gly	31	8.470	1.008
H = His	16	4.372	2.186
I = Ile	20	5.464	1.214
J = ---	0	0.000	0.000
K = Lys	30	8.197	1.242
L = Leu	26	7.104	0.960
M = Met	4	1.093	0.643
N = Asn	20	5.464	1.271
O = ---	0	0.000	0.000
P = Pro	15	4.098	0.788
Q = Gln	11	3.005	0.771
R = Arg	9	2.459	0.502
S = Ser	22	6.011	0.859
T = Thr	28	7.650	1.254
U = ---	0	0.000	0.000
V = Val	27	7.377	1.118
W = Trp	3	0.820	0.631
X = Xaa	0	0.000	0.000
Y = Tyr	19	5.191	1.527
Z = Glx	0	0.000	0.000

Property	Residues	Number	Mole%
Tiny	(A+C+G+S+T)	99	27.049
Small	(A+B+C+D+G+N+P+S+T+V)	190	51.913
Aliphatic	(A+I+L+V)	89	24.317
Aromatic	(F+H+W+Y)	56	15.301
Non-polar	(A+C+F+G+I+L+M+P+V+W+Y)	181	49.454
Polar	(D+E+H+K+N+Q+R+S+T+Z)	185	50.546
Charged	(B+D+E+H+K+R+Z)	104	28.415
Basic	(H+K+R)	55	15.027
Acidic	(B+D+E+Z)	49	13.388

A4.4 Formulation of resolving and stacking gels in SDS- and Native-PAGE

Table A4.4a. Composition of resolving gel for SDS-PAGE

Distilled water	3.4 mL
Acrylamide/bis 30% 37.5:1 (R&M, Msia)	4 mL
Tris-HCl (1.5 M, pH 8.8)	2.5 mL
SDS (10%) (Sigma-aldrich, USA)	100 µL
N,N,N,N-tetramethylethylene-diamine (TEMED) (Bio-Rad)	10 µL
Ammonium persulfate (APS) (R&M, Msia)	32 µL

Table A4.4b. Composition of stacking gel for SDS-PAGE

Distilled water	6.1 mL
Acrylamide/bis 30% 37.5:1 (R&M, Msia)	1.3 mL
Tris-HCl (0.5 M, pH 6.8)	2.5 mL
SDS (10%) (Sigma-aldrich, USA)	100 µL
N,N,N,N-tetramethylethylene-diamine (TEMED) (Bio-Rad)	10 µL
Ammonium persulfate (APS) (R&M, Msia)	100 µL

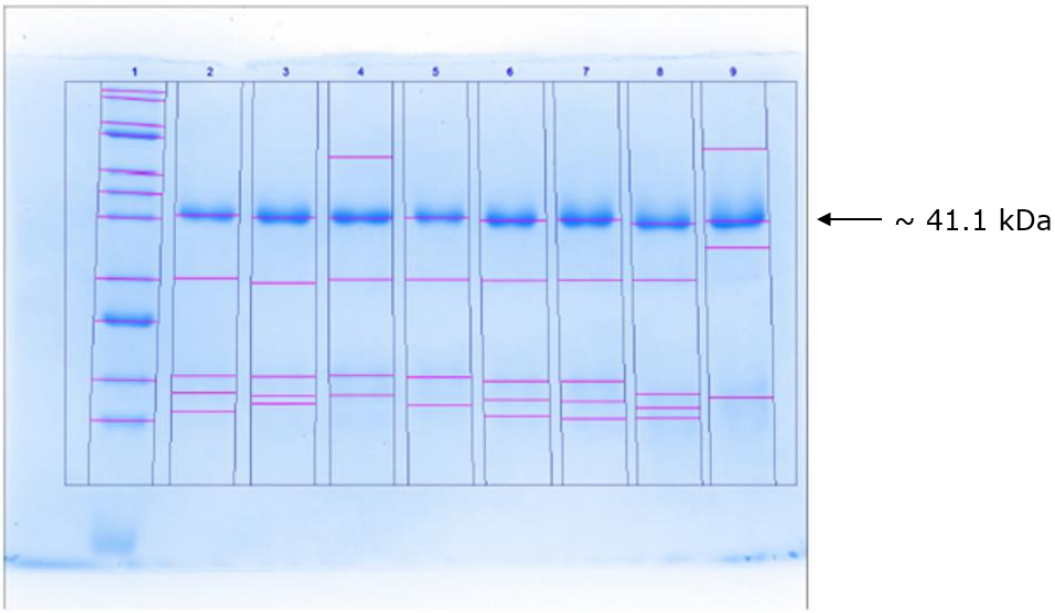
Table A4.4c. Composition of resolving gel for Native-PAGE

Distilled water	3.3 mL
Acrylamide/bis 30% 37.5:1 (R&M, Msia)	4 mL
Tris-HCl (1.5 M, pH 8.8)	2.5 mL
N,N,N,N-tetramethylethylene-diamine (TEMED) (Bio-Rad)	10 µL
Ammonium persulfate (APS) (R&M, Msia)	32 µL

Table A4.4d. Composition of stacking gel for Native-PAGE

Distilled water	6.0 mL
Acrylamide/bis 30% 37.5:1 (R&M, Msia)	1.3 mL
Tris-HCl (0.5 M, pH 6.8)	2.5 mL
N,N,N,N-tetramethylethylene-diamine (TEMED) (Bio-Rad)	10 µL
Ammonium persulfate (APS) (R&M, Msia)	100 µL

A4.5 Determination of protein purity



Lane And Band Analysis

Lane 2

Band No.	Band Label	Mol. Wt. (KDa)	Relative Front	Volume (Int)	Abs. Quant.	Rel. Quant.	Band %	Lane %
1		N/A	0.329	64,757,952	N/A	N/A	83.6	51.4
2		N/A	0.486	1,578,080	N/A	N/A	2.0	1.3
3		N/A	0.728	5,434,240	N/A	N/A	7.0	4.3
4		N/A	0.770	5,332,320	N/A	N/A	6.9	4.2
5		N/A	0.818	386,288	N/A	N/A	0.5	0.3

Lane 3

Band No.	Band Label	Mol. Wt. (KDa)	Relative Front	Volume (Int)	Abs. Quant.	Rel. Quant.	Band %	Lane %
1		N/A	0.335	102,587,968	N/A	N/A	94.6	52.7
2		N/A	0.497	1,131,984	N/A	N/A	1.0	0.6
3		N/A	0.730	3,871,280	N/A	N/A	3.6	2.0
4		N/A	0.777	652,736	N/A	N/A	0.6	0.3
5		N/A	0.797	156,464	N/A	N/A	0.1	0.1

Lane 4

Band No.	Band Label	Mol. Wt. (KDa)	Relative Front	Volume (Int)	Abs. Quant.	Rel. Quant.	Band %	Lane %
1		N/A	0.188	3,209,360	N/A	N/A	2.3	1.4
2		N/A	0.336	100,692,592	N/A	N/A	73.0	43.3
3		N/A	0.489	4,995,536	N/A	N/A	3.6	2.1
4		N/A	0.727	17,214,064	N/A	N/A	12.5	7.4
5		N/A	0.776	11,849,936	N/A	N/A	8.6	5.1

Lane 5

Band No.	Band Label	Mol. Wt. (KDa)	Relative Front	Volume (Int)	Abs. Quant.	Rel. Quant.	Band %	Lane %
1		N/A	0.335	77,926,464	N/A	N/A	81.0	37.5
2		N/A	0.489	4,652,368	N/A	N/A	4.8	2.2
3		N/A	0.731	12,121,536	N/A	N/A	12.6	5.8
4		N/A	0.800	1,524,992	N/A	N/A	1.6	0.7

Lane 6

Band No.	Band Label	Mol. Wt. (KDa)	Relative Front	Volume (Int)	Abs. Quant.	Rel. Quant.	Band %	Lane %
1		N/A	0.342	105,386,960	N/A	N/A	81.2	42.6
2		N/A	0.491	4,794,608	N/A	N/A	3.7	1.9
3		N/A	0.741	9,944,816	N/A	N/A	7.7	4.0
4		N/A	0.787	7,980,560	N/A	N/A	6.1	3.2

Lane 7

Band No.	Band Label	Mol. Wt. (KDa)	Relative Front	Volume (Int)	Abs. Quant.	Rel. Quant.	Band %	Lane %
1		N/A	0.341	126,988,400	N/A	N/A	77.4	45.6
2		N/A	0.490	6,054,944	N/A	N/A	3.7	2.2
3		N/A	0.741	22,930,096	N/A	N/A	14.0	8.2
4		N/A	0.792	5,816,608	N/A	N/A	3.5	2.1
5		N/A	0.835	2,317,392	N/A	N/A	1.4	0.8

Lane 8

Band No.	Band Label	Mol. Wt. (KDa)	Relative Front	Volume (Int)	Abs. Quant.	Rel. Quant.	Band %	Lane %
1		N/A	0.351	111,045,760	N/A	N/A	78.3	46.0
2		N/A	0.490	7,059,024	N/A	N/A	5.0	2.9
3		N/A	0.774	2,722,496	N/A	N/A	1.9	1.1
4		N/A	0.807	2,695,952	N/A	N/A	1.9	1.1
5		N/A	0.833	18,287,472	N/A	N/A	12.9	7.6

Appendices for Chapter 5

A5.1 Protocol of cell proliferation BrdU (colorimetric) ELISA for cell proliferation quantification

An amount of 100 µl of treated cell suspension was transferred from each well of 6-well plate to 96-well plate. BrdU labelling reagent was diluted 1:100 in complete RPMI, and 10 µl of the diluted reagent was added to each well. The plate was incubated for 24 hr at 37˚C in a 5% CO_2 humidified atmosphere. During this labelling incubation period, the pyrimidine analogue is incorporated as a substitute for thymidine into DNA of proliferating cells. After 24 hr, the plate was centrifuged at 300 x g for 10 min. The labelling medium was removed by flicking off and tapping on absorbent tissue. The labelled cells were then dried for 1 hr at 60˚C. The plate was stored at 4˚C and experiment was resumed on the next day.

The experiment was continued with addition of 200 µl FixDenat solution to cells in each well, and the plate was incubated for 30 min at 20˚C. FixDenat solution is added to fix the cells and denature DNA, which is necessary to enhance accessibility of the integrated BrdU for detection by antibody. The solution was then removed by flicking off and tapping. Monoclonal antibody from mouse-mouse hybrid cells (clone BMC 6H8, Fab fragments) conjugated with peroxidase (POD) namely Anti-BrdU-POD solution was diluted 1:100 from stock solution using supplied antibody diluent in the kit, and 100 µl of the diluted anti-BrdU-POD solution was added to cells in each well. The plate was incubated for another 90 min at 20˚C; during this step, the anti-BrdU-POD binds to the BrdU integrated in newly synthesized cellular DNA. The antibody solution was then removed by flicking off and tapping. The wells were washed three times with 200 µl of Washing solution (diluted 1:10 with distilled water). The washing solution was removed by flicking off and tapping.

Subsequently, 100 µl of tetramethyl-benzidine (TMB) substrate solution was added to the cells in each well to detect the immune complexes, which were quantified by measuring the absorbance at wavelength of 370 nm with correction wavelength of 492 nm at 10, 20 and 30 min. It was stated that “the developed color and thereby the absorbance value directly correlate to amount of DNA synthesis and hereby to number of proliferating cells in respective microcultures” (Roche, 2010).

A5.2 Protocol of BD OptIEA mouse IFN-γ and IL-2 ELISA for secretory cytokine profiling

Antibodies and standards were diluted according to lot specific instructions. Immunoplate maxibinding microplate (SPL Life Sciences, Korea) was coated with capture anti-mouse IFN-γ/IL-2 monoclonal antibody that was diluted 1:250 in coating buffer (0.1 M Sodium Carbonate, pH 9.5). The microplate was sealed and incubated overnight at 4˚C. After overnight incubation, the wells were aspirated and washed 5 times with 300 µl Wash Buffer (1X PBS with 0.05% Tween-20). The plate was inverted and blotted on absorbent paper to remove any residual buffer. The wells were blocked with 200 µl Assay Diluent (1X PBS with 10% FBS, pH 7.0) and incubated at room temperature for 1 hr. After overnight incubation, the wells were aspirated and washed 5 times with 300 µl Wash Buffer. The plate was inverted and blotted on absorbent paper to remove any residual buffer.

The recombinant IFN-γ standards were prepared by serial dilutions using Assay Diluent at 31.3 pg/ml, 62.5 pg/ml, 125 pg/ml, 250 pg/ml, 500 pg/ml, 1000 pg/ml and 2000 pg/ml. The recombinant IL-2 standards were prepared by serial dilutions using Assay Diluent at 3.1 pg/ml, 6.3 pg/ml, 12.5 pg/ml, 25 pg/ml, 50 pg/ml, 100 pg/ml and 200 pg/ml. An amount of 100 µl of each recombinant mouse IFN-γ/IL-2 standard, sample, positive and unstimulated controls were pipetted into appropriate wells. The plate was sealed and incubated at RT for 2 hr. All treatments were applied in duplicates. After 2 hr, the wells were aspirated and washed 5 times with 300 µl Wash Buffer. The plate was inverted and blotted on absorbent paper to remove any residual buffer. Subsequently, 100 µl of Working Detector (Detection antibody – Biotinylated anti-mouse IFN-γ/IL-2 + Enzyme reagent - Streptavidin-horseradish peroxidase conjugate) was added to each well and incubated at RT for 1 hr. The detection antibody was diluted 1:250 in Assay Diluent. The

wells were aspirated and washed 10 times with 30 s soaking in Washing Buffer for each wash. The plate was inverted and blotted on absorbent paper to remove any residual buffer.

Substrate Solution was prepared by mixing an equal volume of Substrate A, hydrogen peroxide and Substrate B, 3,3', 5,5' tetramethylbenzidine from TMB Substrate Reagent Set (BD Biosciences, USA). Then, 100 µl of Substrate Solution was added to each well and incubated for 30 min at room temperature in dark. After 30 min incubation, 50 µl of Stop Solution (1M phosphoric acid) was added to each well. Subsequently, absorbance was read at wavelength of 450 nm with correction wavelength of 570 nm within 30 min after addition of Stop Solution using Epoch microplate spectophotometer. The standard curve was plotted with IFN-γ/-IL-2 concentration on x-axis and the mean absorbance of standards on the y-axis. The IFN-γ/IL-2 concentration of samples and control was determined from the plotted standard curve.

A5.3 Immunophenotyping of ConA-stimulated splenocytes culture

As shown in **Figure A5.3**, the lymphocyte population (gated in P1) in ConA-stimulated splenocytes culture was lower in comparison to rFIP-fve-stimulated splenocytes culture. In addition, the population peaks that were stained positively using CD3-and CD4-antibodies in ConA-stimulated splenocyte culture were ambiguous unlike the population peaks in rFIP-fve-stimulated splenocyte culture, which were obvious. Therefore, the ConA-stimulated immune cell population was excluded from analysis and comparison with other mutant proteins. This research focused on analysing and comparing the immune cell population among rFIP-fve and mutant proteins.

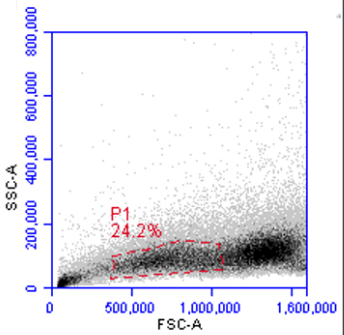
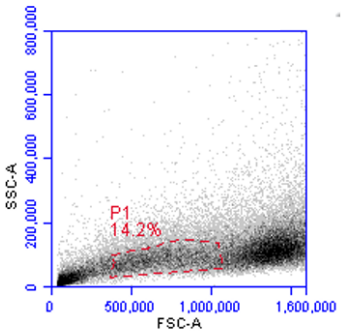
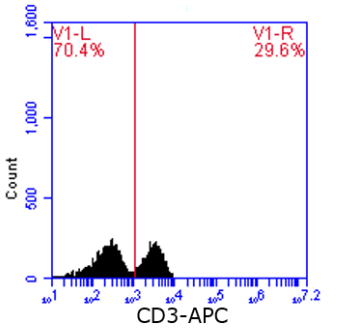
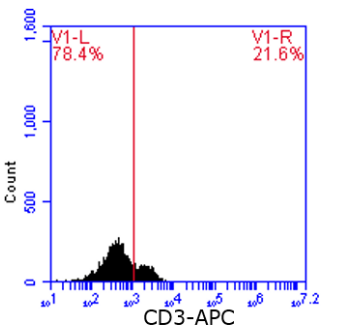
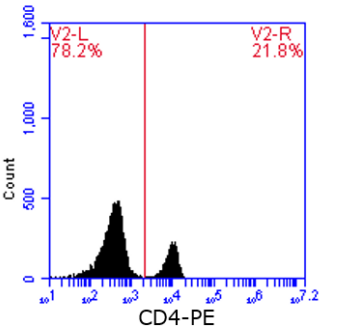
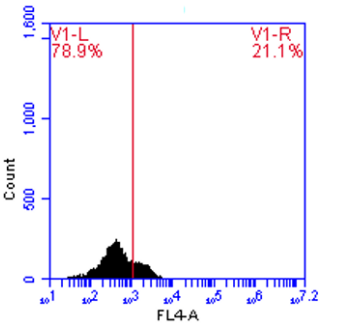
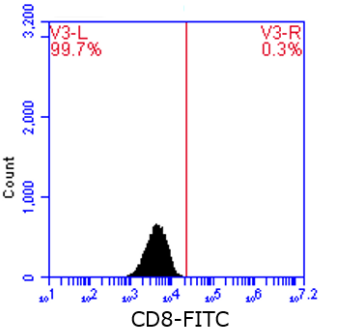
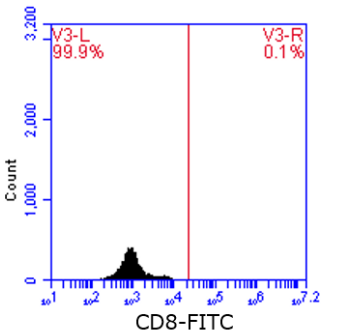
Antibodies	rFIP-fve	ConA
-		
CD3-APC		
CD4-PE		
CD8-FITC		

Figure A5.3. FACS analysis of ConA-stimulated mice splenocytes.